

## General Disclaimer

### One or more of the Following Statements may affect this Document

- This document has been reproduced from the best copy furnished by the organizational source. It is being released in the interest of making available as much information as possible.
- This document may contain data, which exceeds the sheet parameters. It was furnished in this condition by the organizational source and is the best copy available.
- This document may contain tone-on-tone or color graphs, charts and/or pictures, which have been reproduced in black and white.
- This document is paginated as submitted by the original source.
- Portions of this document are not fully legible due to the historical nature of some of the material. However, it is the best reproduction available from the original submission.

CR 73321

AVAILABLE TO THE PUBLIC

---

**DESIGN STUDY**  
**CV-7A TRANSPORT AIRCRAFT MODIFICATION**  
**TO PROVIDE AN**  
**AUGMENTOR-WING JET STOL**  
**RESEARCH AIRCRAFT**

---

By E. H. Kemper and D. J. Renselaer  
March 1969

Distribution of this report is provided in the interest of information exchange. Responsibility for the contents resides in the author or organization that prepared it.

Prepared under Contract No. NAS2-5139 by  
The Los Angeles Division of  
North American Rockwell Corporation,  
Los Angeles, California 90009

for

AMES RESEARCH CENTER

NATIONAL AERONAUTICS AND SPACE DIVISION



(ACCESSION NUMBER) **N69-25291**  
 (THRU) **1**  
 (PAGES) **274**  
 (CODES) **09**  
 (CATEGORY)  
 (NASA CR OR TXR OR AD NUMBER) **NASA CR # 73321**

FACILITY FORM 608

---

**DESIGN STUDY**  
**CV-7A TRANSPORT AIRCRAFT MODIFICATION**  
**TO PROVIDE AN**  
**AUGMENTOR-WING JET STOL**  
**RESEARCH AIRCRAFT**

---

By E. H. Kemper and D. J. Renselaer  
March 1969

Distribution of this report is provided  
in the interest of information exchange.  
Responsibility for the contents resides  
in the author or organization that  
prepared it.

Prepared under Contract No. NAS2-5139 by  
The Los Angeles Division of  
North American Rockwell Corporation,  
Los Angeles, California 90009

for

AMES RESEARCH CENTER

NATIONAL AERONAUTICS AND SPACE DIVISION

TABLE OF CONTENTS

Section	Page
FOREWORD	1
INTRODUCTION AND SUMMARY	3
I PROGRAM DESCRIPTION	15
Flight Test Objectives	15
Design Criteria	16
Engine Availability Survey	17
Propulsion System	17
Control System	18
Structural Modification	18
Performance	19
Schedule and Costs	19
II ENGINE INVESTIGATION	20
Engine Survey	20
Thrust Reverser/Vector Nozzle Survey	24
Propulsion Systems Installation	25
III CONFIGURATION DEVELOPMENT	27
Configuration No. 1 (Figure 3)	39
Configuration No. 2 (Figure 4)	40
Configuration No. 3 (Figure 5)	40
Configuration No. 4 (Figure 6)	41
Configuration No. 5 (Figure 7)	42
Configuration No. 6 (Figure 8)	42
Configuration No. 7 (Figure 9)	43
Configuration No. 8 (Figure 10)	43
Configuration No. 9 (Figure 11)	43
Weight and Balance Data	43
IV AERODYNAMIC PERFORMANCE COMPARISONS	58
Ground Rules for Takeoff and Landing Computations	58
STOL Performance	59
Method of Analysis of Takeoff and Landing Distances	65
STOL Speeds and Maneuver Margins	75

Section		Page
	Expression of Experimental Lift and Drag Data as a Function of Thrust-to-Weight Ratio	84
	Minimum Control Speed	95
	Roll Performance	98
V	CONFIGURATION SELECTION	100
VI	MODIFICATION CONFIGURATION DEVELOPMENT	106
	Propulsion	106
	Orpheus Engine	106
	Viper Compressor/T64-1 Turboshaft Engine	107
	Controls	107
	Aileron Control System	107
	Augmentor Flap System	107
	Augmentor Flap Air Distribution System	111
	Systems	118
	Engine Starting	118
	Engine Controls	118
	Fuel System	118
	Engine Bleed Air System	119
	Hydraulic System	119
	Hazard Protection	137
	Flight Station Modification	140
	Electrical Systems	143
	Structures	145
	Structural Modifications	145
	Structural Loads	147
	Structural Analysis	150
	Flutter Characteristics	150
	Weight, Balance, and Moments of Inertia	151
	Flight Dynamics	151
	Aerodynamics	160
	Performance	160

<b>Section</b>	<b>Page</b>
Longitudinal Stability and Control	169
Lateral and Directional Stability and Control	208
Conclusions and Recommendations	229
Aerodynamics Supporting Data	229
Axis System and Sign Convention	229
Aircraft Drag and Longitudinal Data	231
Lateral and Directional Data	244
REFERENCES	270

DESIGN STUDY  
FOR A  
CV-7A TRANSPORT AIRCRAFT MODIFICATION  
TO PROVIDE AN  
AUGMENTOR WING JET STOL  
RESEARCH AIRCRAFT

By E. H. Kemper and D. J. Renselaer

FOREWORD

This report is a three-volume final report for Contract NAS2-5139, "Design Study for Redefinition of Modifications to a C-8A Transport Aircraft to Provide Augmentor-Wing STOL Research Aircraft." This program has been completed by the Los Angeles Division of the North American Rockwell Corporation for the National Aeronautics and Space Administration Ames Research Center, Moffett Field, California 94035.

The 5-month study resulted in the preliminary design of a CV-7A Buffalo modified to a jet configuration and incorporating the augmentor wing. This aircraft is to be used by NASA-Ames Research Center for jet STOL flight research.

A program plan and estimated costs to carry out detail design, hardware modification, and airworthiness tests were developed as part of the study. Minimum cost was the primary objective.

The description of the study program and the backup data generated during the program is presented in Volume I of this report. Volume II presents the definition of the proposed modification and airworthiness flight testing. The estimated modification program costs are defined in Volume III.

PRECEDING PAGE BLANK NOT FILMED.

## INTRODUCTION AND SUMMARY

The Los Angeles Division of the North American Rockwell Corporation, with the assistance of the de Havilland Aircraft Company of Canada, Limited, has conducted a 5-month study to establish a design concept for a minimum cost program to provide an augmentor-wing jet STOL flight research aircraft.

Considerable effort has been expended over the past 7 years by the de Havilland Company and NASA-Ames, developing and testing the augmentor-wing concept. The three-dimensional capability of the concept was demonstrated on a large-scale (42-foot wingspan) model in late 1966 and 1967 with very encouraging results. A lift coefficient of 6.5 was achieved at a flap-blowing coefficient of 0.9.

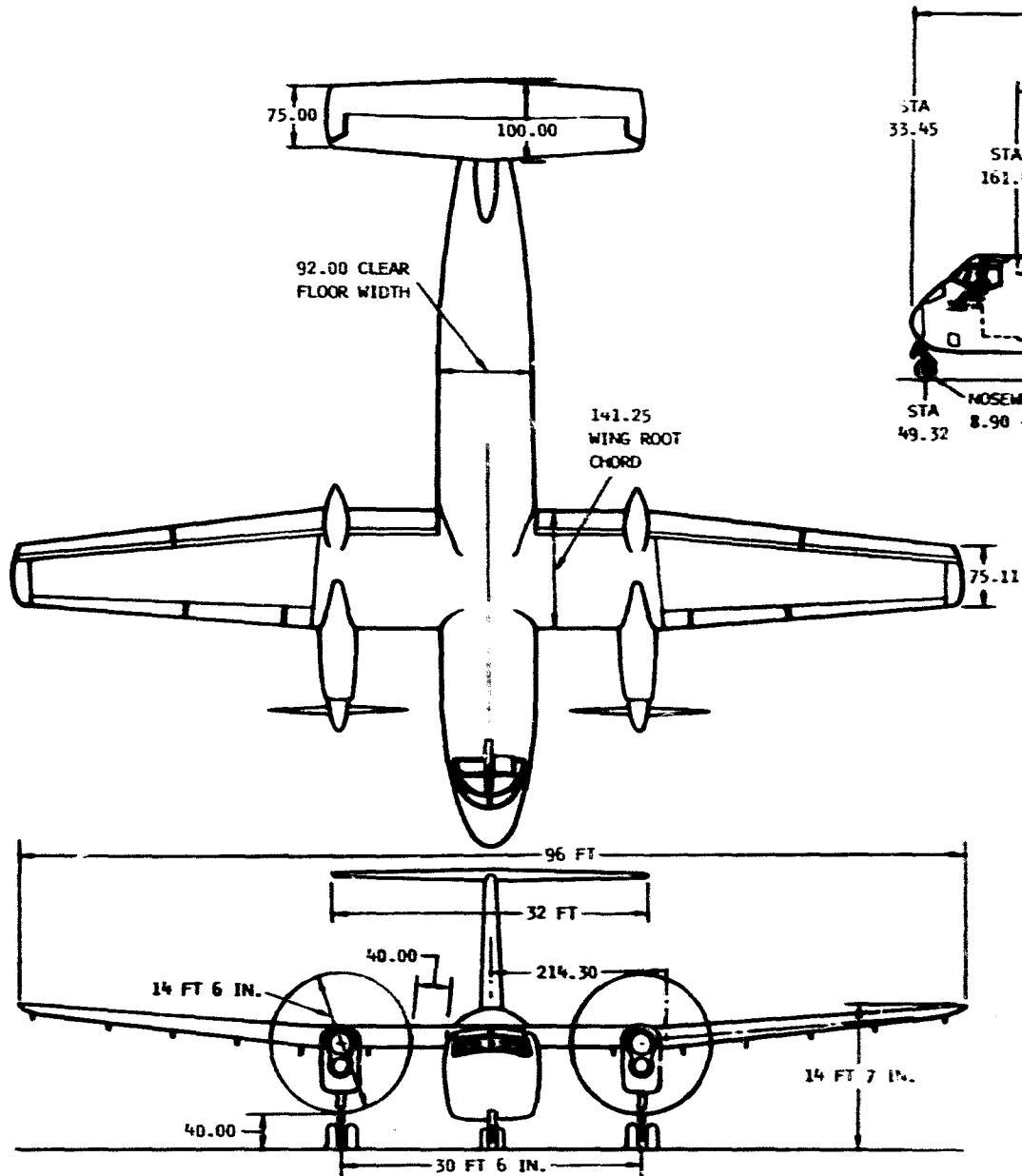
This highly successful test led to submittal of a proposal by de Havilland to the Canadian Government and NASA for continued ground tests of the model and for fabrication of a flight research aircraft to further verify the capability of the augmentor wing under dynamic free-flight conditions. The program for additional wind tunnel model testing and for ground simulation of stability and control systems has been approved. However, the flight research aircraft program was not economically feasible at that time.

The purpose of this study program, therefore, was to reassess the flight research aircraft and to achieve a minimum cost modification design, a program plan, and an estimate of the modification program costs. The aircraft designated for modification was the CV-7A de Havilland Buffalo to be furnished by NASA-Ames (figure 1). The desired STOL performance for the flight research aircraft is 1,000-foot takeoff and landing distance over a 50-foot obstacle.

The NASA-Ames objectives for the flight research program to be conducted with the aircraft are as follows:

1. Demonstrate and evaluate performance of the augmentor-wing concept in a large vehicle and develop data and experience which will serve as the technical foundation for the design of jet STOL operational systems
2. Study environmental signatures (e.g., noise, downwash)
3. Evaluate flight procedures for jet STOL terminal operations under VFR and simulated IFR conditions and to develop operational criteria for jet STOL aircraft





ENGINES - T64-8 GENERAL ELECTRIC  
GROSS WEIGHT 38,000 LB

WING:  
MEAN AERODYNAMIC CHORD 123.00  
ASPECT RATIO 9.85  
AREA 945 SQ FT

VERTICAL TAIL:  
ASPECT RATIO 1.22  
AREA 152 SQ FT

HORIZONTAL TAIL:  
ASPECT RATIO 4.41  
AREA 233 SQ FT

Figure 1. General Arrangement - CV-7A

The principle employed in the augmentor-wing concept is that of increasing circulation around an airfoil by directing a primary jet through a spanwise slot along the wing trailing edge to cause flow entrainment (figure 2). This slot consists of the upper and lower surfaces of what is normally considered wing flap area. The primary jet originates from the inner volume of the wing just forward of the flap hinge line. The flaps deflect the primary jet downward to create the supercirculation field in much the same manner as the jet flap. At the same time, through proper contour, location, and slotting of the forward flap segments, both upper and lower, additional air mass is induced to flow through the flap, augmenting the thrust of the primary jet and increasing the net lift/thrust generation. This latter effect gives rise to the name of the concept.

The primary nozzle is located in the region of the flap leading edge and includes the wing span from the fuselage outboard as far as desired. Depending upon the air source for the jet issuing from this nozzle, it may be supplied through either single or multiple ducting. The latter design would normally be considered, in case the main propulsion system provides the air source, to avoid unsafe air vehicle response in the event of powerplant failure, particularly in roll. The multiple-duct arrangement (cross ducting) also provides the same safety advantages as cross shafting in tilt wing, tilt propeller, etc, concepts.

After passage from the nozzle, the primary jet flows around the upper surface of the lower flap in an action similar to the Coanda effect; however, whereas normal Coanda flow is attached to the surface it follows, the design approach in the augmentor-wing concept separates the jet from the surface by the tertiary intake. This intake performs three functions. Air entrained through it causes low pressure to exist under the primary jet sheet adding to the bend around the Coanda surface. Friction losses are reduced due to the tertiary air stream (low velocity) tending to prevent the primary jet sheet (high velocity) from attaching to the surface. Finally, augmentation of thrust occurs by virtue of the increased momentum of the tertiary air.

Proper location of the Coanda surface with respect to the primary nozzle is important in order to maximize augmented thrust and provide proper exit velocity distribution. However, the shape of the tertiary air intake is apparently not critical nor is the radius of the Coanda surface itself critical (reference 1).

The lower flap acts primarily as one side of the main augmentor channel. In a sense, it also acts as a mechanical, double-slotted flap, particularly with the primary jet off, but understandably not as efficient as it otherwise would be. The gap that exists between the Coanda surface and the lower flap does not serve an entrainment function and hence is not critical. Its main

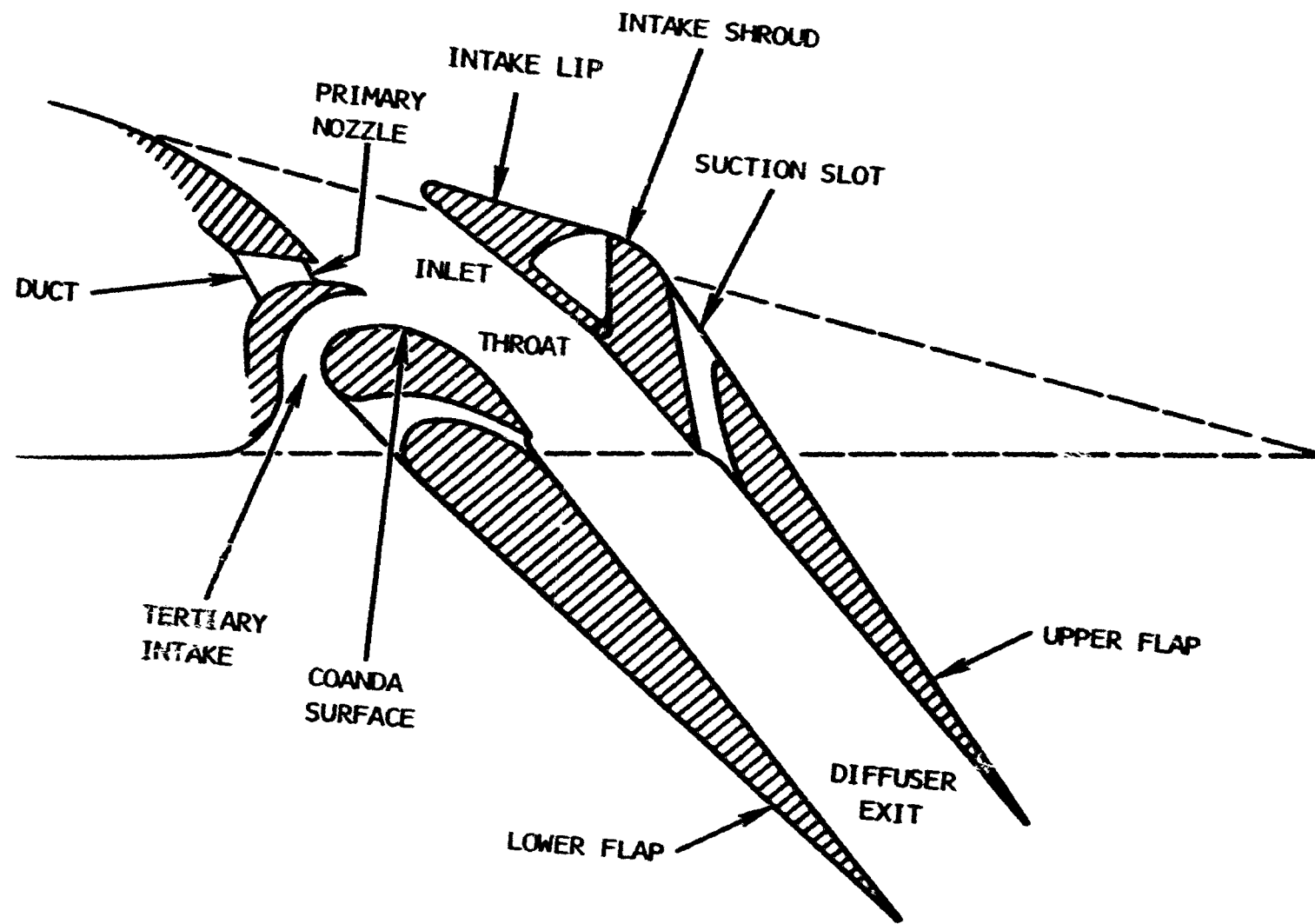


Figure 2. Augmentor Wing Flap Arrangement

purpose is to allow proper positioning of the Coanda surface relative to the nozzle to be maintained as an aid to exit velocity distribution.

The upper flap/intake shroud surface forms the second wall of the augmentor channel. Assuming the Coanda surface/lower flap kinetics have been satisfactorily established, this second wall must be positioned and shaped to optimize the throat and exit width. The intake shroud and upper flap are separated by a BLC suction slot. The purpose is removal of boundary layer on the shroud promoting flow attachment to the shroud. The slot exit is located in the augmentor throat (a region of relatively high negative pressure). The differential pressure across the slot then provides the required pumping action.

Although the upper flap function is almost entirely one of flow containment with reasonable diffusion properties, the intake shroud has several additional requirements. In the closed position, it must fair-in well with the theoretical mold line. In the open position, it must be high enough above the wing to function as an efficient inlet for secondary air capture. It must also turn this flow efficiently, and external surface separation must be avoided.

Special consideration must be given to a means of providing good lateral control at the high-lift coefficients engendered by the augmentor wing. Progress to date, as exhibited by references 2 and 3, indicates that the use of leading edge slats to prevent premature panel stall and aileron blowing to maintain effectiveness at high deflections is successful. However, the adverse yaw characteristics of a conventional trailing edge aileron under these characteristics are exceedingly strong. To counter these tendencies (i.e., improve vehicle response characteristics), a proverse yaw device, such as a spoiler, is used.

A problem normally encountered with a wing trailing-edge-generated super-circulation system is the creation of a correspondingly large pitching moment. This is due to the aft location on the wing of the center of the additional lift. In the case of the augmentor wing, due to the more forward generation of the jet force, plus the secondary circulation for a given improvement in lift, the resulting moment is smaller than a jet flap. Compared to a jet flap, this forward shift results in up to a 50-percent moment reduction. This, in turn, relieves the trim problem considerably, and hence, specific tail volume penalties to accommodate the system are minimized.

## SYMBOLS AND ABBREVIATIONS

A	= constant
a	= forward acceleration, lateral distance, or cruise engine moment arm.
A/C	= aircraft
APU	= auxiliary power unit
ave, av	= average
B	= constant
BLC	= boundary layer control
b	= span (ft)
c	= chord length of mean aerodynamic chord (ft)
CCW	= counterclockwise
$C_D$	= drag coefficient
$C_F$	= equivalent skin friction coefficient
c.g., C.G.	= center of gravity
$C_J$	= thrust coefficient
$C_{J_I}$	= jet flow coefficient for isotropic flow conditions
$C_L$	= lift coefficient
$C_{e\delta_a}$	= rolling moment coefficient due to aileron deflection
$\left(C_{L\delta_e}\right)_H$	= coefficient of lift due to elevator angle based on horizontal tail area
$C_m$	= pitching moment coefficient

$C_{\mu CRIT}$	= critical coefficient of BLC blowing
$C_{n\beta}$	= yawing moment coefficient due to sideslip
$C_{n\delta_a}$	= yawing moment coefficient due to aileron deflection
$C_{n\delta_R}$	= yawing moment coefficient due to rudder deflection
$C_{n\delta_{SP}}$	= yawing moment coefficient due to spoiler deflection
$C_S$	= chord shear (lb)
CW	= clockwise
$C_{y\beta}$	= side force coefficient due to sideslip
$C_{y\delta_R}$	= side force coefficient due to rudder deflection
D	= drag (lb)
DHC	= The de Havilland Aircraft of Canada, Limited
$f^*$	= factor representing the reduction of forces due to three-dimensional effects in a roll mode
F.O.D.	= foreign object damage
fus	= fuselage
fwd	= forward
$F_x$	= accelerating force (lb)
g	= gravitational constant
GE	= General Electric Company
gpm	= gallons per minute
HM	= hinge moment (in.-lb)
HP	= horsepower

$I_{xx}, I_x$	= roll inertia (slug-ft <sup>2</sup> )
$I_{yy}, I_y$	= pitch inertia (slug-ft <sup>2</sup> )
$I_{yz}$	= product inertia (slug-ft <sup>2</sup> )
$I_{zz}, I_z$	= yaw inertia (slug-ft <sup>2</sup> )
K	= constant
KEAS	= knots, equivalent air speed
L	= lift (lb)
$\mathcal{L}$	= rolling moment (ft-lb)
L.E.	= leading edge
$l_H$	= horizontal tail arm (ft)
$l_V$	= vertical tail arm (ft)
Lyc	= Lycoming Division of AVCO
M	= pitching moment (ft-lb)
MAC, mac	= mean aerodynamic chord
MAX	= maximum
$M_C$	= chord bending moment (in.-lb)
$M_{cp}$	= pitching moment due to aerodynamic forces acting at the center of pressure (ft-lb)
$M_H$	= pitching moment due to aerodynamic forces of horizontal tail
$M_N$	= Normal bending moment (in.-lb)
$M_T$	= pitching moment due to cruise engine thrust (ft-lb)
$M_W$	= pitching moment due to weight (ft-lb)
N	= yawing moment (ft-lb)

n mi       ▪ nautical mile  
 NR         ▪ North American Rockwell Corporation  
 N<sub>S</sub>       ▪ normal shear (lb)  
 n         ▪ normal acceleration or load factor  
 n<sub>max</sub>     ▪ maximum normal acceleration reached at C<sub>Lmax</sub>  
 n<sub>0</sub>       ▪ normal acceleration at lift-off speed  
 OEO, oeo   ▪ one engine out  
 p         ▪ rolling velocity (rad/sec)  
 P&W       ▪ Pratt and Whitney Aircraft  
 P/N       ▪ part number  
 P<sub>N</sub>       ▪ load normal to rotated wing chord (lb/in.)  
 psi       ▪ pounds per square inch  
 Q         ▪ hydraulic flow rate (gpm)  
 q         ▪ dynamic pressure (lb/ft<sup>2</sup>)  
 r         ▪ yawing velocity (rad/sec)  
 RPM, rpm   ▪ revolutions per minute  
 RR        ▪ Rolls Royce Limited  
 S, SWING   ▪ wing area (sq ft)  
 S<sub>eff</sub>     ▪ wing area affected by the aileron (sq ft)  
 S<sub>H</sub>       ▪ horizontal tail area (sq ft)  
 SLS       ▪ sea level standard conditions  
 STOL      ▪ short takeoff and landing  
 S<sub>V</sub>       ▪ vertical tail area (sq ft)



$T$  = thrust (lb)  
 $T_C$  = augmentor flap static thrust (lb)  
 $T_{C_N}$  = normal flap thrust (lb)  
 $T_{CR}$  = static cruise engine thrust (lb)  
 $T_H$  = static horizontal thrust (lb)  
 $T_O$  = static force vector existing when augmentor flap blowing is utilized (lb)  
 $T_R$  = reverse thrust (lb)  
 $T_{SA}$  = torque about structural axis (in.-lb)  
 $t$  = time (sec)  
 $t_{AIR}$  = time from lift-off to 50-foot obstacle (sec)  
 $t_{GR}$  = time, ground roll (sec)  
 $V$  = velocity (KEAS), or (ft/sec)  
 $V_a$  = approach speed (KEAS) or (ft/sec)  
 $V_E$  = equivalent air speed (knots)  
 $V_{l_0}$  = velocity at lift-off (KEAS)  
 $V_{LOC}$  = forward velocity at a local wing station (ft/sec)  
 $V_{mc}$  = minimum control speed (KEAS)  
 $V_{min}$  = longitudinal minimum control speed (KEAS)  
 $V_s$  = stall velocity (KEAS)  
 $V/STOL$  = vertical and short takeoff and landing  
 $\bar{V}_H$  = horizontal tail volume  
 $\bar{V}_V$  = vertical tail volume

W	= weight (lb)
WL	= water line
$\ddot{X}$	= forward acceleration (ft/sec <sup>2</sup> )
X <sub>air</sub>	= air distance (ft)
X <sub>BR</sub>	= braking distance (ft)
X <sub>GR</sub>	= ground roll distance (ft)
X <sub>roll</sub>	= rolling distance (ft)
Y	= side force (lb)
y*	= lateral distance where local drag and lift vector changes can be presented as one force change (ft)
Z	= vertical distance (ft)
$\dot{Z}$	= vertical velocity (ft/sec)
$\ddot{Z}$	= vertical acceleration (ft/sec <sup>2</sup> )
$\alpha$	= angle of attack (deg)
$\beta$	= sideslip angle (deg)
$\gamma$	= climb angle (deg)
$\gamma_a$	= approach angle (deg)
$\gamma_\infty$	= steady-state climb angle (deg)
$\Delta$	= determinant
$\delta$	= surface angle (deg)
$\delta_a$	= aileron angle (deg)
$\delta_e$	= elevator angle (deg)
$\delta_f, \delta_f$	= flap angle (deg)

$\delta_R$	= rudder deflection (deg)
$\delta_{SP}$	= spoiler deflection (deg)
$\epsilon$	= downwash angle (deg)
$\theta$	= aircraft attitude angle (deg)
$\dot{\theta}$	= pitch velocity (rad/sec)
$\ddot{\theta}$	= pitch acceleration (rad/sec <sup>2</sup> )
$\mu$	= coefficient of friction
$\rho$	= density (lb/ft <sup>3</sup> )
$\rho_0$	= sea level density
$\tau$	= time constant (sec)
$\phi$	= bank angle (deg)
$\dot{\phi}$	= roll velocity (rad/sec)
$\ddot{\phi}, \phi''$	= roll acceleration (rad/sec <sup>2</sup> )
$\psi$	= yaw angle (deg)
$\dot{\psi}$	= yaw acceleration (rad/sec <sup>2</sup> )
$\partial$	= partial derivative
$\infty$	= infinity

## SECTION I

### PROGRAM DESCRIPTION

The purpose of the study was to establish a preliminary design for the flight research aircraft and develop a modification program plan that will make possible a minimum-cost program consistent with NASA-Ames research objectives for the aircraft. The program consisted of three significant phases.

The first phase was to define the ultimate flight test objectives of the modified aircraft and, based on these objectives, define the design criteria for the modified airplane that will result in an austere yet practical vehicle with which to conduct the flight test program.

The second phase consisted of preliminary studies of subsystems including an engine survey, propulsion system schemes, airframe modifications, and basic performance studies. Based on these preliminary investigations, drawings of nine configuration concepts were made and evaluated to determine relative advantages or disadvantages of each concept. These data were accumulated into an interim report, NA-68-995, "Configuration Evaluation of a CV-7A Buffalo Modification to a Jet-Powered, Augmentor-Wing STOL Aircraft", and submitted to NASA-Ames. Based on this report, a single configuration was selected for the more detailed study and system development.

The third phase consisted of the preliminary design of the selected configuration; the development of a program plan to conduct the detail design, modification, and airworthiness flight testing; and an estimated cost for this program.

Support from de Havilland of Canada personnel provided the necessary background knowledge of both the CV-7A aircraft and the augmentor-wing concept to ensure a satisfactory study effort.

In accomplishing these three phases, the following elements or tasks were considered in the detail necessary to support the program objectives.

#### Flight Test Objectives

The goals of a flight test program would be:

1. Demonstration of the augmentor-wing concept

2. Demonstration of stability, control, and characteristics at very high lift coefficients
3. Investigation of takeoff and landing performance and techniques

### Design Criteria

A study of the available data on the augmentor-wing concept and the CV-7A airplane was accomplished to establish the extent to which these goals might be met with a modified CV-7A. The design criteria were also governed by three primary factors:

1. The aerodynamic parameters to be investigated relative to use of the augmentor-wing concept
2. Use of a modified CV-7A as the flight test vehicle
3. Minimum cost consistent with NASA-Ames objectives

This effort resulted in the definition of the following target characteristics and capabilities to be used as a basepoint of the study.

1. Takeoff gross weight = 45,000 pounds.
2. Landing gross weight = 40,000 pounds.
3. Wing area = 800 square feet.
4. Sink speed at landing gross weight will be 13 fps consistent with minimum modification costs.
5. Normal control power: To be determined.
6. Emergency control power: To be determined.
7. Cold thrust/wing area equal to or greater than 10.
8. Limit, gust, and maneuver load factors and velocities may be limited below the existing unmodified aircraft capabilities.
9. Takeoff and landing distances will be based on sea-level, standard-day conditions. Capabilities at 2500-feet, hot-day conditions will be determined.

10. Cruise and maximum velocity are not critical and may be limited.
11. Range and endurance: To be determined.
12. No fatigue life requirement.
13. The design and installation of the powerplants, fuel system, and related fire protection systems will be equivalent to the intent of AFSCM 80-1.
14. Accessibility and maintainability may be degraded below normal operational requirements.
15. There will be no ejection seat provisions.
16. Cargo bay installations will meet the existing aircraft cargo restraint requirements.
17. Modification of structural design based on minimum cost instead of minimum weight.

#### Engine Availability Survey

Turboprop, turbojet, and turbofan engines were considered in selecting the engines for basic propulsion and for augmentor-wing flap airflow. The prime requirement was that engines must be off-the-shelf; i.e., available from current production or from surplus or spares inventories.

#### Propulsion System

There are two basic functional requirements that must be supplied by the propulsion subsystem. One function is to provide the horizontal thrust required for flight; the other is to supply the pressurized air required for the augmentor-wing system. Therefore, propulsion system arrangements that were considered for the research vehicle requirements are as follows:

1. A two-engine (one per side) turbofan configuration supplying both the horizontal thrust and fan bleed air for the flap system. While this arrangement may be simplest in terms of number of components, the principal disadvantages were (a) the need for a thrust reverser to spoil the excess horizontal thrust developed by use of the high engine rpm setting required to supply adequate airflow to the augmentor-flap system during approach and (b) the undesirable effects

of a single engine failure resulting in simultaneous loss of one-half of the horizontal thrust and one-half of the airflow to the flap system.

2. Arrangements consisting of turbojets or turbofans for horizontal thrust only and separate air supply systems to provide pressurized air for the flap system.

The design objective was to provide the lowest cost system that would be suitable for accomplishing the test program desired. To provide the required safety in the augmentor-wing air supply system, the airflow distribution system must be designed so that no single source failure will result in an unacceptable loss of air to either side of the aircraft.

### Control System

The control system studies were to define the system modification and determine the extent of stability augmentation required to insure a safe flight-test aircraft. These studies were based on the desired characteristics defined by the Design Criteria, the augmentor-wing wind tunnel data, and the estimated center of gravity and mass moment of inertia properties developed for the final configuration as defined by this program.

### Structural Modification

The general approach to the structural modifications aspect of the study was to retain as much as possible of the existing CV-7A structure. The major factors affecting the structure modifications were as follows:

1. Number, type, and location of engines
2. The revised flap system
3. The revised control system
4. The air distribution system from the flap air source to the augmentor-wing nozzles
5. The changes in airframe load distribution due to changes in dead weight distribution, new hardpoints and load inputs from concentrated masses and changes in landing conditions due to revised sink rates
6. The necessity of retaining the present landing gear installations for cost and development considerations

## Performance

During the early portion of the program preliminary performance and control data were developed for each of the configurations based on common ground rules for comparative evaluation purposes. After selection of the configuration to be used for the modification program, detail performance, stability and control data were developed.

## Schedule and Costs

The schedule, cost, and program risk aspects associated with the various configurations developed during the early phases of the program are assumed to be essentially proportional to the number and types of engines required. This approach was considered feasible as the majority of the modification effort was shown to be either associated with the items common to all configurations, such as the augmentor flap system and the slats, or directly associated with the engines and power plant systems installations.

After definition of the final configuration of the research aircraft, the necessary program plan, schedule, and costs were developed.



## SECTION II

### ENGINE INVESTIGATION

This section defines the engine selection and evaluation analysis accomplished prior to the final selection of the aircraft configuration to be used for the research flight test program. Additional engine data were accumulated after the configuration selection and are presented in section VI.

To permit an engine availability survey, a preliminary aircraft performance analysis was accomplished to determine the augmentor flap thrust and aircraft horizontal thrust requirements for both a 40,000-pound and a 45,000-pound aircraft with a wing area of 800 square feet. These data are shown in table I.

#### Engine Survey

The initial survey therefore was based on a vehicle horizontal thrust requirement of 12,000 to 14,000 lbs (SLS) and a flap airflow range of 150 to 250 lb/sec at a compressor pressure ratio of 2.2 to 3.0 to provide the 8,000 to 9,000 pounds of flap thrust.

Turbojet and turbofan versions were considered as candidates for the horizontal thrust engines. For the flap air source, two variations were considered: (1) Turbofan bypass air ducted into the wing with an appropriate valve arrangement for shutting off and diverting the flap airflow, and (2) a compressor unit driven by a turboshaft engine using the compressor section from an existing turbojet engine. The results of this survey are shown in table II.

Several of the candidates from table II were excluded from further consideration due to excessive weight, high or low thrust, probable unavailability, and/or incompatibility with the Buffalo installation. Table III lists the remaining choices in the combinations necessary to provide the air vehicle requirements. Turboshaft/compressor combinations were predicated on proper matching of shaft horsepower, RPM, and direction of rotation.

TABLE I. PRELIMINARY ANALYSIS OF HORIZONTAL THRUST AND FLAP THRUST FOR ENGINE SIZING

Gross weight (lb)	45,000	45,000	40,000	40,000
Wing area (sq ft)	800	800	800	800
Number of flap air engines	2	4	4	4
Flap thrust/weight	0.2	0.2	0.2	0.2
Flap thrust (lb)	9,000	9,000	8,000	8,000
Horizontal thrust/weight	0.3	0.3	0.3	0.2
Horizontal thrust (lb)	13,500	13,500	12,000	8,000
$C_{LMAX}$	5.8	6.7	6.7	6.7
Ground run (ft)	550	405	360	513
Climb angle (radians)	0.262	0.287	0.287	0.173
Acceleration after liftoff (n-1)	0.29	0.11	0.11	0.11
Air distance over 50-ft obstacle (ft)	450	533	518	600
Total distance (ft)	1,000	938	878	1,113

TABLE II. ENGINE SURVEY

THRUST AND FLAP AIR ENGINES

Model	Type	Mfr	Horizontal Thrust SLS (lb)	Fan Air (lb/sec)	Pressure Ratio	Weight (lb)	Used On (availability)
RB163-25	(1)	RR	7,900	80	2.76	2,332	BAC111, Trident
RB163 2	(1)	RR	6,680	107.6	2.2	2,260	BAC111
RB183	(1)	RR	5,000	100	2.275	2,194	F-28
JT8D-5,7	(1)	P&W	8,400	165	1.88	3,156	DC-9, 727, 737

HORIZONTAL THRUST ENGINES

CF700	(1)	GE	4,125 (4)			725	Fan Falcon
CJ610	(2)	GE	2,950 (3)			402	Jet Commander, Learjet
JT12A	(2)	P&W	3,300 (3)			468	Sabreliner, Jetstar
J52	(2)	P&W	7,500 (4)			2,169	A-4F, A6A
J79 (Dry)	(2)	GE	10,500 (4)			2,900	F-104, B58
J57 (Dry)	(2)	P&W	10,500 (4)			4,400	F-100, F102
J65W5, 7	(2)	CW	7,800 (4)			2,795	B-57, F-84F
Orpheus	(2)	RR	5,000 (4)			800	Folland Gnat

TURBOSHAFT ENGINES

Model	Mfr	SHP	RPM	Dir of Rot.	Airflow (lb/sec)	Pressure Ratio	No. of NI Stages	Weight (lb)	Used On (availability)
T55-L-7C	Lyc	2,820	16,000	CW				590	Vertol CH47A
T55-L-11	Lyc	3,750	16,000	CW				670	Vertol CH47C
T64	GE	2,850	13,600	CCW				723	Sikorsky CH53A
T56-PD9,10	A11	7,300	10,400	CW				1,865	(5)

COMPRESSORS

JT12A (Civil J60)	P&W		16,000	CW	48	6.7	9		Sabreliner, T39 Jetstar, T2B
CJ610 (Civil J85 dry)	GE		16,500	CW	44	7	8		Jet Commander, Learjet
YJ85-21	GE		16,600	CW	52	8	9		PFRT 1967
J97	GE		13,900	CW	68	13	14		Available development engine
Viper	RR		13,700	CCW	50	4	7		
J52	P&W		10,700	CW	140	2.8	5		A4F, A6A (6)
J47	P&W		7,900	CW	100	5.4	12		B47, KC97 (7)

- (1) Turbofan
- (2) Turbojet
- (3) Requires four engines
- (4) Requires two engines
- (5) Not available - experimental only
- (6) No suitable turboshaft engine available
- (7) RPM mismatch - requires gearbox

TABLE III. ENGINE SELECTION

THRUST AND FLAP AIR ENGINES

Reqd Per A/C	Model	Horizontal Thrust SLS (lb)	Flap Air (lb/sec)	Pressure Ratio
2	RB163-25 (RR)	7,900	80	2.76
2	RB163-2 (RR)	6,680	107.6	2.2
2	RB183 (RR)	5,000	100	2.275

HORIZONTAL THRUST ENGINES

Reqd Per A/C	Model	Thrust SLS (lb)	Notes
4	CJ610 (GE)	2,950	J85 (Dry) Military version
4	JT12A (P&W)	3,300	J60 Military version
2	J52 (P&W)	7,500	
2	Orpheus (RR)	5,000	

FLAP AIR SOURCES

Reqd Per A/C	Turboshaft Engine Model	Compressor From Model
4	T55-L-7C (Lyc)	JT12A (P&W) CJ610 (GE) YJ85-21 (GE)
4	T64 (GE)	Viper (RR)

This initial survey resulted in the selection of three Rolls-Royce fan jets as the only possible power source for both horizontal thrust and flap air as the P&W JT8D fan jet has a pressure ratio considerably below the estimated minimum requirements.

For horizontal thrust only, eight engines, considered to be off-the-shelf, were evaluated. These were reduced to a total of four for use in the configuration studies. The eliminated engines were considered to have either too low a thrust, or excessive weight with more thrust than required.

The turboshaft engines and compressor listing resulted in several possible choices. The T64 and Viper compressor combination was selected for use in the configuration studies since they have the best overall match of RPM, horsepower requirements, airflow, and pressure ratio.

#### Thrust Reverser/Vector Nozzle Survey

Conventional thrust reversers for ground braking have been developed for the Spey 2 and 23 installations in the BAC-111 and Trident aircraft. These use clamshell doors to block the tailpipe and divert the exhaust through cascaded nozzles on the top and bottom surfaces. They should be usable on the Spey engine configurations of this study but rotated 90 degrees to accommodate the under-wing nacelle location. Some alteration of cascade contours may also be necessary to better direct the exhaust stream for this application.

Dimensionally, the above reversers will fit the J52 engine with minor adaptation of the connecting flange diameters. Cascade nozzle area would have to be adjusted to suit the J52 exhaust gas flow.

For the Orpheus engine installation, the Rolls-Royce Avon engine thrust reverser could be adapted to fit.

A simple clamshell-type reverser has been developed for the JT12A engines. However, installation of these engines side-by-side in an under-wing nacelle would require deflector plates or other means to protect the wing lower surface.

In all cases, the normal-type thrust reversers are not existing installations and would require development. It is assumed, at this point, that this development would be comparable for all engines and is ignored as being a constant factor for the initial evaluations.

For inflight thrust modulation, the Pegasus-type, hot-gas vectoring nozzle could be considered as a possibility for adaptation to one of the horizontal thrust engines but is much larger than required. The vectoring nozzle used on the Rolls-Royce RB193 engine is also a possibility. However, at the time of the original configuration evaluation, adequate data on these nozzles were not available, and therefore they were not considered at this time.

### Propulsion Systems Installation

The various configurations, as defined in section III, were evaluated for comparison of propulsion and related systems installation problems. The factors considered included engine modification required, engine installation (mounting, accessories, systems attachment, servicing, etc), flap air system power source and air source, air inlets and exhaust, hazard protection (fire detection, fire extinguishing, compartmentation, and cockpit indication), fuel system, control system, instrumentation, starting systems, and bleed air systems.

As would be expected, the order of rating of the configurations follows inversely the number of power plant units used, with only slight variations due to engine locations.

Configurations No. 1 and 5, utilizing two Rolls-Royce RB163-25 engines for both horizontal thrust and flap air, emerge equally as the preferable choice. Their superiority is due principally to the capability of using existing CV-7A systems with only a minimum of modifications to suit the new engine package.

Configuration No. 7 follows, utilizing two Rolls-Royce RB183-1 Spey, Junior engines for flap air and horizontal thrust. To supplement the Spey, Junior horizontal thrust, one Pratt and Whitney JT12A turbojet has been added in the aft fuselage over the cargo doors. A significant increase in the modification effort is entailed in the addition of this engine and its peripheral systems in the cargo bay and the crew compartment.

Configurations No. 2, 3, 4, and 6 rank essentially equal. All employ either two Pratt and Whitney J52 turbojets or two Rolls-Royce Orpheus turbojets for horizontal thrust. Flap air is supplied by four turbocompressor units (General Electric T-64 turboshaft engine driving a modified compressor section from a Rolls-Royce Viper turbojet). The additional four power plant installations and the development problems encountered in

adapting compressor units to this use add a large measure of complexity and cost to these configurations.

Configuration No. 8 ranks last in this evaluation. It utilizes four Pratt and Whitney JT12A turbojets for horizontal thrust and four turbocompressor units (described in the preceding paragraph) for flap air. The multiplicity of power plant installations gives this configuration its low ranking.

One factor not included in the above evaluation is the flexibility gained by separating the flap air source from the horizontal thrust engines. This allows variation of the flap air delivery without affecting the horizontal thrust setting. Conversely, it allows variation of the horizontal thrust without change in the flap air. This capability is particularly advantageous for the subject test program.

From the standpoint of propulsion systems, configuration No. 8 is eliminated from further consideration. Configurations No. 2 and 6, with J52 engines, are also eliminated as providing no advantage over the Orpheus installations of configurations No. 3 and 4 and having the disadvantage of being considerably heavier.

Configuration No. 7, with the two Rolls-Royce RB183-1 Spey, Junior fanjets and a P&W JT12 turbojet, has no significant advantage over configurations No. 1 and 5 and is also eliminated because of its increased complexity with the third engine.

Thus, configurations No. 1 and 5, with two engines supplying both horizontal thrust and flap air, and configurations No. 3 and 4, with separate power sources for horizontal thrust and for flap air, remain in contention for final evaluation.

## SECTION III

### CONFIGURATION DEVELOPMENT

This section defines the development of the various configurations utilizing the engine selection data. It also includes the weight and balance data generated for these configurations. The configuration selected for the research aircraft and its definition is presented in section VI of this volume.

The various aircraft configurations are based on the engine selection investigation with the primary requirements of defining the possible engine locations. A summary of the various engine arrangements used is shown in table IV. Three-view drawings of these configurations are shown in figures 3 through 11.

It has been assumed for all configurations that the existing wing fuel provisions will be replaced by a fuselage cargo bay installation. This provides the capability of routing flap air ducting through the main wing box area between spars and permits the maximum flap chord. This approach is necessary as any system requiring the relocation of the existing rear spar would require the design and fabrication of a new wing which is outside the scope of this program.

The existing landing gear will be retained and locked in the extended position. Preliminary data from de Havilland indicate that the higher gross weight landing condition of 40,000 pounds is possible with the installation of the production aircraft larger wheels and tires and without any major structural changes in the area of the main gear primary structure.

All configurations are shown with an aileron span of 15 percent of the total wing span. The various supporting systems, such as flap actuation, engine controls, fire detection and prevention, fuel system, electrical system, etc, are either common to all configurations or are dependent upon the configuration selection for requirements. These areas will be defined after selection of the specific modification configuration.

These configurations were arranged with the assumption that normal jet thrust reversing could be obtained without major development. Therefore, the engine installations were located to prevent direct hot-gas impingement on the main gear strut or tires and to provide necessary clearance for tailpipe routing by the main gear trunnion fitting.

As an alternate thrust reverser system, the split, vectored-thrust type nozzle was investigated. This type would allow locating the horizontal



TABLE IV. CONFIGURATION ARRANGEMENT SUMMARY

Configuration No.	Engines	Location
1	2 Spey RB163-25	Under wing at inboard edge of main landing gear trunnion fitting
2	2 P&W J52-P-8A  2 GE T64-1  2 GE T64-1	Under wing below gear trunnion fitting and inboard of main landing gear strut  Under wing just outboard of main landing gear in common pod with J52 engines  Above wing center section at fuselage
3	2 Orpheus  2 GE T64-1  2 GE T64-1	In existing nacelles in landing gear well  In existing nacelles using existing T64 installation provisions  Below wing on outer wing panel
4	2 Orpheus  2 GE T64-1  2 GE T64-1	In existing nacelles in landing gear well  In existing nacelles using existing T64 installation provisions  Above wing center section at fuselage
5	2 Spey RB163-25	Under wing between main landing gear and fuselage
6	2 P&W J52-P-8A  2 GE T64-1  2 GE T64-1	Under wing below gear trunnion fitting and inboard of gear strut  Pylon mounted above wing at main gear wing station  Above wing center section at fuselage

TABLE IV. CONFIGURATION ARRANGEMENT SUMMARY (CONCLUDED)

Configuration No.	Engines	Location
7	2 Spey RB183  1 P&W JT12A	Under wing between main landing gear and fuselage  Mounted in cargo bay under retracted upper cargo door
8	4 P&W JT12A  2 GE T64-1  2 GE T64-1	Dual engine pods mounted below existing T64 installation and ahead of main gear strut  In existing nacelle area using existing T64 installation provisions  Above wing center section at fuselage
9	2 Orpheus  4 GE T64-1	Pod mounted on upper fuselage shoulder aft of wing  Mounted in pairs in modified existing nacelles

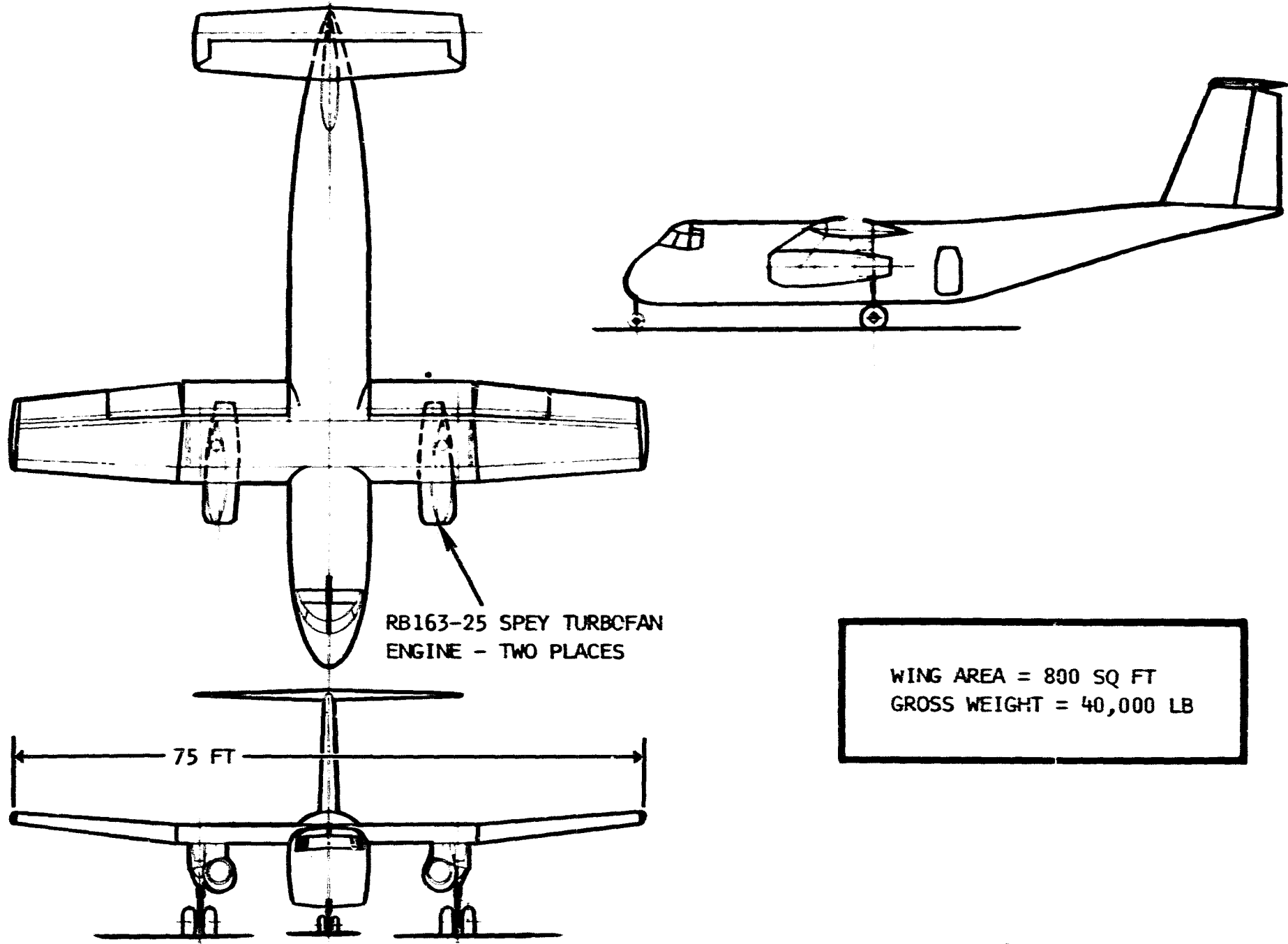


Figure 3. Configuration No. 1

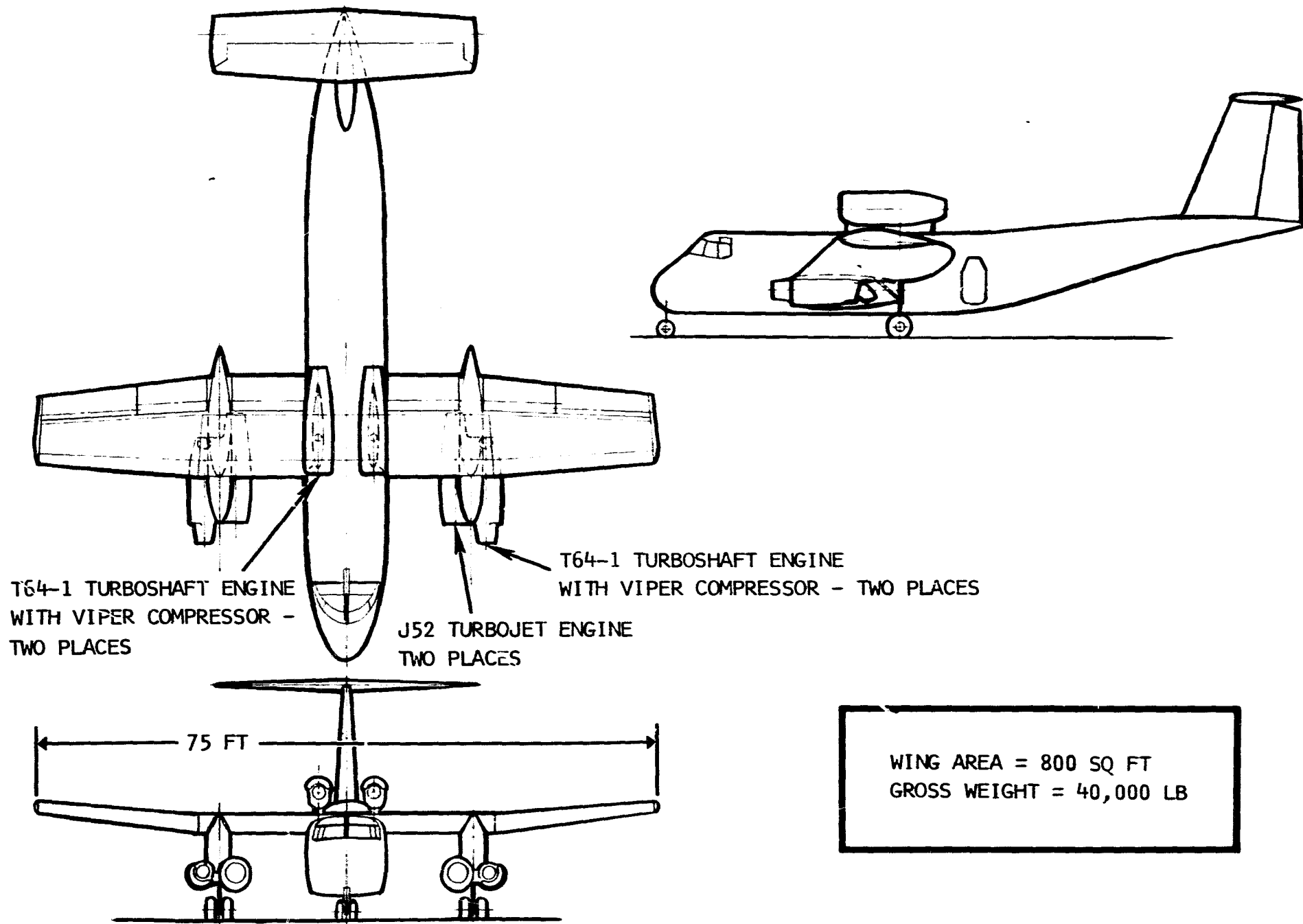


Figure 4. Configuration No. 2

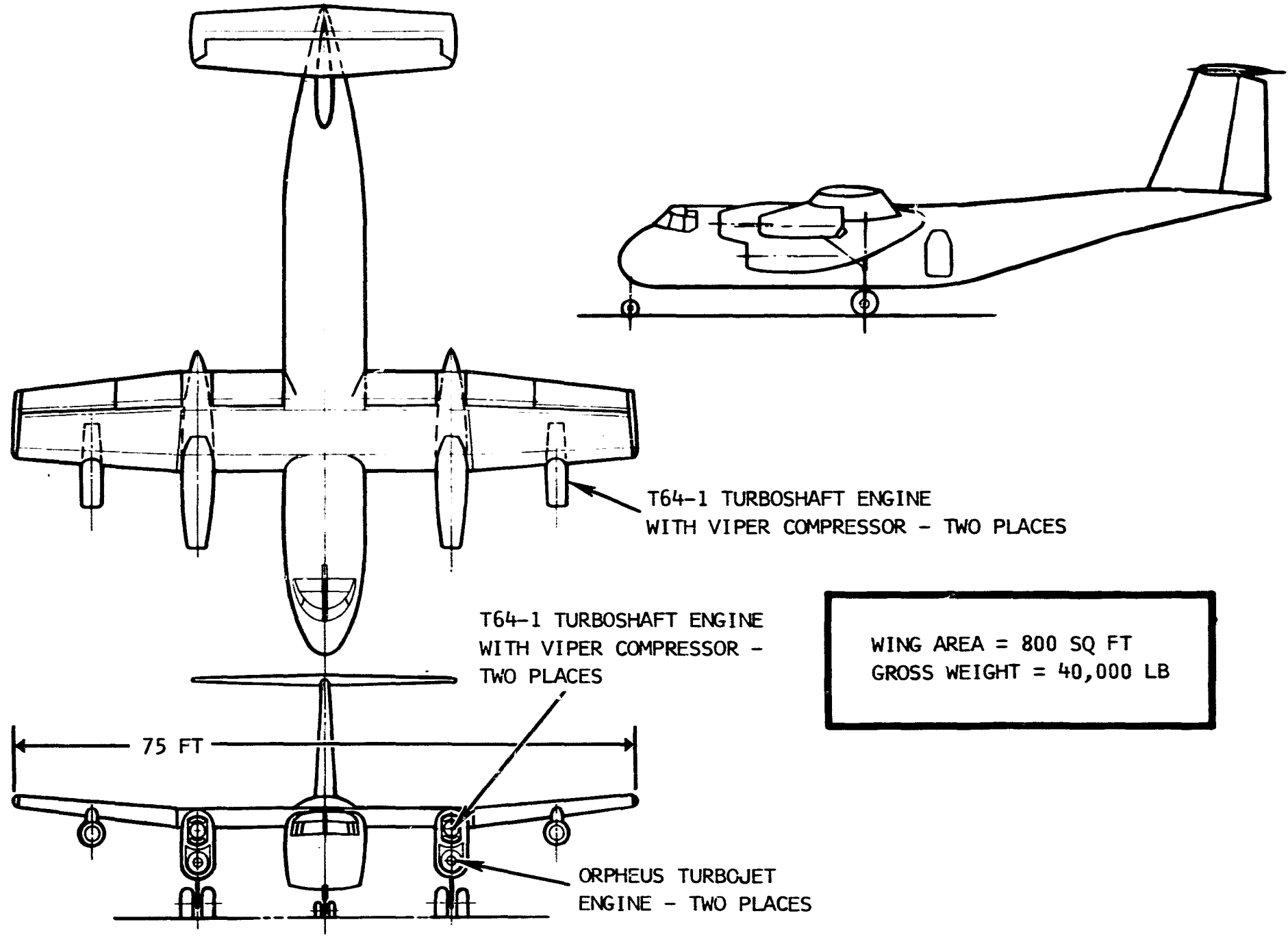


Figure 5. Configuration No. 3

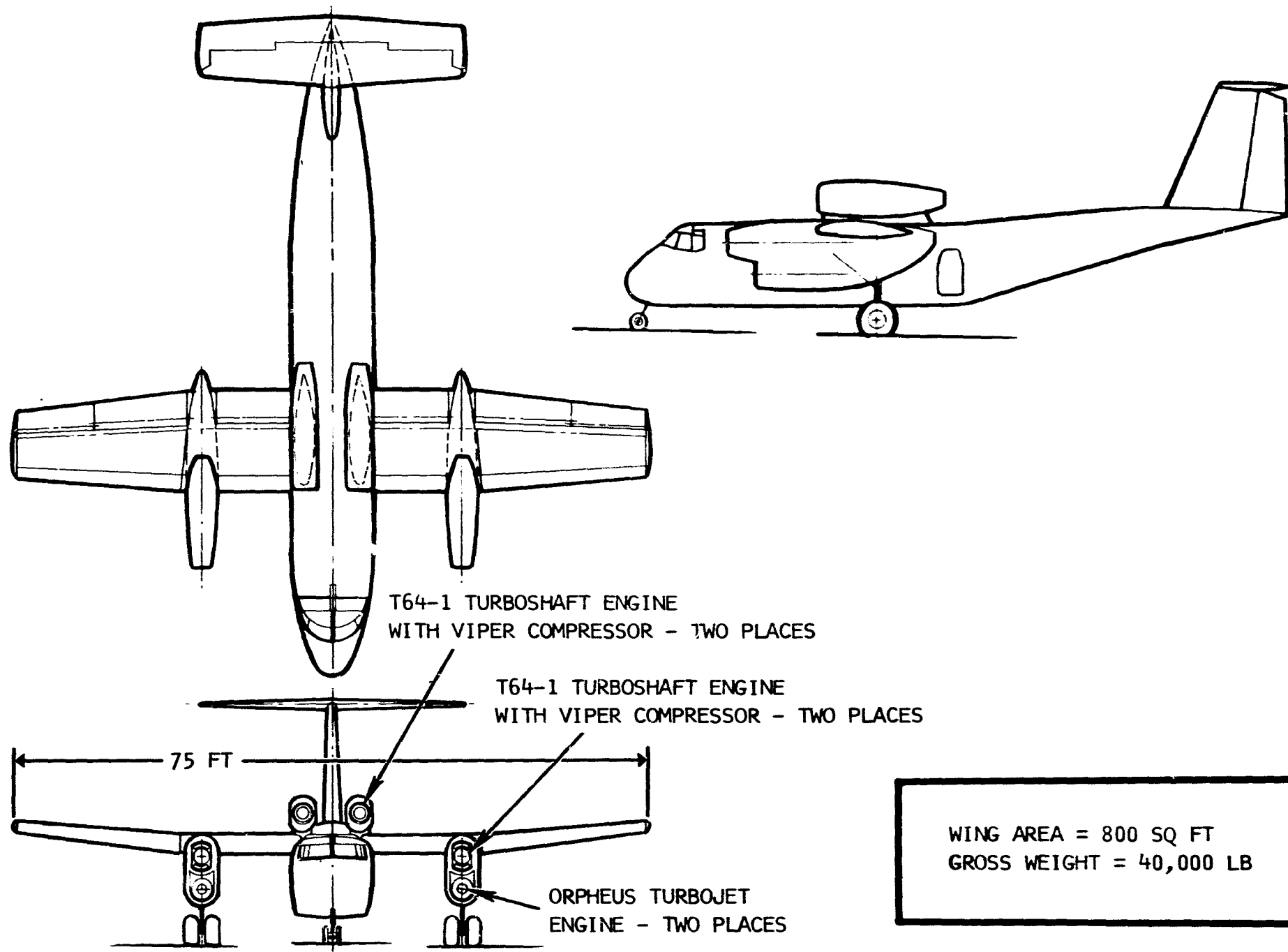


Figure 6. Configuration No. 4

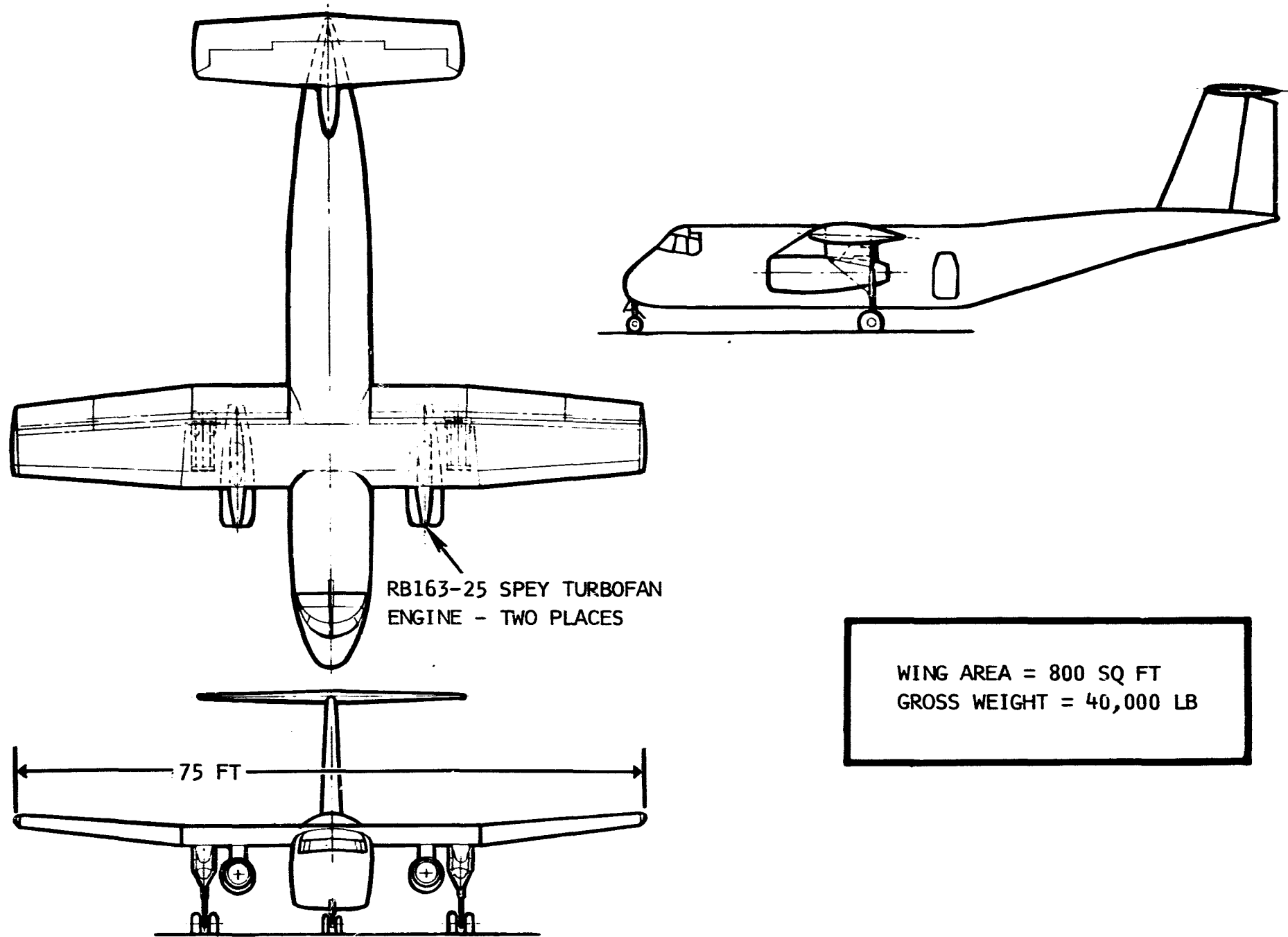


Figure 7. Configuration No. 5

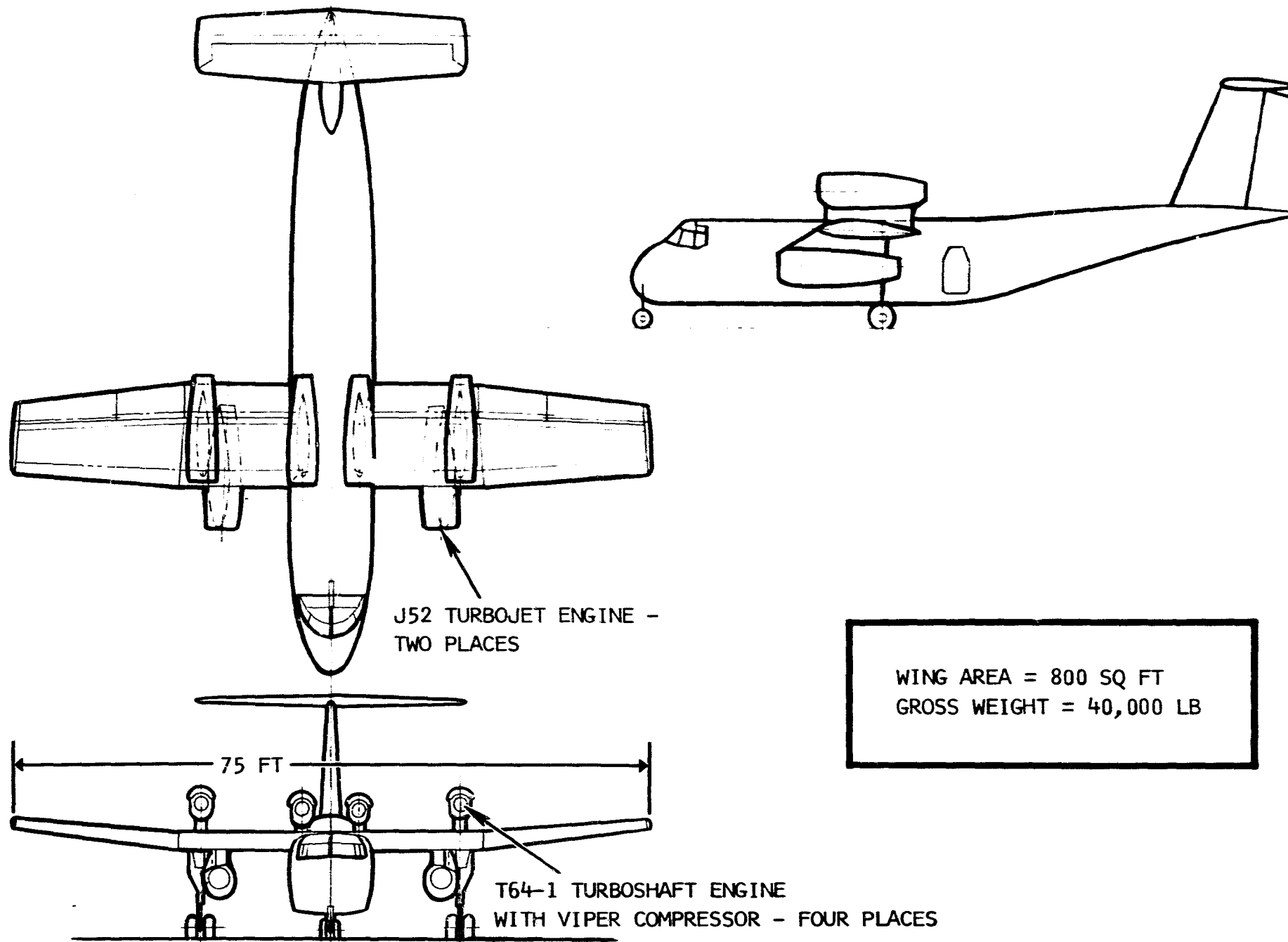
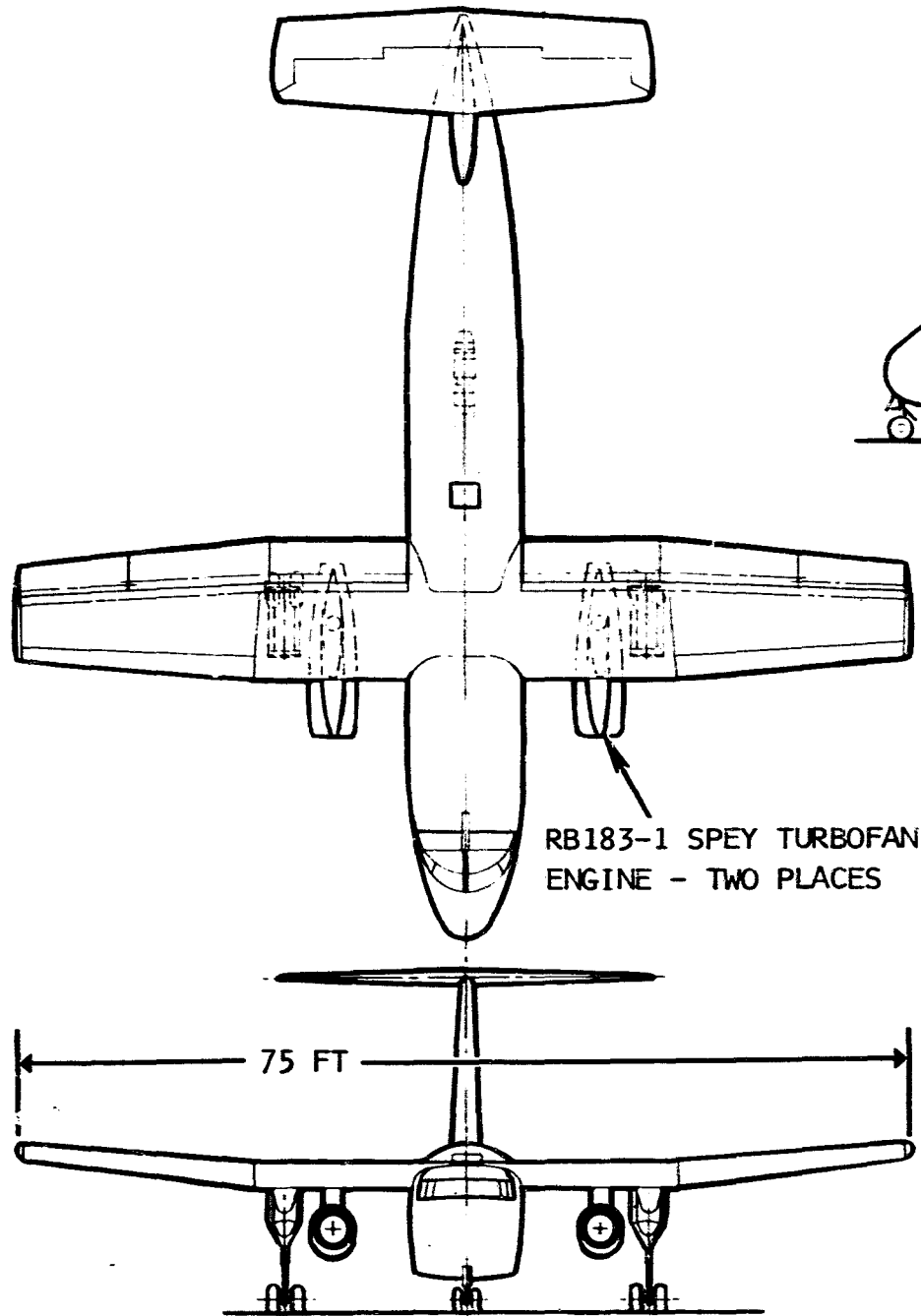
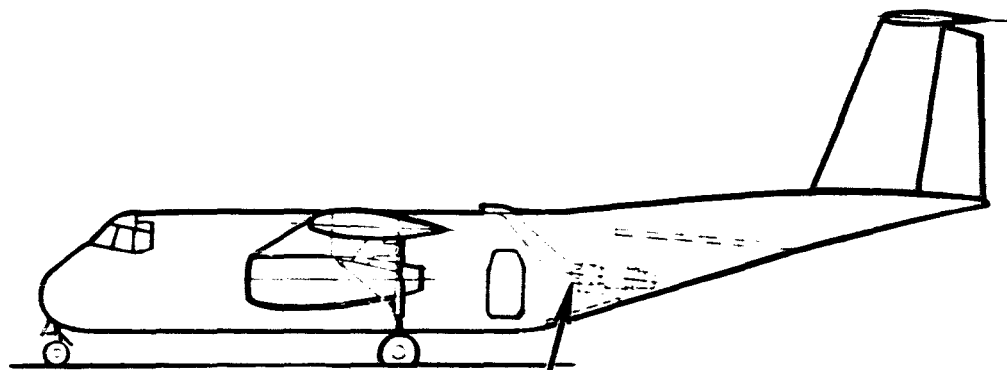


Figure 8. Configuration No. 6





RB183-1 SPEY TURBOFAN  
ENGINE - TWO PLACES



JT12A TURBOJET ENGINE -  
ONE PLACE

WING AREA = 800 SQ FT  
GROSS WEIGHT = 40,000 LB

Figure 9. Configuration No. 7

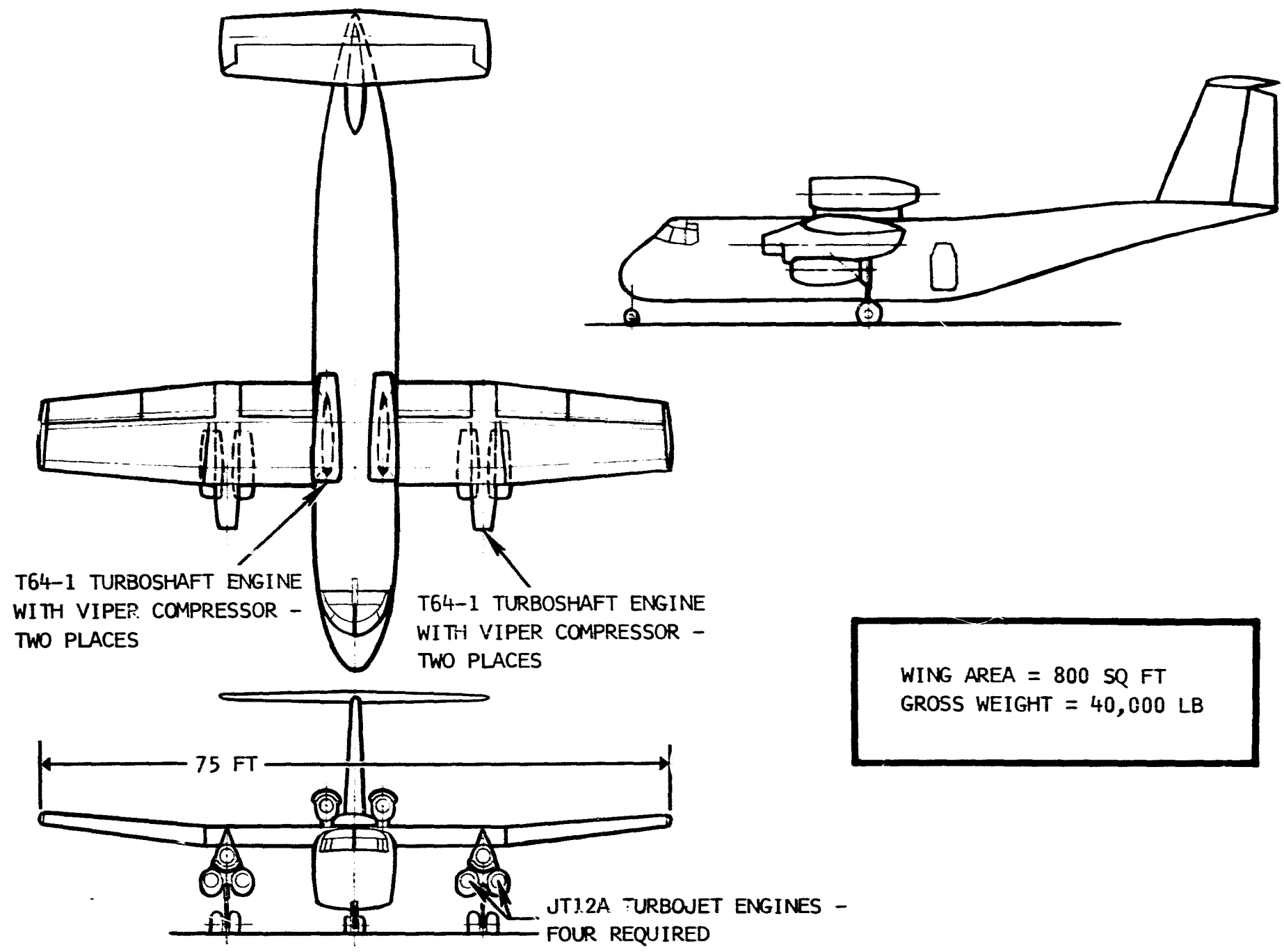


Figure 10. Configuration No. 8

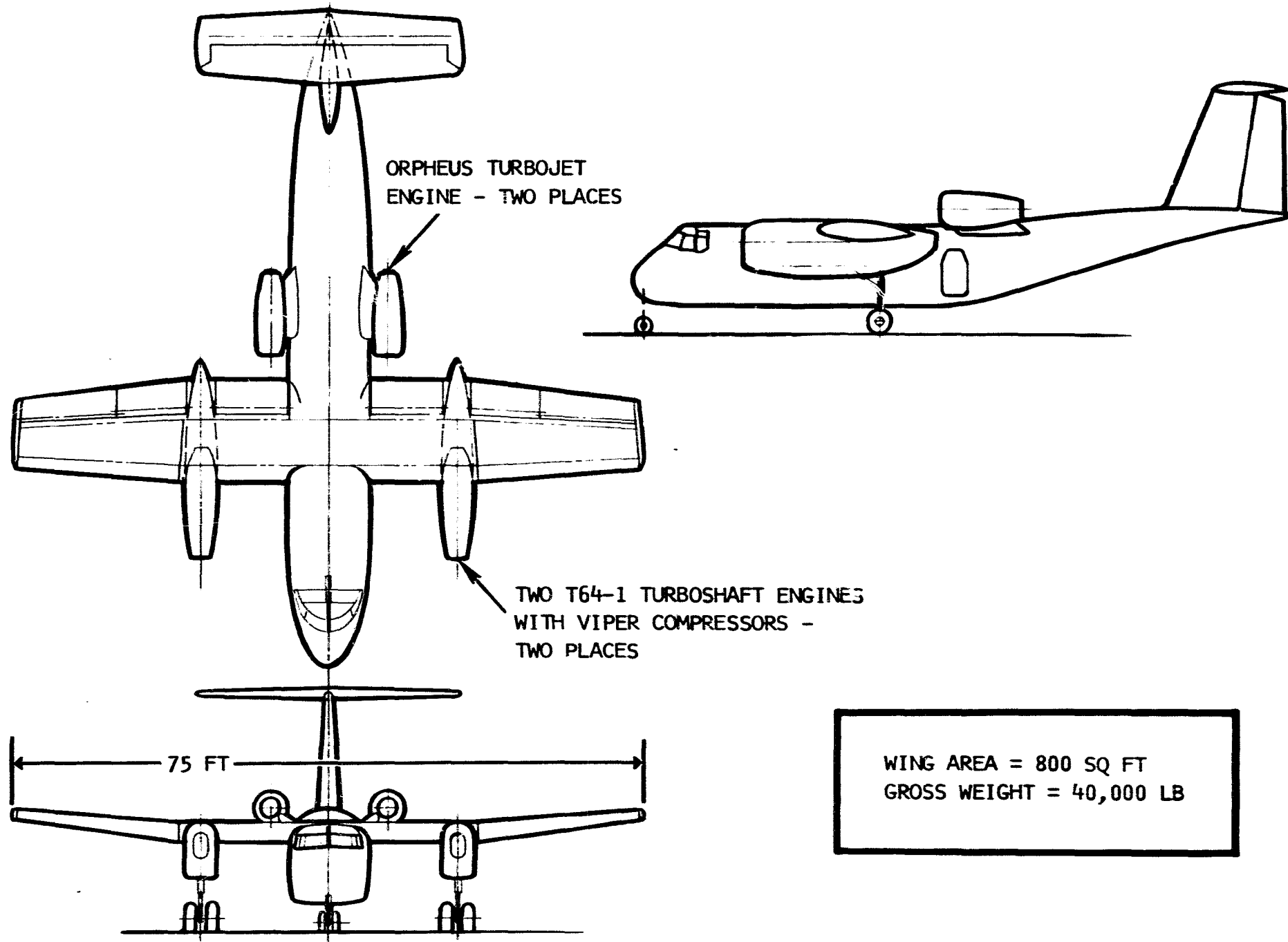


Figure 11. Configuration No. 9

thrust engines in line with the main gear and could improve the overall installation subject to center-of-gravity verification. As there are no vectored thrust nozzles available for the engines being considered for this program, a development and proof-testing program would be required for configurations No. 3 and 4. The other configurations were based on the use of the normal clamshell-type thrust reversers which were not available for all the engines considered, and therefore, some development and testing would be required.

### Configuration No. 1 (Figure 3)

A Spey 25 engine is pylon-mounted just inboard of the main landing gear support fitting and low enough to clear the flap travel envelope. The outboard pylon structure is attached to and supports the inboard portion of the main landing gear fitting. The outboard portion of this fitting is supported by a separate pylon structure which carries the moment reaction up to the front spar and provides the shear transfer into the lower wing skins between the spars.

The large pylon supporting the engine is a relatively fat pylon to cover the large diameter duct and diverter valve assembly required for routing the flap air into the wing between the spars. The location inboard of the landing gear decreases the structural modification complexity from that required if the large-diameter flap air duct was routed into the wing between the heavy machined ribs providing backup structure for the main landing gear. While several of the relatively light former ribs would require modification to support the engine loads, the major landing gear backup ribs would only be revised to provide routing provisions for the outboard flap air.

With the engines located further aft with respect to the wing than the turboshaft engines, gear boxes, and propellers on the existing Buffalo aircraft installation, the torsional loads on the wing center section are reduced.

Because this configuration is a two-engine installation, as is the existing Buffalo aircraft, the various cable, plumbing, and wiring systems should require relatively minor revisions.

This configuration will be used as a basepoint for evaluating the relative structural modification complexity of all configurations presented. It is assumed for this phase of the study that schedule and costs will vary essentially as the complexity of structural modifications required. The augmentor flap design and installation is assumed to be essentially the same for all configurations and is ignored in determining the relative modification complexities.

### Configuration No. 2 (Figure 4)

This configuration has two J52 turbojets for horizontal thrust and four T64 turboshaft engines driving air compressors for providing the flap air.

The J52 is mounted alongside the main gear for tailpipe clearance and forward of the main gear to prevent impingement on the main gear of the exhaust gases during thrust reverser use. A T64 air compressor unit is shown mounted on the outboard side of the J52 and forward to provide clearance for the J52 thrust reverser gases.

This installation provides a relatively balanced loading through the pylon and into the wing structure, and the pylon provides the necessary main gear trunnion fitting stabilizing structure.

The T64 air compressor unit supplies only one-fourth of the flap air, and the ducting through the pylon and into the wing box is considerably smaller than that required by configuration No. 1. Therefore, the arrangement would require less complex structural modifications in the highly loaded area of the wing.

The packaging of the J52 and a T64 air compressor in the same pylon results in considerably higher torsional loading on the center wing box than that resulting from configuration No. 1.

The third and fourth T64 air compressor units are pylon-mounted symmetrically above the fuselage on the wing carry-through structure. While this installation provides good carry-through structure down into the main fuselage structure supporting the wing, it does require that the flap air ducting be routed through the upper wing skin.

While the local wing structural modifications for the pylon installation at the main gear location is essentially the same as for configuration No. 1, the increased torsional loading increases the complexity. In addition, the use of the four turboshaft air compressor units adds four additional areas of structural and systems modifications.

It is estimated that this configuration would be several times as complex as configuration No. 1 and is rated as a less desirable arrangement.

### Configuration No. 3 (Figure 5)

This configuration is based on the maximum utilization of the existing nacelle structure and main landing gear supporting structure.

The T64 turboshaft engine is mounted in its existing location with the air compressor unit replacing the existing gear box and propeller. This requires modification for supporting the air compressor, for the air compressor inlet ducting, and for the addition of the flap air ducting into the wing.

The Orpheus turbojet is mounted in the wheel well area of the existing nacelle. This would require a redesign of the existing main gear drag brace to clear the engine installation. The present lower nacelle structure would be replaced in part with a new temperature resistant structure. This installation would require the development of a split exhaust and thrust reverser system. The Orpheus installation could be revised by moving the engine forward, adding a normal clamshell thrust reverser and then providing a split tail pipe to clear the main gear strut. This, however, would increase the torsional loading on the wing center section and is not believed warranted for consideration at this time.

The flap air ducting into the wing is the same as configuration No. 2 and less complex structurally than configuration No. 1.

The third and fourth T64 air compressor units are suspended under the outer wing panels. The outer wing panel would require structural revisions for this installation.

This configuration is also considered to be considerably more complex than configuration No. 1 but not significantly different from configuration No. 2.

#### Configuration No. 4 (Figure 6)

This configuration is identical to configuration No. 3 except that the outboard T64 air compressors have been moved to a position above the wing at the fuselage.

This not only eliminates the necessity for structural revisions to the outer wing panels but provides a major decrease in roll and yaw inertias.

This configuration is also much more complex than configuration No. 1, due primarily to the greater number of engines. It is, however, believed to be less complex than configurations No. 2 and 3 and is rated as a reasonable structural arrangement.

### Configuration No. 5 (Figure 7)

This configuration has the same powerplant and systems setup as configuration No. 1, but the engines are located further inboard and completely dissociated from the main gear area of the wing.

This installation also requires structural revisions to the wing center-section former ribs in the area of the pylon. It requires a smaller pylon than configuration No. 1 as there is no tie-in with the landing gear trunnion fitting.

For main gear trunnion support, two relatively thin pylons are added at each gear location to stabilize the trunnion fitting and transfer the gear loads into the wing structure. These pylons also pick up the existing drag brace forward attachments.

While this configuration is essentially the same as configuration No. 1 and is considered to be a good structural arrangement, it is slightly less complex. The engine pylon and the landing gear support modifications are separate areas, and the design coordination would, therefore, be somewhat less critical.

### Configuration No. 6 (Figure 8)

This configuration, as drawn, is not a realistic approach. After completion of the three-view drawing and the weight, balance, and roll inertia calculations, it was realized that there was no reason for mounting the T64 air compressor units above the wing at the main landing gear location. A more practical and less complex modification would result if these units were left in their existing locations on the present CV-7A as has been done in configurations No. 3 and 4.

The J52 would stay essentially as shown but would be side-mounted on the inboard side of the T64 air compressor nacelle instead of having its own pylon.

As this revision will have minor effects on the roll inertia calculations, the three-view drawing was not revised.

This overall configuration has no significant differences from configuration No. 2.

#### Configuration No. 7 (Figure 9)

This configuration is basically the same as configuration No. 5 with the addition of a JT12A turbojet installed in the aft end of the cargo bay for additional horizontal thrust. The RB163-25 Spey, Junior turbofan engine replaces the RB163-25 Spey used on configuration No. 5.

The general structural modification would be more complex than configuration No. 5 and, therefore, also more complex than configuration No. 1 due primarily to the addition of the third engine.

#### Configuration No. 8 (Figure 10)

This configuration uses four JT12A turbojets for horizontal thrust and four T64 air compressor units for flap air. The T64 air compressor units are located in the same manner as the previous configurations, and the JT12A turbojets are mounted in pairs directly in front of the main gear struts.

This configuration is much more complex than any of the previous configurations.

#### Configuration No. 9 (Figure 11)

In this configuration, two T64 air compressor units are mounted in each of the existing nacelles, and the two Orpheus turbojets are mounted on the aft fuselage.

This arrangement does not balance, using the basic ballasting ground rules that have been assumed for this phase of the study. Therefore, it has been dropped from the study.

From the standpoint of structural arrangements, the two-engine configurations No. 1 and 5 are shown to require the least design and manufacturing effort. For arrangements using separate power sources for horizontal thrust and flap air, configuration No. 4 is considered to require the least modification effort.

#### Weight and Balance Data

These weight and balance data are the results of the preliminary configuration analysis. The baseline aircraft was established by the correlation of



two reports: The "Weight Statement," D.H.C. 5.3.G.1, issue 18, and the "Moment of Inertia Report," D.H.C. 5.3.G.8.

The design assumptions for the weight estimates were as follows: 10 pounds/foot for wing modifications for augmentor wing; 1500 pounds/running foot, limit load for ballast on cargo floor; 320 pounds for wing and aileron structural removals. Engine cowl and pylons were scaled from similar installations. No accounting was made for engine controls and similar installations as it was assumed that the ballast installations allowed sufficient margins for the smaller detail items and unknowns. Other weights removed were taken from the weight statement. Fuel for all configurations was assumed to be in the fuselage-mounted ferry tanks. The takeoff gross weight was established as 40,000 pounds, and all configurations were ballasted to this weight. The wing fuel system components were not removed and will tend to make the moment of inertia estimates conservative.

A summary of the weight, balance, and inertia values for the configurations is shown in table V. A comparison of the configurations with respect to the amount of ballast required to meet the 40,000-pound takeoff weight and the minimum required for balance is shown in table VI. Table VII is a summary of the inertia characteristics calculated. The inertia values for the unmodified CV-7A aircraft are shown for comparison.

The derivation of the baseline aircraft data is shown in table VIII with the calculations for the various modification configurations shown in tables IX through XVII.

From the weight and balance standpoint, there are no significant differences between the configurations. However, from the inertia standpoint, configurations No. 1, 4, 5, and 7 are better than all others.

TABLE V. WEIGHT AND INERTIA SUMMARY

Configuration	Takeoff Weight	Center of Gravity			Ballast (lb)	Moment of Inertia Slug-Ft <sup>2</sup>			
		Fus Sta	WL	% MAC		I <sub>xx</sub> (Roll)	I <sub>yy</sub> (Pitch)	I <sub>zz</sub> (Yaw)	I <sub>yz</sub> (Product)
1	40,000	345.98	155.7	33.1	8,760	159,782	230,847	348,549	34,447
2	40,000	348.32	162.0	35.0	4,412	187,634	-	-	-
3	40,000	348.46	161.0	35.1	7,842	224,475	-	-	-
4	40,000	348.32	164.0	35.0	8,042	163,603	232,584	346,364	27,752
5	40,000	348.29	154.2	35.0	8,760	143,487	221,436	331,935	36,245
6	40,000	348.32	171.0	35.0	4,212	179,147	-	-	-
7	40,000	348.42	156.0	35.1	8,474	146,093	-	-	-
8	40,000	348.30	164.0	35.0	6,440	174,169	-	-	-
9	40,000	354.07	-	39.7	8,442	This vehicle will not balance.			

TAKEOFF GROSS WEIGHTS WITH MINIMUM BALLAST

1	33,940	345.99		33.1	2,700
2	36,588	348.32		35.0	1,000
3	33,658	348.46		35.1	1,500
4	34,458	348.32		35.0	2,500
5	35,240	348.29		35.0	4,000
6	38,788	348.32		35.0	3,000
7	35,026	348.42		35.1	3,500
8	36,560	348.30		35.0	3,000
9	40,000	354.07		39.7	8,442

TABLE VI. MINIMUM TAKEOFF WEIGHT

Configuration	CG % MAC	Min Gross Weight (lb)	Ballast Reqd for 40,000 Lb A/C	Min Ballast Reqd	Weight Diff
1	33.1	33,940	8,760	2,700	6,060
2	35.0	36,588	4,412	1,000	3,312
3	35.1	33,658	7,842	1,500	6,342
4	35.0	34,458	8,042	2,500	5,542
5	35.0	35,240	8,760	4,000	4,760
6	35.0	38,788	4,212	3,000	1,212
7	35.1	35,026	8,474	3,500	4,974
8	35.0	36,560	6,440	3,000	3,440

TABLE VII. MOMENT OF INERTIA

40,000 LB MAX GROSS WEIGHT

Config- uration	CG % MAC	$I_{xx}$ (Roll)	%	$I_{yy}$ (Pitch)	%	$I_{zz}$ (Yaw)	%	$I_{yz}$ (Product)	%
CV7A*	**	272,706	100	216,279	100	448,883	100	25,525	100
1	33.1	159,782	58.5	230,847	106.5	348,549	77.9	34,447	135
2	35.0	187,634	68.7						
3	35.1	224,475	82.4						
4	35.0	163,603	59.8	232,584	107.5	346,364	77.4	27,752	108.8
5	35.0	143,487	52.6	221,436	102.2	331,935	74	36,245	142
6	35.0	179,147	65.6						
7	35.1	146,093	53.6						
8	35.0	174,169	63.9						

\*Buffalo max gross wt = 38,000 lb  
moments of inertia in slug-ft<sup>2</sup>

\*\*CG for condition shown in report, D.H.C. 5.3.G.1  
issue 18, is 40% of MAC.

TABLE VIII. DERIVATION OF BASELINE VEHICLE

Item	Weight	Horizontal CG	
		Arm	Moment
Operational weight empty	23,696	344.39	8,160,665
Three-man crew (DHC 5.3.G.1, Issue 18)			
Less:			
Usable oil	- 90	245	- 22,050
Trapped oil	- 50	276	- 13,800
Trapped fuel	-1,000	355	- 35,500
Engines	-2,310	257.33	- 594,432
Engine mounts	- 129	235.22	- 30,343
Propellers	-1,529	197	- 301,213
Exhaust system	- 246	370.91	- 91,244
Starters	- 39	262	- 10,218
APU	- 105	264.75	- 27,799
Nacelles	-1,570	290.33	- 455,818
Wing tip and aileron (100 inches)	- 320	351.64	- 112,525
Baseline vehicle three-man crew	17,208	375.74	6,465,723

TABLE IX. WEIGHT SUMMARY - CONFIGURATION NO. 1

Item		Weight	Horizontal CG	
			Arm	Moment
Base vehicle		17,208	375.74	6,465,723
Plus:				
Engines (2) RB163-25 Spey		4,624	302	1,396,448
Nacelles		2,400	312	748,800
Engine fluids		100	302	30,200
Wing beef-up, ducts, flaps		668	384	256,512
Ballast - forward		5,790	212	1,227,480
Ballast - aft		2,970	510	1,514,700
Operational weight empty	32.1%	33,760	344.78	11,639,863
Plus: Forward fuselage fuel		+3,120	319.7	997,464
Plus: Aft fuselage fuel		+3,120	385.2	1,201,824
Takeoff gross weight	33.1%	40,000	345.98	13,839,151
Less: Forward fuselage fuel		-3,120	319.7	-997,464
Gross weight - Most aft CG	34.9%	36,880	348.20	12,841,687
Plus: Forward fuselage fuel		+3,120	319.7	997,464
Less: Aft fuselage fuel		-3,120	385.2	-1,201,824
Gross weight - Most fwd CG	30.4%	36,880	342.66	12,637,327

$$I_x (\text{Roll}) = 159,782 \text{ slug-ft}^2 \text{ at } 40,000 \text{ lb}$$

TABLE X. WEIGHT SUMMARY - CONFIGURATION NO. 2

Item	Weight	Horizontal CG		
		Arm	Moment	
Base vehicle	17,208	375.74	6,465,723	
Plus:				
Engines (2) P&W J52-P-8A	4,200	291	1,222,200	
Engines (2) GE T64-6A lower	1,786	270	482,220	
Engines (2) GE T64-6A upper	1,786	370	660,820	
Nacelles (2) lower engines (4)	3,000	290	870,000	
Nacelles (2) upper engines	400	370	148,000	
Fluids - engines	300	310	93,000	
Wing beef-up, ducting, flap	668	384	256,512	
Ballast - forward	2,400	212	508,800	
Ballast - aft	2,012	510	1,026,120	
Operational weight empty	34.4%	33,760	347.55	11,733,395
Plus: Forward fuselage fuel		3,120	319.7	997,464
Plus: Aft fuselage fuel		3,120	385.2	1,201,824
Takeoff gross weight	35.0%	40,000	348.32	13,932,683
Less: Forward fuselage fuel		-3,120	319.7	-997,464
Gross weight - most aft CG	37.0%	36,880	350.74	12,935,219
Plus: Forward fuselage fuel		+3,120	319.7	+997,464
Less: Aft fuselage fuel		-3,120	385.2	-1,201,824
Gross weight - most fwd CG	32.5%	36,880	345.20	12,730,859

$I_x$  (Roll) = 187,634 slug-ft<sup>2</sup> at 40,000 lb

TABLE XI. WEIGHT SUMMARY - CONFIGURATION NO. 3

Item		Weight	Horizontal CG	
			Arm	Moment
Base vehicle		17,208	375.74	6,465,723
Plus:				
Engines (2) Orpheus - inbd		1,800	310	558,000
Engines (2) GE T64-6A - inbd		1,786	260	464,360
Engines (2) GE T64-6A - outbd		1,786	334	596,524
Nacelles (2) inboard		1,570	310	486,700
Nacelles (2) outboard		800	344	275,200
Engine fluids		300	300	90,000
Wing beef-up, ducting, flaps		668	384	256,512
Ballast - forward		4,877	212	1,033,924
Ballast - aft		2,965	510	1,512,150
Operational weight empty	34.5%	33,760	347.72	11,739,093
Plus: Forward fuselage fuel		+3,120	319.7	997,464
Plus: Aft fuselage fuel		+3,120	385.2	1,201,824
Takeoff gross weight	35.1%	40,000	348.46	13,938,381
Less: Forward fuselage fuel		-3,120	319.7	-997,464
Gross weight - most aft CG	37.1%	36,880	350.89	12,940,917
Plus: Forward fuselage fuel		+3,120	319.7	+997,464
Less: Aft fuselage fuel		-3,120	385.2	-1,201,824
Gross weight - most forward CG	32.6%	36,880	345.35	12,736,557

$I_x$  (Roll) = 224,475 slug-ft<sup>2</sup> at 40,000 lb



TABLE XII. WEIGHT SUMMARY - CONFIGURATION NO. 4

Item		Weight	Horizontal CG	
			Arm	Moment
Base Vehicle		17,208	375.74	6,465,723
Plus:				
Engines (2) Orpheus - lower		1,800	310	558,000
Engines (2) GE T64-6A lower		1,786	260	464,360
Engines (2) GE T64-6A - upper		1,786	370	660,820
Nacelles (2) lower		1,570	310	486,700
Nacelles (2) upper		600	370	222,000
Engine fluids		300	310	93,000
Wing beef-up, ducting, flaps		668	384	256,512
Ballast - forward		5,285	212	1,120,420
Ballast - aft		2,757	510	1,406,070
Operational weight empty	34.4%	33,760	347.56	11,733,605
Plus: Forward fuselage fuel		+3,120	319.7	997,464
Plus: Aft fuselage fuel		+3,120	385.2	1,201,824
Takeoff gross weight	35.0%	40,000	348.32	13,932,893
Less: Forward fuselage fuel		-3,120	319.7	-997,464
Gross weight - most aft CG	37.0%	36,880	350.74	12,935,429
Plus: Forward fuselage fuel		+3,120	319.7	+997,464
Less: Aft fuselage fuel		-3,120	385.2	-1,201,824
Gross weight - most forward CG	32.5%	36,880	345.20	12,731,069

$I_x$  (Roll) = 163,603 slug-ft<sup>2</sup> at 40,000 lb

$I_y$  (Pitch) = 232,584 slug-ft<sup>2</sup> at 40,000 lb

$I_z$  (Yaw) = 346,364 slug-ft<sup>2</sup> at 40,000 lb

$I_{yz}$  = 27,752 slug-ft<sup>2</sup> at 40,000 lb

TABLE XIII. WEIGHT SUMMARY - CONFIGURATION NO. 5

Item		Weight	Horizontal CG	
			Arm	Moment
Base vehicle		17,208	375.74	6,465,723
Plus:				
Engines (2) RB163-25 Spey		4,624	343	1,586,032
Nacelles (2)		2,400	353	847,200
Engine Fluids		100	343	34,300
Wing beef-up, ducting, flaps		668	384	256,512
Ballast - forward		6,460	212	1,369,520
Ballast - aft		2,300	510	1,173,000
Operational weight empty	34.3%	33,760	347.52	11,732,287
Plus: Forward fuselage fuel		+3,120	319.7	997,464
Plus: Aft fuselage fuel		+3,120	385.2	1,201,824
Takeoff gross weight	35.0%	40,000	348.29	13,931,575
Less: Forward fuselage fuel		-3,120	319.7	-997,464
Gross weight - most aft CG	36.9%	36,880	350.71	12,934,111
Plus: Forward fuselage fuel		+3,120	319.7	+997,464
Less: Aft fuselage fuel		-3,120	385.2	-1,201,824
Gross weight - most forward CG	32.4%	36,880	345.17	12,729,751

$$I_x \text{ (Roll)} = 143,487 \text{ slug-ft}^2 \text{ at } 40,000 \text{ lb}$$

TABLE XIV. WEIGHT SUMMARY - CONFIGURATION NO. 6

Item		Weight	Horizontal CG	
			Arm	Moment
Base vehicle		17,208	375.74	6,465,723
Plus:				
Engines (2) P&W J52-P 8A - lower		4,200	302	1,268,400
Engines (4) GE T64-6A - upper		3,572	370	1,321,640
Nacelles (2) - lower		2,400	312	748,800
Nacelles (4) - upper		1,200	370	444,000
Engine fluids		300	336	100,800
Wing beef-up, ducting, flaps		668	384	256,512
Ballast - forward		3,425	21.2	726,100
Ballast - aft		787	510	401,370
Operational weight empty	34.4%	33,760	347.55	11,733,345
Plus: Forward fuselage fuel		+3,120	319.7	997,464
Plus: Aft fuselage fuel		+3,120	385.2	1,201,824
Takeoff gross weight	35.0%	40,000	348.32	13,932,633
Less: Forward fuselage fuel		-3,120	319.7	-997,464
Gross weight - most aft CG	37.0%	36,880	350.74	12,935,169
Plus: Forward fuselage fuel		+3,120	319.7	+997,464
Less: Aft fuselage fuel		-3,120	385.2	-1,201,824
Gross weight - most forward CG	34.4%	36,880	345.20	12,730,809

$$I_x(\text{Roll}) = 179,147 \text{ slug-ft}^2 \text{ at } 40,000 \text{ lb}$$

TABLE XV. WEIGHT SUMMARY - CONFIGURATION NO. 7

Item	Weight	Horizontal CG		
		Arm	Moment	
Base vehicle	17,208	375.74	6,465,723	
Plus:				
Engines (2) RB183-1 Spey Jr	4,046	300	1,213,800	
Engine (1) JT-12A P&W	468	584	273,312	
Nacelles (2)	2,400	310	744,000	
Air inlet - aft engine	98	524	51,352	
Engine mount and shroud - aft	100	574	57,400	
Tail pipe	109	654	71,286	
Heat shield - aft	50	654	32,700	
Replace aft cargo door	-	-	-575	
Engine fluids	150	395	45,425	
Wing beef-up, ducting, flaps	668	384	256,512	
Ballast - forward	6,000	212	1,272,000	
Ballast aft	2,474	510	1,261,740	
Less: Cargo door mechanism	-11	651	-7,161	
Operational weight empty	34.5%	33,760	347.68	11,737,514
Plus: Forward fuselage fuel	+3,120	319.7	997,464	
Plus: Aft fuselage fuel	+3,120	385.2	1,201,824	
Takeoff gross weight	35.1%	40,000	348.42	13,936,802
Less: Forward fuselage fuel	-3,120	319.7	-997,464	
Gross weight - most aft CG	37.0%	36,880	350.85	12,939,338
Plus: Forward fuselage fuel	+3,120	319.7	+997,464	
Less: Aft fuselage fuel	-3,120	385.2	-1,201,824	
Gross weight most forward CG	32.6%	36,880	345.31	12,734,978

$$I_x(\text{Roll}) = 146,093 \text{ slug-ft}^2 \text{ at } 40,000 \text{ lb}$$

TABLE XVI. WEIGHT SUMMARY - CONFIGURATION NO. 8

Item	Weight	Horizontal CG		
		Arm	Moment	
Base vehicle	17,208	375.74	6,465,723	
Plus:				
Engines (4) P&W JT-12A	1,872	312	584,064	
Engines (2) GE T64-6A - lower	1,786	296	528,656	
Engines (2) GE T64-6A - upper	1,786	370	660,820	
Nacelles (2) lower	3,000	334	1,002,000	
Nacelles (2) upper	600	370	222,000	
Engine fluids	400	323	129,200	
Wing, beef-up, ducting, flaps	668	384	256,512	
Ballast - forward	4,700	212	996,400	
Ballast - aft	1,740	510	887,400	
Operational weight empty	34.4%	33,760	347.53	11,732,775
Plus: Forward fuselage fuel		3,120	319.7	997,464
Plus: Aft fuselage fuel		3,120	385.2	1,201,824
Takeoff gross weight	35.0%	40,000	348.30	13,932,063
Less: Forward fuselage fuel		-3,120	319.7	-997,464
Gross weight most aft CG	36.9%	36,880	350.72	12,934,599
Plus: Forward fuselage fuel		+3,120	319.7	+997,464
Less: Aft fuselage fuel		-3,120	385.2	-1,201,824
Gross weight most forward CG	32.5%	36,880	345.18	12,730,239

$$I_x \text{ (Roll)} = 174,169 \text{ slug-ft}^2 \text{ at } 40,000 \text{ lb}$$

TABLE XVII. WEIGHT SUMMARY - CONFIGURATION NO. 9

Item	Weight	Horizontal CG		
		Arm	Moment	
Base vehicle	17,208	375.74	6,465,723	
Plus:				
Engines (2) Orpheus - upper	1,800	550	990,000	
Engines (2) GE T64-6A - lower	1,786	308	550,088	
Engines (2) GE T64-6A - lower	1,786	252	450,072	
Nacelles (2) upper	1,570	536	841,520	
Nacelles (2) lower	2,000	322	644,000	
Engine fluids	300	370	111,000	
Wing beef-up, ducting, flaps	668	384	256,512	
Ballast - forward	8,442	196	1,654,632	
Operational weight empty	39.9%	33,760	354.37	11,963,547
Plus: Forward fuselage fuel		3,120	319.7	997,464
Plus: Aft fuselage fuel		3,120	385.2	1,201,824
Takeoff gross weight	39.7%	40,000	354.07	14,162,835
Less: Forward fuselage fuel		-3,120	319.7	-997,464
Gross weight - most aft CG	42.0%	36,880	356.98	13,165,371
Plus: Forward fuselage fuel		+3,120	319.7	+997,464
Less: Aft fuselage fuel		-3,120	385.2	-1,201,824
Gross weight - most forward CG	37.5%	36,880	351.44	12,961,011

° Most aft CG 0.5% aft of aft limit

° Does not balance under ground rules established (ballast on cargo floor only)

° No inertia estimates made

## SECTION IV

### AERODYNAMIC PERFORMANCE COMPARISONS

#### Ground Rules for Takeoff and Landing Computations

The takeoff and landing distances are computed using ground rules with simplifying assumptions appropriate for the selection of one of various engine layouts. The ground rules used are as follows:

The takeoff ground run is made using a friction coefficient  $\mu = 0.10$  and a takeoff flap setting. The total takeoff distance is computed using sea-level standard conditions and an obstacle height of 50 feet. All engines are operating with takeoff power; however, the speeds used during the takeoff are based on critical-engine-out safety margins. The maximum normal acceleration used after lift-off is limited to 90 percent of  $C_{L_{max}}$ .

The lift-off speed is the lowest speed that can satisfy all of the following safety criteria.

$$V \geq 1.2 V_{s_{\text{oeo}}}$$

$$n_{\text{max}} \geq 1.2 \text{ when all engines are operating at maximum takeoff power}$$

$$n_{\text{max}} \geq 1.1 \text{ with the critical engine inoperative and the remaining engines at a 10-percent emergency overrating}$$

The subscript oeo pertains to the one-engine-out condition with the critical engine inoperative.  $V_s$  designates the stall speed. The symbol  $n_{\text{max}}$  denotes the maximum normal acceleration reached at  $C_{L_{\text{max}}}$ .

During the climb to the 50-foot obstacle, the velocity is assumed to be constant as an approximation. No ground effect is included in the computations.

Upon engine failure, the available power and the flap settings must provide a positive rate of climb. Ten-percent emergency overrating of the remaining engines is used in conjunction with the engine failure.

The landing distance is computed using a constant rate of sink of 13 feet/second and a constant forward speed between the 50-foot obstacle and the ground. Again, sea-level standard conditions are used.

The approach speed is the lowest speed that can satisfy all of the following safety criteria:

- $n_{\max} \geq 1.2$  when all engines are operating at maximum takeoff power
- $n_{\max} \geq 1.1$  with the critical engine inoperative and the remaining engines at a 10-percent emergency overrating
- $C_L \geq 0.90 C_{L_{\max}}$  with all engines operating in the approach power setting

Upon touch down, a time delay of 2 seconds is used before activation of brakes and thrust reversers. For computational purposes, no speed change is assumed during the 2 seconds, and after elapse of this time, the effectiveness of the brakes and thrust reversers is assumed to be instantaneous. An average friction coefficient of  $\mu = 0.30$  is used during braking, assuming no aerodynamic lift exists. A decelerating force due to reversing the horizontal thrust engine exhaust is equal to 50 percent of the takeoff thrust.

The computations are made independent of the minimum control speed,  $V_{mc}$ , so that the effects of this speed can be assessed separately.  $V_{mc}$  is based on one engine being inoperative and the remaining engines producing takeoff power. For safe operation, the lift-off speed and the final approach speed during takeoff and landing must be at least 110 percent of the minimum control speed.

#### STOL Performance

Short takeoff and landing distances have been computed on the basis of the aforementioned ground rules, and the results are presented in table XVIII. The methods for the determination of the distances and a description of the aerodynamic data used are presented in a subsequent portion of this section.

All distances are determined for the sea-level standard condition, a uniform nominal weight of 40,000 pounds, and a uniform wing reference area of 800 square feet. Also, a single flap angle of 50 degrees is used for all takeoffs and landings. No optimization with regard to the flap angle is attempted. Lift loss due to trimming is neglected.



TABLE XVIII. STOL PERFORMANCE COMPARISON

Configuration	1	2	3	4	5	6	7	8	9
W (lb)	40,000	40,000	40,000	40,000	40,000	40,000	40,000	40,000	40,000
S (sq ft)	800	800	800	800	800	800	800	800	800
W/S (lb/sq ft)	50	50	50	50	50	50	50	50	50
Horizontal thrust (lb)	2 x 7,955	2 x 7,500 +4 x 150	2 x 7,120 +4 x 150	2 x 6,900 +4 x 150	2 x 7,955	2 x 7,500 +4 x 150	2 x 5,200 +5,000	4 x 3,000 +4 x 150	2 x 5,000 +4 x 150
Flap air thrust (lb)	2 x 3,555	4 x 2,340	4 x 2,340	4 x 2,340	2 x 7,075	4 x 2,340	2 x 3,800	4 x 2,340	4 x 2,340
(T/W) total	0.187	0.160	0.160	0.160	0.177	0.160	0.133	0.133	0.150
Takeoff regardless of $V_{MC}$ :									
$\delta_f$	30°	30°	30°	30°	30°	30°	30°	30°	30°
$C_{LMAX}$ OED	4.5	7.0	7.0	7.0	4.5	7.0	4.5	7.0	7.0
$V_{SOEO}$ (KEAS)	58.5	46.0	46.0	46.0	58.5	46.0	57.2	46.0	46.0
$V_{LO}$ (KEAS)	70.0	55.0	55.0	55.0	70.0	55.0	49.7	55.0	55.0
$n_{max}$ , normal	1.61	1.33	1.33	1.33	1.61	1.33	1.61	1.33	1.33
Ground distance (ft)	550	510	455	455	550	510	625	570	455
Air distance (ft)	370	420	445	445	370	420	355	455	495
Total distance (ft)	920	770	900	900	920	730	980	825	950
$\gamma_{OED}$	+9.2°	+8.9°	+8.4°	+8.4°	+9.2°	+8.9°	+8.7°	+11.5°	+5.4°
Landing regardless of $V_{MC}$ :									
$\delta_f$	30°	30°	30°	30°	30°	30°	30°	30°	30°
$C_{LMAX}$ OED	4.5	7.0	7.0	7.0	4.5	7.0	4.5	7.0	7.0
$V_{SOEO}$ (KEAS)	58.5	46.0	46.0	46.0	58.5	46.0	57.2	46.0	46.0
$V_a$ (KEAS)	65.0	51.0	51.0	51.0	65.0	51.0	63.5	51.0	51.0
$n_{max}$ , normal	1.46	1.20	1.20	1.20	1.46	1.20	1.46	1.20	1.20
Air distance (ft)	425	337	335	335	425	337	408	328	333
2-second delay (ft)	220	170	170	170	220	170	210	170	170
Ground distance (ft)	377	235	270	270	377	235	405	255	276
Total distance (ft)	1,020	740	775	775	1,020	740	1,025	755	755
$\gamma_a$	-6.8°	-8.6°	-8.6°	-8.6°	-6.8°	-8.6°	-7.0°	-8.7°	-8.6°
OED bank angle at $V_{MC}$	5.5°	5.5°	4.2°	4.2°	4.7°	5.2°	3.0°	2.7°	2.8°
$V_{MC}$ (KEAS) actual, disregard $V_S$	51.0	49.5	44.2	44.2	46.7	48.6	58.0	35.4	31.0
V(KEAS) Min reqd for takeoff	65.8	50.0	50.0	50.0	65.8	50.0	62.5	50.0	50.0
V(KEAS) Min reqd for landing	59.0	46.5	46.5	46.5	59.0	46.5	57.8	46.5	46.5
$\theta^{**}$ at $V_a$ (rad/SEC <sup>2</sup> )	0.55	0.29	0.24	0.24	0.54	0.60	0.32	0.32	—

The landing approach is made with partial horizontal thrust reversal for flight path control. The approach is also made with a partial power setting for the flap airflow.

This partial flap air power setting is such that the total flow used for the wing lift augmentation from all normally operating engines is equal to the flow available in the one-engine-out condition. This is the least amount of airflow needed for the one-engine-out condition and provides the necessary lift equilibrium at the normal approach speed.

An increase of the flap airflow to the level obtained from takeoff power settings may not be used to lower the stall speed but gives an increased normal acceleration capability. However, a smaller angle of attack is needed as well as a greater horizontal thrust reversal during the approach. Because the stall speeds involved are unchanged, no significant decrease in landing distance is realized with the higher power setting, and thus the landing distances quoted are applicable for either power setting.

The results in table XVIII show that all takeoff distances are less than 1,000 feet. Also, all configurations show a positive climb angle,  $\gamma_{oeo}$ , after failure of a critical engine. In all cases, the critical engine is one providing horizontal thrust.

The takeoff distances are also presented graphically in figure 12 as a function of horizontal and flap thrust. As expected, an increase of horizontal thrust results in a shorter takeoff distance, and also, an increase in the flap thrust results in a shorter takeoff distance. The latter is related to a decrease in required speeds because of an effect on  $C_{L_{max}}$ .

Because of this dependency of  $C_{L_{max}}$  on the flap thrust,  $T_c$ , and because the takeoff distance is a function of  $1/C_{L_{max}}$  and  $1/(T_c/W)$ , the results are also expressed parametrically versus  $1/\left(\frac{T_c}{W} \frac{T_H}{W}\right)$  in figure 13. The small scatter in that figure includes the effect of two versus four engines that provide the flap airflow.

Table XVIII shows that the landing distances generally are also less than 1,000 feet. Only in the cases where the flap thrust is less than 8,000 pounds, does the landing distance exceed the 1,000-foot goal.

Landing distances are plotted in figure 14 where the level of the flap thrust is shown to be significant. The reason for this lies again in the fact that the airflow effects the  $C_{L_{max}}$  strongly. The horizontal thrust does

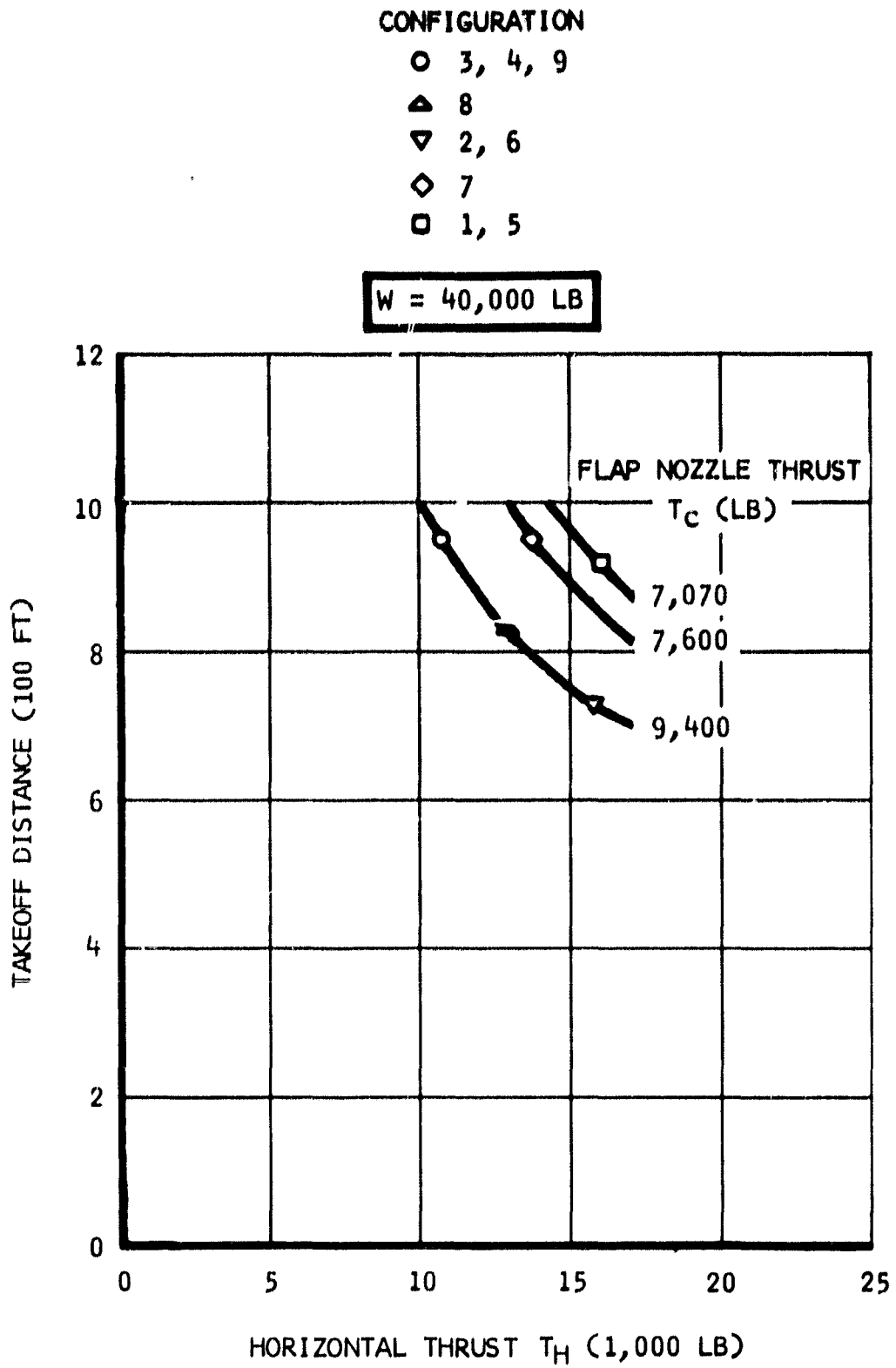


Figure 12. Takeoff Distance Over 50-Foot Obstacle  
at Sea Level Standard Condition

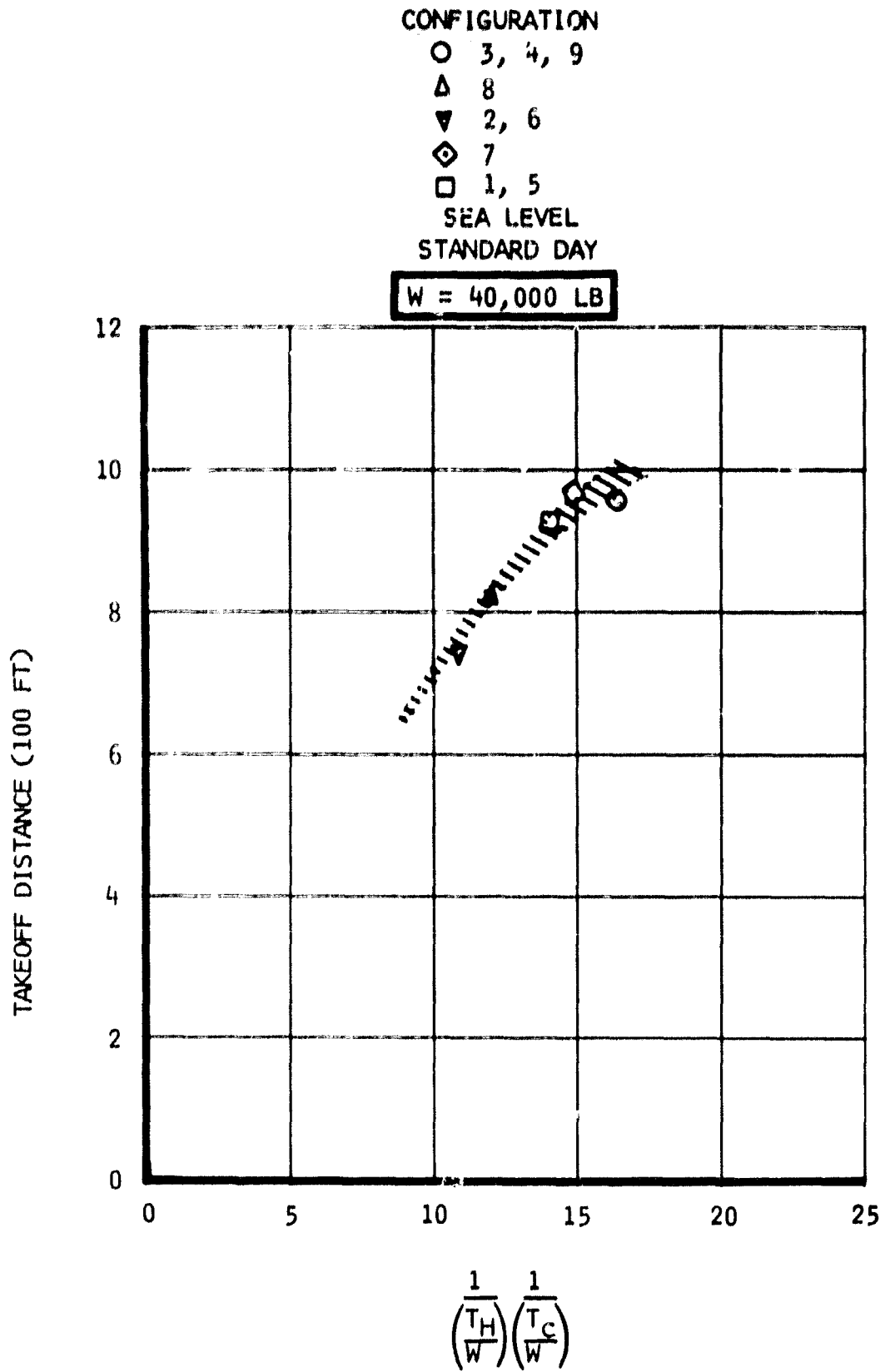


Figure 13. Takeoff Distance Versus Thrust Parameters

CONFIGURATION

- 3,4,9
- △ 8
- ▽ 2,6
- ◇ 7
- 1,5

W = 40,000 LB

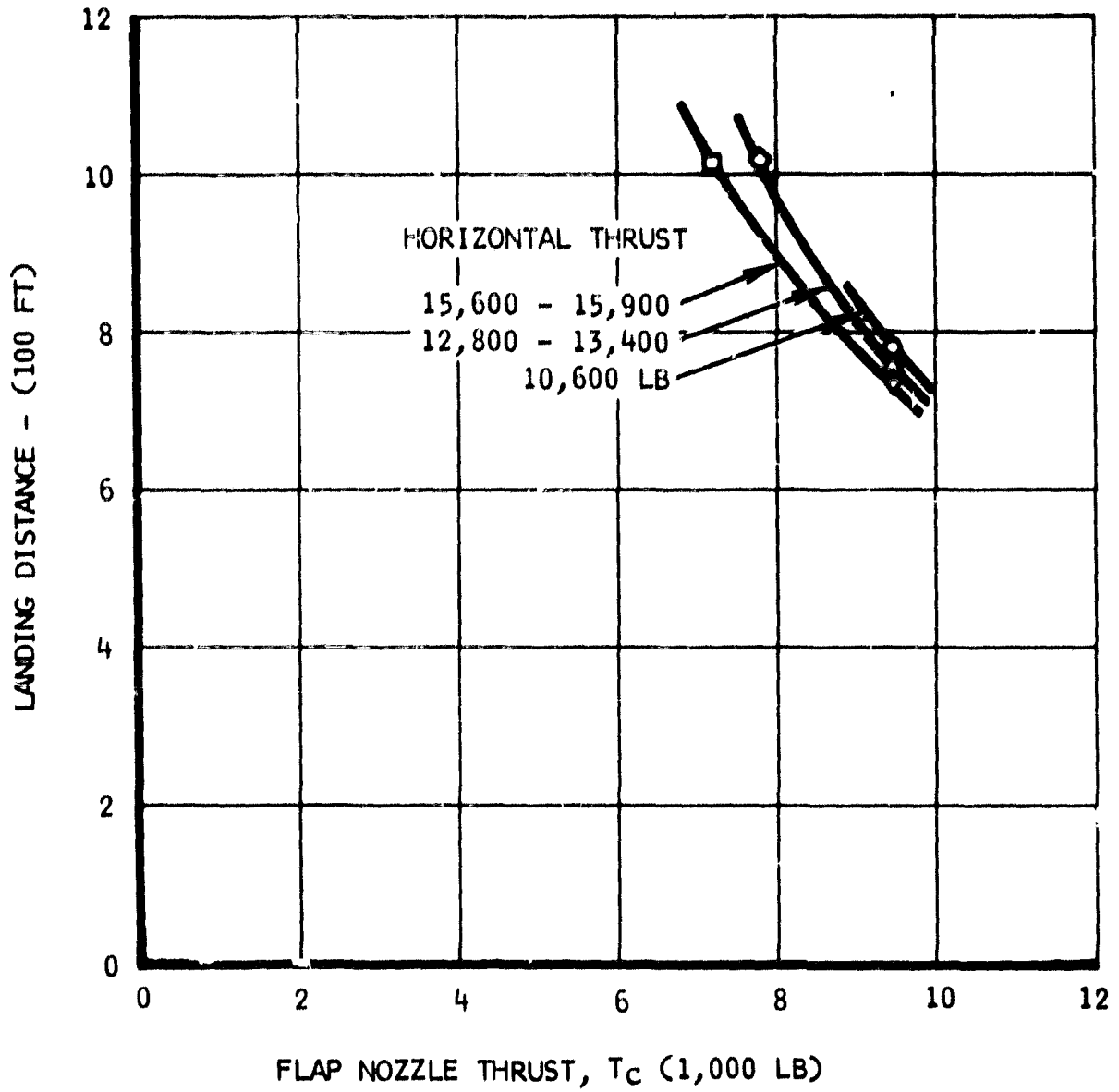


Figure 14. Landing Distance Over 50-Foot Obstacle at Sea Level Standard Condition

not enter into the approach speed, and its effect is limited to the braking distance on account of the thrust reversing. The overall effect of the horizontal thrust is minor in comparison to the flap thrust.

The approach speed,  $V_a$ , is lower than the lift-off speed,  $V_{lo}$ , in all cases investigated. It is not necessary to have the approach speed equal to the lift-off speed; however, if it is desired to have these speeds equal by increasing the approach speed, then the landing distance is approximately 13 percent greater for each 10-percent speed increase.

The approach angle,  $\gamma_a$ , varies between 6.8 and 8.7 degrees for all cases investigated.

#### Method of Analysis of Takeoff and Landing Distances

The takeoff distances over the 50-foot obstacle are determined from figure 15. In this figure, the ground roll distance is

$$X_{GR} = \frac{\left(\frac{1}{\rho_o q}\right)}{C_{L_{max}}} \cdot \frac{\left(\frac{W}{S}\right) \left(\frac{V_{lo}}{V_s}\right)^2}{\frac{T_{H1}}{W} (1 + \psi_1)} \cdot \frac{1}{\rho/\rho_o} \quad (1)$$

Herein,  $(T_{H1}/W) (1 + \psi_1)$  is the average forward force during the ground run, nondimensionalized by the Aircraft weight.  $T_{H1}$  is the static horizontal thrust of the vehicle. Often,  $(1 + \psi_1)$  does not differ much from unity.

The equation for the ground roll distance is used as the abscissa in the figure. The parameter

$$(1 + \psi_2) \frac{\sqrt{\frac{T_{H1}}{W} (1 + \psi_1)}}{\sqrt{n_o - 1}} \quad (2)$$

in the figure determined the climb distance. Herein,  $n_o$  is the maximum normal acceleration allowed during the climb and is  $(0.90) n_{max}$ . The factor  $(1 + \psi_2)$  also does not differ much from unity and is separately shown in figure 16. Therein,  $\gamma_v$  is the steady-state climb angle at the climb speed.

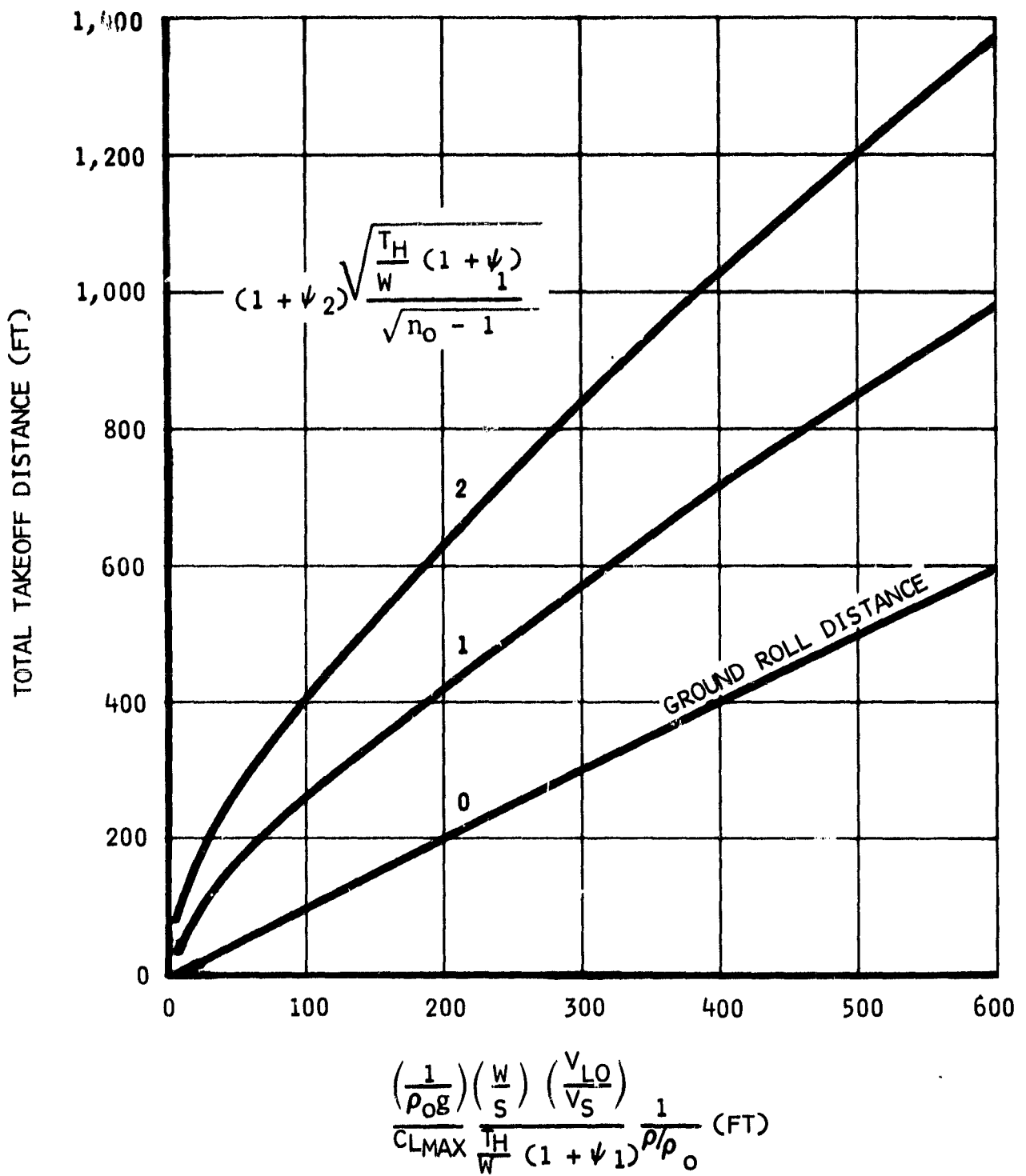


Figure 15. Determination of Takeoff Distance Over 50-Foot Obstacle

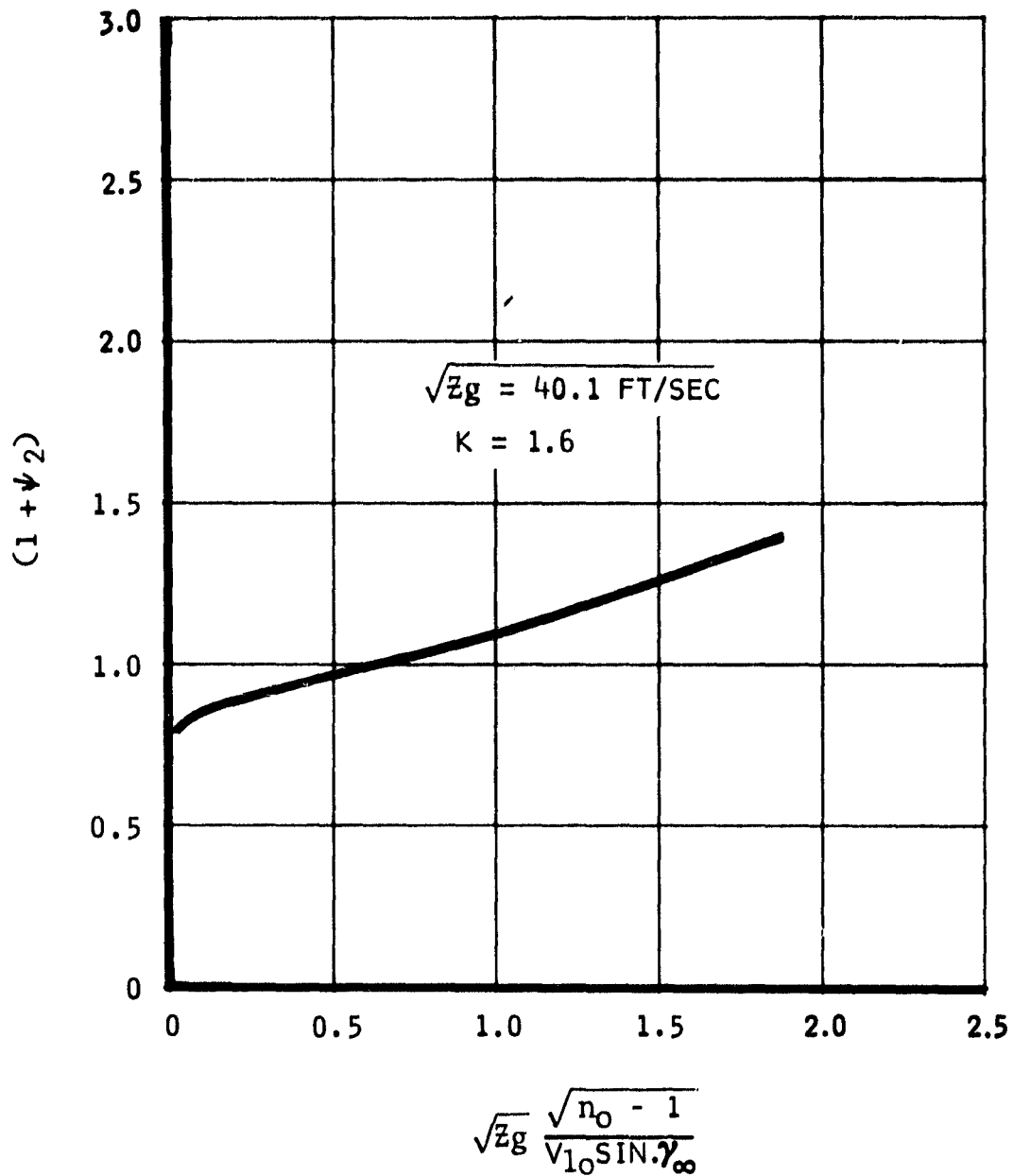


Figure 16. Correction Factor  $(1 + \psi_2)$  for Takeoff Air Distance Computations



or, using the static flap thrust,  $T_c$ , as a parameter:

$$\left(\frac{F_x}{W}\right)_{ave} = \frac{T_{H_{ave}}}{W} - \mu + \frac{T_c}{W} \left( -\frac{D_{ave}}{T_c} + \mu \frac{L_{ave}}{T_c} \right) \quad (7)$$

Herein, the average horizontal thrust is the static thrust,  $T_H$ , minus the average intake momentum drag of the engines.

The average drag and lift,  $D_{av}$  and  $L_{av}$ , are the averages between the static condition and the lift-off speed. They include the power effects from the flap airflow. For example,  $D_{av}$  is negative when the forward thrust component of  $T_c$  for the augmentor wing is greater than the power-off drag of the airplane.

Because the static horizontal thrust generally contributes the most in the preceding equation, the other terms are treated as a correction factor  $(1 + \psi_1)$  to this thrust:

$$\left(\frac{F_x}{W}\right)_{ave} = \frac{T_H}{W} (1 + \psi_1) \quad (8)$$

in which

$$(1 + \psi_1) = \frac{T_{H_{ave}}}{T_H} + \frac{\frac{T_c}{W} \left( -\frac{D_{ave}}{T_c} + \mu \frac{L_{ave}}{T_c} \right) - \mu}{\frac{T_H}{W}} \quad (9)$$

The value of  $At = t/\tau$  can now be solved for a given obstacle height:

$$e^{-t/\tau} - \frac{t}{\tau} - 1 = \frac{Z}{\left(\frac{-B}{A^2}\right)} \quad (21)$$

The solution is

$$\frac{t}{\tau} = (1 + \psi_2) K \sqrt{\frac{Z}{\left(\frac{-B}{A^2}\right)}} \quad (22)$$

in which  $K$  is an arbitrary constant and in which  $\psi_2$  is a function of  $\sqrt{Z / \left(\frac{-B}{A^2}\right)}$ . The value of  $\psi_2$  is generally near zero for a proper choice of the value of  $K$ . Choosing  $K = 1.6$  and substituting the other constants yields

$$\frac{t}{\tau} = (1 + \psi_2) (1.6) \frac{\sqrt{Z_g (n_o - 1)}}{V \sin \gamma_\infty} \quad (23)$$

$(1 + \psi_2)$  is given in figure 16. The steady-state climb angle is  $\gamma_\infty$  and is determined from

$$\tan \gamma_\infty \approx \frac{-D}{L} + \frac{T_H}{W} \quad (24)$$

where  $D$  and  $L$  are the drag and lift including the flap thrust effects.

The climb distance becomes

$$X_{\text{air}} = V \left(\frac{t}{\tau}\right) \tau = \left(\frac{t}{\tau}\right) \frac{V}{A} \quad (25)$$

Pertinent values for the various configurations depend on the aerodynamics as affected by the propulsion characteristics and are derived later. The following is limited to the derivation of equations.

The ground distance is found from

$$X_{GR} = \frac{V_{10}^2}{2a} \quad (3)$$

in which

$$a = g \left( \frac{F_X}{W} \right)_{ave} \quad (4)$$

so that

$$X_{GR} = \frac{\left( \frac{W}{S} \right)}{C_L \left( \frac{F_X}{W} \right)_{ave} \rho g} = \frac{\left( \frac{1}{\rho_0 g} \right) \left( \frac{W}{S} \right)}{C_L \left( \frac{F_X}{W} \right)_{ave} \left( \frac{\rho}{\rho_0} \right)} = \quad (5)$$

$$\frac{\left( \frac{1}{\rho_0 g} \right) \left( \frac{W}{S} \right) \left( \frac{V_{10}}{V_s} \right)^2}{C_{L_{max}} \left( \frac{F_X}{W} \right)_{ave} \left( \frac{\rho}{\rho_0} \right)}$$

The average accelerating force,  $F_{X_{av}}$ , is determined from

$$F_{X_{ave}} = T_{H_{ave}} - D_{ave} - \mu (W - L_{ave}) \quad (6)$$

The climb trajectory after lift-off is determined from equations governing a lift and a drag equilibrium. The lift equilibrium is given by

$$\ddot{z} \frac{W}{g} = L_{\alpha=0} + \frac{dL}{d\alpha} \alpha - W \quad (10)$$

Using the Symbol  $\gamma$  to denote the flight path angle, the drag equilibrium is given by

$$\ddot{x} \frac{W}{g} = F_{x \alpha=0} + \frac{dF_x}{d\alpha} \alpha - W \sin \gamma \quad (11)$$

It is now assumed that the climb will be made at a constant speed, so that  $\dot{x} = 0$ . Also, it is assumed that  $dF_x/d\alpha = \text{constant}$ . Its value is always negative. The angle of attack can then be found and is

$$\alpha = \frac{W \sin \gamma - F_{x \alpha=0}}{\frac{dF_x}{d\alpha}} \quad (12)$$

It is seen that the angle of attack must become smaller when  $\gamma$  increases to satisfy the constant-speed condition.

In the preceding equation,  $\sin \gamma$  is now substituted by  $Z/V$ . Subsequently, the angle of attack is substituted into the lift equation which then obtains the following general form, with A and B being constants:

$$\ddot{z} + A\dot{z} + B = 0 \quad (13)$$

Solutions of this equation are

$$z = \frac{-B}{\Lambda^2} \left[ e^{-At} - At - 1 \right] \quad (14)$$

$$\dot{z} = \frac{B}{\Lambda} \left[ e^{-At} - 1 \right] \quad (15)$$

$$\ddot{z} = -B \left[ e^{-At} \right] \quad (16)$$

A time constant is associated and is  $\tau = 1/A$ . The constants can be found from conditions at  $t = 0$  and  $t = \infty$ :

$$t = 0 \rightarrow \ddot{z}_0 = -B = (n_0 - 1)g \quad (17)$$

$$t = \infty \rightarrow \dot{z}_\infty = -\frac{B}{A} = V \sin \gamma_\infty \quad (18)$$

so that

$$A = \frac{(n_0 - 1)g}{V \sin \gamma_\infty} \quad (19)$$

$$\frac{-B}{A^2} = \frac{V^2 \sin^2 \gamma_\infty}{(n_0 - 1)g} \quad (20)$$

$$x_{\text{air}} = (1 + \psi_2) (1.6) \frac{\sqrt{z_g (n_o - 1)}}{V \sin \gamma_\infty} \left[ \frac{v^2 \sin \gamma_\infty}{(n_o - 1) g} \right] \quad (26)$$

$$x_{\text{air}} = (1 + \psi_2) \frac{(1.6) \sqrt{z}}{\sqrt{(n_o - 1) g}} (v) \quad (27)$$

Substituting

$$v = \left[ \frac{\frac{W}{S} \left( \frac{v_{10}}{v_s} \right)^2}{\frac{1}{2} \frac{\rho}{\rho_o} (\rho_o) c_{L, \max}} \right]^{\frac{1}{2}} \quad (28)$$

yields

$$x_{\text{air}} = (1 + \psi_2) (1.6 \sqrt{z}) \left[ \frac{\frac{2W}{S} \left( \frac{v_{10}}{v_s} \right)^2}{\frac{\rho}{\rho_o} c_{L, \max} \rho_o g} \right]^{\frac{1}{2}} \left( \frac{1}{\sqrt{n_o - 1}} \right) \quad (29)$$

or

$$x_{\text{air}} = (1 + \psi_2) (1.6 \sqrt{z}) \frac{\sqrt{\frac{T_{11}}{W} (1 + \psi_1)}}{\sqrt{n_o - 1}} \quad (30)$$

$$\left[ \frac{\left( \frac{1}{\rho_o g} \right) \left( \frac{W}{S} \right) \left( \frac{v_{10}}{v_s} \right)^2}{c_{L, \max} \frac{T_{11}}{W} (1 + \psi_1)} \left( \frac{1}{\rho_o} \right) \right]^{\frac{1}{2}}$$

Using this relation, the total takeoff distance  $X = X_{gr} + X_{air}$  is shown graphically in figure 15.

The landing distance consists of an air distance, a ground roll distance without braking, and a braking distance. The air distance is computed from

$$X_{air} = \frac{z}{-\frac{dz}{dt}} V_a \quad (31)$$

Herein,  $V_a$  is the approach speed, and  $dz/dt$  is the tolerated sink speed. No ground effect is taken into account.

The rolling distance without braking is computed allowing a time delay,  $\Delta t$ , before the brakes are applied:

$$X_{roll} = \Delta t \left( V_a \right) \quad (32)$$

Rolling friction and airplane drag are neglected, resulting in a constant speed during the delay.

The braking distance is determined from

$$X_{BR} = \frac{V_a^2}{2a} \quad (33)$$

in which

$$2a = \frac{2F_x}{\frac{W}{g}} = 2g \left[ \frac{D_{ave}}{W} + \frac{\mu W}{W} + \frac{T_R}{T_H} \left( \frac{T_H}{W} \right) \right] \quad (34)$$

Ignoring the relatively small value of the aerodynamic drag,  $D_{av}$ , this yields

$$X_{br} = \frac{V_a^2}{2g \left[ \mu + \frac{T_R}{T_H} \left( \frac{T_H}{W} \right) \right]} \quad (35)$$

Herein,  $T_R/T_H$  is the ratio of thrust reversal of the hot-gas thrust  $T_H$ .

### STOL Speeds and Maneuver Margins

Certain relations exist between the speed margins and maneuver margins depending on the maximum lift characteristics of the airplane. In the present analysis, the lift values are taken directly from the NASA-Ames 40 x 80 wind tunnel test 294. No correction of the wind tunnel data to a different wing planform, chord ratio, or basic airplane drag was attempted. Also, the improvement of the augmentor efficiency developed after this test is not incorporated. The use of the wind tunnel data directly is considered adequate for selecting one engine layout above others.

Test data for a selected flap angle of 50 degrees are presented in figure 17. In this figure, a speed parameter is used,  $2/(T_c/S)$ , which is the reciprocal value of the thrust coefficient  $C_J$  quoted in the wind tunnel test. The ratio  $(L/T_c)_{max}$  is found from the wind tunnel data using

$$\left( \frac{L}{T_c} \right)_{max} = \frac{C_{L_{max}} q S}{T_c} = \frac{C_{L_{max}}}{C_J} \quad (36)$$

$C_J$  includes the blowing over the ailerons.

In the figure, the curve for  $(L/T_c)_{max}$  not only represents the maximum lift obtainable at given values of the speed parameter but also represents the minimum speed conditions for given weight or lift and given thrust  $T_c$ . The curve is valid for all thrust and speed combinations considered for the vehicle.



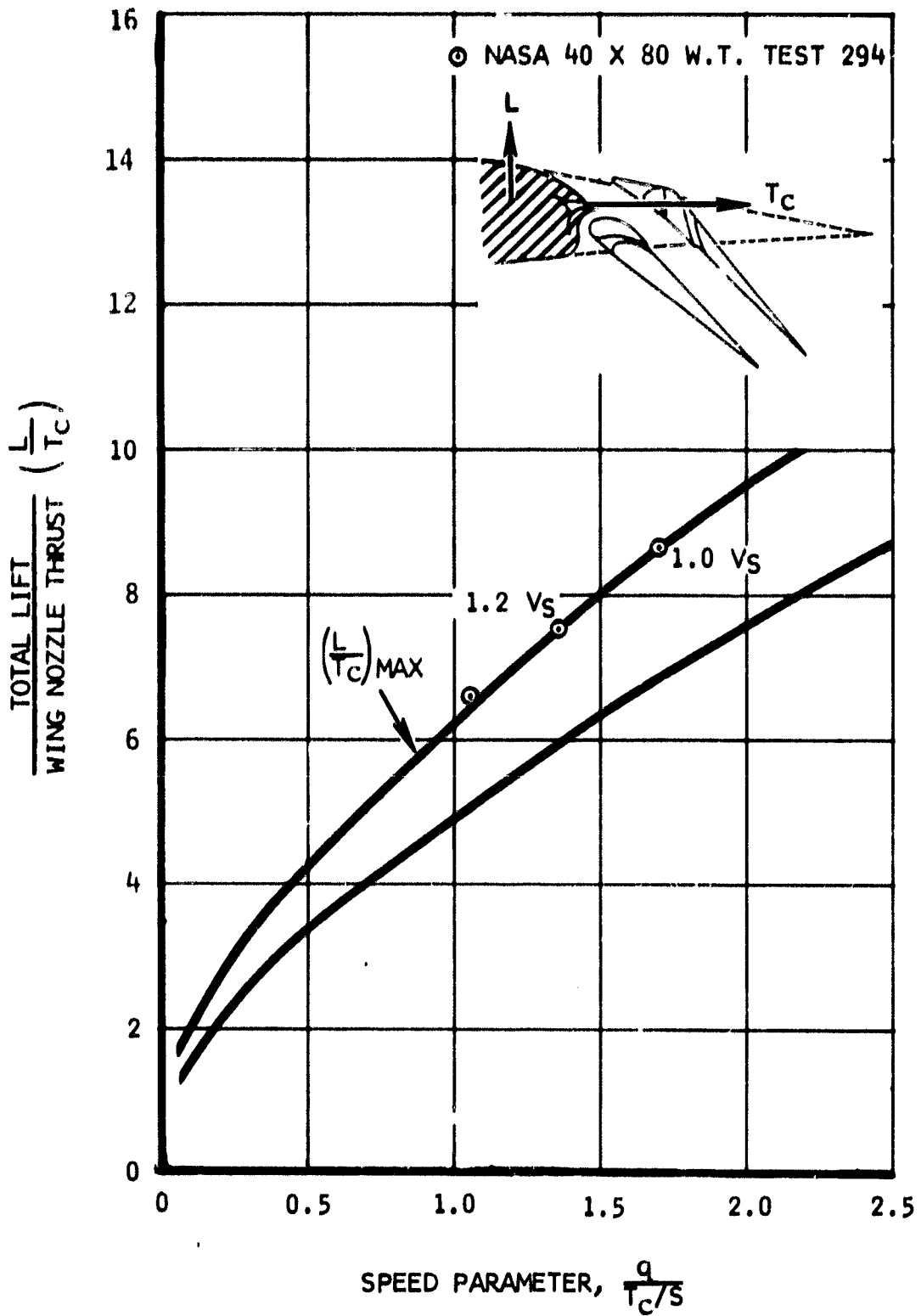


Figure 17. Lift Versus Speed Parameter at a 50-Degree Flap Angle

The curve is very suitable to analyze the effect of safety requirements that have to be met during takeoff and landing. The takeoff safety requirements are based on a 20-percent speed margin with respect to the one-engine-out stall speed,  $V_{s_{oeo}}$ , and some minimum normal acceleration requirements.

Because the curve for  $(L/T_C)_{\max}$  is valid for all thrust settings, it can be used also for the one-engine-out condition. Thus, the curve labeled 1.0  $V_s$  also represents the stall speed in the one-engine-out case, provided the correct one-engine-out thrust level for  $T_C$  is taken.

A 20-percent speed margin can now simply be added to this curve for given values of  $L$  (i.e., weight) and  $T_C$ . This is accomplished by multiplying the dynamic pressure values by  $(1.2)^2$ . This new curve satisfies the speed margin for all combinations of lift and thrust.

The new curve at  $1.2 V_s$  is now compared with the curve for  $1.0 V_s$ . The shapes of the two curves are similar, and  $L/T_C$  values of the lower curve can be easily expressed as a ratio of those of the upper curve at given values of the speed parameter. The ratios are presented in figure 18, and it is seen that the ratio is nearly constant for this configuration and the chosen flap angle of 50 degrees, and is about 0.815.

Thus, when the speed parameter is increased by a factor  $(1.2)^2$  keeping the thrust and lift at any constant value, then only 81.5 percent of the maximum lift capability is used. This is again shown in figure 19, where the ratio is plotted as a function of a change in  $q/(T_C/S)$ .

This implies that in the one-engine-out condition at  $1.2 V_{s_{oeo}}$ , a load factor can be pulled equal to  $n = 1/0.815 = 1.23$ . This exceeds the minimum required value of  $n = 1.1$ , so that this maneuvering requirement is covered for the present configuration by the required speed margin.

It should be noted that in conventional power-off aerodynamics, a speed margin of 20 percent results in  $n = 1.44$ . However, in STOL conditions, a certain speed margin generally results in a lesser maneuver margin than in conventional conditions.

The preceding discussion was made on the basis of one-engine-out conditions. The question arises as to what is the maximum maneuverability with all engines operating normally at the maximum takeoff power. It is required that a normal acceleration of at least  $n = 1.2$  can be obtained in that condition. Furthermore, the available maneuver margin needs to be known for the takeoff climb computation.

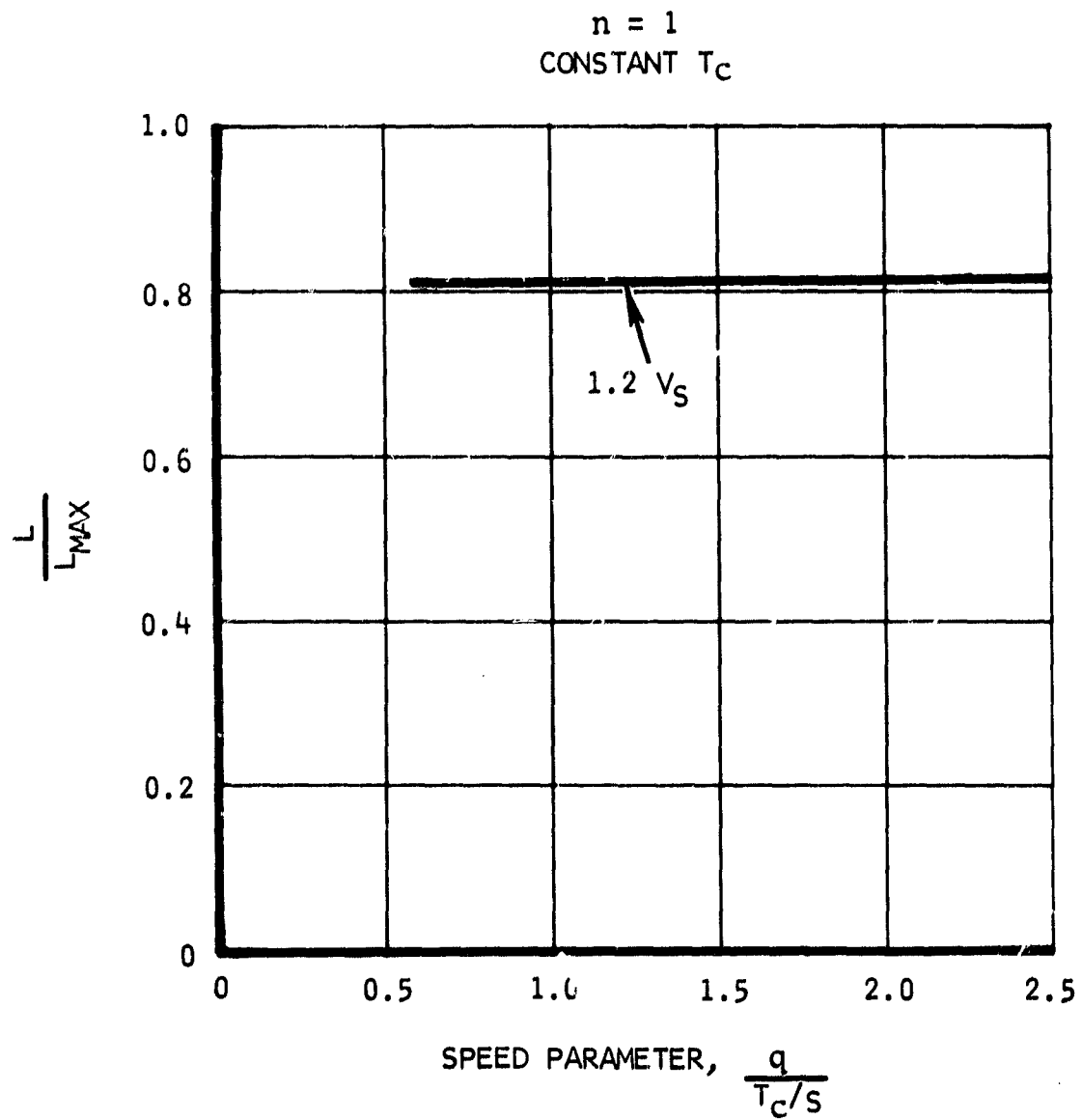


Figure 18. Ratio of Lift to Maximum Lift at a Speed of  $1.2 V_S$

n = 1  
CONSTANT T<sub>C</sub>

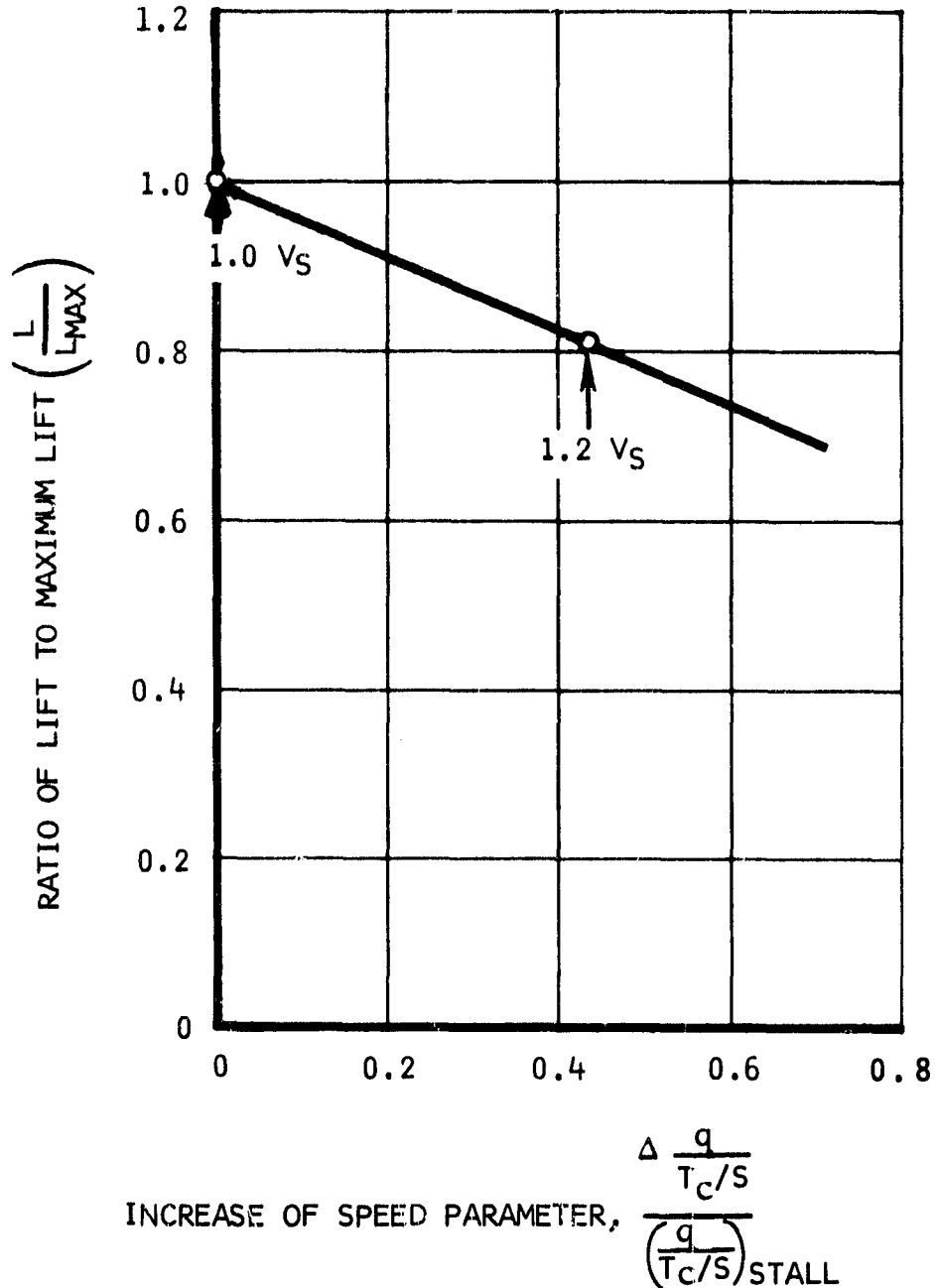


Figure 19. Ratio of Lift to Maximum Lift at Various Speeds Above Stall Speed

The analysis of this capability is made for a speed equal to  $1.2 V_{s_{oeo}}$ . Using this speed but a higher thrust,  $T_c$ , than before, changes the value of the speed parameter. Figure 17 again is applicable because it is valid for all speed-to-thrust relationships. In this figure, an increase of  $T_c$  for a given speed results in a decrease of the speed parameter and thus in a decrease of the maximum value for  $L/T_c$ . Multiplication of this new  $L/T_c$  value with the new  $T_c$  value yields the new maximum lift. Pertinent equations become

$$L_{\max, \text{ new}} = \left( \frac{L}{T_c} \right)_{\text{new}} \left( T_{c \text{ new}} \right) \quad (37)$$

or

$$L_{\max, \text{ new}} = \frac{\left( \frac{L}{T_c} \right)_{\text{new}}}{\left( \frac{L}{T_c} \right)_{\text{old}}} \left( \frac{L}{T_c} \right)_{\text{old}} \left( T_{c \text{ new}} \right) \quad (38)$$

By comparison, the old maximum lift value is

$$L_{\max, \text{ old}} = \left( \frac{L}{T_c} \right)_{\text{old}} \left( T_{c \text{ old}} \right) \quad (39)$$

The ratio of the new maximum lift to the old becomes

$$\frac{L_{\max, \text{ new}}}{L_{\max, \text{ old}}} = \frac{\left( \frac{L}{T_c} \right)_{\text{new}}}{\left( \frac{L}{T_c} \right)_{\text{old}}} \left( \frac{T_{c \text{ new}}}{T_{c \text{ old}}} \right) \quad (40)$$

This ratio is plotted as a function of the speed parameter in figure 20, using an arbitrary 50-percent increase in  $T_c$ . It is seen that the increase in maximum lift is nearly constant and is about 19 percent. Thus, in spite of the decrease in  $(L/T_c)_{\max}$ , the value of  $L_{\max}$  is increasing at the constant speed, which is the case in general. The increase in maximum lift for other thrust increases at constant speed is presented in figure 21.

Thrust increases under consideration are those from the one-engine-out level to the full, normal takeoff level. The increases are different for designs with two engines and four engines providing the cold-gas flow for the augmentation. The associated thrust and lift increment are as follows, using a 10-percent thrust overrating in the one-engine-out case (see figure 21):

Number of Engines Providing Flap Air	Normal Thrust Level	One-Engine-Out Thrust Level	$\frac{\Delta T_c}{T_{c_{\text{ooo}}}}$	$\frac{L_{\max \text{ new}}}{L_{\max \text{ old}}}$
2	$T_{c_n}$	$0.55 T_{c_n}$	0.82	1.31
4	$T_{c_n}$	$0.825 T_{c_n}$	0.21	1.08

Because the normal acceleration capability in the one-engine-out case was  $n_{\max} = 1.23$ , the maximum normal acceleration for all engines operating becomes  $n_{\max} = (1.23) (1.31) = 1.61$  for the two-engine case and  $n_{\max} = (1.23) (1.08) = 1.33$  for the four-engine case. Both cases have an acceleration capability exceeding the minimum required value for normal operation of  $n_{\max} = 1.2$ .

These normal accelerations are obtained with a takeoff speed margin of 20-percent. If the normal acceleration capability would have been insufficient, a larger speed margin would have been required.

The preceding computations are made for takeoff. Similar computations can be made for landing, except no speed margin is used as a requirement. The requirement exists that a normal acceleration can be obtained at least equal to  $n = 1.1$  in the one-engine-out case and  $n = 1.2$  with all engines operating with takeoff power. Another requirement states that the lift coefficient shall not exceed  $0.90 C_{L_{\max}}$  during the landing.

In the present study, the total airflow for the wing lift augmentation in landing is reduced to that of the one-engine-out level, even though all

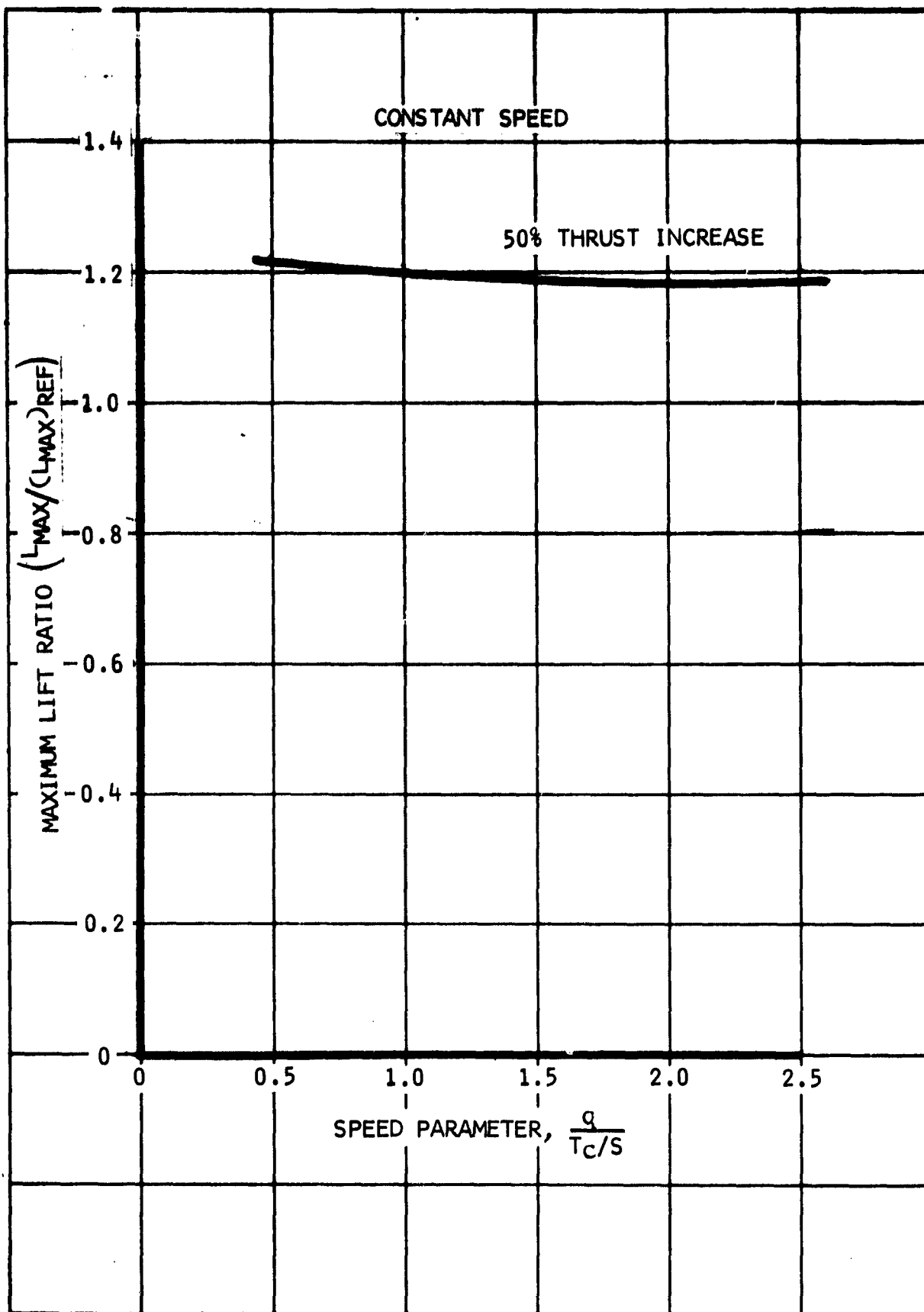


Figure 20. Effect of Thrust Increase on Lift Increase as a Function of the Speed Parameter

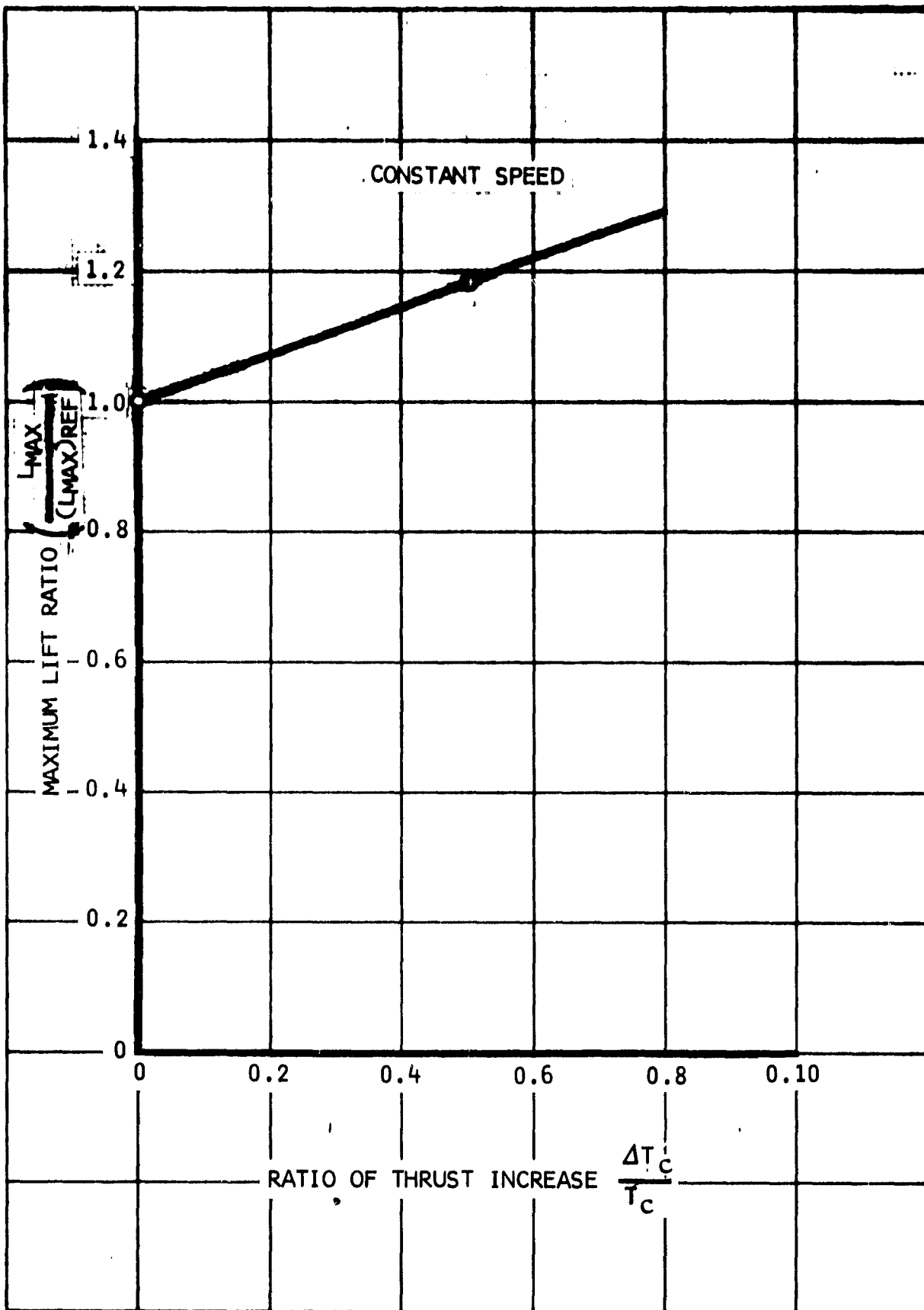


Figure 21. Average Lift Increase as a Function of Thrust Increase



engines are in good operating condition, i.e., the approach is made with a partial power setting. Furthermore, the landing approach is made in a steady-state condition, which means that no pullup is carried out. In that condition, the 90-percent  $C_{L_{max}}$  requirement is synonymous with  $L/L_{max} = 0.90$  to be applied to the one-engine-out condition.

The normal acceleration requirement of  $n = 1.1$  for the one-engine-out case results in  $L/L_{max} = 1/1.1 = 0.91$  as a requirement and is slightly less critical.

It is now necessary to determine the speed at which  $L/L_{max} = 0.90$  can be satisfied. Figure 19 shows that this occurs at  $q = 1.23 q_{s_{oeo}}$ . This means that the above engine-out requirements are met at  $V = 1.11 V_{s_{oeo}}$ .

When at this speed the power is increased to the maximum takeoff level on all engines, the normal acceleration capability is increased by a factor 1.31 for a dual-engine layout, and a factor 1.08 for a four-engine layout. Thus, the resultant normal acceleration capability is

$$n_{max} = 1/0.90 = 1.11 \text{ for one engine out} \quad (41)$$

$$n_{max} = 1.11 \cdot 1.08 = 1.20 \text{ for all engines operating at takeoff power in a four-engine configuration} \quad (42)$$

$$n_{max} = 1.11 \cdot 1.31 = 1.46 \text{ for all engines operating at takeoff power in a two-engine configuration} \quad (43)$$

It is seen that the minimum required acceleration of 1.20 in the normal operating condition is just met at the aforementioned speed. At higher speeds, as may be required to maintain an adequate margin to the minimum control speed,  $V_{mc}$ , a larger normal acceleration capability is available.

#### Expression of Experimental Lift and Drag Data as a Function of Thrust-to-Weight Ratio

In a parametric performance study such as the present study involving different engines, it is desired to present the aerodynamic characteristics

in terms of thrust-to-weight ratios. In this form, the data have been used in the determination of takeoff and landing performance.

The takeoff and landing performance is related to  $C_{L_{\max, oeo}}$ , and it is possible to express this coefficient in terms of that thrust-to-weight ratio. Previously, the maximum lifting capability was expressed in terms of  $(L/T_c)_{\max}$  versus the speed parameter  $q/(T_c/S)$ . Such a plot is again presented in figure 22, and it is seen that the  $C_{L_{\max}}$  value is found from the ratio of the value of the ordinates of each point along the curve:

$$C_{L_{\max, oeo}} = \frac{\left(\frac{L}{T_c}\right)_{\max, oeo}}{\frac{q}{T_{c_{oeo}}/S}} \quad (44)$$

Also, at each point along the curve, a certain value of  $(L/T_c)_{\max, oeo}$  exists, so that  $C_{L_{\max, oeo}}$  can be related to it. This is carried out in figure 23.

At the stall condition, it is now assumed that  $L_{\max} = W$ , which means that the effect of trimming the airplane on the lifting capability is neglected. Furthermore, the thrust to be used for  $C_{L_{\max}}$  is the one-engine-out thrust  $T_{c_{oeo}}$ . This thrust is related to the installed normal flap thrust  $T_{c_n}$  by

$$T_{c_{oeo}} = \frac{T_{c_n}}{\left(\frac{T_{c_n}}{T_{c_{oeo}}}\right)} \quad (45)$$

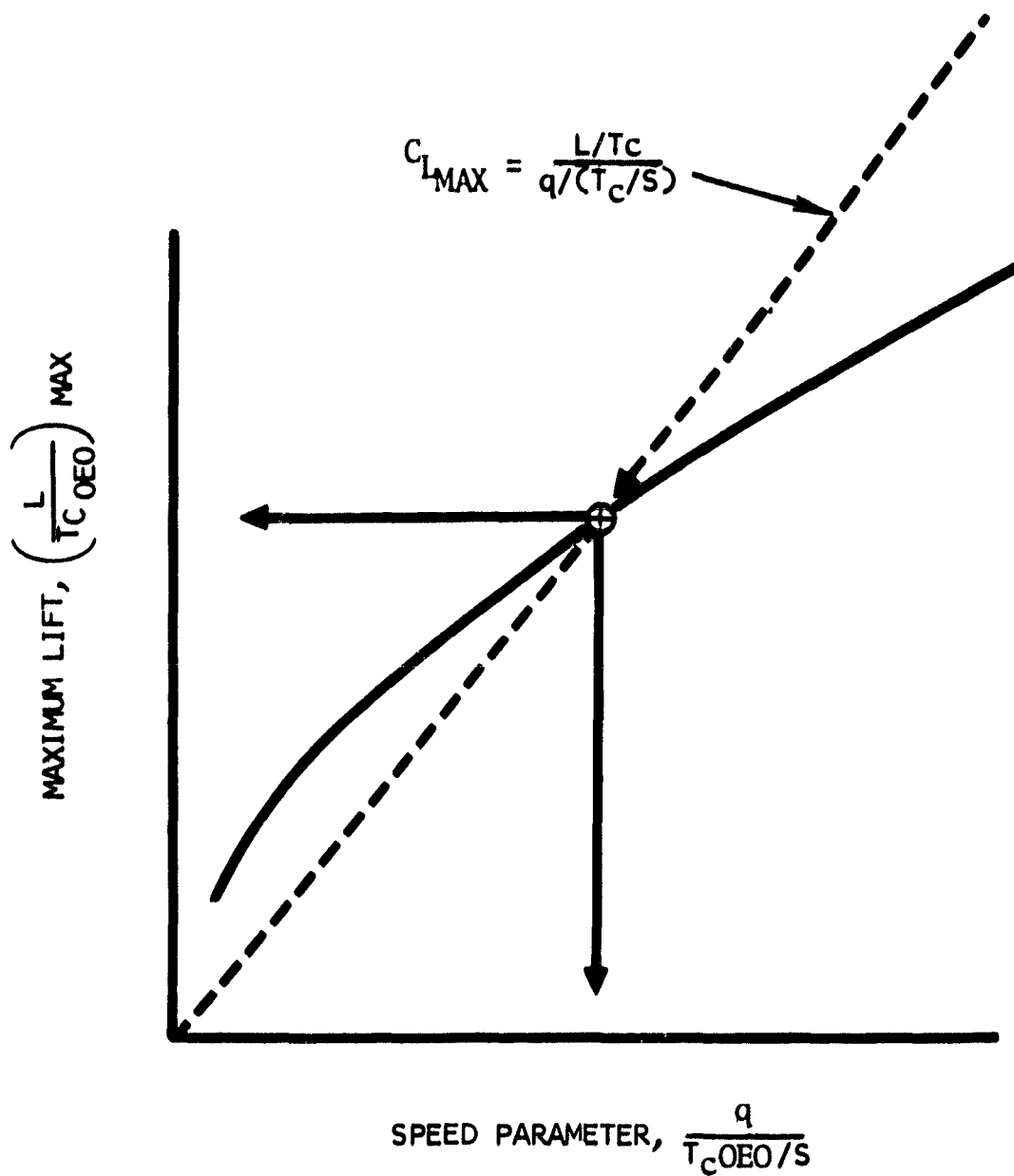


Figure 22. Relation Between  $C_{L\text{MAX}}$ ,  $\frac{q}{Tc/S}$ , and  $\frac{L}{Tc} \text{ MAX}$

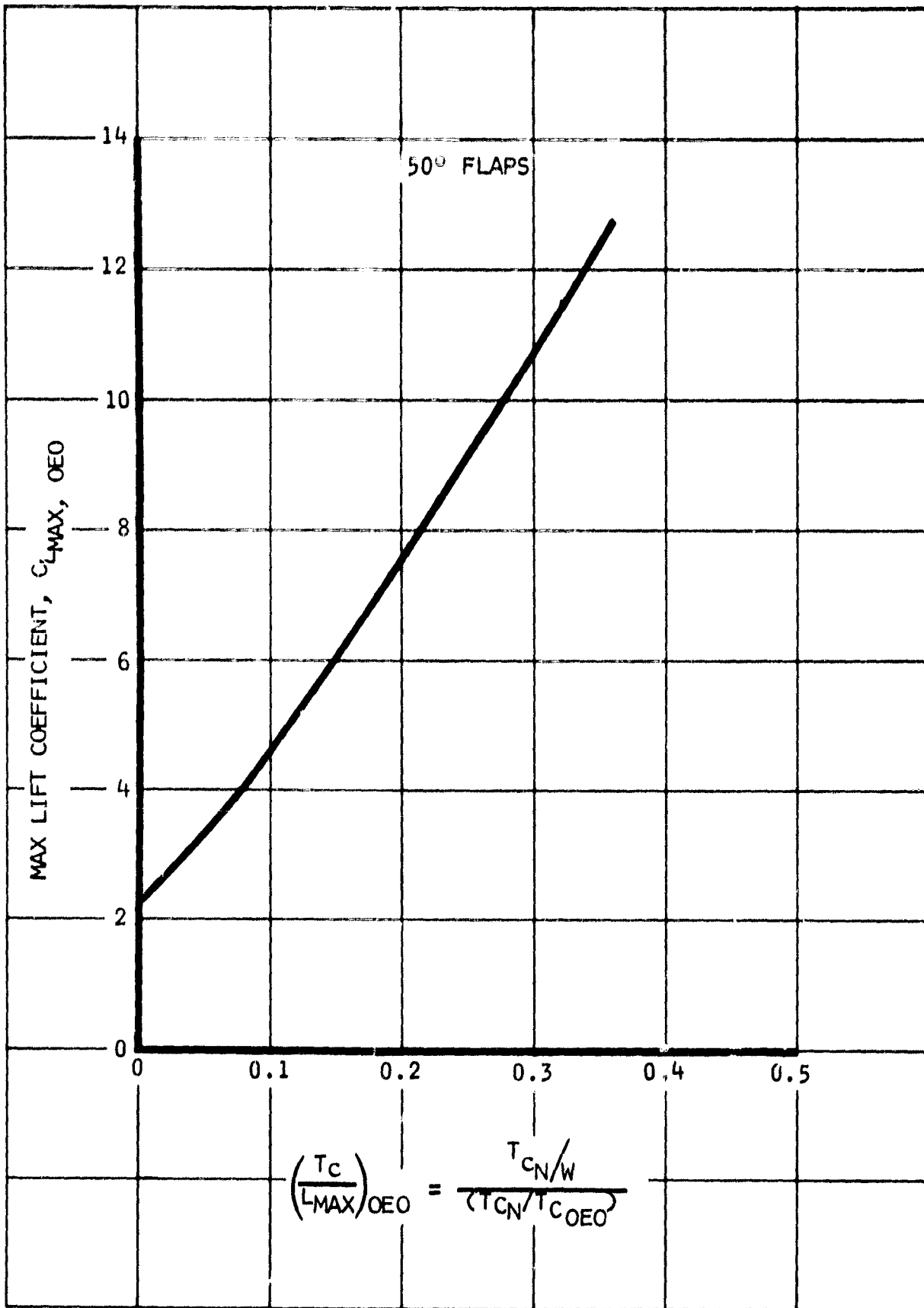


Figure 23. One-Engine-Out Maximum Lift Coefficient Versus Thrust-to-Weight Ratio

in which  $T_{c_n} / T_{c_{oo}}$  = 1.21 for four-engine designs for flap air supply and 1.82 for two-engine designs. This yields for use in the abscissa in figure 25

$$\frac{T_{c_{oo}}}{L_{\max}} = \frac{T_{c_n}}{\left(\frac{T_{c_n}}{T_{c_{oo}}}\right) W} \quad (46)$$

Because  $(T_{c_n} / T_{c_{oo}}) = \text{constant}$ , it is seen that  $C_{L_{\max}}$  is a function of the ratio of the installed flap thrust to the weight of the airplane for a given wing geometry and flap angle.

Also, the drag in the ground roll and takeoff climb can be expressed in terms of this thrust-to-weight ratio. To prove this, it is first shown that the speed parameter is a function of this ratio.

The dynamic pressure at the lift-off speed is determined from

$$q = \frac{W/S}{C_{L_{\max, oeo}}} \left(\frac{V_{10}}{V_s}\right)^2 \quad (47)$$

where  $(V_{10}/V_s) = 1.2$  is the takeoff speed margin. This dynamic pressure is to be taken regardless of whether one engine is inoperative or not. However, the thrust used for the takeoff computation is the normal takeoff thrust for all engines operating,  $T_{c_n}$ . Thus, the speed parameter becomes

$$\frac{q}{T_c} = \frac{\frac{W}{S}}{C_{L_{\max, oeo}}} \cdot \frac{(1.2)^2}{\left(\frac{T_{c_n}}{S}\right)} = \frac{(1.2)^2}{C_{L_{\max, oeo}} \left(\frac{T_{c_n}}{W}\right)} \quad (48)$$

where  $C_{L_{max, oeo}}$  is a function of  $T_{c_n}/W$  and  $T_{c_n}/T_{c_{oeo}}$  as shown above. Therefore, the whole right-hand side of the equation becomes a function of only these variables, and the speed parameter can be expressed in terms of them. This is carried out in figure 24. These results are used hereafter.

The average accelerating force during the ground roll, as shown previously, is

$$\frac{F_{x_{ave}}}{W} = \left( \frac{T_{c_n}}{W} \right) \left( \frac{-D_{ave}}{T_c} + \mu \frac{L_{ave}}{T_c} \right) - \mu + \frac{T_H}{W} \quad (49)$$

where

$T_H$  = thrust from hot-gas flow

$$\frac{D_{ave}}{T_c} = \frac{1}{2} \left[ \left( \frac{D}{T_c} \right)_{V=0} + \left( \frac{D}{T_c} \right)_{V_{10}} \right] \quad (50)$$

The value of  $(D/T_c)_{V_{10}}$  is obtained from

$$\left( \frac{D}{T_c} \right)_{V_{10}} = \frac{C_D q S}{T_c} = C_D \left( \frac{q}{S} \right)_{V_{10}} \quad (51)$$

in which  $C_D$  is found from test data shown in figure 25 and taken from NASA-Ames test 294. The coefficient  $C_D$  used belongs to  $\alpha = 0$ , this being the attitude for ground roll. The value at zero velocity is estimated at

$$\left( \frac{D}{T_c} \right)_{V=0} = -0.70 \quad (52)$$

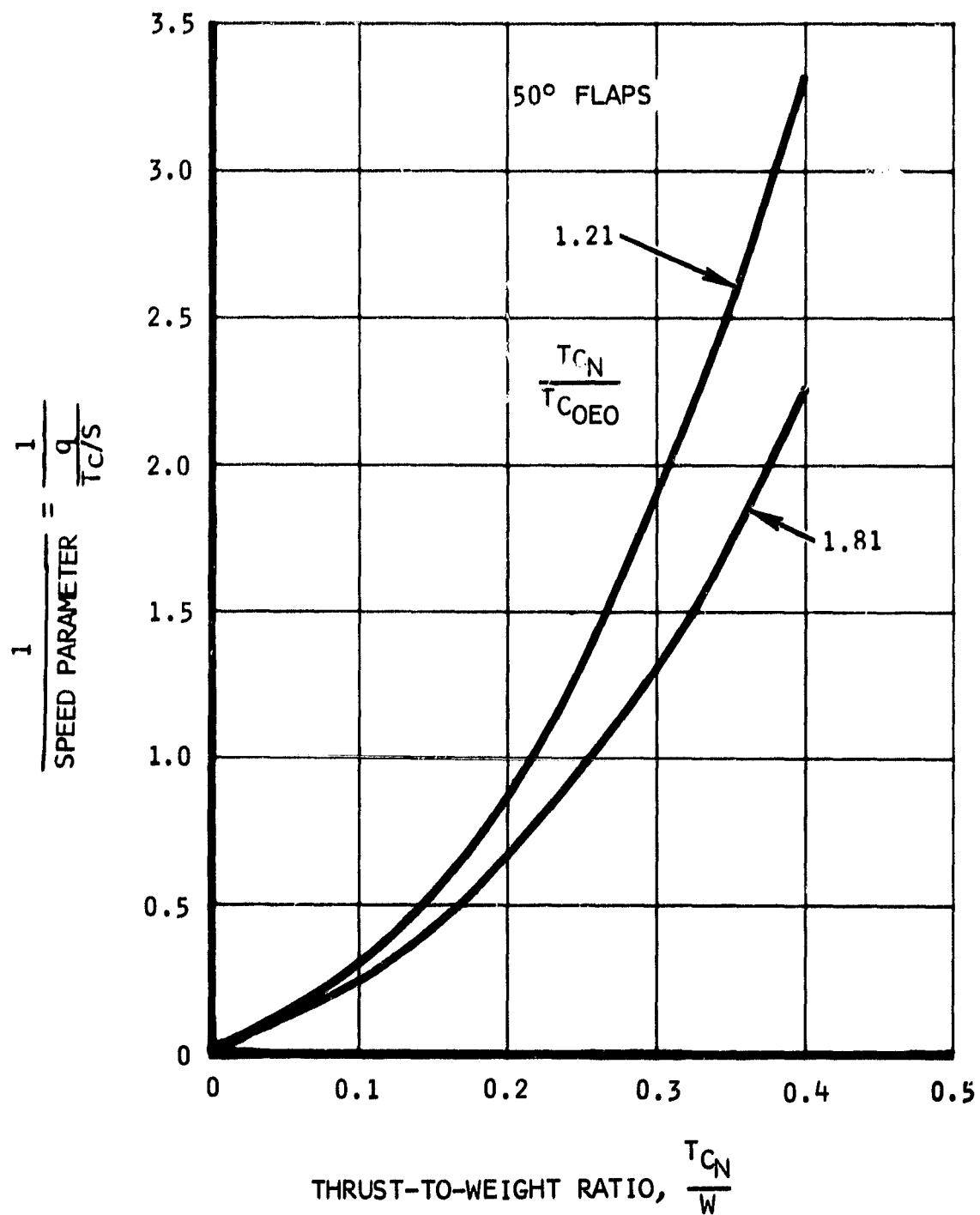


Figure 24. Relation Between Speed Parameter and Thrust-to-Weight Ratio at Liftoff Speed

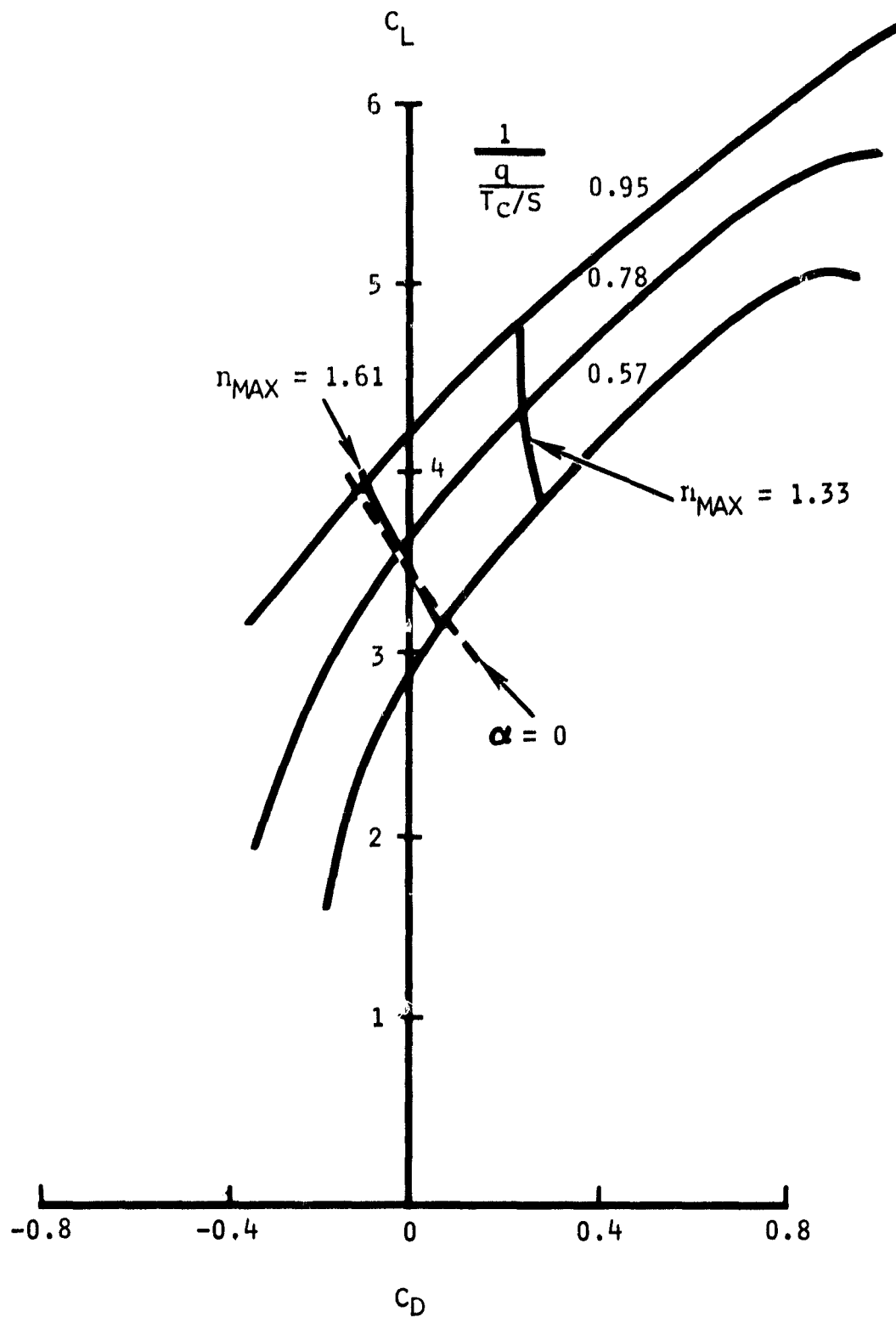


Figure 25. Power-On Drag Polars for 50 Degree Flap Setting



The lift is treated similarly as follows:

$$\frac{L_{ave}}{T_c} = \frac{1}{2} \left[ \left( \frac{L}{T_c} \right)_{V=0} + \left( \frac{L}{T_c} \right)_{V_{10}} \right] \quad (53)$$

where

$$\left( \frac{L}{T_c} \right)_{V_{10}} = C_L \left( \frac{q}{T_c/S} \right)_{V_{10}} \quad (54)$$

$$\left( \frac{L}{T_c} \right)_{V=0} = 0.98 \quad (55)$$

It is seen that, for a given flap angle, wing geometry, and friction coefficient  $\mu$ , the following bracket becomes only a function of the speed parameter:

$$\left( \frac{-D_{ave}}{T_c} + \mu \frac{L_{ave}}{T_c} \right) = f \left( \frac{q}{T_c/S} \right) \quad (56)$$

Thrust-to-weight ratios can now be substituted for the speed parameter, and results are presented in figure 26.

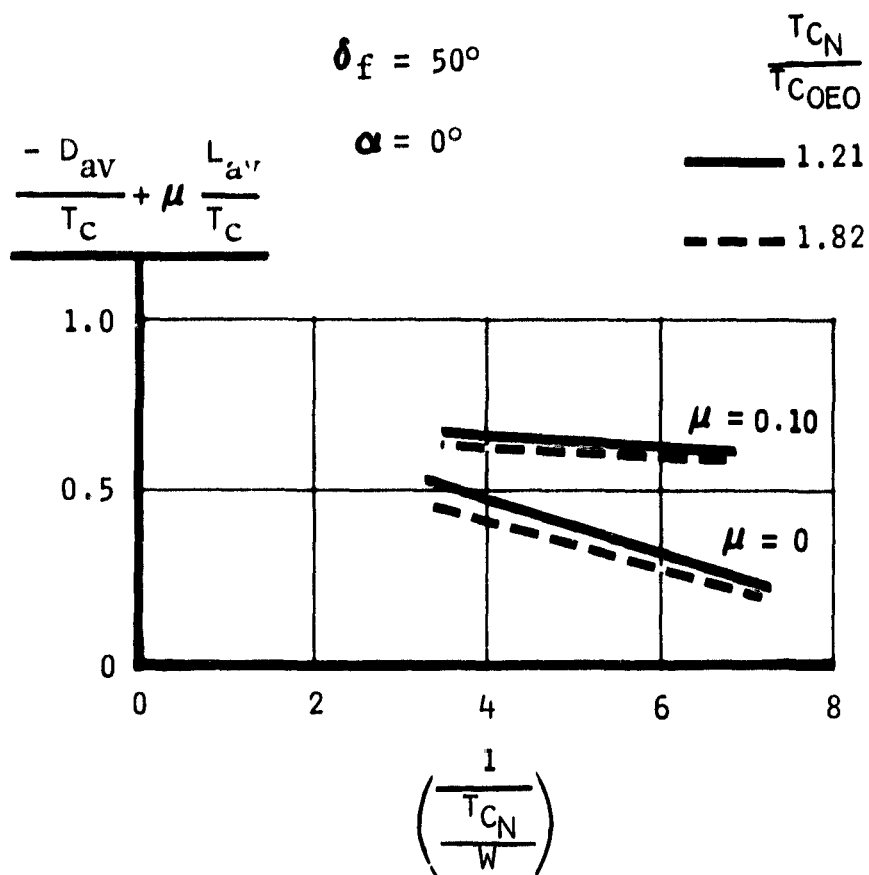


Figure 26. Aerodynamic Effects in Ground Roll as a Function of Thrust-to-Weight Ratio

A similar approach is used in establishing the steady-state climb angle,  $\gamma_\infty$ . This angle is used as a parameter in the determination of the climb distance to the 50-foot obstacle.

The speeds are assumed to be the same as those at lift-off; the slight increase in speed that generally exists after lift-off is neglected. Figure 25 can again be used, giving  $C_L$  and  $C_D$  values that determine the climb angle at zero hot-gas thrust:

$$\frac{-D}{L} = \frac{-C_D}{C_L} = \tan \gamma_\infty \approx \gamma_\infty \quad \text{at } T_H = 0 \quad \text{at } T_H = 0 \quad (57)$$

Contrary to the ground roll condition where a zero angle of attack was used, a lift condition is taken consistent with maneuver margins previously computed, i.e.:

$$n_{\max} = 1.61 \text{ for two flap air engines} \quad (58)$$

$$(T_{cN}/T_{cOEO} = 1.82)$$

$$n_{\max} = 1.33 \text{ for four-flap air engines} \quad (59)$$

$$(T_{cN}/T_{cOEO} = 1.21)$$

The  $C_L$  and  $C_D$  values are then only a function of the speed parameter which, as shown above, is in turn a function of the thrust-to-weight ratio. Thus, also the climb angle can be expressed in terms of this ratio, which is carried out in figure 27.

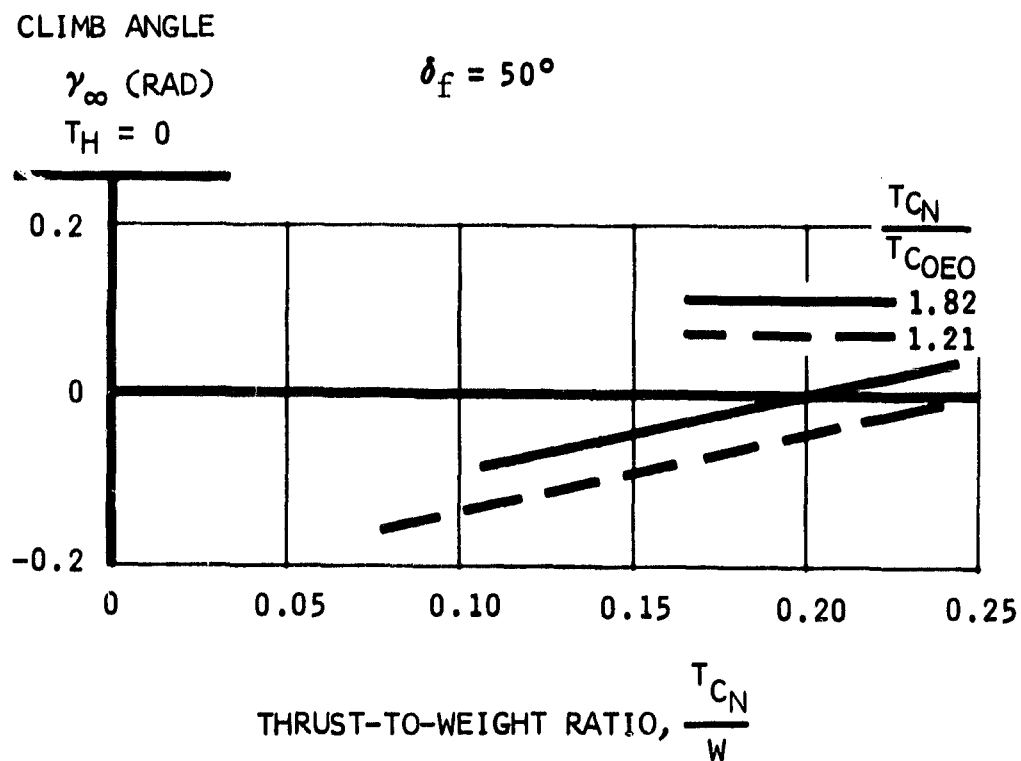


Figure 27. Effect of Thrust-to-Weight Ratio on the Steady-State Climb Angle

The total climb angle consists of the above angle, plus the increment obtained from any direct thrust such as the horizontal thrust. This increment is

$$\Delta \gamma_{\infty, T_H} = \frac{T_H}{W} \quad (60)$$

so that the total climb angle becomes

$$\gamma_{\infty} = \gamma_{\infty} \quad , \quad T_H = 0 + \frac{T_H}{W} \quad (61)$$

#### Minimum Control Speed

The minimum control speed with the critical engine inoperative is determined using the simplifying assumption that the roll control has negligible effects on the yawing moment, lift, and sideforce. The minimum speed is determined from the following yawing moment equation:

$$\left(\frac{T}{W}\right) \left(\frac{a}{b}\right) = \left(C_{n\beta} \cdot \beta + C_{n\delta_R} \cdot \delta_{R_{\max}}\right) \left(\frac{qS}{W}\right) \quad (62)$$

where "a" is the lateral distance of the inoperative engine to the airplane plane of symmetry. This equation is presented in figure 28 by the dotted line labeled "max sideslip."

The side force or the vertical tail needed for the yawing moment equilibrium can be expressed in terms of the bank angle  $\phi$  and the sideslip angle used. Elimination of the sideslip angle yields a relation of  $(T/W)a/b$  versus  $qS/W$  for given bank angles:

$$\left(\frac{T}{W}\right) \left(\frac{a}{b}\right) = \frac{C_{n\beta}}{C_{y\beta}} \sin \phi + \left[ C_{n\delta_R} \delta_{R_{\max}} \right] \quad (63)$$

$$\frac{C_{n\beta}}{C_{y\beta}} \left( C_{y\delta_R} \delta_{R_{\max}} \right) \left[ \frac{qS}{W} \right]$$

Also, this equation is graphically presented in figure 28. If the bank angle is critical, this equation prevails above that of the maximum sideslip.

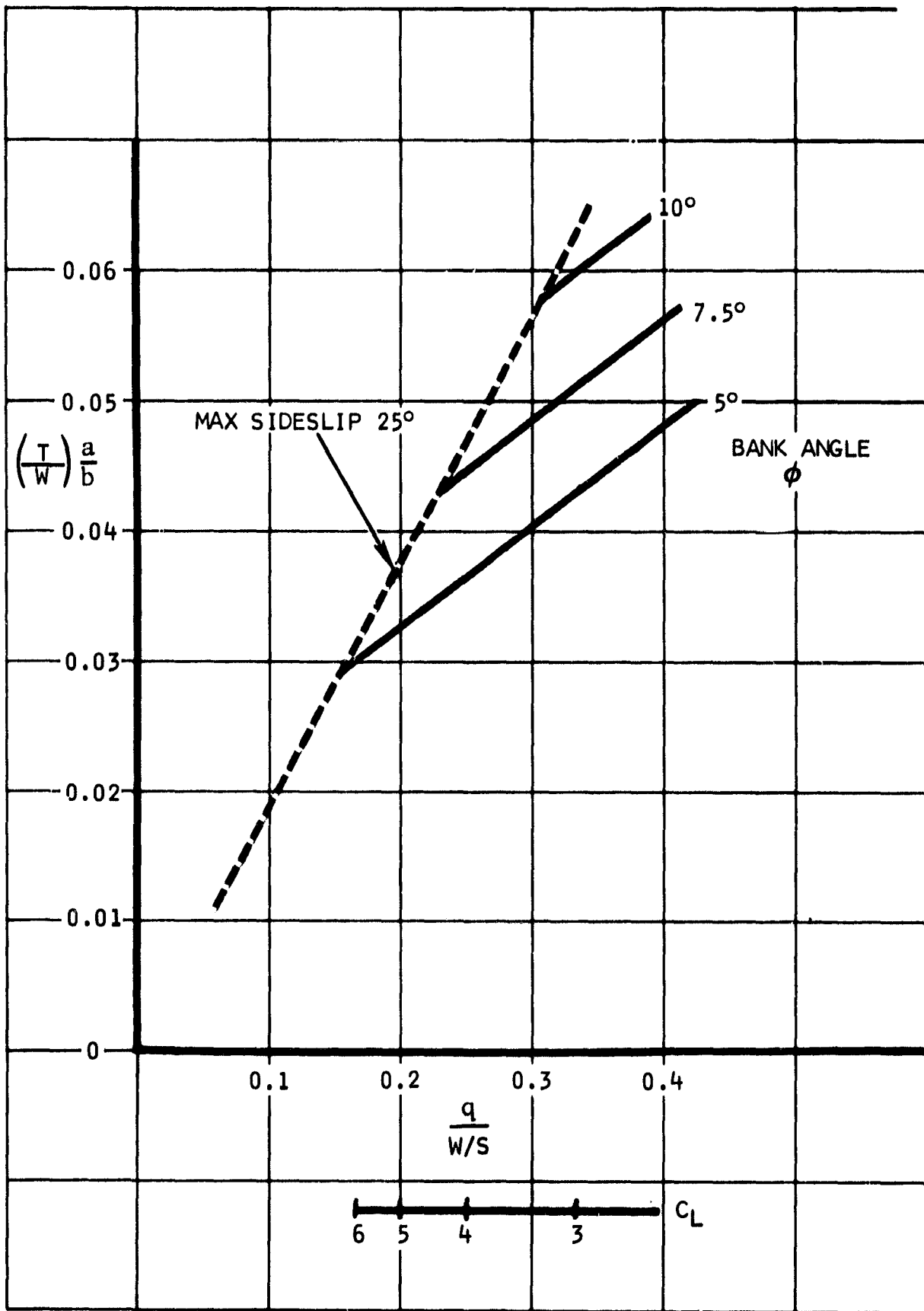


Figure 28. Determination of Minimum Control Speed Condition

Figure 28 is determined using the following preliminary values:

$$C_{n\beta} = 0.00280 \quad (64)$$

$$C_{y\beta} = 0.0141 \quad (65)$$

$$C_{n\delta_R} \delta_{R_{\max}} = 0.119 \quad (66)$$

$$C_{y\delta_R} \delta_{R_{\max}} = 0.218 \quad (67)$$

$$\beta_{\max} = 25 \text{ deg} \quad (68)$$

$$W = 40,000 \text{ lb} \quad (69)$$

Results for the configurations under investigation are shown in table XIX. Herein the most critical engine is that which supplies the horizontal thrust.

TABLE XIX. MINIMUM CONTROL SPEEDS

Configuration	$\left(\frac{T}{W}\right) \left(\frac{a}{b}\right)$	$\phi$ Deg	$V_{mc}$ (KEAS)
1	0.0325	5.5	51.0*
2	0.0313	5.3	49.5
3	0.0249	4.2	44.2*
4	0.0249	4.2	44.2*
5	0.0277	4.7	46.7*
6	0.0302	5.2	48.9
7	0.0182	3.0	38.0*
8	0.0160	2.7	35.4*
9	0.0120	2.0	31.0*

It should be noted that the preceding equations pertain only to yawing moment and sideforce equilibrium, disregarding considerations of maximum lift. For this reason, the computed minimum control speeds of many configurations are lower than the one-engine-out stall speed. In table XIX, these are indicated by an asterisk. Though the airplane is flyable below the one-engine-out stall speed with all engines operating,  $V_{S_{oeo}}$  should be substituted for  $V_{MC}$  in those cases. Also, it should be noted that  $V_{MC}$  is 5 percent higher than shown when the 10-percent emergency overrating is used for the remaining engines.

### Roll Performance

The roll performance is only investigated in terms of initial roll acceleration at the approach speed for airplane weights of 40,000 pounds.

The roll acceleration is determined from

$$\ddot{\phi} = \frac{L}{I} \quad (70)$$

in which

$$L = q \left( S b C_{l_{\delta_a}} \delta_a \right) \quad (71)$$

The coefficient,  $C_{l_{\delta_a}}$ , is determined using the Weissinger lifting surface theory, and is, for an ideal 100-percent chord flap, equal to

$$\left( C_{l_{\delta_a}} \right)_{100\% \text{ chord}} = 0.00247 \text{ deg}^{-1} \quad (72)$$

For preliminary investigation, use is made of

$$\frac{C_{l\delta_a}}{(C_{l\delta_a})_{100\% \text{ chord}}} \cdot \delta_a = 40 \text{ deg} \quad (73)$$

$$S = 800 \text{ sq ft} \quad (74)$$

$$b = 79 \text{ ft} \quad (75)$$

which results in the following relation:

$$\ddot{\phi} = \frac{6250}{I} (q) \quad (76)$$

The roll accelerations become as shown in table XX for the various configurations

TABLE XX. ROLL ACCELERATIONS

Configuration	I	q	$\ddot{\phi}$
1	161,300	14.3	0.554
2	187,600	8.8	0.293
3	224,500	8.8	0.245
4	163,600	8.8	0.336
5	149,500	14.3	0.598
6	179,100	8.8	0.307
7	146,100	13.7	0.586
8	174,200	8.8	0.316
9	-	8.8	-



## SECTION V

### CONFIGURATION SELECTION

The selection of the final configuration was the result of essentially a three-step evaluation.

The first step was contained in the Configuration Evaluation Report NA-68-995. As a result of this evaluation, the configurations which utilized the J52 engines, the JT12A engines, or the RB183-1 Spey, Junior engines were eliminated from consideration. The 7,500-pound thrust available from the J52 was not required, and its weight is approximately 270 percent of the Orpheus turbojet which will provide adequate thrust for this program.

The JT12A was eliminated as four of these engines would be required to provide the necessary horizontal thrust. The Spey, Junior (RB183-1) would provide adequate thrust and also flap air. However, the compressor pressure ratio of 2.27 was considered too marginal for a program base.

This removed configurations No. 2, 6, 7, and 8 from consideration. Configuration No. 9 was previously removed because of center-of-gravity problems. Configuration No. 3 was dropped from consideration because of its relatively high roll moments of inertia when compared to the rest of the configurations.

As a result, only three configurations remained for evaluation. Of these, configurations No. 1 and 5 were essentially the same and differed only in that the two RB163-25 Spey turbofan engines were located at slightly different wing stations for landing gear considerations. This difference was negligible from the standpoint of overall evaluation. These two arrangements both used the same power source to provide horizontal thrust and flap air.

The other configuration, No. 4, was a different basic approach in that two Orpheus engines provided the horizontal thrust, and four GE T64 turboshaft engines driving modified Viper compressor sections were used as the augmentor flap air source.

These two types of configurations were compared as follows:

Configuration No. 1 or No. 5

1. Two-engine installation - less complex and utilizes existing aircraft systems. Results in low design and fabrication costs.
2. Single-engine-out reduces horizontal thrust and flap air is approximately one-half.
3. Change in horizontal thrust results in similar change in flap air quantity.
4. Engine procurement expected to require long lead time. Revision of engine internal fan air routing not expected to require major development.
5. Engine procurement costs expected to be high
6. Requires development of modulating thrust reversal system to cancel horizontal thrust while maintaining high engine power setting to provide flap air during landing approach.
7. Provides no capability of independent variations in horizontal thrust and flap air due to single-source system.
8. Two-engine system requires large diameter ducting and creates local structural problems.

Configuration No. 4

- Six-engine installation - requires four additional sets of powerplant and related systems installations. Higher design and fabrication costs.
- Single-engine-out is essentially one-sixth of available power.
- Horizontal thrust and flap air supply can be varied independently.
- Horizontal thrust engines expected to be available. Turbohaft engines available. Modification of compressor sections not expected to require major development.
- Engine procurement costs estimated to be less than one-half as high as for configuration No. 1 or 5.
- Requires development of modulating thrust reversal system, but high horizontal thrust settings are not required during landing approach as flap air source is a separate system.
- Complete freedom for independent variations in flap air and horizontal thrust due to separate sources for each system.
- Four-engine air source requires smaller ducting and less complex structural problems.

Based on these comparisons, it was recommended that the configuration No. 4 type of aircraft system be selected for detail definition.

As a result of discussions between personnel from NASA-Ames, NR, and de Havilland Aircraft of Canada, it was mutually agreed that the configuration No. 4 type of aircraft system would be utilized.

It was agreed that the two T64 turboshaft engine and air compressor units which were located on top of the wing above the fuselage would be relocated to a position on the side of the fuselage. These were first located in line with the cabin windows completely forward of the wing to provide the least interference with the augmentor-flap system and the cargo bay fuel tank installations. NASA-Ames desired a location further aft which resulted in the configuration shown in figure 29.

It had been determined that full thrust reversing for all the engines considered would require at least some development, but it was also agreed that this capability would not be required. Information from Rolls-Royce, received after completion of the Configuration Evaluation Report (reference 4), indicated that a vectoring nozzle installation was available for the Orpheus engine. This installation would fulfill the program requirements for thrust vectoring during landing approach and would be acceptable with the decision to remove the full thrust reversing requirement. With this arrangement, the landing roll distances will be calculated.

The performance calculations used in the configuration evaluation were based on the development of takeoff and landing capabilities for each configuration. It was mutually agreed that all future landing calculations would be based on a 65-knot approach speed.

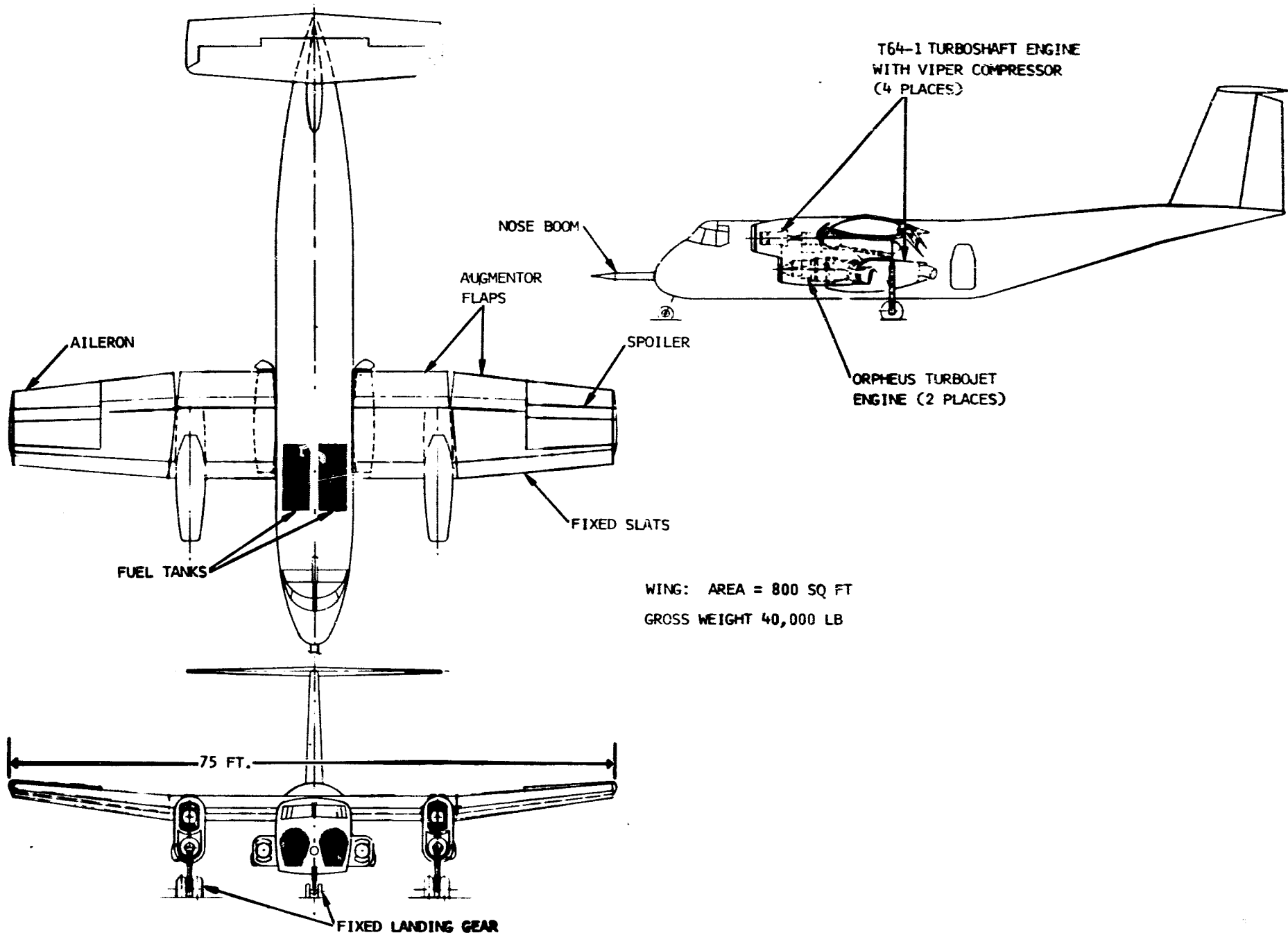


Figure 29 Augmentor-Wing configuration

## SECTION VI

### MODIFICATION CONFIGURATION DEVELOPMENT

Final selection of the aircraft configuration permitted definition of the requirements for the various systems and detail studies of methods for meeting those requirements. This section describes the system configurations which evolved.

#### Propulsion

Orpheus engine. - Contacts were made with Rolls-Royce Limited personnel concerned with the Orpheus engines and with the Pegasus rotating nozzles to verify the availability of this configuration and its ability to meet the requirements of the program. In addition, it was determined that surplus Orpheus Mark 100 engines, presently held by the U.K. Ministry of Technology, might be made available to this research program.

The Orpheus Mark 100 engine is a 4,200-pound thrust engine that would be automatically up-rated, during overhaul, to 4,520 pounds thrust. It has been demonstrated that with additional, relatively simple revisions, the engine can be up-rated to 5,000 pounds thrust. Bench testing necessary to clear the Orpheus/vectoring nozzle combination for the 200-hour flight life of this research aircraft would also provide the flight clearance for the 5,000-pound thrust rating.

The rotating nozzle assembly is currently operational on Pegasus engines in the Hawker-Siddeley P1127 Harrier aircraft. It is adaptable to the smaller Orpheus engine by using only one nozzle with a new adapter section. This provides a single side-mounted vectoring nozzle installation supported by the engine structure with minimum interface requirements to the aircraft structure.

The RB-193 vectoring nozzle was also investigated for possible use with the Orpheus Mark 100 engines. While it is compatible, the present design requires that the major support be furnished by aircraft structure. This would increase the structural complexity of the nacelles, and would also require that aircraft structural parts be fabricated and delivered to the engine manufacturer for use during the ground testing of the engine. As this nozzle design is still in the ground test and development phase of its program, it is not considered for use on this program.

A second alternative method has been investigated. This employs the Orpheus engine with a split tailpipe to pass the hot exhaust around the landing

gear strut, and an available, two-position, diverter valve in each leg of the tailpipe to direct the hot gas laterally when forward thrust is not desired.

The Orpheus Mark 100 turbojet is normally equipped with a 4-kva generator and a single, 3,000-psi, 4-gpm hydraulic pump. It also provides approximately 3 pounds-per-second of bleed air.

Viper compressor/T64-1 turboshaft engine. - A modified compressor section from a Rolls-Royce Viper turbojet engine will be direct-driven by the output shaft of the T64-1 turboshaft engine. These two units are compatible from the standpoint of horsepower and rotation speeds.

### Controls

Aileron control system. - The aileron control system was based on the following requirements:

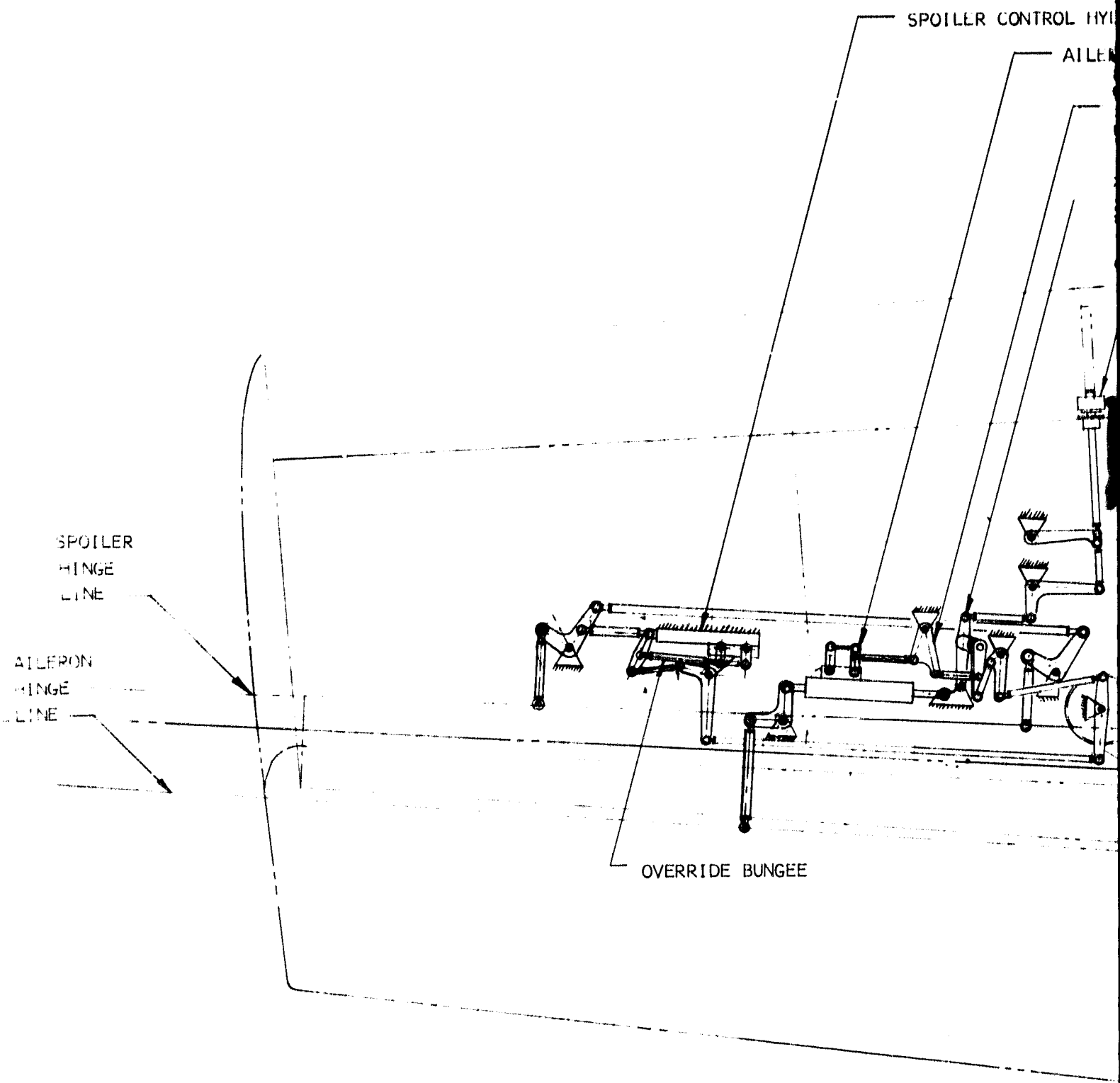
1. Deflections of +27 degrees and -18 degrees during cruise conditions
2. Drooped 20 degrees when flaps are extended
3. Deflections of +54 degrees and -36 degrees when in drooped position
4. Full deflection from neutral in one-half second
5. BLC when in drooped position
6. Full-powered system
7. Spoilers operating with up-aileron travel.

In the original CV-7A system, aileron droop was directly coupled to the flap deflection system. The proposed configuration requires that BLC air be provided to the ailerons at all drooped positions to prevent aileron stall and loss of roll control effectiveness. Since the augmentor flaps can be extended without the flap air system operations and therefore, no BLC air available to the aileron, the aileron droop actuation system has been separated from the flap actuation system.

The proposed aileron and flap control systems are illustrated schematically in figure 30.

Augmentor flap system. - While it was desirable to provide an augmentor-wing flap arrangement that duplicated the configuration of the model tested in

PRECEDING PAGE BLANK NOT FILMED. 109-A



109-B

POTTER CONTROL HYDRAULIC ACTUATOR

AILERON CONTROL HYDRAULIC ACTUATOR

AILERON CONTROL NONLINEAR GEARING MECH

AILERON DROOP & GEARING CHANGER MECH

AILERON DROOP & GEARING CHANGER JACK ASSY

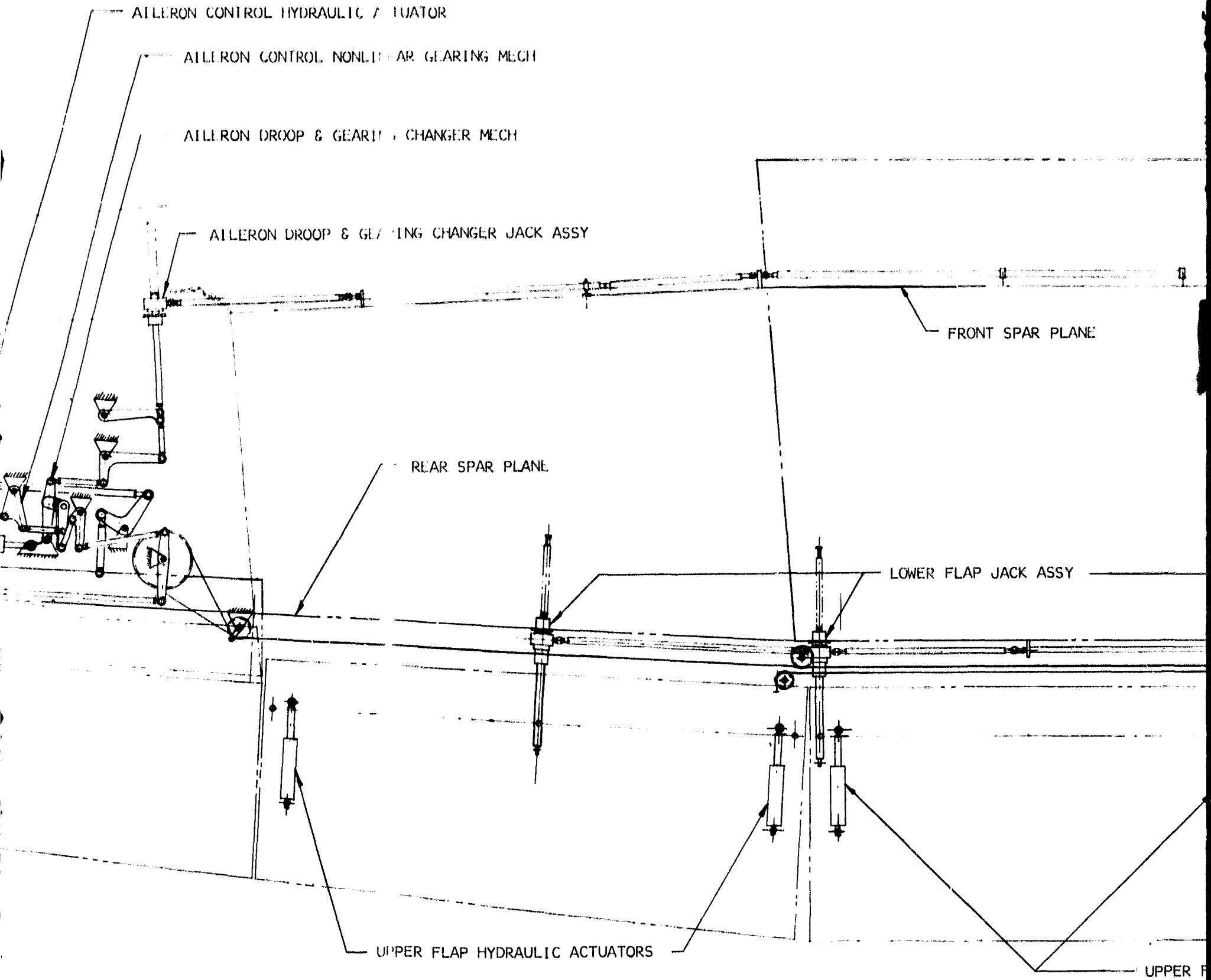
FRONT SPAR PLANE

REAR SPAR PLANE

LOWER FLAP JACK ASSY

UPPER FLAP HYDRAULIC ACTUATORS

UPPER F





109-C

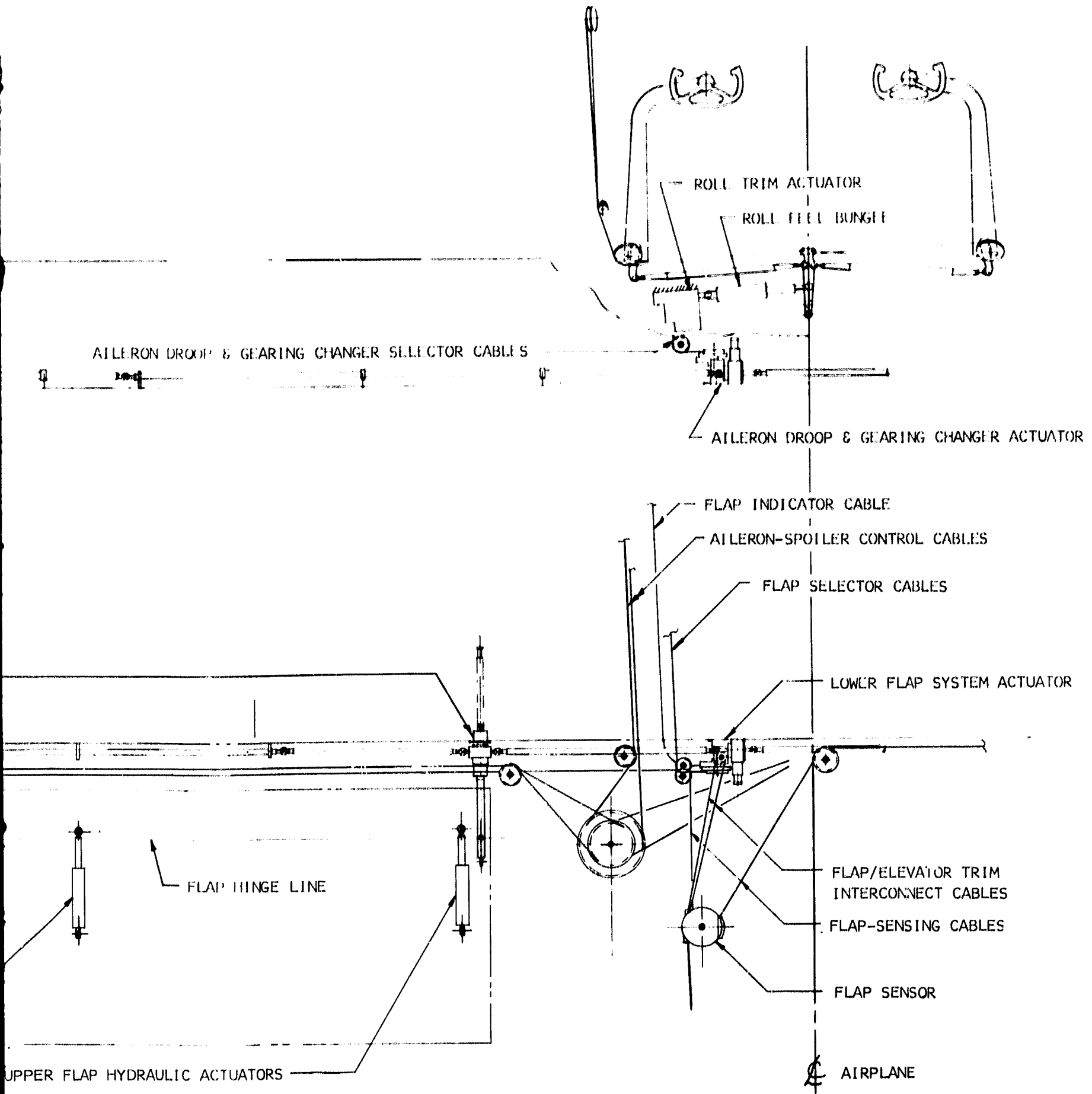


Figure 30. Controls System Schematic

PRECEDING PAGE BLANK NOT FILMED.

the NASA/Ames/de Havilland 40 by 80 wind tunnel program that goal was not compatible with the minimum modification requirement of this program.

To obtain the same flap chord to wing chord ratio and space for the flap air plenum chambers, either the rear spar would have to be moved forward, a major wing structure modification, or the wing chord would have to be increased. The program requirement for increased wing loading was accomplished by removing approximately 10 feet of each outer wing panel to reduce the total wing area. Any increase of the wing chord would require a further reduction in wing span, and was not considered feasible.

Within the above restrictions and providing approximately 60 square inches of area for each nozzle plenum chamber, the augmentor flap configuration of figure 31 was developed.

The operating mechanism shown performs two functions. The upper flap is extended and locked in its proper position by hydraulic cylinders incorporated in the lower flap structure. The total flap system is then rotated about the hingeline by hydraulically actuated jackscrews mounted under the wing.

As the total flap assembly is rotated to the extended position, the upper flap lip is operated by a nonlinear linkage to maintain a reasonable relationship to the airflow over the wing.

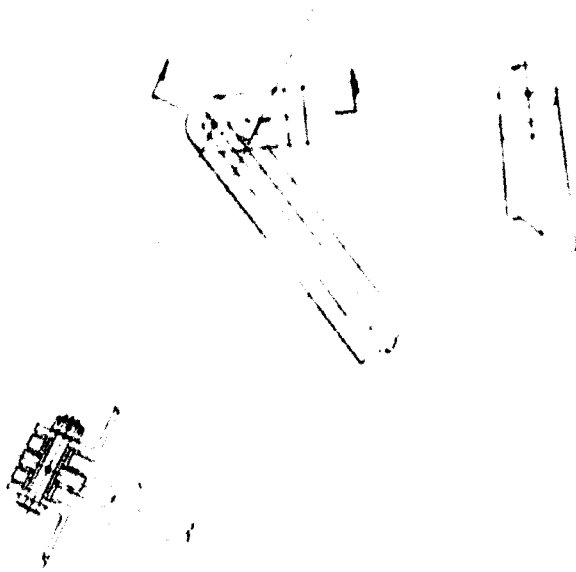
Augmentor flap air distribution system. - The flap air distribution system consists of three principal areas: the air distribution ducting from the compressor outlets to the flap plenum chamber, the flap plenum chamber and nozzle assemblies, and the aileron boundary layer control (BLC) distribution system.

In each area a basic system requirement is the maintenance of balanced forces about the aircraft roll axis under single-failure conditions in the air system. To accomplish this purpose, the flap plenum chamber in each wing was divided laterally into two sections. Each of these sections was divided into an upper and lower plenum. The air from each of the four compressors was ducted to two of the above eight plenum chambers in such a manner that each compressor supplied the plenum at the same span-wise location on each wing. In this way any engine, compressor or duct malfunction will affect the airflow to the augmentor flap symmetrically about the aircraft roll axis. The distribution system is illustrated in figure 32. With the four air supply systems separated, the possibility of adverse intercompressor effects due to stall or variations in pressure and air flows is virtually eliminated.

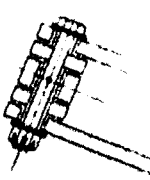
The plenum chamber cross-section dimensions and nozzle location, figure 33, were dictated by the rear spar location and the flap chord requirements.

PRECEDING PAGE BLANK NOT FILMED.

113-A



SECT E E  
SCALE: FULL



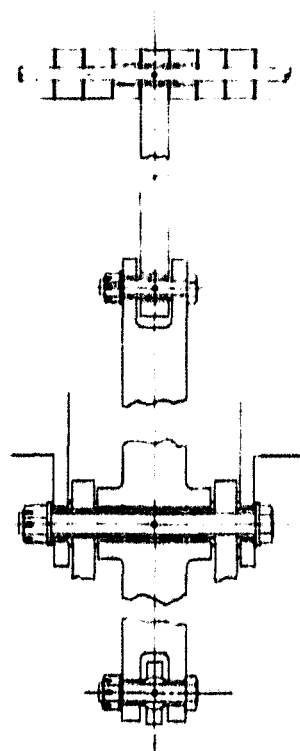
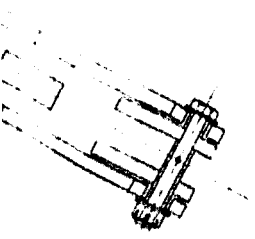
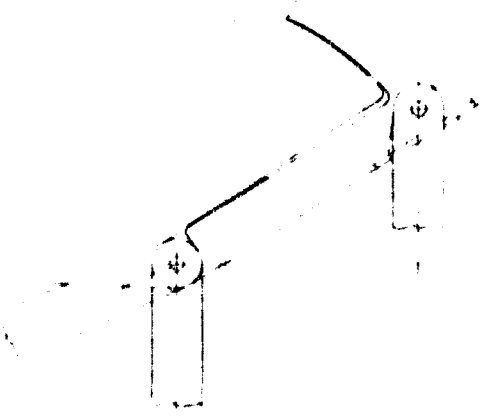
SECT C-C  
SCALE: FULL

FOLDOUT BEAM

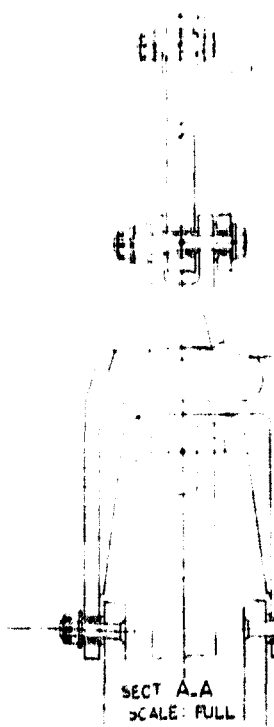
113 - B



SECT D-D  
SCALE: FULL



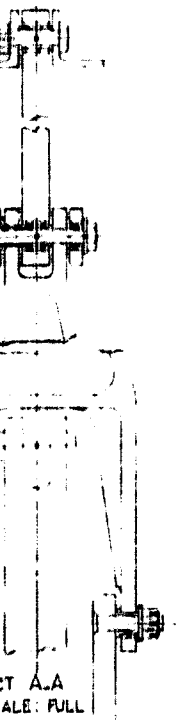
SECT B-B  
SCALE: FULL



SECT A-A  
SCALE: FULL

**FOLDOUT FRAME**

113-C



CT A.A  
ALE: FULL

FOLDOUT FRAME

113-D

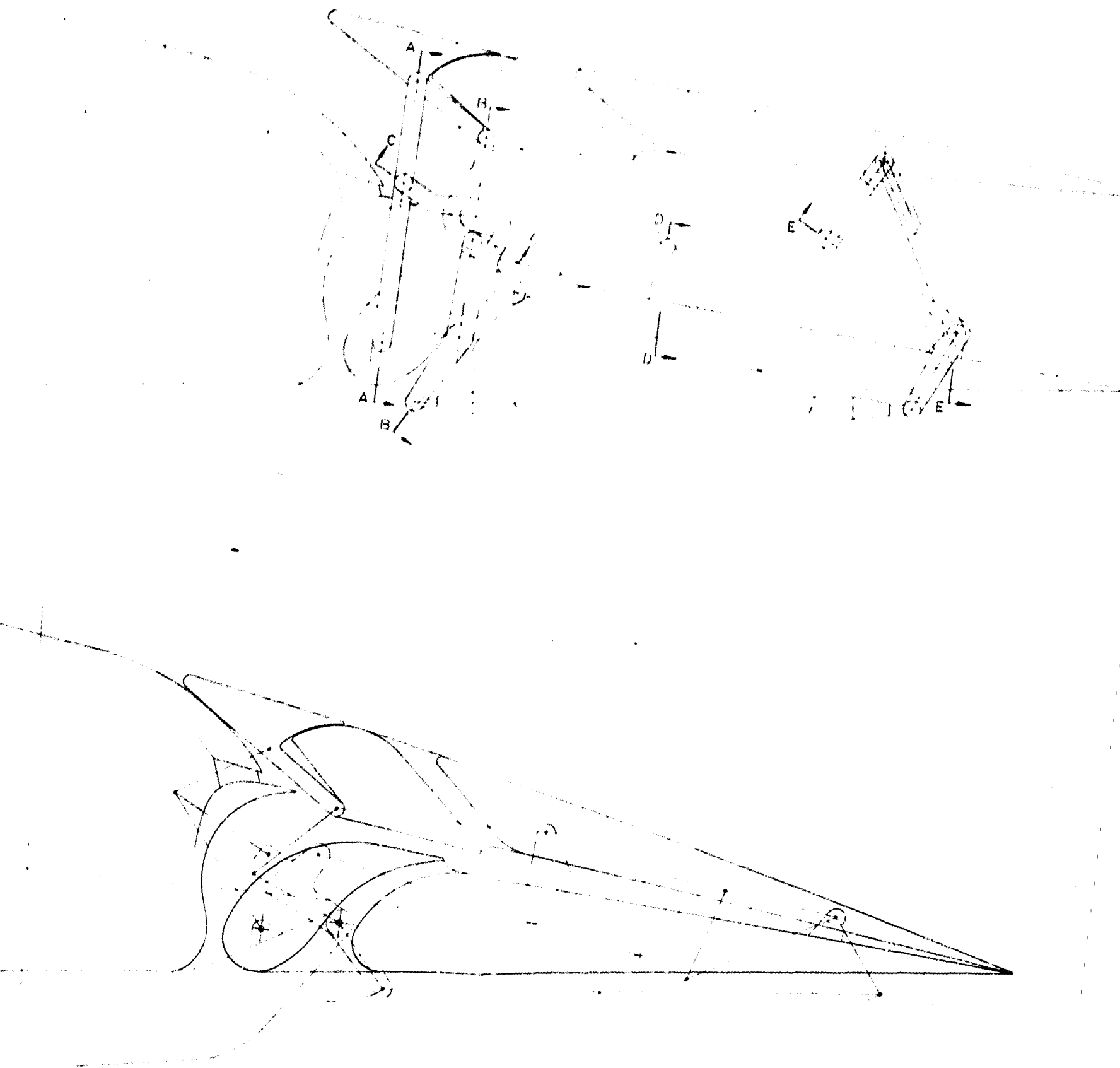
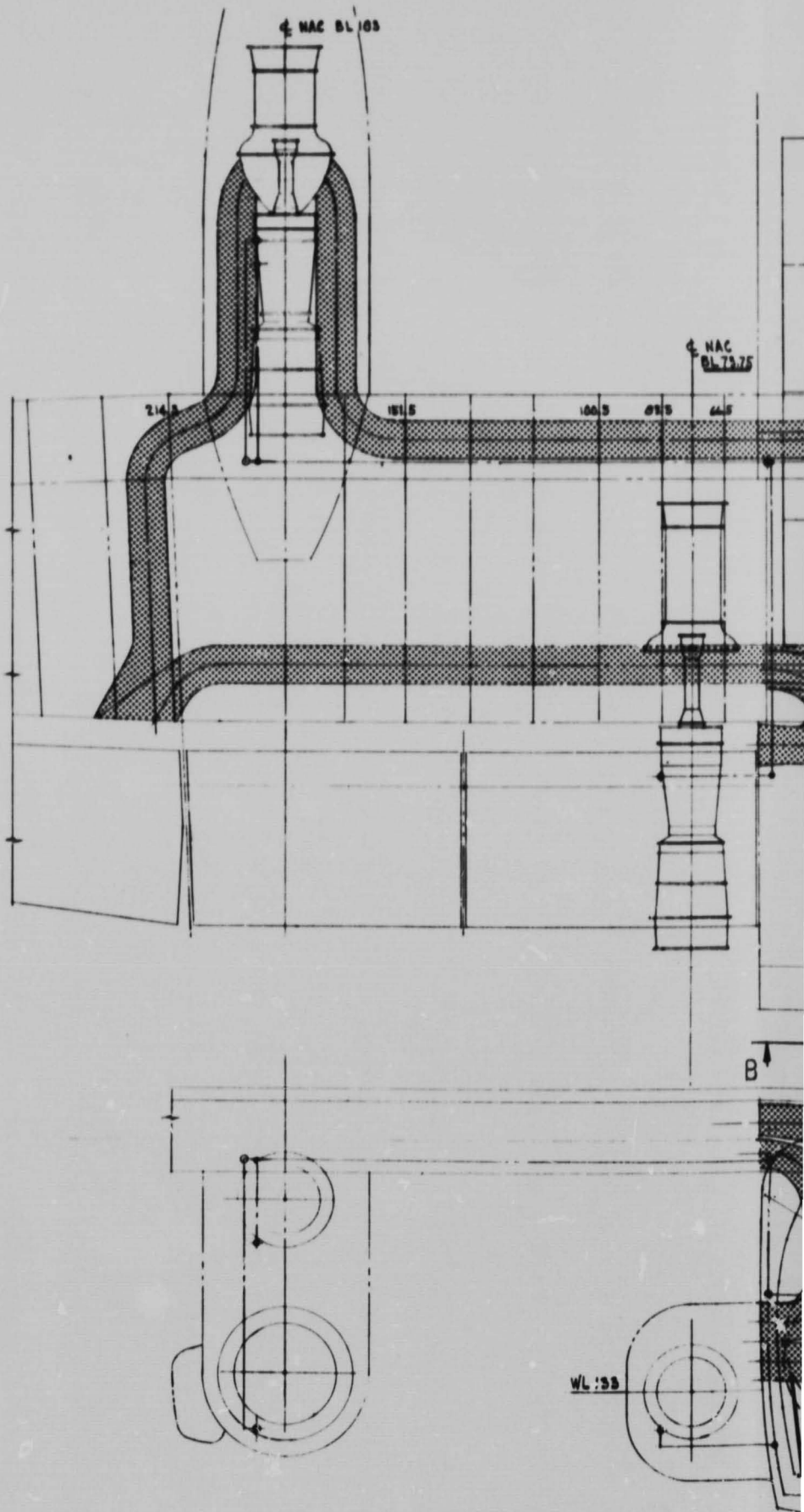


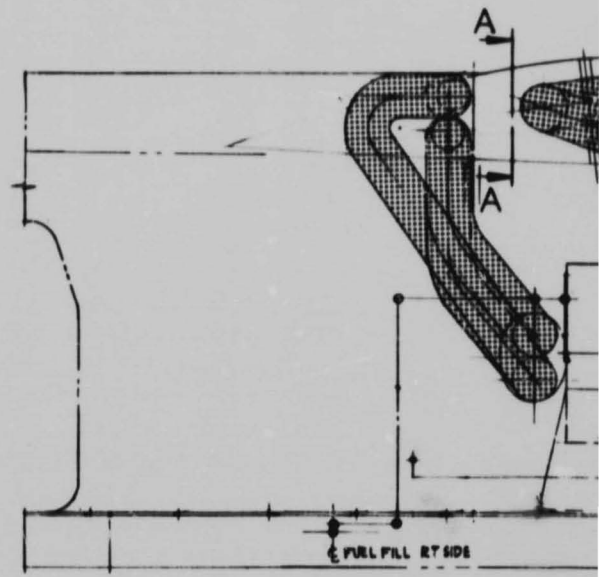
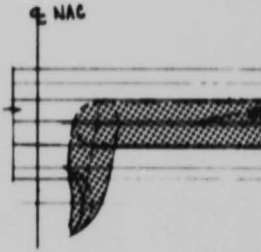
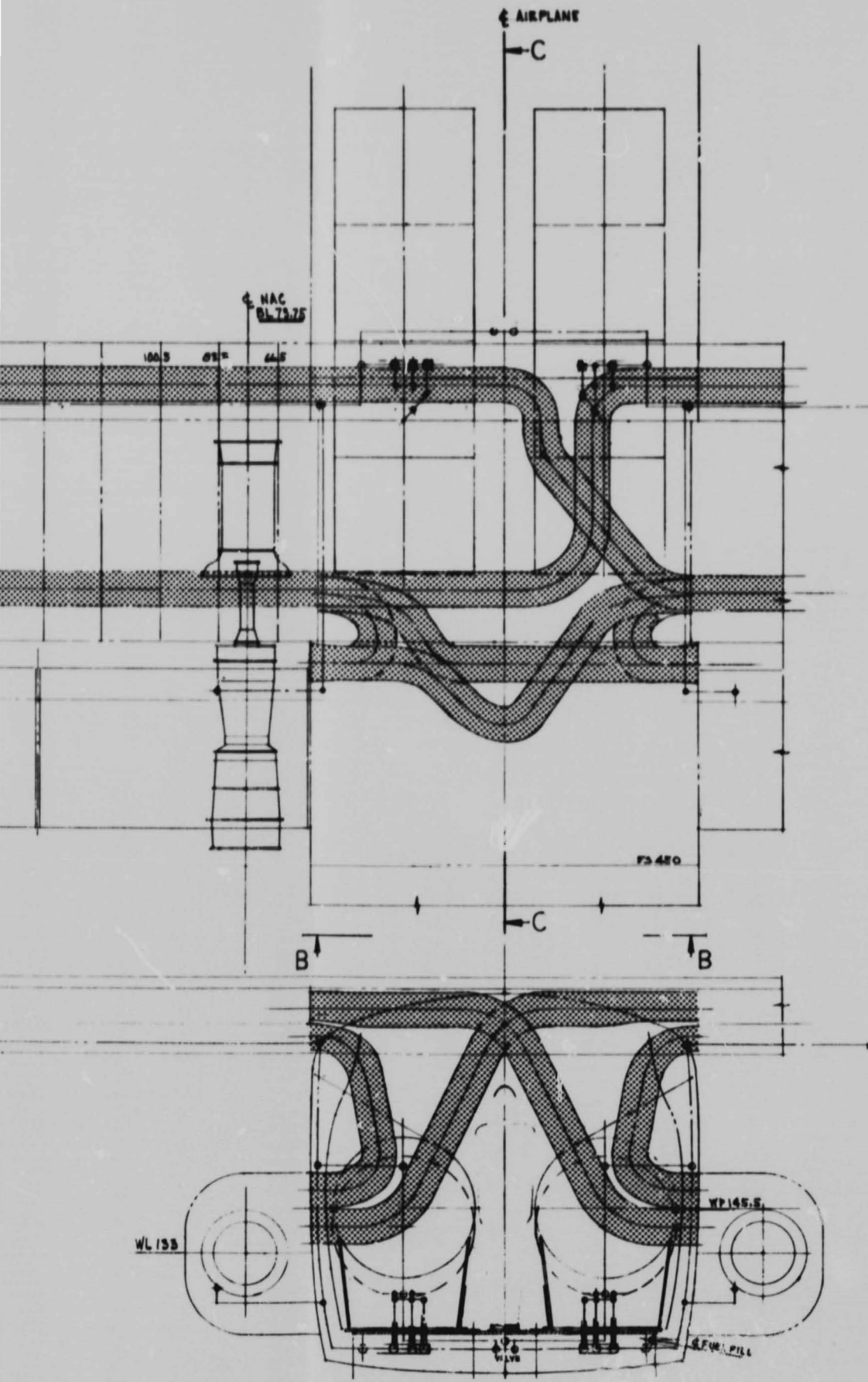
Figure 31. Augmentor Flap and Mechanism.

FOLDOUT FRAME



FOLDOUT FRAME

115-B



SECTI

FOLDOUT FRAME



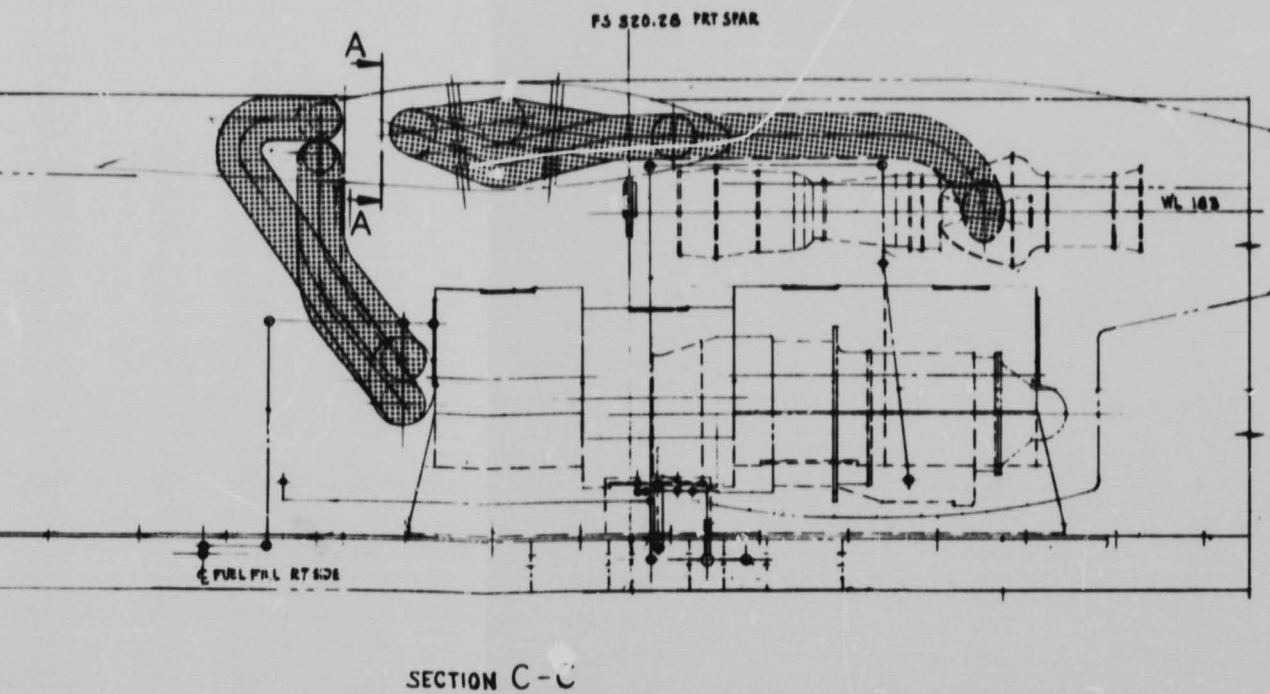
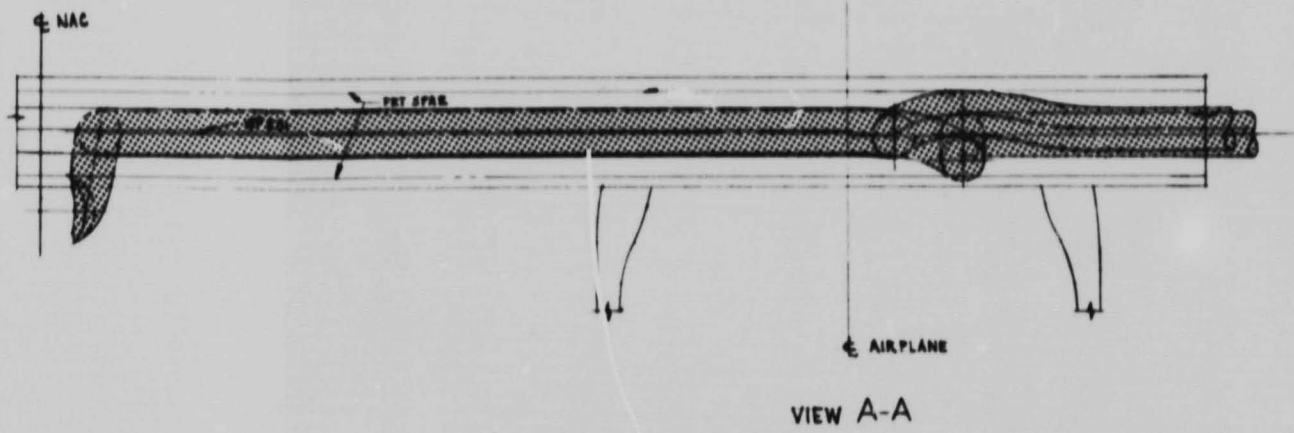


Figure 32. Ducting - Air Supply

FOLDOUT FRAME

**Page intentionally left blank**

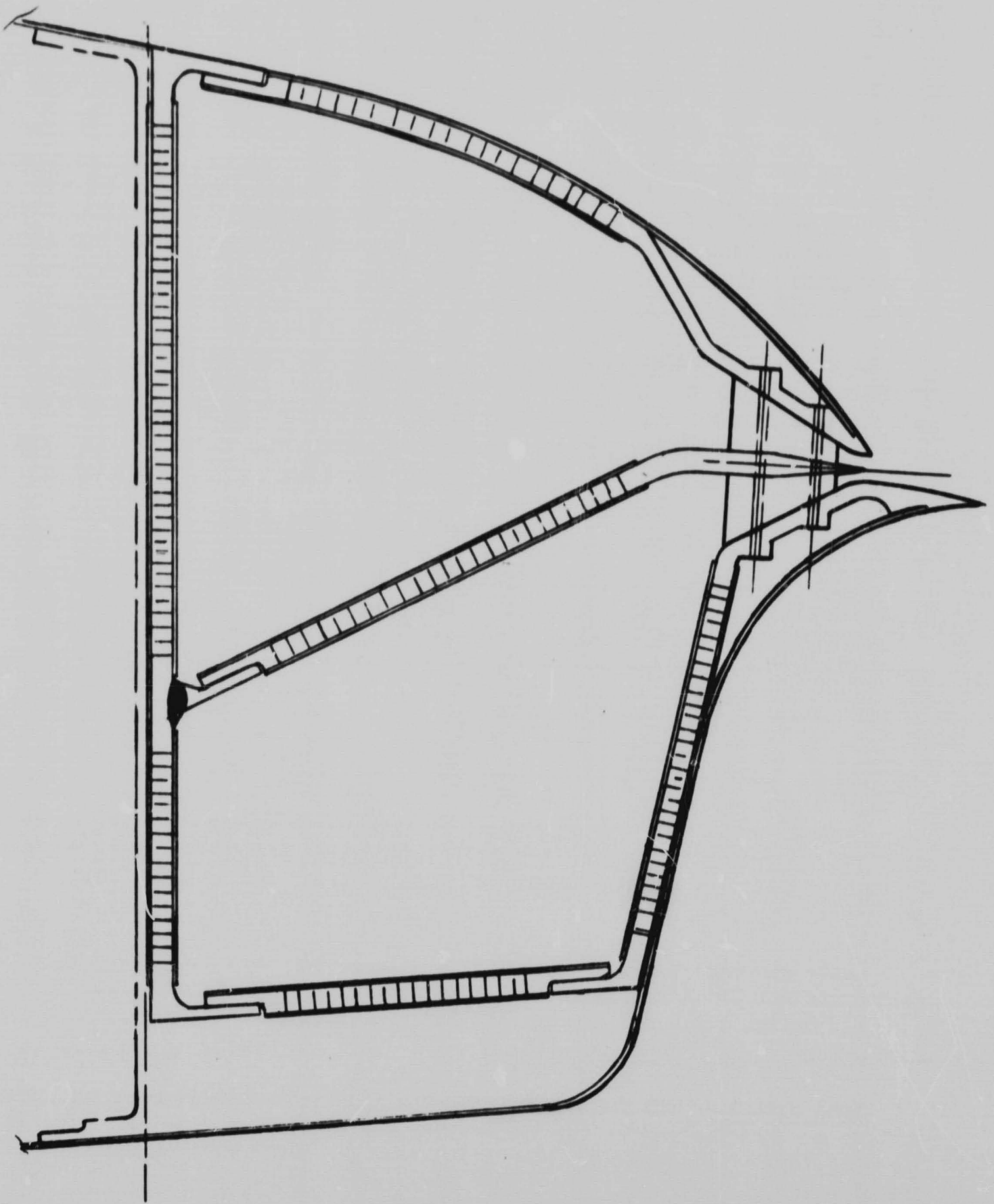


Figure 33. Air Duct - Augmentor-Wing

Each nozzle configuration is essentially the same as that used in the NASA/Ames/de Havilland wind tunnel model program. Tunnel testing by de Havilland has also indicated that the dual plenum chamber with split nozzles will provide essentially the same characteristics as the single-nozzle plenum chamber arrangement used on the NASA/Ames/de Havilland 42-foot augmentor-wing wind tunnel model.

Using the dual-ducting arrangement from each air source, shown in figure 32, permits the use of approximately 10-inch-diameter ducting with an air flow mach number of 0.2 for ducting efficiency calculations. The 10-inch ducting is compatible with the aircraft structure without causing major structural modification problems. Sealed slip joints are used to provide the necessary expansion and to simplify installation.

As shown in figure 32, the aileron BLC air is supplied from two of the compressor ducting systems. Each system supplies air to one half of the aileron span on each side of the wing, thus, insuring a symmetrical change in aileron efficiency in case of an air system malfunction.

### Systems

Engine starting. - Ground starting for all engines will be accomplished by engine-mounted air turbine starters using a ground air source connected at the right-hand outboard nacelle. Cross-ship bleed-air ducting will be used to route air to each engine for starting. A shutoff valve in each engine starter air supply duct will open when starting for that engine is initiated.

Air or ground starting of the flap air engines will utilize bleed air from the Orpheus engines through the cross-ship ducting.

Engine controls. - Cockpit engine controls will be as described under Flight Station Modifications. A single lever will control the power setting on each engine with a lever to control each rotating nozzle for thrust directional control.

Cable routings through the fuselage will follow essentially the same paths as the present CV-7A systems to minimize aircraft modification. The cam tube assembly in the cabin ceiling will be modified for the revised switching requirements.

Fuel system. - The fuel system for the modified aircraft must supply six turbine engines instead of the two turbine engines on the original aircraft. The wing tank provisions have been eliminated and replaced by a cargo bay installation.

The system schematic, shown in figure 34, provides all the basic requirements of an economical and straightforward arrangement. The fuel tanks are floor mounted on each side of the cargo bay separated by approximately a 20-inch isleway. These tank assemblies consist of four aluminum 33-inch long by 40-inch diameter modules welded together. One of these modules is lower than the others, as shown in figure 35, to act as a sump tank. One-way-swing check valves in each intermodule bulkhead permit fuel flow to the sump tank but not back to the other tank sections. Each module contains a normal bladder cell for increased safety. Intermodule venting and system overboard venting is provided.

The sump tanks are interconnected and each contains three fuel pumps. One pump is an electrically driven unit as used on the existing aircraft. The other two are bleed-air-driven pumps as used on the production Buffalo aircraft. This system provides system safety under electrical failure conditions.

The tanks are supported by a cradle assembly attached to the floor and are restrained longitudinally by the cargo tiedown provisions of the basic aircraft. The installation is designed to be compatible with the 200 pounds per square foot floor loading restrictions of the cargo bay.

Refueling and defueling will utilize the present aircraft single-point connector relocated, as necessary, to accommodate the fuselage-mounted nacelles.

Engine bleed air system. - The existing duct system from the wing nacelles to the air-conditioning system in the fuselage will be retained. Bleed-air ducting from the engines in the fuselage-mounted nacelles will tee into the cross-ship ducting to provide air start capabilities to these engines. The outboard nacelle engines will connect with the cross-ship ducting in the same manner as the original installation.

Additional ducting from the cross-ship ducting in the fuselage area will provide air for the air-driven fuel pump operation.

The existing refrigeration package will be retained. Portions of the system may be deactivated, if required.

Hydraulic system. - The hydraulic system for the modified aircraft supplies hydraulic power for the operation of the ailerons, spoilers, rudder, upper and lower flaps, nosewheel steering and brakes.

The proposed hydraulic system is shown to have additional functions when compared with the present system described in reference 5. The comparison is shown in the simplified schematic diagram, figure 36. The system consists of a utility system and a primary system, each deriving power from two engine-driven hydraulic pumps and a self-displacing accumulator. To provide redundancy for flight control functions, both systems are used to operate the

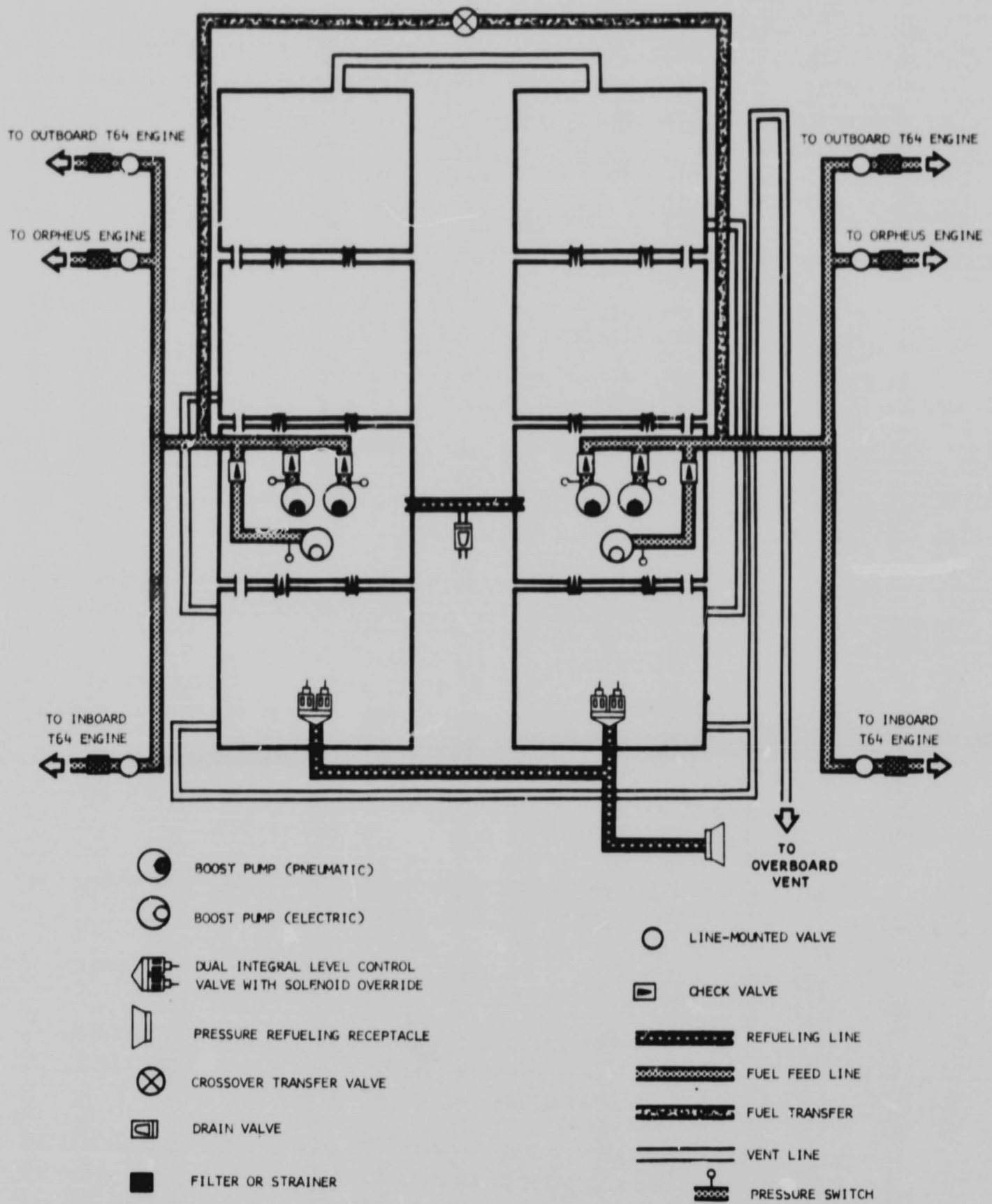


Figure 34. Fuel System Schematic

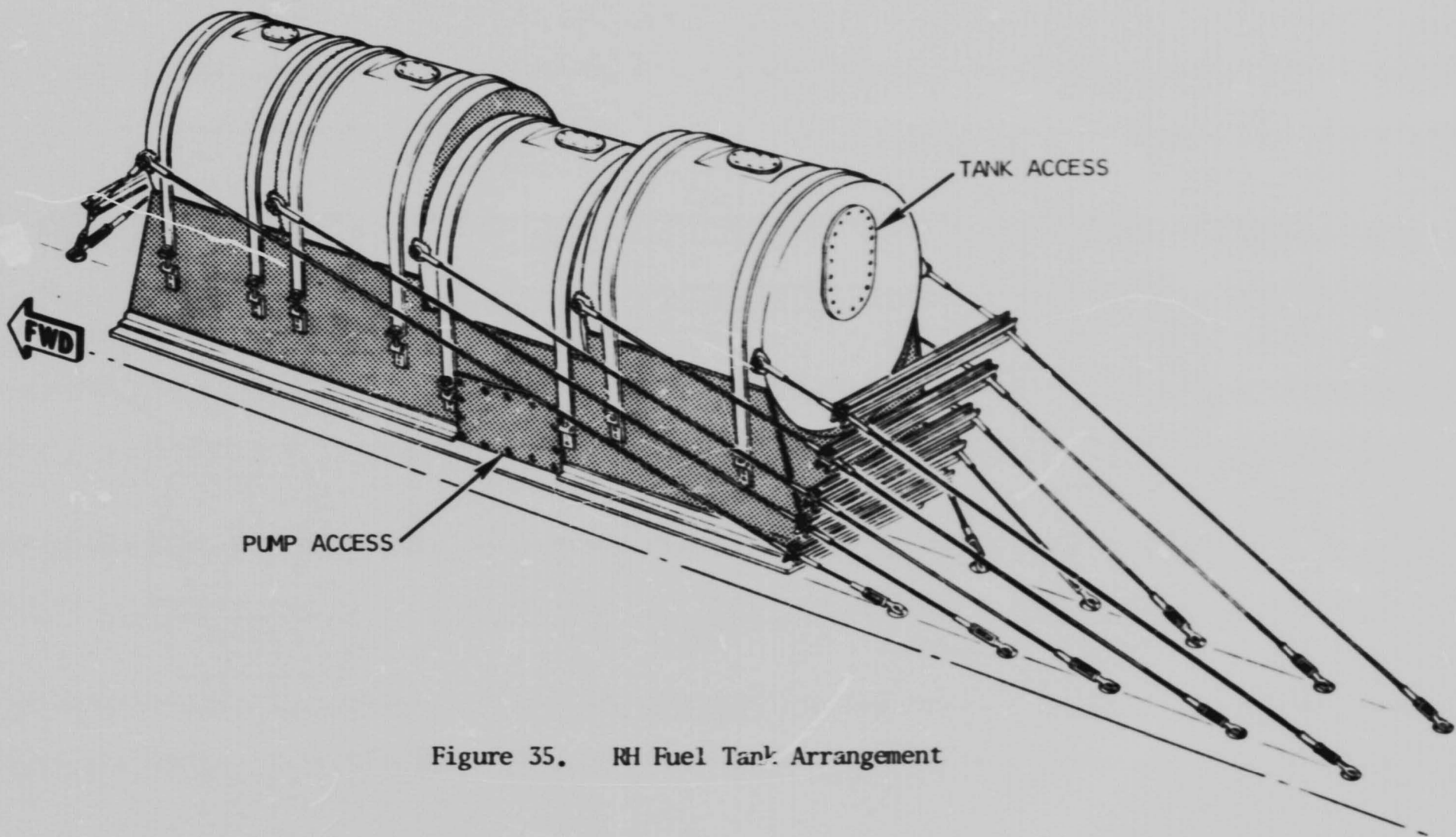


Figure 35. RH Fuel Tank Arrangement

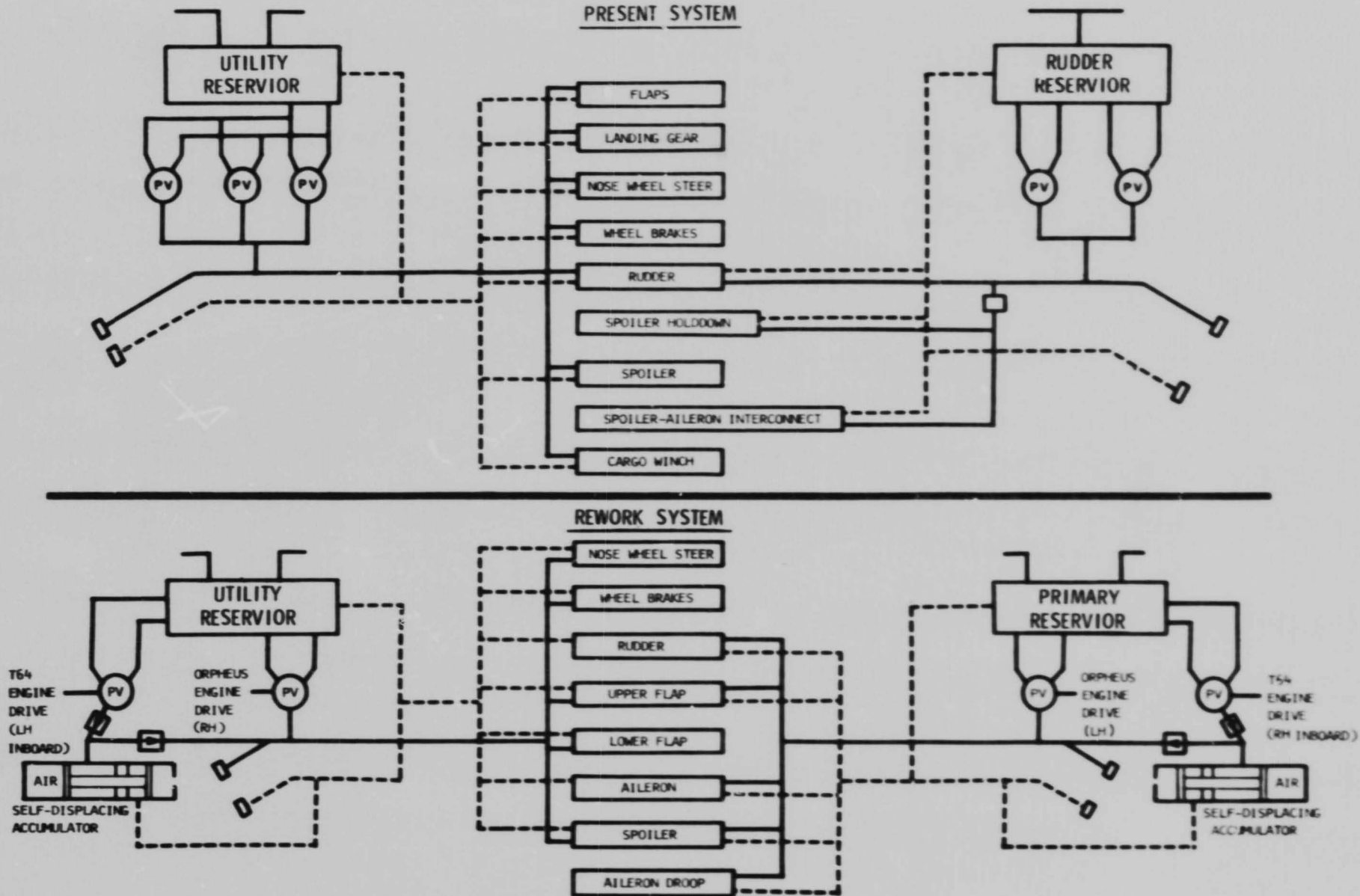


Figure 36. Simplified Hydraulic System Schematic



aileron, spoiler, and rudder by applying hydraulic power to separate sections of dual tandem actuators. In addition, the utility system supplies power to the brakes, steering, lower flaps, and a portion of the upper flaps. The remaining cylinders of the upper flaps and the aileron droop actuator are powered by the primary system. Since the cargo winch will not be operated, and the landing gear will remain extended and pressurized during flight, these services will not be considered in the hydraulic load analysis.

A detailed schematic diagram of the proposed hydraulic system is shown in figure 37.

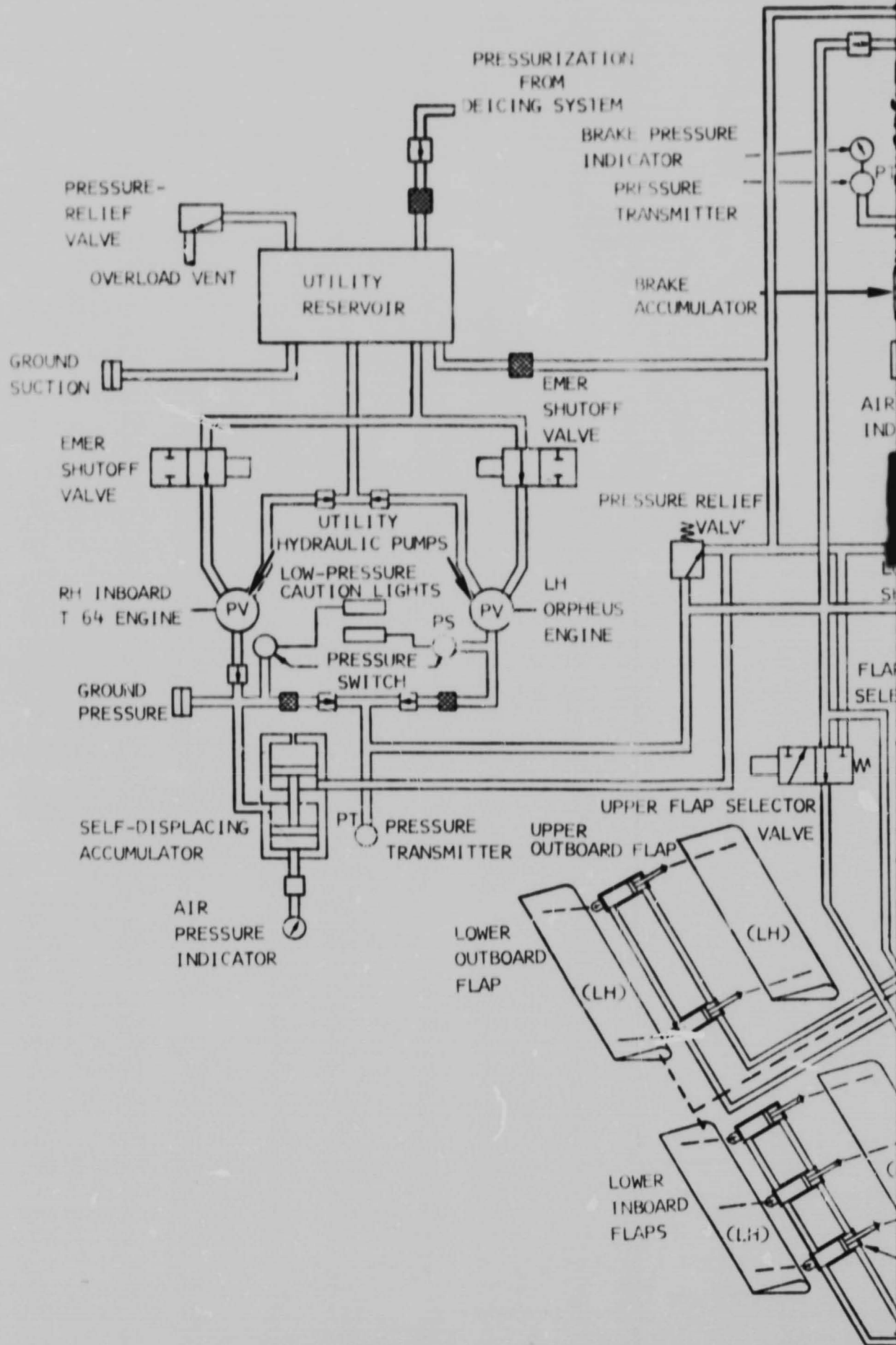
The utility system supplies power to the primary flight control surfaces (rudder, aileron, and spoiler), nosewheel steering, brakes, and flaps as shown in figures 36 and 37. The power is supplied by two pumps: a Lockheed Mark 8 hydraulic pump capable of 8.1 gpm at 4,460 rpm (maximum engine speed driven by one of the two Orpheus engines) and a New York Airbrake hydraulic pump (P/N 65W01022) taken from the present rudder system and capable of 3.7 gpm at 4,421 rpm (maximum engine speed) driven by one of the two inboard T64 engines. A 100-cubic-inch self-displacing accumulator is placed in the T64 engine-driven pump pressure line to meet peak flow rate demands during flight. Each pump is supplied through a suction line from a 2.32-gallon reservoir which is pressurized at 18 to 22 psi with air from the bleed-air system. The fluid is delivered through a system filter to the various functions at a nominal 3,000 psi. A relief valve is provided to relieve any excessive pressure buildup. The pump pressure warning lights and emergency shutoff valves will be identical to the present system. In general, the utility hydraulic power supply system is very similar to the present de Havilland Buffalo system (figures 36 and 37), except for the addition of the accumulator. Rework would include the removal of the auxiliary power unit, and the relocation and replacement of the system pumps.

The primary hydraulic system powers the primary flight control functions of the rudder, aileron, and spoiler control surfaces. The power is supplied by two pumps identical to the utility system, but driven by the symmetrically opposite engines as shown in figure 37. Due to the increased load requirements, a portion of the present rudder system will be modified to form a part of the primary system. These modifications include enlarging the reservoir to 2.32 gallons (same as utility reservoir) increasing line sizes, adding a 100-cubic-inch self-displacing accumulator, and installing a different pump arrangement.

The augmentor flaps require actuation of both the lower flaps and upper flaps (figure 37). The lower flaps will be actuated by the present flap system modified to meet requirements indicated in figure 38. The plan is to use the present hydraulic flap motor but provide the increased power by driving

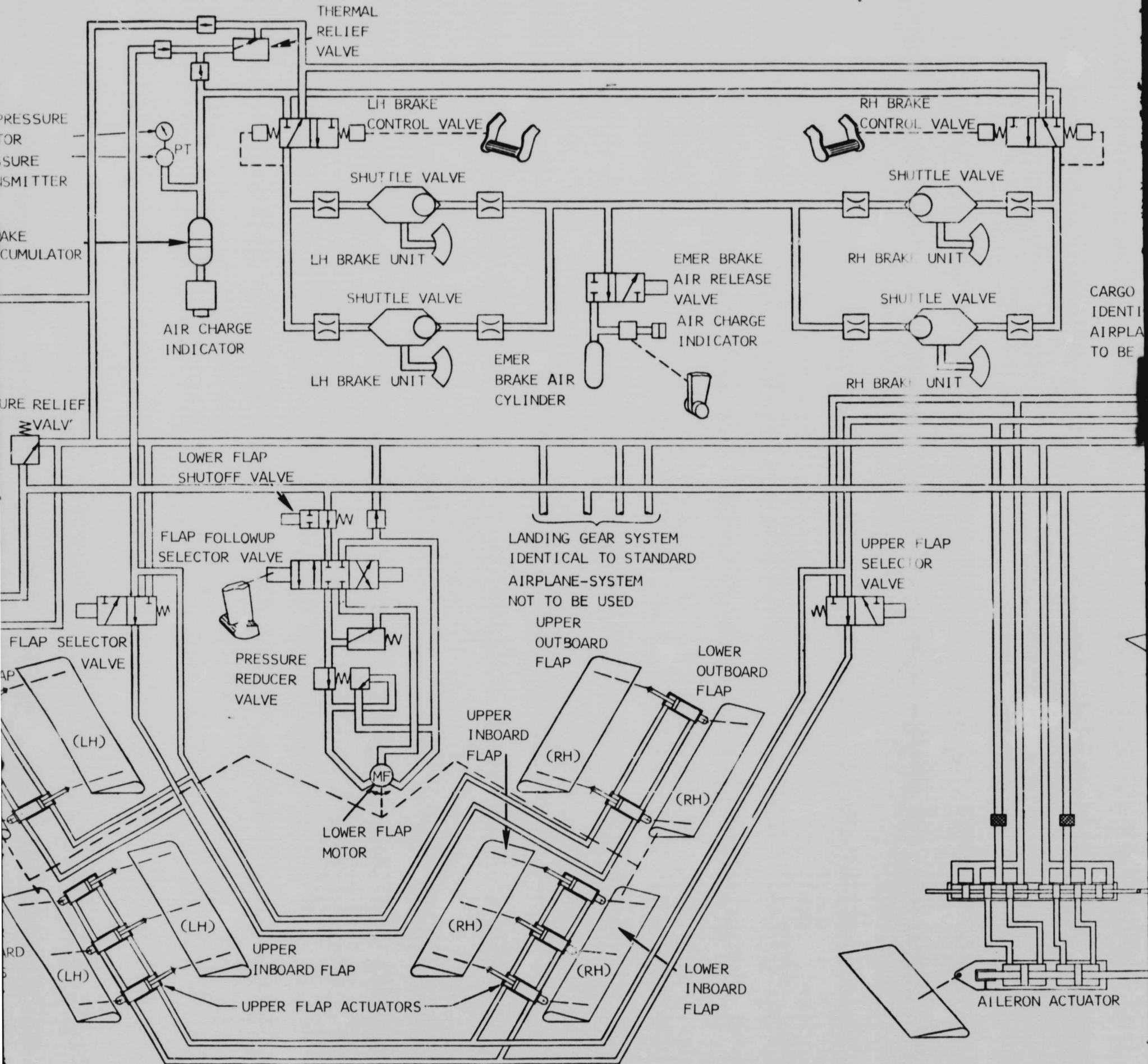
125-A

PRECEDING PAGE BLANK NOT FILMED.



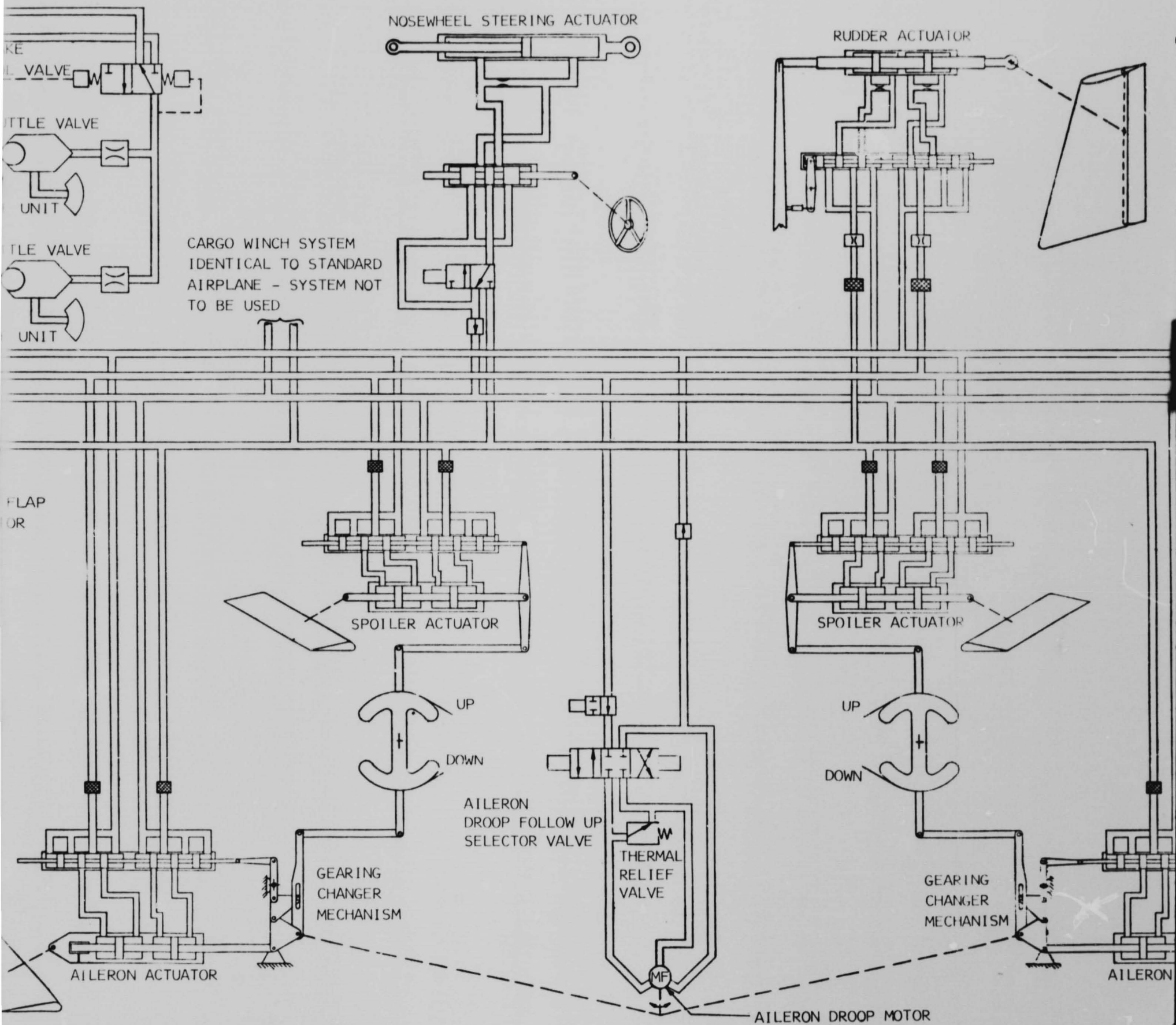
FOLDOUT FRAME

125-B



FOLDOUT FRAME

125-C



CARGO WINCH SYSTEM  
IDENTICAL TO STANDARD  
AIRPLANE - SYSTEM NOT  
TO BE USED

FLAP  
OR

FOLDOUT FRAME

125-D

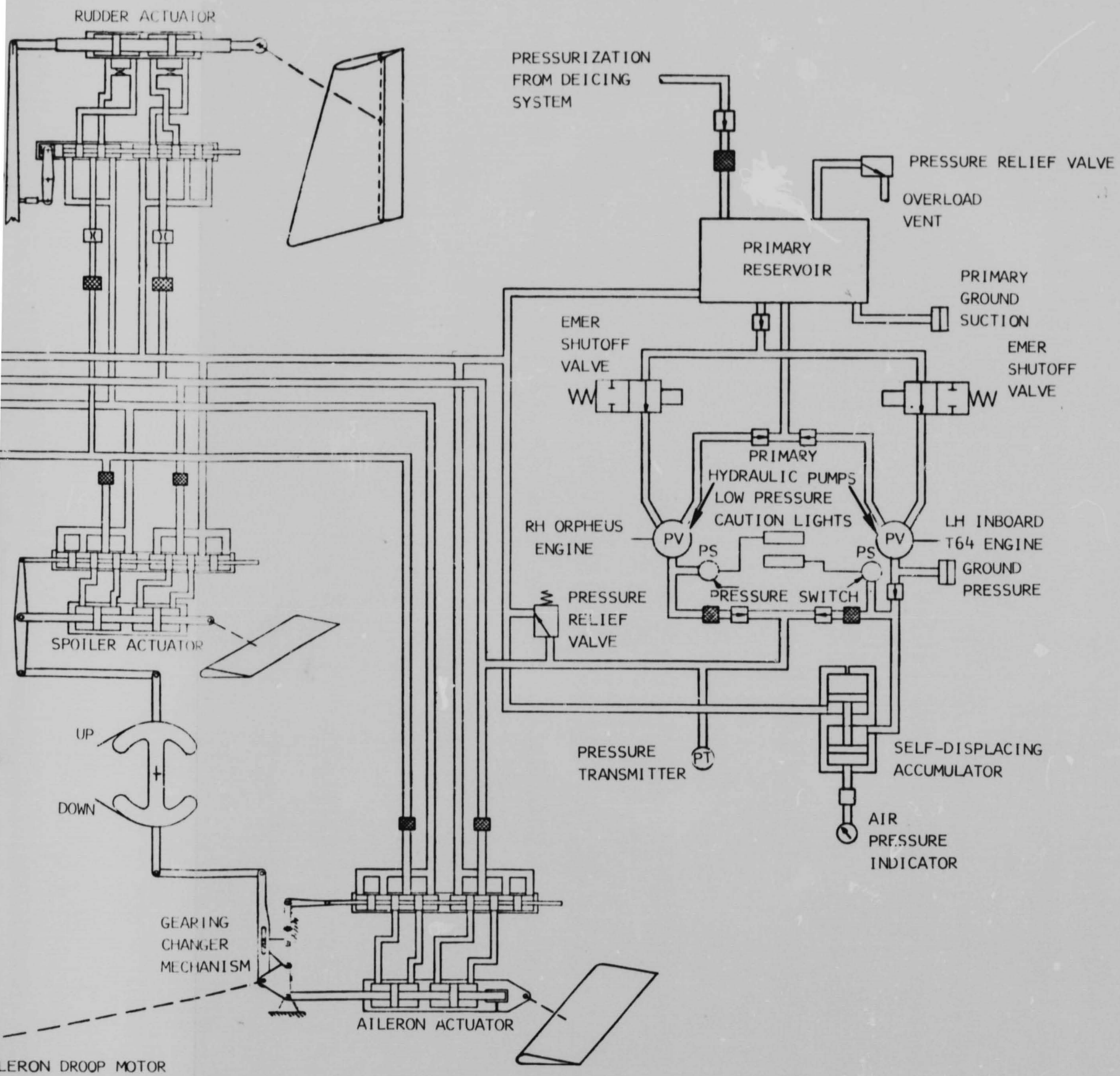


Figure 37. Detail Schematic - Hydraulic System

FOLDOUT FRAME

PRECEDING PAGE BLANK NOT FILMED.

$$\begin{aligned}HM_{MAX} &= -322.1 \text{ IN.LB/IN.} \times 2 (147.6 + 97.8)/\text{AIRPLANE} \\ &= (-322.1)(490.8) \\ &= 158,000 \text{ IN.-LB}\end{aligned}$$

$$\text{RATE} = 8^\circ/\text{SEC}$$

$$\begin{aligned}HP &= \frac{HM \text{ RATE}}{378,150} \times \frac{1}{\text{EFF}} \\ &= \frac{(158,000)(8)}{378,150} \cdot \frac{1}{.80} \\ &= \underline{4.2} \leftarrow\end{aligned}$$

$$\begin{aligned}Q &= \frac{1,714.6 \text{ HP}}{(\text{PSI})(\text{EFF})} \\ &= \frac{(4.2)(1,714.6)}{(2,000)(0.9)} = \underline{4.0 \text{ GPM}}\end{aligned}$$

Figure 38. Lower Flap Hydraulic Power Requirements

the motor at a higher speed. The larger flow rate dictates larger lines, a larger pressure reducer, shutoff valve, and flap selector valve. The upper flaps are actuated by five actuators per wing which are pressurized at all times. The two actuators on the outboard flap, are powered by the utility system and the three actuators, on the inboard flap, by the primary system. Two electrically operated three-way valves control the actuators in each system. The requirements of each actuator, and thus of each system, are shown in figure 39. Since the actuation of the upper flaps is not concurrent with the lower flaps, the upper flap load requirements are not considered in the hydraulic load analysis.

The present spoiler system as shown in figure 2.7.3 of reference 5 will be modified by removing the hold-down actuators, lock-in quadrants, and landing mode select valves, and replacing the single system actuators with dual-tandem actuators.

Ten micron (absolute) filters will be placed in the pressure lines to protect the servo valves. The flight requirements for the actuators are shown in figure 40, and the two critical design points are indicated in figure 41.

The rudder actuator will not be modified but flow rate requirements were calculated (figure 42) to conduct a complete load analysis for the total hydraulic system. It should be noted that the rudder actuation is reduced from two-thirds of a cycle per second to one-third of a cycle per second.

The aileron system will be actuated by two new dual-tandem actuators. To size the actuator, the aerodynamic requirements of down aileron and up aileron are considered for both up-flap and down-flap conditions as shown in figure 43. Two critical points, shown in figure 44, for the down-flap condition, were used to size the actuator.

The additional aileron droop and gearing changer mechanism requires a hydraulic motor, a selector valve, and a thermal relief valve. This system is connected into the primary system but the flow rate required is negligible due to the low load and actuation requirements. Thus, the aileron droop and gearing changer mechanism is not considered in the hydraulic load analysis.

No changes are contemplated for the brake and steering subsystem. For the hydraulic load analysis (tables XXI and XXII), the flow rate required for the steering system is based on information supplied by de Havilland. The brake flow rate requirements are chosen with consideration given to the potential energy available from the present hydraulic accumulator and the emergency air bottle. (See figure 2.7.3 of reference 5 and figure 37.)

The hydraulic load analysis indicates the flow rate required and the flow rate available with both thrust engines operating (tables XXI and XXII).

STROKE = 4.5 INCHES IN  $\approx$  2 SECONDS

LOAD:

42 LB/IN. (74 IN.) = 3108 LB

$$HP = \frac{(LOAD)(STROKE)}{6,600 (TIME)}$$

$$HP = \frac{(3108)(4.5)}{(6,600)(2)} = 1.09 \text{ HP}$$

$$Q = \frac{HP (1714)}{P}$$

$$Q = \frac{1.09(1714)}{3,000} = 0.62 \text{ GPM}$$

$$\underline{(Q) \text{ PRIMARY}} = (6)(0.62) = \underline{3.72 \text{ GPM}}$$

$$\underline{(Q) \text{ UTILITY}} = (4)(0.62) = \underline{2.48 \text{ GPM}}$$

Figure 39. Upper Flap Hydraulic Power Requirements



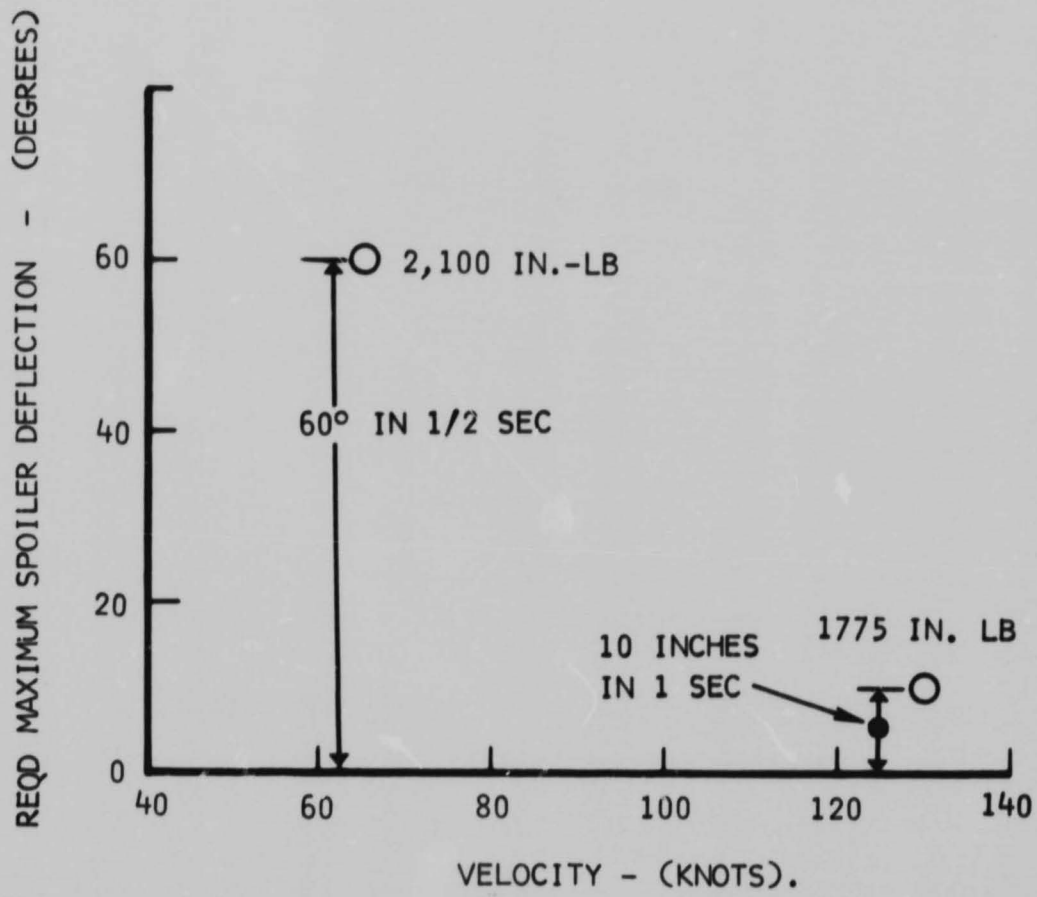
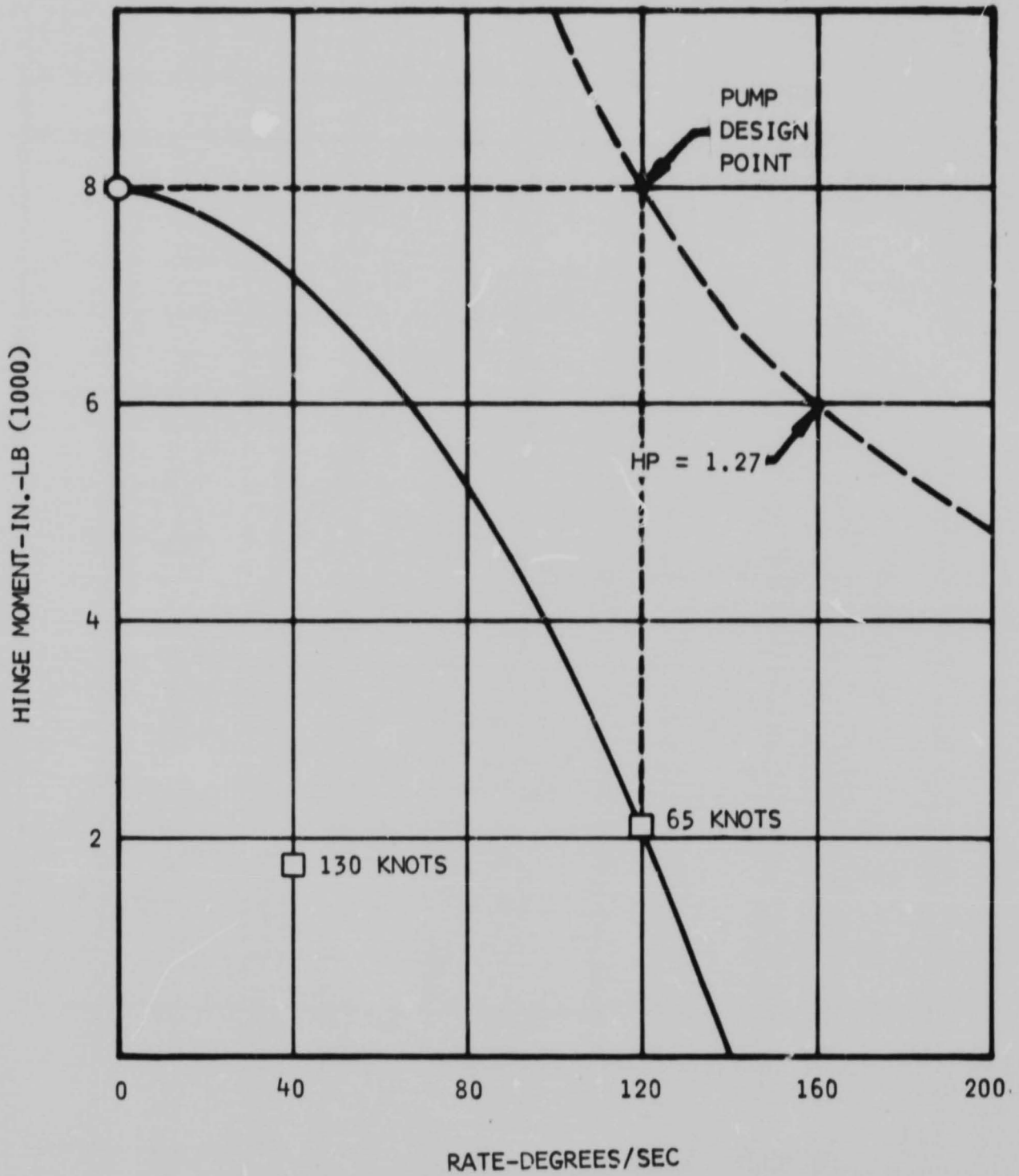


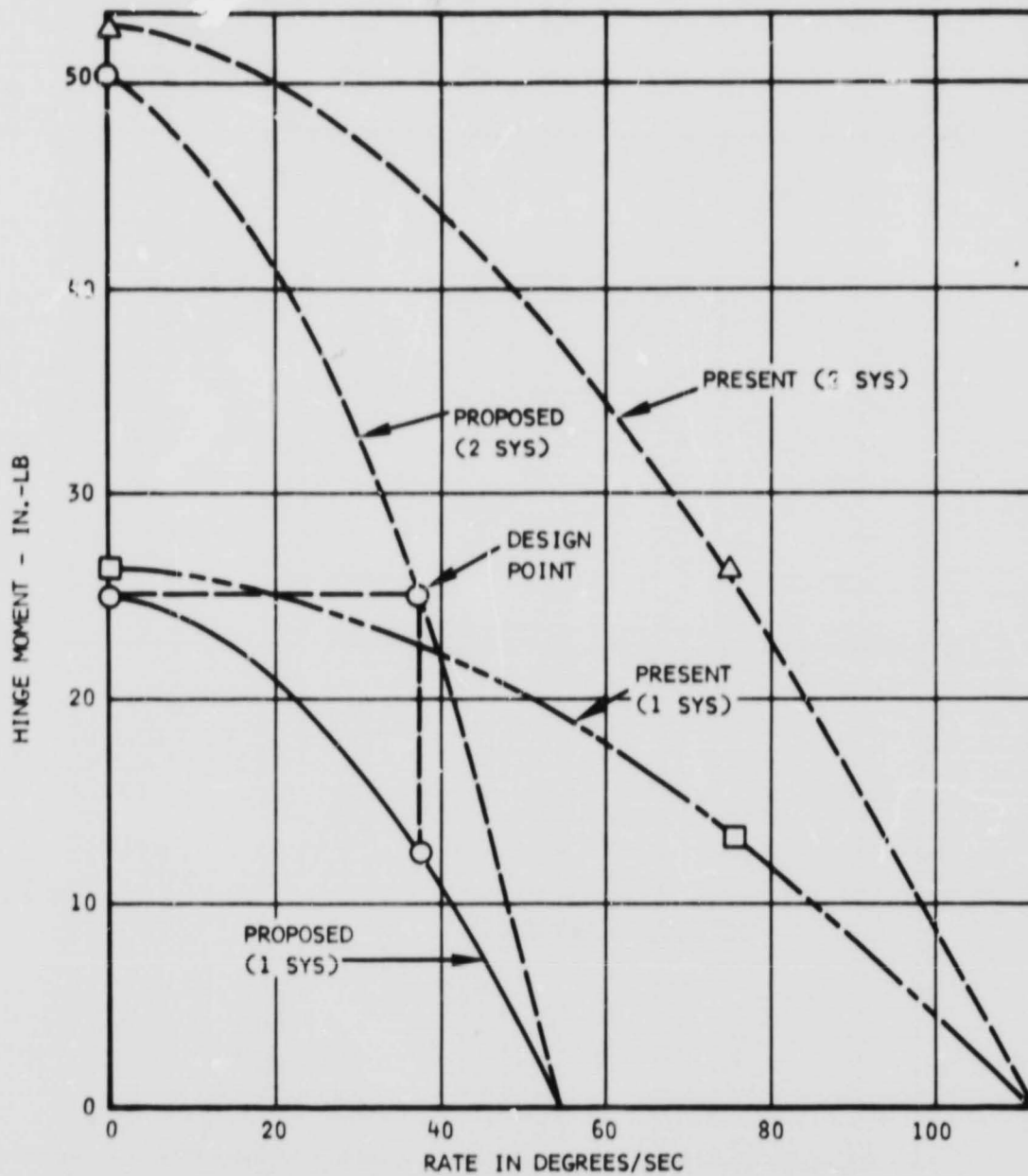
Figure 40. Spoiler Deflection Requirements



$$\begin{aligned}
 Q &= \frac{(HM)(RATE)}{P} \\
 &= \frac{(8,000)(120^\circ) \frac{\pi}{180} \frac{60}{231}}{3,000} \\
 &= 1.46 \text{ GPM/SYS} \\
 &= 2.8 \text{ GPM/AIRPLANE}
 \end{aligned}$$

$$\begin{aligned}
 HP &= \frac{(HM)(RATE)}{378,150} \\
 &= \frac{(8,000)(120)}{378,150} \\
 &= 2.54/\text{SYS}
 \end{aligned}$$

Figure 41. Spoiler Power Requirements



GIVEN HM = 50,400 IN.-LB (2 SYS)

RATE = 37 1/2 °/SEC

$$Q = \frac{(25,200)(37.5)}{3,000} \frac{\pi}{180} \frac{60}{231}$$

$$Q = 1.43 \text{ GPM}$$

$$HP = \frac{(3,000)(1.43)}{1,714} = 2.5 \text{ HP}$$

GIVEN Q = 3 GPM; RATE = 75°/SEC

$$HM = \frac{PQ}{\text{RATE}} = (3,000)(3) \frac{231}{60} \frac{180}{\pi}$$

$$= 26,420 \text{ IN.-LB (1 SYS)}$$

$$HP = \frac{(26,420)(75)}{378,150}$$

$$= 5.25$$

Figure 42. Rudder Power Requirements

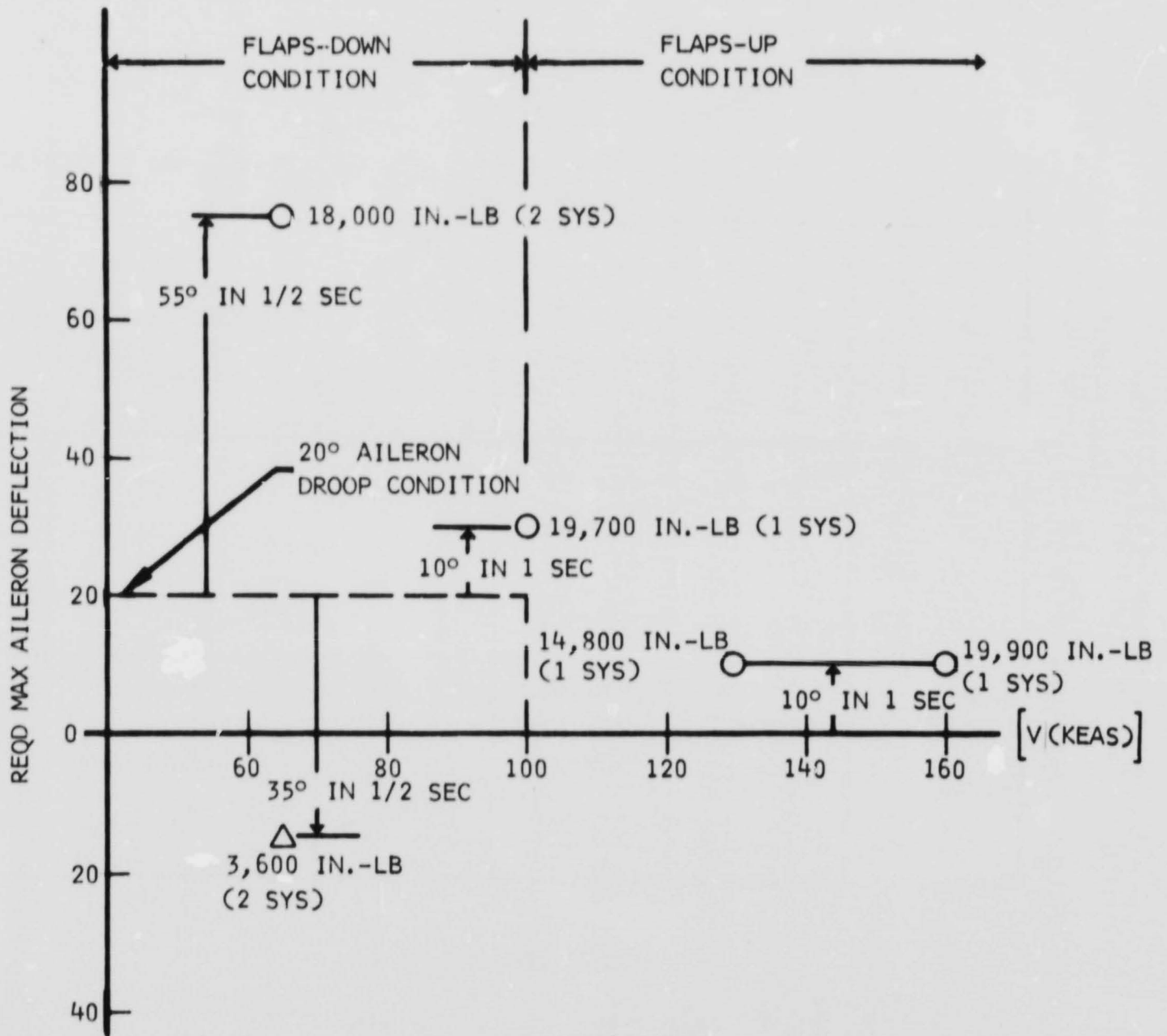
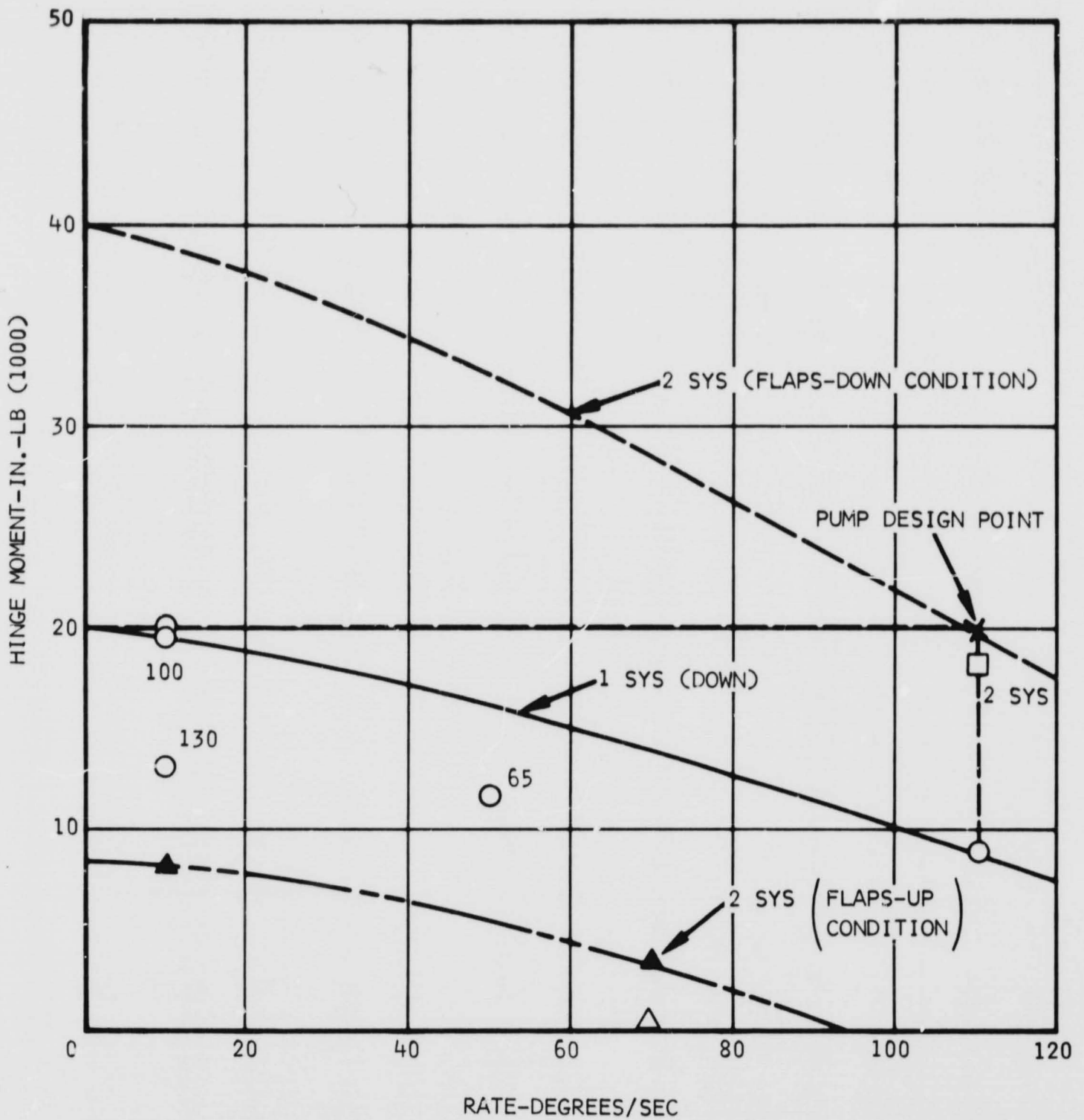


Figure 43. Aileron Deflection Requirements



$$Q_P = \frac{(20,000)(110)}{3,000} \frac{\pi}{180} \frac{60}{231}$$

$$= 3.33 \text{ GPM}$$

$$\frac{1.67}{5.00 \text{ GPM/SYS}}$$

$$10.0 \text{ GPM/AIRPLANE}$$

$$HP = \frac{(20,000)(110)}{378,150} = 5.82 \text{ HP}$$

$$Q_P = \frac{HP (1714)}{P} = 3.33 \text{ GPM}$$

Figure 44. Aileron Actuator Requirements

TABLE XXI. LOAD ANALYSIS - UTILITY HYDRAULIC SYSTEM

FUNCTION SYSTEM	TAXI	TAKEOFF AND CLIMB		CRUISE	DESCENT		ROLL	
		ROLL	CLIMB		INITIAL	FINAL	INITIAL	FINAL
	GPM	GPM	GPM	GPM	GPM	GPM	GPM	GPM
BRAKES (EMERGENCY)	0.5	0	0	0	0	0	0	0.5 (4.0)
NOSE WHEEL STEERING	1.0	2.5	0	0	0	0	0	2.5
FLAPS	4.0	0	0	4.0	4.0	0	0	0
SPOILER	0	1.5	1.5	0.6	1.0	1.5	1.5	0
AILERON	0	5.0	5.0	1.2	2.5	5.0	5.0	0
RUDDER	0	0	1.5	0.3	0.7	1.5	1.5	0
INTERNAL LEAKAGE	0.25	0.25	0.25	0.25	0.25	0.25	0.25	0.25
REQUIRED SIMULTANEOUS FLOW	5.75	9.25	8.25	6.35	8.45	8.25	8.25	3.25

FLOW SOURCE	PUMP CAPACITY (GPM)							
ORPHEUS (% ENGINE SPEED)	3.25 (40%)	8.1 (100%)	8.1 (100%)	7.65 (94.5%)	6.1 (75%)	4.85 (60%)	4.05 (50%)	2.85 (35%)
T64 (DIRECT)	0	3.7	3.7	0	3.7	3.7	3.7	0
AVAILABLE TOTAL FLOW	3.25	11.8	11.8	7.65	9.8	8.55	7.75	2.85
T64 ACCUMULATOR REQUIREMENT	2.50	0	0	0	0	0	0.5	0.40

TABLE XXII. LOAD ANALYSIS - PRIMARY HYDRAULIC SYSTEM

FUNCTION SYSTEM	TAXI	TAKEOFF AND CLIMB		CRUISE	DESCENT		ROLL	
		ROLL	CLIMB		INITIAL	FINAL	INITIAL	FINAL
	GPM	GPM	GPM	GPM	GPM	GPM	GPM	GPM
SPOILER	0	1.5	1.5	0.6	1.0	1.5	1.5	0
AILERON	0	5.0	5.0	1.2	2.5	5.0	5.0	0
RUDDER	0	0	1.5	0.3	0.7	1.5	1.5	0
INTERNAL LEAKAGE	0.25	0.25	0.25	0.25	0.25	0.25	0.25	0.25
REQUIRED SIMULTANEOUS FLOW	0.25	6.75	8.25	2.35	4.45	8.25	8.25	0.25

FLOW SOURCE	PUMP CAPACITY (GPM)							
ORPHEUS (% ENGINE SPEED)	3.25 (40%)	8.1 (100%)	8.1 (100%)	7.65 (94.5%)	6.1 (75%)	4.85 (60%)	4.05 (50%)	2.85 (35%)
T64 (DIRECT)	0	3.7	3.0	0	3.7	3.7	3.7	0
AVAILABLE TOTAL FLOW	3.25	11.8	11.8	7.65	9.8	8.55	7.75	2.85
T64 ACCUMULATOR REQUIREMENT	0	0	0	0	0	0	0.5	0

The utility system hydraulic load analysis is shown in table XXI. Sufficient pump flow rate is available to handle the required flow rate during all phases of operation except taxi and initial roll upon landing. The deficiency during taxi is tolerable since it only means a slow actuation rate for the wing flaps. The deficiency during roll will be taken care of by fluid energy stored in the self-displacing accumulator.

The hydraulic load analysis for the primary system is shown in table XXII. It also indicates a deficiency during initial roll upon landing. This deficiency will also be met by accumulator fluid discharge.

As described above, the 100-cubic-inch accumulator in each system supplements the hydraulic pumps during periods of peak demand. Table XXIII shows the maximum number of applications possible for various combinations of services for each hydraulic system.

Table XXIV shows the hydraulic load analysis when one thrust engine is inoperative during landing phase. The function flow rate requirements are based on aerodynamic requirements for two conditions. One condition, when the thrust engine nozzle is pointing aft, requires full rudder, three-quarter spoiler, and three-quarter aileron. The other condition requires full aileron and minor rudder inputs, and occurs when the thrust engine nozzle is vertical. The noted deficiency in flow rate is to be overcome by the self-displacing accumulators in each system.

Hazard protection. - Compartmentation requirements for the new engine arrangement were evaluated relative to the fire detection and extinguishing capabilities necessary for the research vehicle. This tentatively resulted in the identification of six fire zones (each engine compressor compartment) where both fire detection and extinguishing will be required, and six zones (each engine hot section and tailpipe) where only detection of overheat or engine burnthrough is required.

Coverage of the above zones requires 12 fire-detection loops and cockpit indicator circuits. Six of the present CV-7A type tee-handles in the cockpit, one for each engine, will indicate and locate the hazardous condition. If a compressor compartment fire is indicated, the pilot will shut down that engine and discharge the extinguisher to that compartment. If the fire condition continues, a second extinguisher shot is available. If a hot section overheat is indicated, engine shutdown will correct the problem.

The increased number of fire zones and the increased compartment volume to be covered will require additional extinguisher storage quantity and distribution equipment.



TABLE XXIII. SELF-DISPLACING ACCUMULATOR CAPACITY

I. UTILITY SYSTEM

FUNCTIONS IN SERVICE	NUMBER OF APPLICATIONS
AILERON SPOILER	6
AILERON SPOILER RUDDER	4
AILERON SPOILER STEERING	4
AILERON SPOILER STEERING RUDDER	3

II. PRIMARY SYSTEM

FUNCTIONS IN SERVICE	NUMBER OF APPLICATIONS
AILERON SPOILER	6
AILERON SPOILER RUDDER	4

TABLE XXIV. HYDRAULIC LOAD ANALYSIS DURING DESCENT

I. ENGINE NOZZLE POINTING AFT

	FUNCTION	DESCENT FLOW RATE (GPM)**
REQUIRED	FULL RUDDER	1.5
	3/4 AILERON	3.75
	3/4 SPOILER	1.12
	SIMULTANEOUS	6.37
AVAILABLE	T64 (DIRECT)	3.7
	T64 ACCUMULATOR REQUIREMENT	2.67

II. ENGINE NOZZLE POINTING VERTICALLY DOWN

	FUNCTION	DESCENT FLOW RATE (GPM)**
REQUIRED	FULL AILERON	5.0
	RUDDER	0.5
	SIMULTANEOUS	5.5
AVAILABLE	T64 (DIRECT)	3.7
	T64 ACCUMULATOR REQUIREMENT	1.8

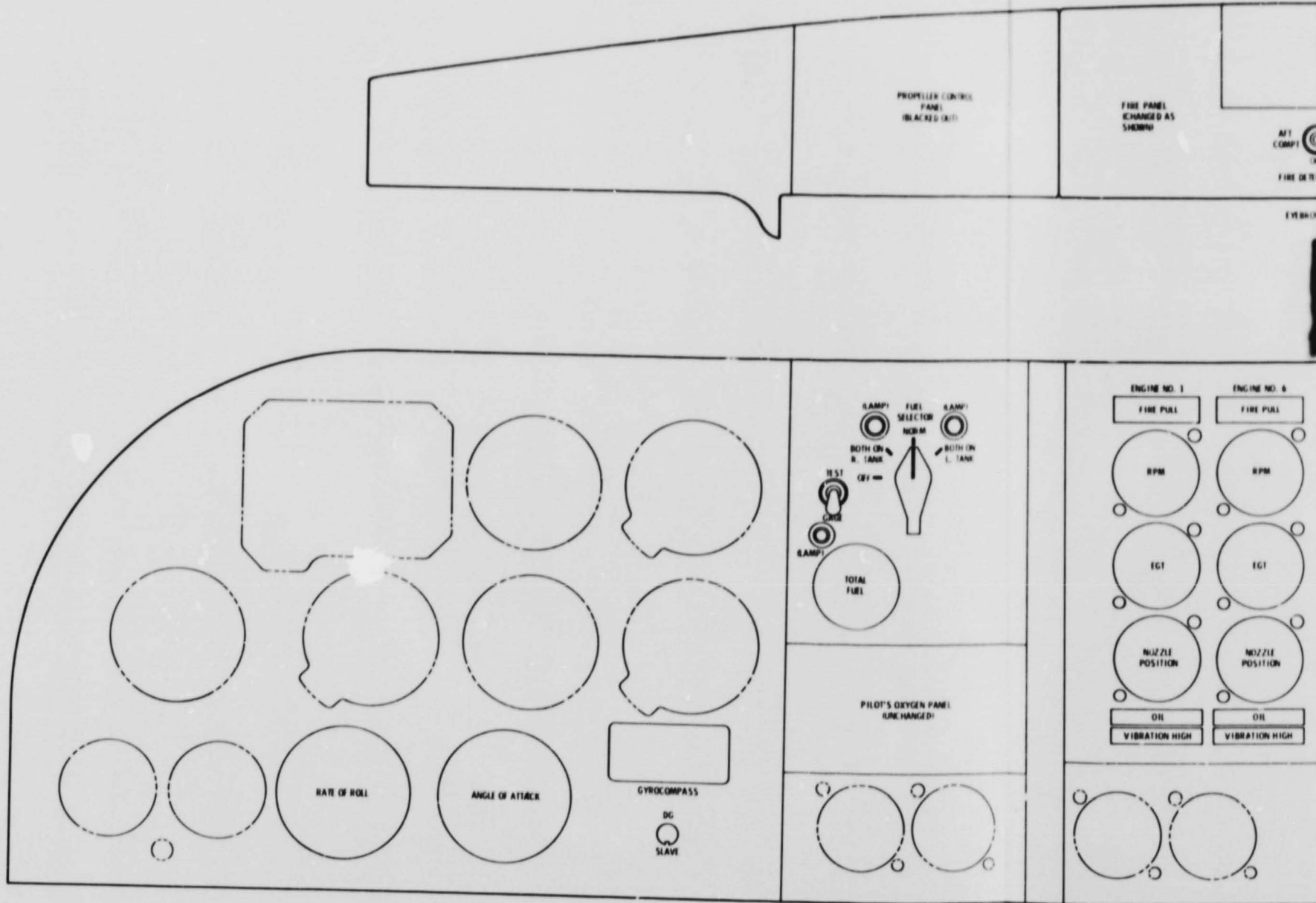
\*\*DESCENT FLOW RATE PER SYSTEM

Flight station modification. - The flight station modification consists of revisions to the instrument panel and the overhead controls. The center portion of the instrument panel, as noted in figure 45, will be replaced with a new panel for the new engine instruments and related indicator lights. The two thrust engine instrument displays will be juxtaposed near the pilot for optimum scanning during normal flight. The two columns will relate to the left and right thrust engines as will the left and right overhead thrust engine throttle controls. The flap air engine instruments will be grouped near the center for optimum viewing by either pilot for STOL operations. The four columns of flap air engine instruments and related indicator lights will be positioned in a left-to-right manner to relate to the left-to-right positioning of the respective engines in the same manner as the overhead throttle controls are to be positioned for the flap air engines. A fire warning light and shut-down control will be provided at the top of each column of engine instruments to provide immediate fuel cutoff capability to each engine. The standard engine health indicators of RPM and EGT will be provided for each engine as shown in figure 45. A dual pressure indicator will be installed for each flap air system to provide an indication of the pressure differential between the compressor discharge and the flap air plenum chamber for duct failure indication. Indicator lights will alert the pilots to engine oil malfunction or excessive engine vibration for the respective thrust engines. Indicator lights labeled "ENGINE OIL," "COMPRESSOR OIL," "ENGINE VIBRATION," "COMPRESSOR VIBRATION," "COMPRESSOR VIBRATION," or "OVERSPEED" will also alert the pilots to malfunctions for each flap air system.

A rate-of-roll indicator and an angle-of-attack indicator will be added to the pilot's panel as shown in figure 45.

In the group of overhead controls the landing gear lever, propeller control levers, APU lever, and fuel levers will be deleted as they will not be required in the modified configuration. The thrust engines will utilize the existing engine throttles with minor modifications. The thrust directional control levers will be added to an existing shaft at a position to the right of the thrust engine throttles. This will group the companion controls most frequently used in STOL operations. On an existing shaft located aft of the flap actuating lever, four controls will be added for the flap air engine. Each lever in the left-to-right manner will control the respective flap air engine located from left to right in the engine pattern. On an existing overhead panel between the thrust and flap air engine throttles a control will be added for raising and lowering of the upper flap sections, and four adjacent lights will indicate when the four upper flap sections are in the fully raised position. These indicators provide the pilot with the information needed to determine when the lift engines may be started. In addition to the upper flap control, another control will be added forward of the flap actuating lever which will lower the ailerons to their droop position for STOL operations.

141-A



FOLDOUT FRAME

141-B

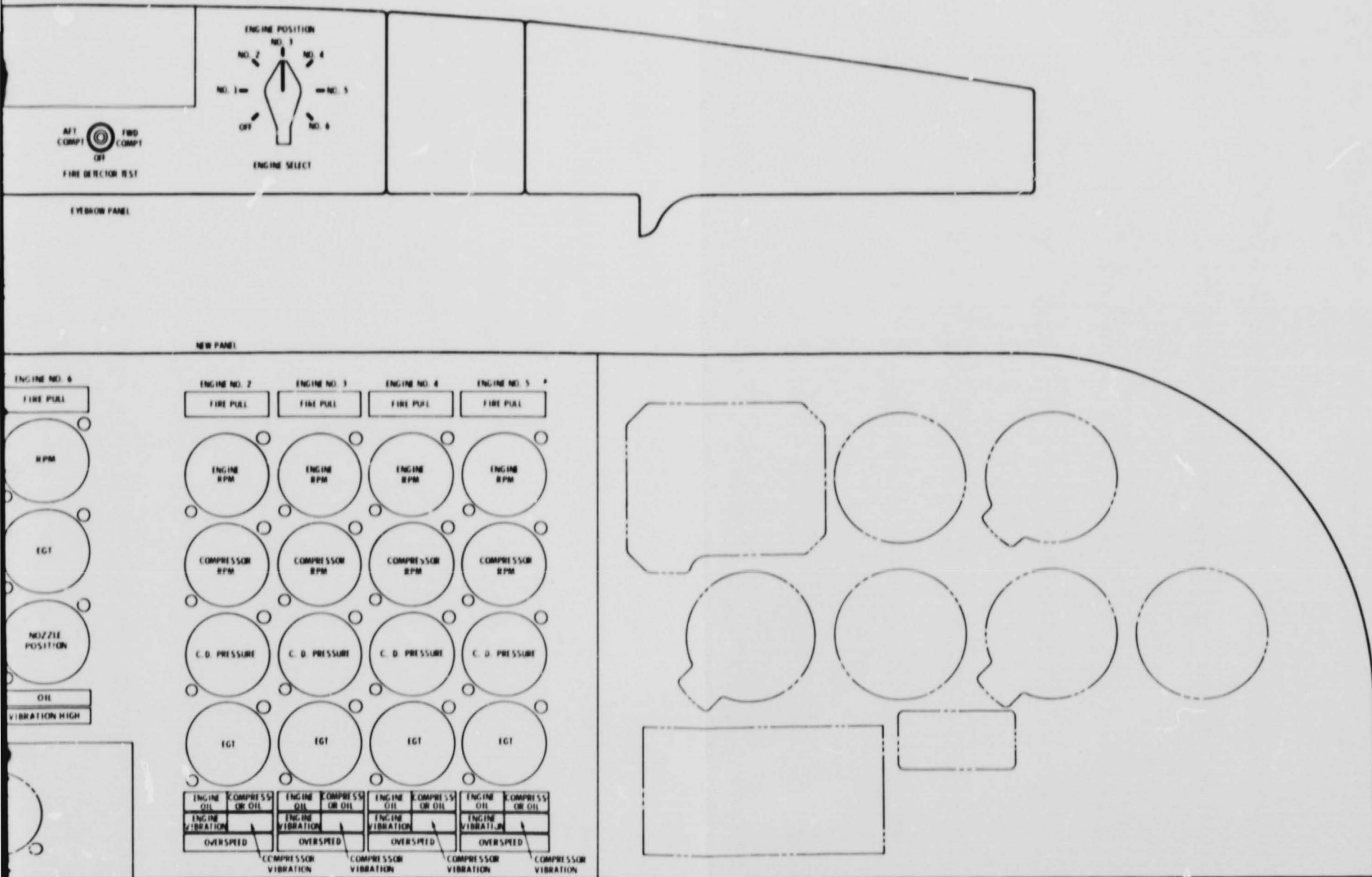


Figure 45. Instrument Panel

FOLDOUT FRAME

FOLDOUT FRAME

Suitable safeguards will be provided to require activation of the flap air engines prior to drooping the ailerons. This will insure a supply of boundary layer control air for the ailerons to retain roll control of the vehicle when the ailerons are drooped.

On the pilot's instrument panel, the existing fuel control panel will be modified to suit the new fuel system. A total fuel quantity gage will be added. No other fuel controls will be required.

Electrical systems. - The engine changes required deletion of the two existing engine-mounted 20-kva generators and the 10-kva generator on the auxiliary power unit (APU) and their replacement with two generators compatible with the Rolls-Royce Orpheus Mark 100 engines. Due to the engine accessory drive restrictions, it was decided to utilize the same generators as used on these engines in current airplanes. As these generators are rated at 4 kva each, the generating capacity would be reduced from 40 kva to 8 kva.

Several options were considered in order to arrive at the most desirable electrical power system adequate for the airplane. The USA-built generators were not considered as the British generator mounting pad standards differ from those used in the USA, and special adaptors for utilizing USA-built generators was considered undesirable from the viewpoint of cost. In addition, the idea of either customizing the Orpheus engines to accept USA generators or customizing USA generators to install on the Orpheus engines was rejected because of probable high cost and the spares problem associated with such customized equipment.

An electrical load analysis supplied by de Havilland was reviewed in detail to determine the actual electrical loads on the system and for any loads that could be removed as not necessary for the intended use of the modified airplane.

Decisions were made to deactivate long-range navigation and communication systems and the autopilot components shown in the load analysis. Anti-icing loads except pitot heaters and stall warning heaters were also to be deactivated. These load reductions added to the deleted de-icing and control loads associated with the propellers, deactivated landing gear indicators and controls (gear locked down), and some of the cargo compartment lighting brought the total loads to within the capacity of a single, 4-kva generator. The objective of establishing feasibility of a system adequate for the aircraft with one generator inoperative was considered extremely important; especially due to lack of a backup such as existed prior to deletion of the APU. However, the estimates of the new loads being added along with flight test instrumentation requirements showed the potential loads would exceed the capacity of a single generator.

Further analysis revealed that conversion losses for 400-cycle loads were considerable and would increase due to engine instrument increase. This is because of the unique prototype installation in the airplane which takes the variable frequency output of the generators, converts it to 28 volts dc at 85 percent efficiency, then converts again to 400-cycle ac through rotary inverters at 40 percent efficiency. Therefore, the generator(s) must put out 2.94 watts for each watt demanded by the loads on the 400-cycle buses.

Study of the load analysis charts revealed that peak loading on the generators occurs during landing so subsequent effort concentrated on this phase of flight.

The following decisions were reached that justify acceptance of the 4-kva generators.

1. The electrical fuel pumps would be monitored off if one generator becomes inoperative.
2. Replace the inefficient rotary inverters with wye to delta transformers. This is possible because the output of the proposed generators is both frequency and voltage regulated.
3. Monitor off pitot heaters and stall warning heaters if one generator is off. This is considered acceptable since the modified airplane is essentially a fair-weather airplane, and it is unlikely this equipment would be essential for controlled flight or landing.
4. Monitor off flight test instrumentation loads if one generator is off.

With these changes reflected in the load analysis charts, the demands on the generating system are well within the capacity of one generator with a reserve of approximately 1,300 watts.

The generators, manufactured by Plessey Co. Ltd., Romford, England, are defined by the following extracts from communications received from the manufacturer's representative.

Weight	38 pounds
Voltage	120-208 vac $\pm 1.5$ percent 3 phase
Power factor	1.0 to 0.8 lag
Frequency	400 cps $\pm 1.5$ percent
Rated output	4 kva

Cooling air temperature range -40° F to +114° F

Abnormal ratings

3 kva for ground running (no forced air cooling)

5 kva for 2 minutes

6 kva for 30 seconds

4 kva for 2 minutes with engines at 110 percent rpm

Structures

Structural modifications. - The structural modifications are associated with several main areas. These are the installation of the following:

1. The new flaps and ailerons aft of the existing rear spar
2. The spoiler on top of the existing outer wing upper skin surface
3. The flap air and BLC distribution ducting through the wing and in the fuselage
4. The new fuselage mounted nacelles
5. The new powered aileron and spoiler control system
6. The fixed slat on the wing leading edge
7. The rerouted and revised cables, plumbing and electrical systems
8. The attachment interface of the outboard nacelles on the wing structure
9. The attachment of the inboard nacelles on the fuselage

The investigations of these structural modification areas have verified the feasibility of utilizing existing state-of-the-art materials and fabrication methods.

The flaps, ailerons, and spoilers are conventional sheet metal construction. Bonded aluminum or nonmetallic honeycomb may be utilized where economical. The aileron hinge and jackscrew support fittings are attached



to the lower surface of the main wing box structure. Mounting pads on these fittings will eliminate the necessity of machining extensive surface areas to match an existing wing surface.

The flap actuating linkage will be profiled links and bellcranks without the extensive pocket machining usually done to obtain minimum weight. The aileron and spoiler control system linkage will also be based on a minimum machining approach except in those areas where the extra mass may be detrimental to system operation requirements.

The spoiler is mounted outside the wing upper surface just forward of the ailerons and has the same span as the ailerons. A nonstructural fairing is installed forward of the spoiler to retain a smooth airfoil section.

The flap air ducting from the outboard engines is routed within the leading edge of the wing, wherever possible, and through the main wing box between spars only where other, more accessible space, is not available. The ducting from the two inboard, or fuselage-mounted engines, is in the cabin and does not affect the main wing structure.

The fuselage-mounted nacelles are located immediately forward of the cargo bay entrance door and just low enough on the side of the fuselage to provide minimum clearance with the extended flaps. This location permits routing the flap air ducts through an existing cargo bay window opening and, thus, requires minimum fuselage structural modification for this ducting. The primary engine mount is in the area of the main fuselage frame that provides the rear spar support.

The new aileron and spoiler control system is to be installed in the outer wing panel, primarily between the front and rear spars. As the wing fuel provisions of the basic CV-7A have been removed, the total outer panel area is available and has good accessibility through the fuel tank access doors in the lower wing skin. Structural modification of the ribs will be required for mechanism clearance and support. Revisions of the leading edge structure is also required for routing of the aileron droop torque shaft installation.

The fixed slat installation is essentially an external modification with all the supporting structure added to the outside of the existing leading edge structure. The slat is attached to the support structure with splice plates. This installation permits slat relocation, if necessary, by replacement of simple splice plates instead of total support system revisions. In addition, the slat can be easily removed when not required.

While any electrical, plumbing, or systems installations or revisions require structural modifications to some degree, the CV-7A is basically a low-density aircraft and, therefore, does not present major routing problems.

It is expected that many local revisions will be required to provide structural clearances and mechanism support backup structure, but no major redesign of the primary aircraft structural elements is to be accomplished.

Provisions will be incorporated in the wing and fuselage to insure that adequate overboard air passages exist to prevent over pressurization of the structure by flap air distribution ducting failure.

Structural loads. - The following criteria were used in a preliminary evaluation of structural loads. The criteria are also considered adequate for the establishment of the structural integrity of the proposed modification. The criteria, from DHC Report AEROC 5.4.G.2, used in the design of the unmodified CV-7A aircraft are also shown in table XXV for comparison.

TABLE XXV. STRUCTURAL LOADS ANALYSIS

	Modified Aircraft	CV-7A Aircraft
Design takeoff weight, pounds	40,000	38,000
STOL landing weight, pounds	40,000	34,000
Conventional landing weight, pounds	40,000	36,500
Maximum speed, flaps up, KEAS	160	291
Maximum speed, flaps down, STOL, KEAS	100*	115
Max. speed, flaps down, conventional, KEAS	130	115
STOL landing rate of descent, fps	13	13
Conventional landing rate of descent, fps	10	10
Flight load factor at takeoff weight with flaps up	2.5	3.22
Flight load factor, flaps down	2.0	2.0
nW, (load factor x weight), flaps up	100,000	122,360
nW, flaps down	80,000	76,000

\*STOL mode for modified aircraft is with augmentation.

A review of design wingloads for the unmodified aircraft indicates that the wing flight-load bending moments for the proposed modification would be reduced because the span of the modified wing is approximately 78 percent of the unmodified wing. However, due to the increased landing weight, the modified aircraft would be expected to have higher wingloads, from the nacelle inboard, during the landing impact at a limit descent velocity,  $V_V = 13$  fps. The landing condition producing the maximum wing torsion is the DH-11 case (ref DHC Report AEROC 5.4.W.2) where main gear limit load is 2.0 and the drag factor is 0.80. A comparison of resulting net ultimate wing loads at wing stations 54.35 and 167.7 for the unmodified and modified aircraft is shown in table XXVI. Also shown are the loads for the modified aircraft when  $V_V = 12$  fps.

TABLE XXVI. BASIC LOADS

Wing Station		Unmodified A/C	Modified Aircraft	
		$V_V = 13$ fps	$V_V = 13$ fps	$V_V = 12$ fps
54.4	N <sub>S</sub>	43,800	54,840	48,900
	M <sub>N</sub>	7,124,000	7,494,000	6,787,000
	T <sub>SA</sub>	-8,126,000	-8,510,000	-7,308,000
	C <sub>S</sub>	29,900	37,700	32,500
	M <sub>C</sub>	4,258,000	4,500,000	3,910,000
167.7	N <sub>S</sub>	42,200	52,440	47,200
	M <sub>N</sub>	2,230,000	2,114,000	2,092,000
	T <sub>SA</sub>	-8,046,000	-8,430,000	-7,208,000
	C <sub>S</sub>	30,400	36,400	30,950
	M <sub>C</sub>	372,000	642,000	602,000

Loads on the augmentor flap components have been estimated from wind tunnel tests conducted by NASA/Ames and DHC for a similar augmentor configuration with and without blowing. Loads on the intake door, shroud, Coanda surface, and flap are presented for the  $\delta_f = 70$  degrees conditions at  $V = 100$  KEAS with blowing, and at 130 KEAS without blowing. Loads shown in table XXVII are normal to the rotated wing chord. Moments for the upper surface components are about the intake leading edge hinge point; and, for the lower surface components, the moments are about the flap hinge line. Limit loads and moments are shown per inch of span, i.e., lb/in. and in. lb/in.

TABLE XXVII. AUGMENTOR FLAP LOADS

Condition		Component	V = 100 KEAS	V = 100 KEAS
			$\delta_f = 70^\circ$ $C_{J_I} \neq 0$	$\delta_f = 70^\circ$ $C_{J_I} = 0$
Intake	Fwd of Hinge	$P_N$ HM	6.8 lb/in. 29.8 in. lb/in.	2.8 17.3
	Aft of Hinge	$P_N$ HM	3.5 -10.4	0.2 -0.5
Upper Flap		$P_N$ HM	-24.0 385	-0.8 7.6
Coanda Section		$P_N$ HM	42.3 103	3.6 2.8
Lower Flap		$P_N$ HM	33.2 -506	19.4 -325.0

Loads on the slat have been estimated also from wing tunnel tests conducted on a similar slat configuration. Slat chord is at -60 degrees with respect to the wing chord line. Loads normal and parallel to the slat chord and moments about the slat leading edge are shown in table XXVII for maximum positive and negative load conditions. Limit loads are shown as lb/in. of span and in lb/in. of span.

TABLE XXVIII. SLAT LOADS

Parameter	Condition	
	A	B
$V_E$ (KEAS)	130	160
$\alpha$ (deg)	23	-13
$\delta_f$ (deg)	70	0
Normal load (lb/in.)	+28.6	-11.8
Chord load (lb/in.)	+1.7	-1.5
L.E. moment (in. lb/in.)	-234	+105

Structural analysis. - A comparison of wingloads for the modified aircraft to those of the existing aircraft for a landing condition of 13 feet per second, indicate an increase of 5 percent in bending and torque, and 25 percent in shear at station 54.4. At station 167.7, the loads also show an increase in shear and torsion of about the same magnitude as station 54.4; however, this is accompanied by a 5-percent decrease in normal bending.

A search of the existing DHC-5 stress analysis (AEROC 5.4.W.3) indicates a margin of safety of 5 percent in the center section covers which should be adequate for the increased loads.

The margin of safety in the front and rear spars is zero for current loads and would, therefore, show a slightly negative margin for the higher loads at ultimate.

A detailed analysis will be made for the wing center section to determine the exact level for the new loads. Sink-speed restrictions or slight beefup will be made, as necessary.

Areas of the wing and fuselage affected by the routing of the control system, air ducting, control surface hinges, or nacelle modification will be reanalyzed to insure adequate strength and stiffness for the revised loads.

The area aft of the rear spar of the wing including the new control surfaces, and associated control systems and actuators will be completely analyzed to show adequate structural integrity.

The fuselage-mounted fuel tanks, including the tiedown to the cargo deck and any associated fuselage modification, and the fixed leading edge slat along with necessary wing modification in this area, will be completely analyzed for the appropriate loading conditions.

Flutter characteristics. - The proposed changes in the wing will affect the wing flutter characteristics. Reducing the wingspan will tend to increase the wing natural frequencies of importance in flutter and to change their ratios to each other. Also the reduced engine pitching inertia will tend to result in the wing torsional frequencies being higher in an absolute sense and higher in relation to wing bending modes. While a critical wing bending-torsion flutter problem is not anticipated, particularly in view of the reduced limit speed of 160 KIAS, flutter analyses must be conducted to investigate the possibility of unfavorable bending-torsion frequency ratios.

In addition to the above, proposed changes to the flaps and ailerons pose potential flutter and aeroelastic problems that must be analyzed. Due to their double construction, the flaps tend to have weight, static unbalance, and mass moment of inertia values approximately twice as large as normal. Flutter

analyses must be conducted to develop flap and aileron designs having satisfactory combinations of mass parameters and rotational frequencies. Another area to be investigated is the possibility of flap aeroelastic divergence due to suction between the upper and lower flap panels.

Weight, balance, and moments of inertia. - Weight, balance, and inertia data for a baseline vehicle were established by correlating weight data from the 18th issue of the DHC 5.3.G.1 Weight Statement, with inertia and weight distribution from the DHC 5.3.G.8 Inertia Report. Incremental weight changes for the additions and deletions of structural or system components have been applied to the baseline vehicle to establish the weight empty for the configuration.

These weight, balance, and inertia data include calculations from design layouts for the flaps, ailerons, spoilers, wing fairing for spoilers, nacelles, fuel system, fuel tanks, and surface controls. Engine weights were obtained from engine manufacturer's information. Weights for test instrumentation are based on vendor data. The ballast for the initial test flight loadings has been located to maintain a center of gravity range between 35.5 percent MAC and 40 percent MAC.

The group weight data for the modified aircraft are shown in tables XXIX and XXX. Derivation of the basic CV-7A aircraft empty weight for use with this modification program and the weight build up to the 40,000-pound research aircraft is defined in tables XXXI through XXXIV.

### Flight Dynamics

The basic philosophy that was used in defining the proposed modification was to rely on the suitability of the unmodified aircraft as having safe and reasonable handling qualities for the design mission which is that of a research vehicle under controlled conditions. In addition, configuration changes which have been included were specifically chosen to improve handling qualities over those of the unmodified aircraft. These include removing the fuel from the wings and shortening the span to increase roll control. These mission requirements and the design modification approach permit a minimum of sophistication at reduced costs. To obtain maximum effectiveness from any design, however, and to justify its adequacy for the intended mission, detailed handling qualities analyses must be made.

It is intended that these detailed analyses will be conducted during the initial phase of the design effort. They will utilize the predicted aerodynamic derivatives for the proposed modification, and will evaluate static and dynamic aircraft handling qualities parameters and responses to pilot inputs at:

AN-9103-D

TABLE XXIX.  
GROUP WEIGHT STATEMENT  
WEIGHT EMPTY

PAGE \_\_\_\_\_  
MODEL \_\_\_\_\_  
REPORT \_\_\_\_\_

1	<b>WING GROUP</b>					4,776
2	CENTER SECTION - BASIC STRUCTURE					1,886
3	INTERMEDIATE PANEL - BASIC STRUCTURE					
4	OUTER PANEL - BASIC STRUCTURE (INCL. TIPS LBS.)					974
5						
6	SECONDARY STRUCTURE (INCL. WINGFOLD MECHANISM LBS.)					
7	AILERONS (INCL. BALANCE WEIGHT LBS.)					175
8	FLAPS - TRAILING EDGE					1,074
9	ATTACHMENTS TO WING					220
10	SLATS					168
11	SPOILERS					81
12	SPEED BRAKES					
13	JOINTS & FAIRINGS					198
14						
15	<b>TAIL GROUP</b>					1,030
16	STABILIZER - BASIC STRUCTURE					348
17	FINS - BASIC STRUCTURE (INCL. DORSAL LBS.)					281
18	SECONDARY STRUCTURE (STAB. & FINS)					
19	ELEVATOR (INCL. BALANCE WEIGHT LBS.)					226
20	RUDDERS (INCL. BALANCE WEIGHT LBS.)					148
21	EMPENNAGE ASSEMBLY					27
22						
23	<b>BODY GROUP</b>					4,736
24	FUSELAGE OR HULL - BASIC STRUCTURE					
25	BOOMS - BASIC STRUCTURE					
26	SECONDARY STRUCTURE - FUSELAGE OR HULL					
27	- BOOMS					
28	- SPEEDBRAKES					
29	- DOORS, PANELS & MISC.					
30						
31	<b>ALIGHTING GEAR GROUP - LAND (TYPE: _____)</b>					1,674
32						
33	LOCATION	WHEELS, BRAKES TIRES, TUBES, AIR	STRUCTURE	CONTROLS		
34	MAIN	433	914	17	1,364	
35	NOSE	112	194	4	310	
36						
37						
38						
39						
40	<b>ALIGHTING GEAR GROUP - WATER</b>					
41	LOCATION	FLOATS	STRUTS	CONTROLS		
42						
43						
44						
45						
46	<b>SURFACE CONTROLS GROUP</b>					911
47	COCKPIT CONTROLS					100
48	AUTOMATIC PILOT					
49	SYSTEM CONTROLS (INCL. POWER & FEEL CONTROLS 42 LBS.)					341
50	BOUNDARY LAYER CONTROLS - DUCTING ETC.					470
51	<b>ENGINE SECTION OR NACELLE GROUP</b>					2,170
52	INBOARD - SIDE FUSELAGE					600
53	CENTER					
54	OUTBOARD					1,570
55	DOORS, PANELS & MISC.					
56						
57	<b>TOTAL (TO BE BROUGHT FORWARD)</b>					15,297

AN-9103-D

NAME \_\_\_\_\_

DATE \_\_\_\_\_

TABLE XXIX. (CONCLUDED)  
**GROUP WEIGHT STATEMENT**  
**WEIGHT EMPTY**

PAGE \_\_\_\_\_

MODEL \_\_\_\_\_

REPORT \_\_\_\_\_

1 PROPULSION GROUP				9,174
2	AUXILIARY	GAIN		
3	ENGINE INSTALLATION		5,492	
4	AFTERBURNERS (IF FURN. SEPARATELY)			
5	ACCESSORY GEAR BOXES & DRIVES			
6	SUPERCHARGERS (FOR TURBO TYPES)			
7	AIR INDUCTION SYSTEM			
8	EXHAUST SYSTEM		132	
9	COOLING SYSTEM			
10	LUBRICATING SYSTEM		100	
11	TANKS			
12	COOLING INSTALLATION			
13	DUCTS, PLUMBING, ETC.			
14	FUEL SYSTEM		3,177	
15	TANKS - PROTECTED			
16	- UNPROTECTED			
17	PLUMBING, ETC.			
18	WATER INJECTION SYSTEM			
19	ENGINE CONTROLS		156	
20	STARTING SYSTEM		117	
21	PROPELLER INSTALLATION			
22				
23				
24	AUXILIARY POWER PLANT GROUP			
25	INSTRUMENTS & NAVIGATIONAL EQUIPMENT GROUP			129
26	HYDRAULIC & PNEUMATIC GROUP			424
27	INSTRUMENTATIONS			180
28				
29	ELECTRICAL GROUP			817
30				
31				
32	ELECTRONICS GROUP			453
33	EQUIPMENT			
34	INSTALLATION			
35				
36	ARMAMENT GROUP (INCL. GUNFIRE PROTECTION LBS.)			
37	FURNISHINGS & EQUIPMENT GROUP			1,506
38	ACCOMMODATIONS FOR PERSONNEL		424	
39	MISCELLANEOUS EQUIPMENT		65	
40	FURNISHINGS		166	
41	EMERGENCY EQUIPMENT		108	
42	CARGO HANDLING (INCL. RAMPS)		743	
43	AIR CONDITIONING & ANTI-ICING EQUIPMENT GROUP			557
44	AIR CONDITIONING		327	
45	ANTI-ICING		230	
46				
47	PHOTOGRAPHIC GROUP			
48	AUXILIARY GEAR GROUP			
49	HANDLING GEAR			
50	ARRESTING GEAR			
51	CATAPULTING GEAR			
52	ATO GEAR			
53	PAINT - EXTERNAL SURFACES			102
54				
55	MANUFACTURING VARIATION			
56	TOTAL FROM PG. 2			15,297
57	WEIGHT EMPTY			28,639



AN-9103-D

NAME \_\_\_\_\_  
DATE \_\_\_\_\_

TABLE XXX.  
GROUP WEIGHT STATEMENT  
USEFUL LOAD & GROSS WEIGHT

PAGE \_\_\_\_\_  
MODEL \_\_\_\_\_  
REPORT \_\_\_\_\_

1 LOAD CONDITION				TEST	FERRY
2				FLIGHTS	
3 CREW (NO. 3 )				600	600
4 PASSENGERS (NO. )					
5 FUEL		Type	Gals.		
6 UNUSABLE				195	260
7 INTERNAL				6,543	8,693
8					
9					
10 EXTERNAL					
11					
12 BOMB BAY					
13					
14 OIL					
15 TRAPPED				37	37
16 ENGINE				101	101
17					
18 FUEL TANKS (LOCATION )					
19 WATER INJECTION FLUID ( GALS)					
20					
21 BAGGAGE					
22 CARGO					
23					
24 ARMAMENT					
25 GUNS (Location)		Pla. or Pla.	Qty.	Cal.	
26					
27					
28					
29					
30					
31					
32 AMMUNITION					
33					
34					
35					
36					
37					
38					
39 INSTALLATIONS (BOMB, TORPEDO, ROCKET, ETC.)					
40 BOMB OR TORPEDO RACKS					
41					
42					
43					
44					
45					
46 EQUIPMENT					
47 PYROTECHNICS					
48 PHOTOGRAPHIC					
49					
50 OXYGEN					
51					
52 MISCELLANEOUS					
53 BALLAST				3,885	1,670
54					
55 USEFUL LOAD				11,361	11,361
56 WEIGHT EMPTY				28,639	28,639
57 GROSS WEIGHT				40,000	40,000

\*If not specified as weight empty.

TABLE XXXI. WEIGHT EMPTY DERIVATION BEFORE MODIFICATION

Item	Weight	Horizontal CG	
		Arm	Moment
Weight empty (AEROC: 5.3.G.1 Issue 18)	22,855	350.58	8,012,506
Less:			
Engines	2,320	257.33	597,006
Engine mounts	129	235.22	30,343
Propellers	1,529	197.00	301,213
Exhaust system	246	370.91	91,244
Starters	39	262.00	10,213
Engine controls	78	198.90	15,514
Fuel system	719	347.40	249,781
Lubrication system	113	243.40	27,504
APU	98	264.50	25,921
Nacelles	1,530	291.28	445,658
Wing tip	400	352.00	140,800
Flaps	556	403.85	224,541
Ailerons	152	392.40	59,645
Spoilers	42	394.00	16,548
Weight empty less items removed	14,904		5,776,570

TABLE XXXII. WEIGHT EMPTY DERIVATION FOR MODIFIED AIRCRAFT

Item	Weight	Horizontal CG	
		Arm	Moment
Weight empty less items removed	14,904		5,776,570
Add:			
Wing			
Ailerons	175	405.00	70,875
Flaps - upper	587	406.70	238,733
- lower	462	411.70	190,205
- interconnect linkage	25	411.30	10,283
Attachments - flap	60	382.00	22,920
- aileron	7	392.00	2,744
Slats	168	296.33	49,783
Spoilers	81	385.00	31,185
Fairing - spoilers	88	338.00	29,744
Fuselage			
Beef-up - Side-mounted engines	48	371.50	17,832
Surface controls			
Change to flap and aileron controls	40	396.00	15,840
Nacelles			
Side fuselage	600	380.00	228,000
Wing	1,570	270.00	423,900
Propulsion			
Engines: T64 - side fuselage (2)	1,846	399.00	736,554
T64 - wing (2)	1,846	262.00	483,652
Orpheus - wing (2)	1,800	275.50	495,900
Exhaust system	132	382.20	50,450
Starters	117	295.00	34,515
Engine controls	156	295.00	46,020
Fuel system - tanks	1,429	296.80	424,127
- cradles for tanks	1,582	296.80	469,241
- plumbing	166	311.00	51,626
Lubrication system	100	330.60	33,060
Air ducting - wing	355	370.00	131,350
- fuselage	115	390.00	44,850
Instrumentation - flight test	180	482.00	86,760
Weight empty - after modification	28,639		10,196,719

TABLE XXXIII. USEFUL LOAD AND TAKEOFF GROSS WEIGHT FOR FLIGHT TEST

Item	Weight	Horizontal CG		
		Arm	Moment	
Useful load - flight test				
Oil - trapped	37	312	11,544	
- engine	101	312	31,512	
Fuel - unusable	195	314	61,230	
- usable	6,543	314	2,054,502	
Crew (3)	600		76,380	
Useful load - flight test - no ballast	7,476		2,235,168	
Weight empty	28,639		10,196,719	
Takeoff gross weight - no ballast - most forward CG	31.7%	36,115	344.23	
12,431,887				
Add ballast				
Forward fuselage	500	182	91,000	
Aft fuselage	3,385	412	1,394,620	
Takeoff gross weight - flight test - with ballast	34.7%	40,000	347.9	
13,917,507				
Less usable fuel	-6,543		-2,054,502	
Landing Gross weight - with ballast - most aft CG	40.0%	33,457	354.57	
11,863,005				
Moment of Inertia - Slug-Ft <sup>2</sup>				
Takeoff Gross Weight	I <sub>XX</sub> (Roll)	I <sub>YY</sub> (Pitch)	I <sub>ZZ</sub> (Yaw)	I <sub>XZ</sub> (Product)
40,000 lb	149,444	203,778	313,464	29,517

TABLE XXXIV. USEFUL LOAD AND TAKEOFF GROSS WEIGHT FOR FERRY

Item	Weight	Horizontal CG	
		Arm	Moment
Useful load - ferry			
Oil - trapped	37	312.0	11,544
- engine	101	312.0	31,512
Fuel - unusable	260	297.2	77,272
- usable	8,693	297.2	2,583,560
Crew (3)	600	127.3	76,380
Useful load - ferry - no ballast	9,691		2,780,268
Weight empty	28,639		10,196,719
Takeoff gross weight - no ballast - most forward CG	38,330	338.56	12,976,987
			27.1%
Add ballast	1,670	423	706,470
Takeoff gross weight - ferry - with ballast	40,000	342.09	13,683,457
			30.0%
Less usable fuel	-8,693		-2,583,560
Landing gross weight - with ballast most aft CG	31,307	354.55	11,099,897
			40.0%

representative flight conditions throughout the anticipated flight envelope. Aircraft configurations and flight conditions to be examined are listed in table XXXV:

TABLE XXXV. HANDLING QUALITIES ANALYSIS CONFIGURATIONS AND FLIGHT CONDITIONS

Configuration	Airspeed (KEAS)	CG Position (% MAC)
Takeoff		
40,000 lb $\delta_f = 50^\circ$	60	30, 35, 40
	70	30, 35, 40
	85	30, 35, 40
	100	30, 35, 40
Landing		
34,600 lb $\delta_f = 50^\circ$	100	35
34,600 lb $\delta_f = 80^\circ$	100	30, 35, 40
	85	30, 35, 40
	70	30, 35, 40
	65	30, 35, 40

The parameters define during these analyses will be compared directly with criteria presented in references 6 to 8.

The results of these analyses will indicate whether or not control or stability augmentation is necessary, and will provide the basis for proposing incorporation of such. The analyses will also aid in specification of the basic hydromechanical flight control system characteristics such as feel forces, pilot control-to-surface gearing, flap control-to-elevator gearing, and the various aileron and flap actuator characteristics. This approach will facilitate achieving the best system characteristics for the intended mission of the proposed configuration, and will provide a basis for the control system ground checkout requirements.

Flight test maneuvers, aircraft configuration, and flight conditions will be defined to allow in-flight evaluation of handling qualities (pilot ratings). Parameters determined during the handling qualities analysis will be compared with those obtained in flight.

## Aerodynamics

Performance. - The takeoff distance for 40,000 pounds gross weight and all engines operating is computed to be 890 feet. Of this distance, 541 feet is consumed for the ground run with  $\mu = 0.03$ , and the remainder is to clear a 50-foot obstacle.

The computation is carried out for a sea-level standard-day condition, and with the flaps extended to 50 degrees throughout the takeoff. During the ground run, only 75 percent thrust from the T64-1 engines is used for the lift augmentation in order to prevent premature main gear lift off. Lift-off and climb to 50 feet is achieved at a constant speed of 60 knots by applying 100-percent thrust augmentation and a rotation of the airplane.

The highest normal acceleration used during the climb is 90 percent of  $n_{\max}$ , where  $n_{\max} = 1.60$ . The steady-state climb angle associated with these takeoff conditions is 15.9 degrees.

In case of failure of one of the T64-1 lift augmentor engines immediately after lift off, the distance to clear the 50-foot obstacle is increased to 1,093 feet. Again, 90 percent of  $n_{\max}$  is used, where in this case  $n_{\max} = 1.40$ . The associated steady-state climb angle is 9.0 degrees.

The speed of 60 knots is chosen equal to the landing speed. Slightly lower speed are possible because the stall speeds are lower for the takeoff flap setting of 50 degrees than for the landing flap setting of 80 degrees. An estimated takeoff time history is presented in figure 46.

The landing distance for the 40,000-lb aircraft over a 50-foot obstacle at the sea-level standard-day condition is computed to be 1,124 feet without thrust reversal, and 883 feet with theoretical 100 percent thrust reversal using full rotation of Pegasus nozzles during the braking.

The air distance is 390 feet using the flight speed of 60 knots and a sink rate of 13 ft/sec. The associated glide path angle is -7.4 degrees. A time delay of 2 seconds after touchdown is used before the brakes and/or thrust reversal is used, based on C-130 STOL test experience. During that time, the speed is assumed constant and the ground distance traveled is 203 feet. Braking is accomplished with a braking coefficient of  $\mu = 0.30$  as the airplane is not equipped with an antiskid device.

The speed of 60 knots provides an adequate margin to the one T64-1 engine-out stall speed of 50.5 knots with the flaps at 80 degrees, and to the elevator limit speed of 51 knots. This landing speed should also be used for lower weight landings so that adequate pitch acceleration is available.

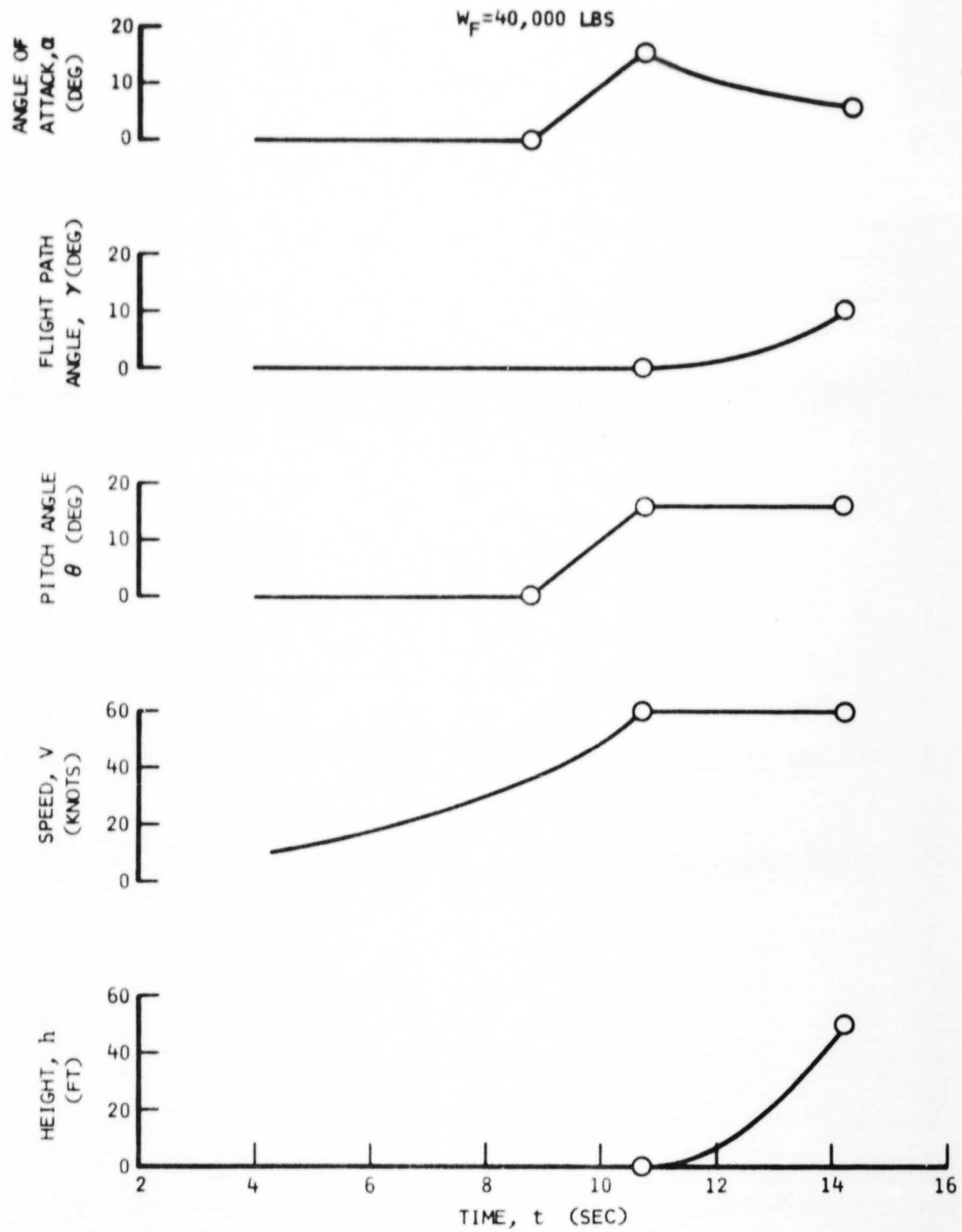


Figure 46. Take-off Time History



Maximum normal accelerations at 40,000 pounds are  $n_{\max} = 1.45$  for normal operation and  $n_{\max} = 1.29$  for one T64-1 engine inoperative. The following methods are used to determine previously mentioned distances.

The take-off ground distance is computed using

$$X_{GR} = \left( \frac{1}{\rho_{0g}} \right) \left( \frac{q}{\frac{T_{CR}}{W} (1 + \psi_1)} \right) \left( \frac{1}{\rho_0} \right) \quad (77)$$

Herein,  $q$  is the free stream dynamic pressure at liftoff,  $T_{CR}$  is the static cruise engine thrust of 10,000 pounds, and  $(1 + \psi_1)$  is a factor accounting for the airplane drag. The factor is generally about 0.80 for conventional takeoff, but is about 1.20 for the augmentor wing because the separate power source for the lift augmentation adds a thrusting effect. More specifically, the factor is determined from

$$(1 + \psi_1) = \frac{T_{CR}}{T_{CR} \text{ ave}} + \frac{\frac{T_0}{W} \left( \frac{-D_{ave}}{T_0} + \mu \frac{L_{ave}}{T_0} \right) - \mu}{\frac{T_{CR}}{W}} \quad (78)$$

Herein is

$$\frac{D_{ave}}{T_0} = \frac{1}{2} \left[ \left( \frac{D}{T_0} \right)_{V=0} + \left( \frac{D}{T_0} \right)_{V_{10}} \right] \quad (79)$$

$$\frac{L_{ave}}{T_0} = \frac{1}{2} \left[ \left( \frac{L}{T_0} \right)_{V=0} + \left( \frac{L}{T_0} \right)_{V_{10}} \right] \quad (80)$$

$$\left( \frac{D}{T_0} \right)_{V=0} = -\cos \delta_F \quad (81)$$

$$\left( \frac{L}{T_0} \right)_{V=0} = \sin \delta_F \quad (82)$$

$T_0$  is a reference thrust associated with the lift augmentation, and described more in detail in the longitudinal stability and control discussion.

$(L/T_0)V_L/C$  is obtained from the same section at  $-0^\circ$  at the speed parameter,  $q/(T_0/S)$ , for lift-off. Similarly,  $(D/T_0)V_{10}$  is obtained from the supporting data discussion.

The total distance to climb to 50 feet altitude above the runway is determined from figure 47. Herein,  $n_o$  is the initial normal acceleration used at lift-off. It is a percentage of  $n_{\max}$  where

$$n_{\max} = \left( \frac{L}{T_o} \right)_{\max} \left( \frac{T_o}{W} \right) \quad (83)$$

The value of  $(L/T_o)$  is found in the stability and control discussion for the speed parameter at lift-off.

Also needed in the figure is the value of the factor  $(1 + \psi_2)$ . This factor is a function of the obstacle height  $Z$  and the steady-state climb angle  $\gamma_\infty$ . The factor also can be determined from figure 47 and is near unity in the region of interest.

For detail computation, the climb angle  $\gamma_\infty$  is determined from

$$T_{\text{an}} \gamma_\infty \approx \frac{\frac{-D}{T_o}}{\frac{L}{T_o}} + \frac{T_{\text{cr}}}{W} \quad (84)$$

Where  $L/T_o \approx W/T_o$ , and where  $D/T_o$  is found at the value of  $L/T_o$  from the drag polar of  $D/T_o$  versus  $L/T_o$  existing for the speed parameter associated with the climb speed.  $L/T_o$  as well as  $D/T_o$  include the effect of the wing augmentation, but do not include the cruise engine effects. The drag polar is taken from NASA/Ames data of test 294, by making use of

$$\frac{L}{T_o} = \frac{C_L q S}{T_o} = C_L \frac{q}{\frac{T_o}{S}} = \frac{C_L}{C_J} \quad (85)$$

$$\frac{D}{T_o} = C_D \frac{q}{\frac{T_o}{S}} = \frac{C_D}{C_J} \quad (86)$$

$$\frac{q}{\frac{T_o}{S}} = \frac{1}{C_J} \quad (87)$$

The climb is assumed to take place at constant speed. The small speed increase that is inevitable immediately after lift-off is neglected.

(88)

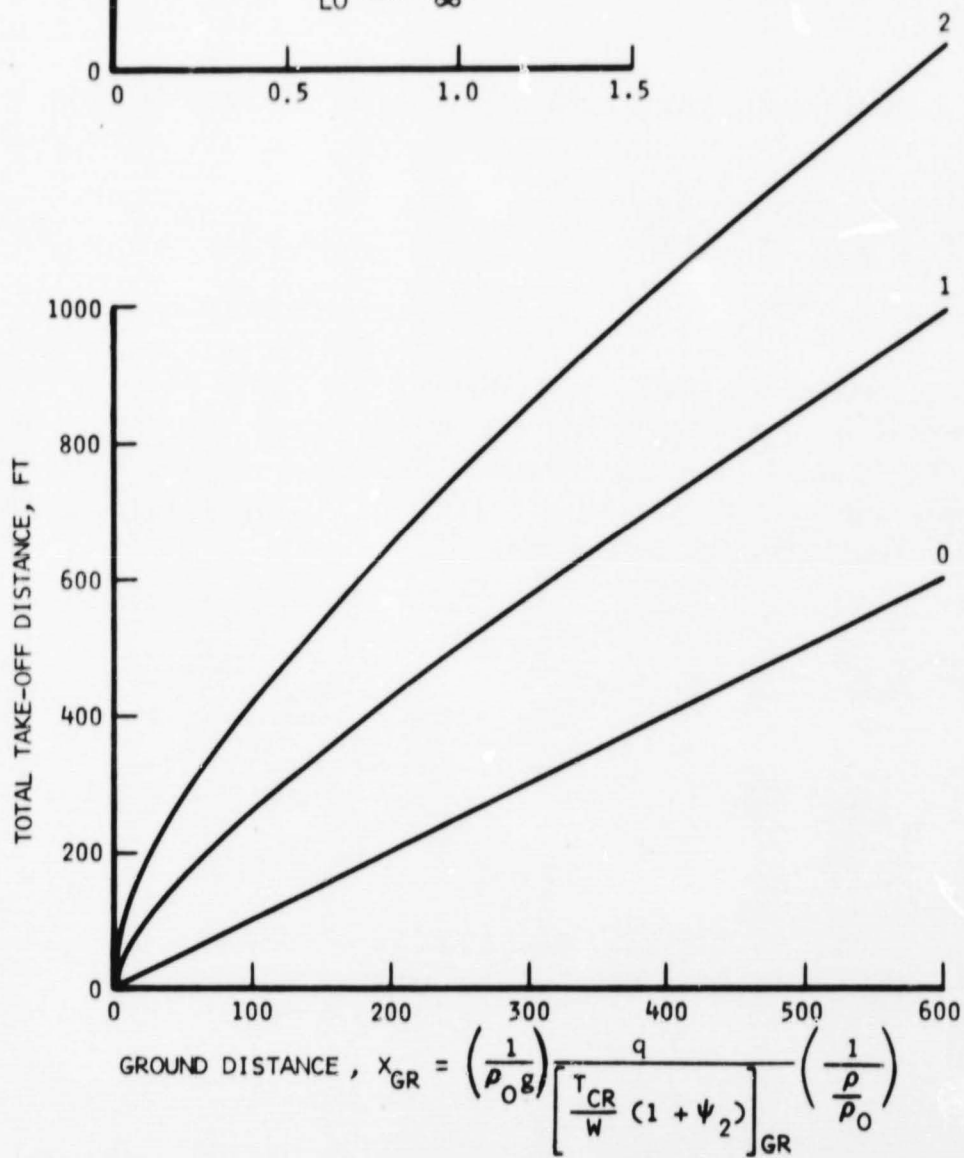
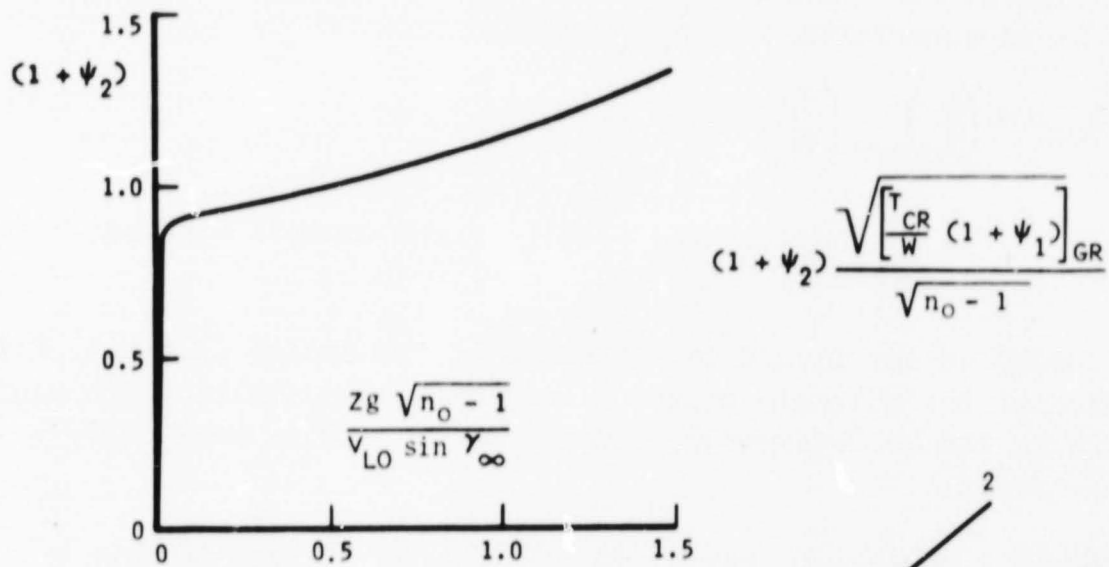


Figure 47. Determination of Take-off Distance

The time required to reach liftoff speed in the previously shown time history (figure 46) is determined from

$$t_{GR} = \frac{V_{lo}}{g \frac{T_{cr}}{W} (1 + \psi_1)} \quad (108)$$

The time duration from lift-off to the 50-foot obstacle is

$$t_{AIR} = \frac{X_{AIR}}{V} = \frac{X_{TOT} - X_{GR}}{V} \quad (89)$$

The flight path angle of  $\gamma$  as a function of time is determined from figure 48 using

$$\gamma = \frac{\dot{Z}}{V} \quad (90)$$

Herein,  $Z$  is a vertical distance. In the derivation of the equations, a linear relation between  $\dot{Z}$  and  $Z$  is assumed, which means a linear relation is taken between  $\alpha$  and  $\gamma$  at constant speed. Thus,  $\alpha$  can be interpolated linearly between the values indicated in figure 48 for  $\gamma = 0$  and  $\gamma_{\infty}$ . The airplane altitude angle  $\theta$  is then determined from

$$\theta = \alpha + \gamma \quad (91)$$

A derivation of the equations for the takeoff distance is presented in section IV.

The landing distance is computed from: (1), the air distance

$$X_{AIR} = \frac{Z}{\frac{dZ}{dt}} \cdot V \quad (92)$$

(2), a rolling distance without braking with a duration of  $\Delta t = 2$  seconds

$$X_{ROLL} = V \cdot \Delta t \quad (93)$$

and, (3) the braking distance

$$X_{BR} = \frac{V^2}{2a} \quad (94)$$

W = 40,000 LBS

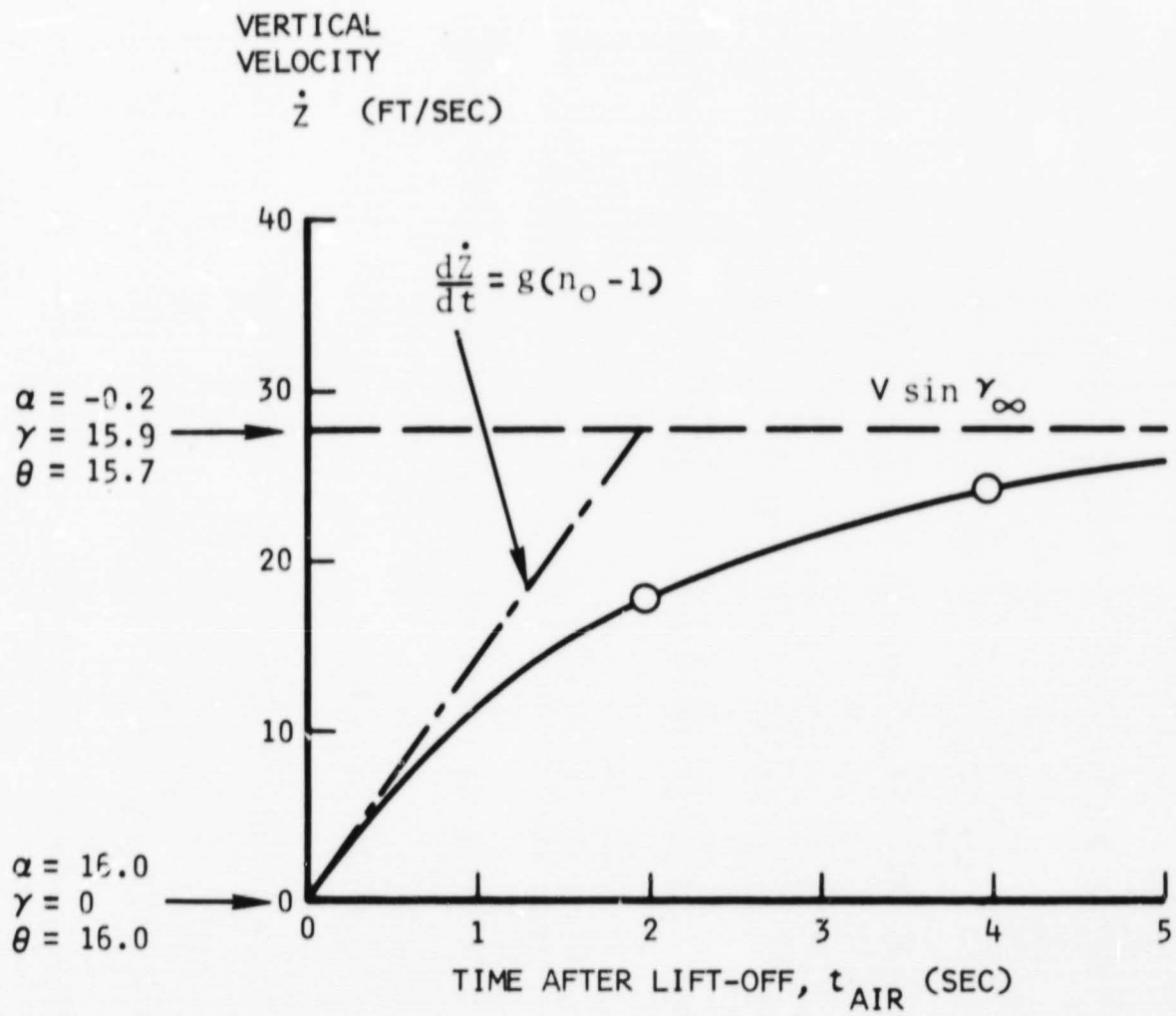


Figure 48. Vertical Velocity Versus Time During a Normal STOL Takeoff

Here

$$2a = 2g \left[ \frac{D_{ave}}{W} + \frac{\mu(W - L_{ave})}{W} + \frac{T_R}{T_{CR}} \left( \frac{T_{CR}}{W} \right) \right] \quad (95)$$

and

$$\frac{D_{ave}}{W} = \frac{C_D q_{ave} S}{W} = \frac{1/2 q_{TD} C_D S}{W} \quad (96)$$

$$\frac{L_{ave}}{W} = \frac{C_L q_{ave} S}{W} = \frac{1/2 q_{TD} C_L S}{W} \quad (97)$$

$$\frac{T_R}{T_{CR}} = \text{Thrust reversal factor} \quad (98)$$

No ground effect has been considered in the landing and takeoff computations.

For ferry and test capability, correlation of number of takeoffs versus climb time is shown in figure 49. The data of this correlation are of a preliminary nature and are to provide an approximate assessment of the test capabilities of the modified aircraft.

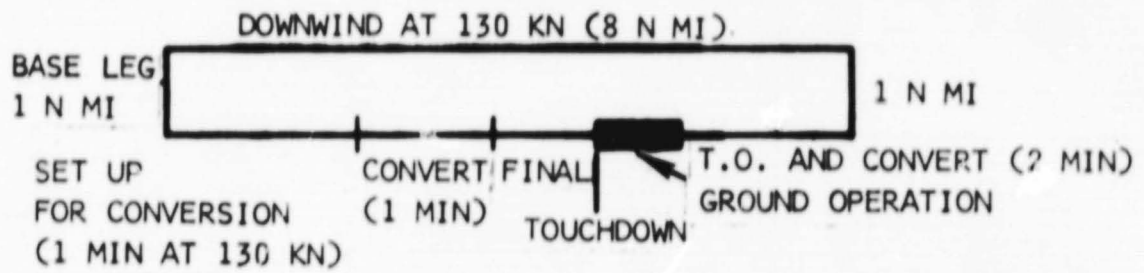
The performance is based on the drag data utilizing the T64 blowing engines and the Orpheus Mark 803 engine data. The fuel flows are increased 5 percent to allow for installation losses.

The typical takeoff and landing pattern is also shown in figure 49. The cruise time is computed for 130 knots at 1000 feet altitude. A total number of six patterns can be flown with full fuel.

The ground rules used in the typical pattern for takeoff and landing are as follows:

- ° Takeoff - 1-1/2 minutes at maximum power for all engines for takeoff and conversion to flaps up at 130 knots and 1,000 feet.
- ° Landing - 1 minute for setup for conversion at 130 knots at power for level flight
  - 1 minute for conversion from 130 knots flaps up to 65 knots flaps down with 75 percent power on T64 engines and 50 percent on cruise engines
  - 1 1/2 minutes on descent at 65 knots to touchdown with T64's at 75 percent and 50 percent on cruise engines.

TYPICAL PATTERN



TOTAL NUMBER OF PATTERS  $\cong$  6  
 T.O. WT = 40,000 LB (8,400 LB FUEL)

START ENGINES - 200 LB  
 RESERVE (5%) - 420 LB

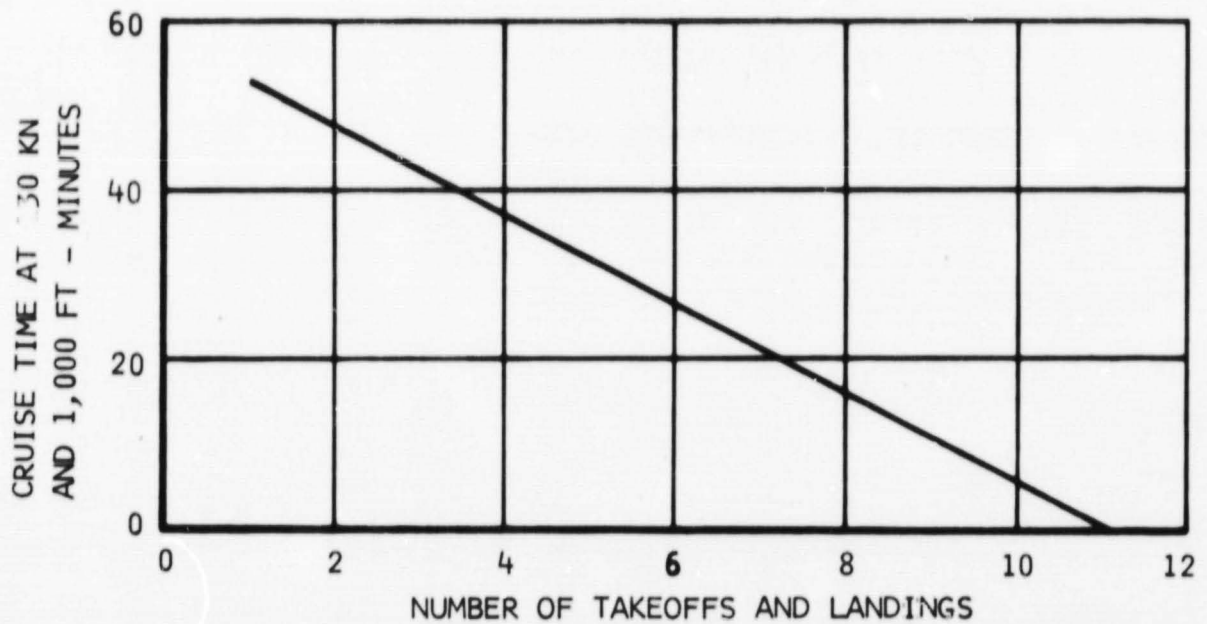


Figure 49. Modified Buffalo Takeoff and Landing Test Capability

For the time between landing and the next takeoff there is a 1-minute allowance at idle power on all engines. The fuel reserve (5 percent of initial fuel) is 420 pounds.

With the previously mentioned reserve and a normal takeoff (without T64 engines) a ferry range of approximately 135 n mi would be attainable at 130-knot cruise at 5,000 feet.

Longitudinal stability and control. - Steady-state longitudinal characteristics, such as airplane angle of attack and elevator position versus speed, is presented in figures 50 through 54 for an airplane weight of 40,000 pounds. The first three figures show the characteristics of the airplane without lift augmentation (i.e., in the conventional flight mode) for flaps at 0, 50, and 80 degrees. The other figures show characteristics with lift augmentation (in the STOL mode) for flaps at 50 and 80 degrees. All data are shown for idle cruise thrust.

The airplane generally exhibits stability in terms of elevator angle versus speed when the downwash characteristics are as expected (solid lines). Only a slight instability with speed is exhibited with lift augmentation when the downwash characteristics are significantly different (dashed lines). The two different downwash characteristics are obtained from different sets of experimental data which will be discussed later. Unstable characteristics versus speed are common for airplanes utilizing high lift coefficients.

The figures also show the speed limits encountered for the various flap settings and lift augmentations. These limits include wing stall, tail stall, mechanical elevator limits, and flow separation at the leading edge slats (LE slat stall at high speed). Without augmentation, the flaps-up stall speed is 90 knots; and, the flaps-down high-speed limits are 125 to 130 knots as limited by slat stall. Recommended speed range for operating the flaps without augmentation is 110 to 125 knots. A speed margin with respect to the slat stall speed need not be taken into account as exceeding this speed probably does not lead to dangerous condition. It is, however expected that airframe buffeting will be experienced at higher speeds.

With lift augmentation and at a flap angle of 80 degrees, the low-speed limit is 50 knots which is set by the one T64 engine-out stall speed. The high-speed limit is 68 knots set by slat stall. Thus, short-field landings should be limited to a speed range of 60 to 68 knots. It appears that this speed range can be increased slightly by the use of a somewhat lower flap angle.

Conversions between conditions with and without lift augmentations are to be carried out between 100 and 105 knots at flap angles of 50 degrees using a speed margin of 20 percent with respect to the stall speed without augmentation.



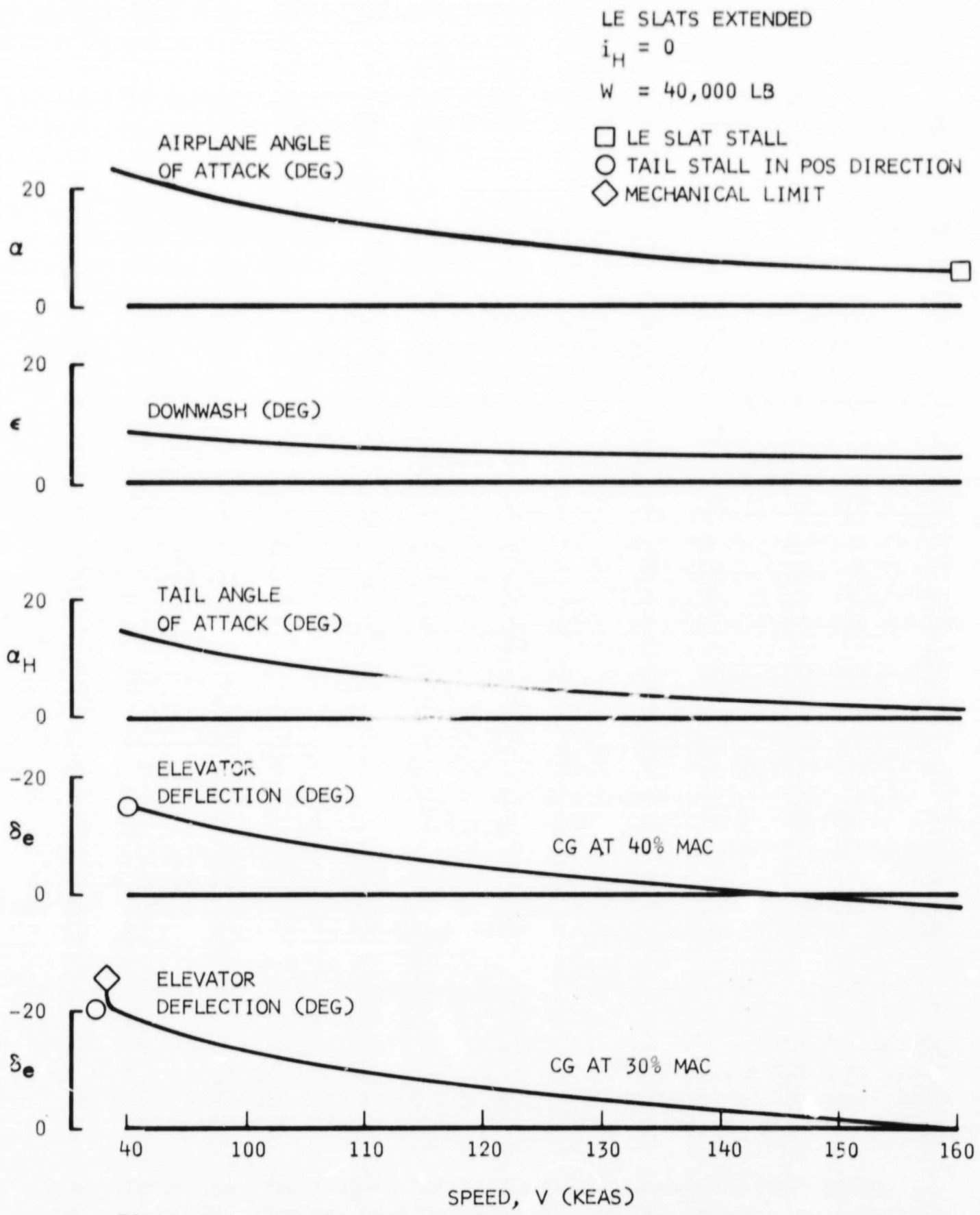


Figure 50. Steady-state Longitudinal Characteristics Flaps Up, No Augmentation, Idle Cruise Thrust

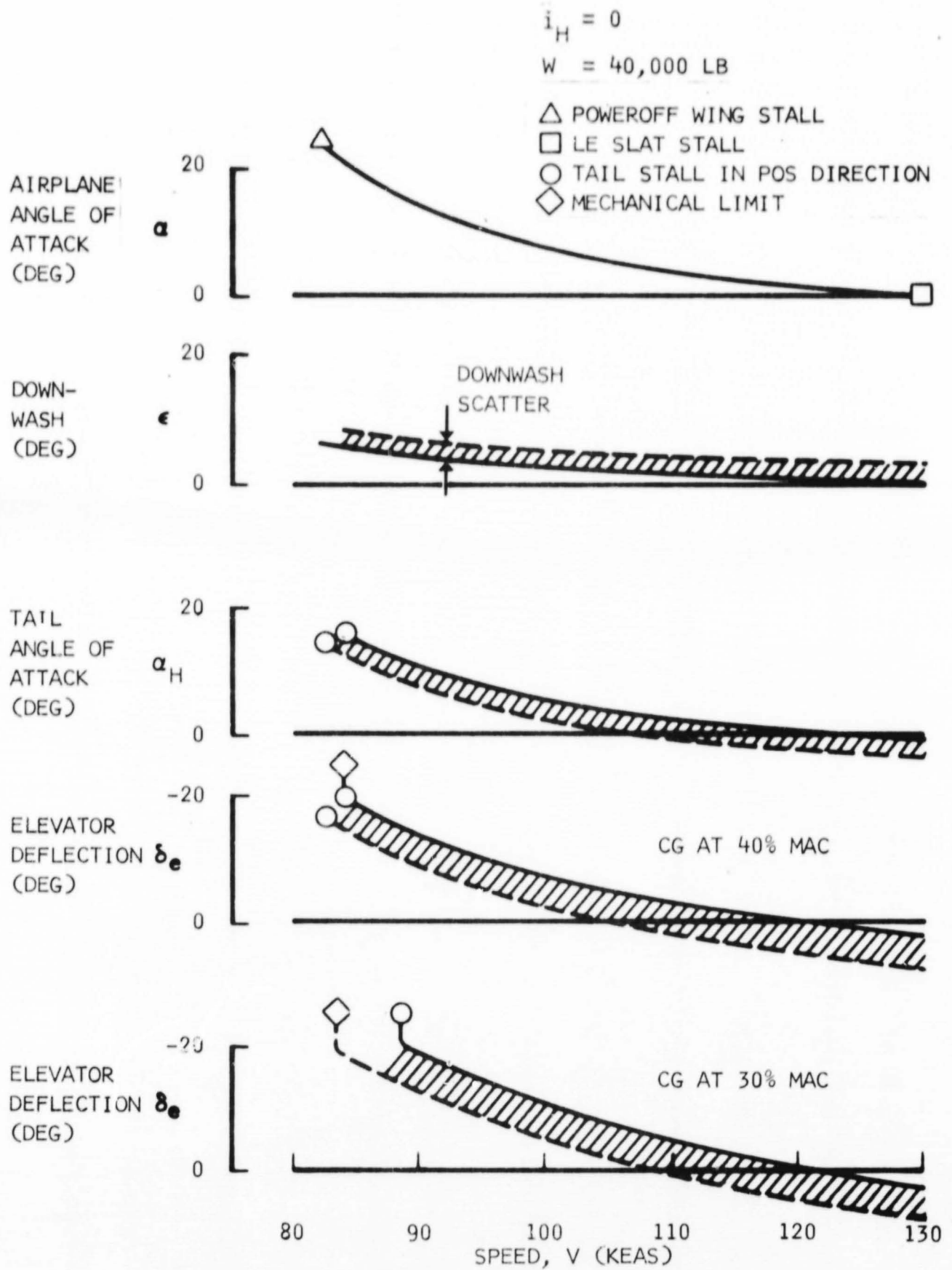


Figure 51. Steady-state Longitudinal Characteristics Flaps 50°, No Augmentation, Idle Cruise Thrust

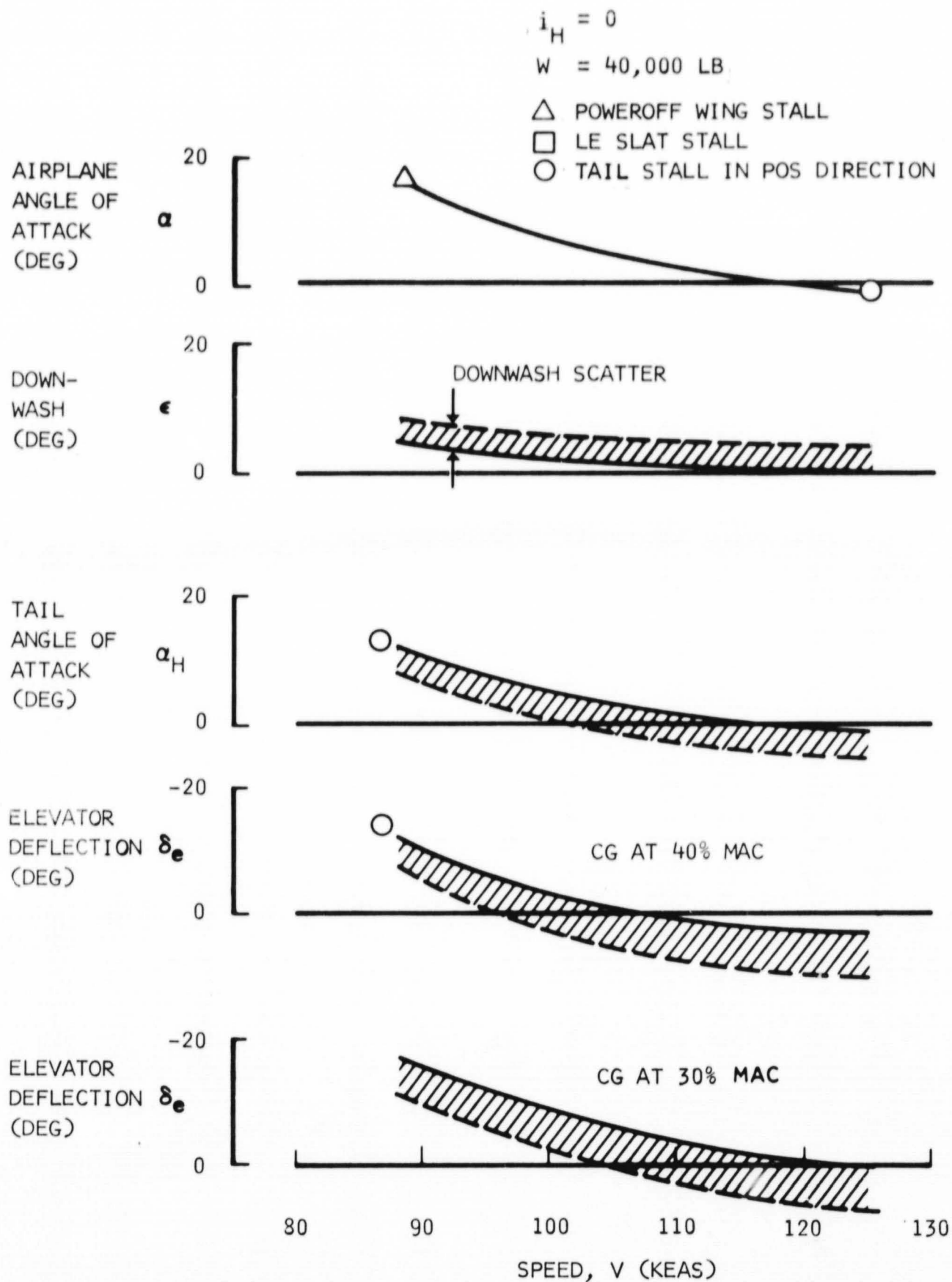


Figure 52. Steady-state Longitudinal Characteristics Flaps 80°, No Augmentation, Idle Cruise Thrust

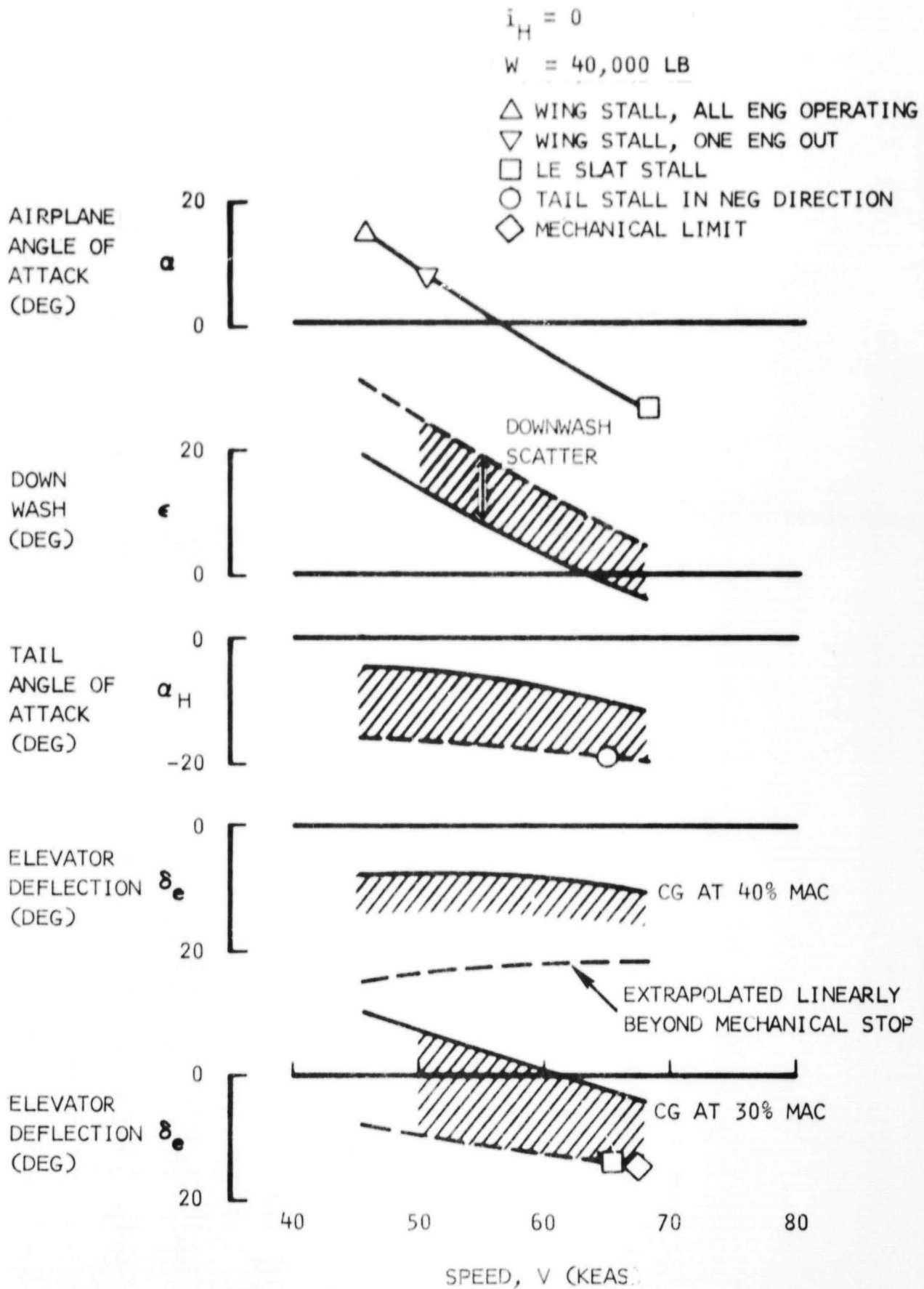


Figure 53. Steady-state Longitudinal Characteristics Flaps 80°, Max Augmentation, Idle Cruise Thrust

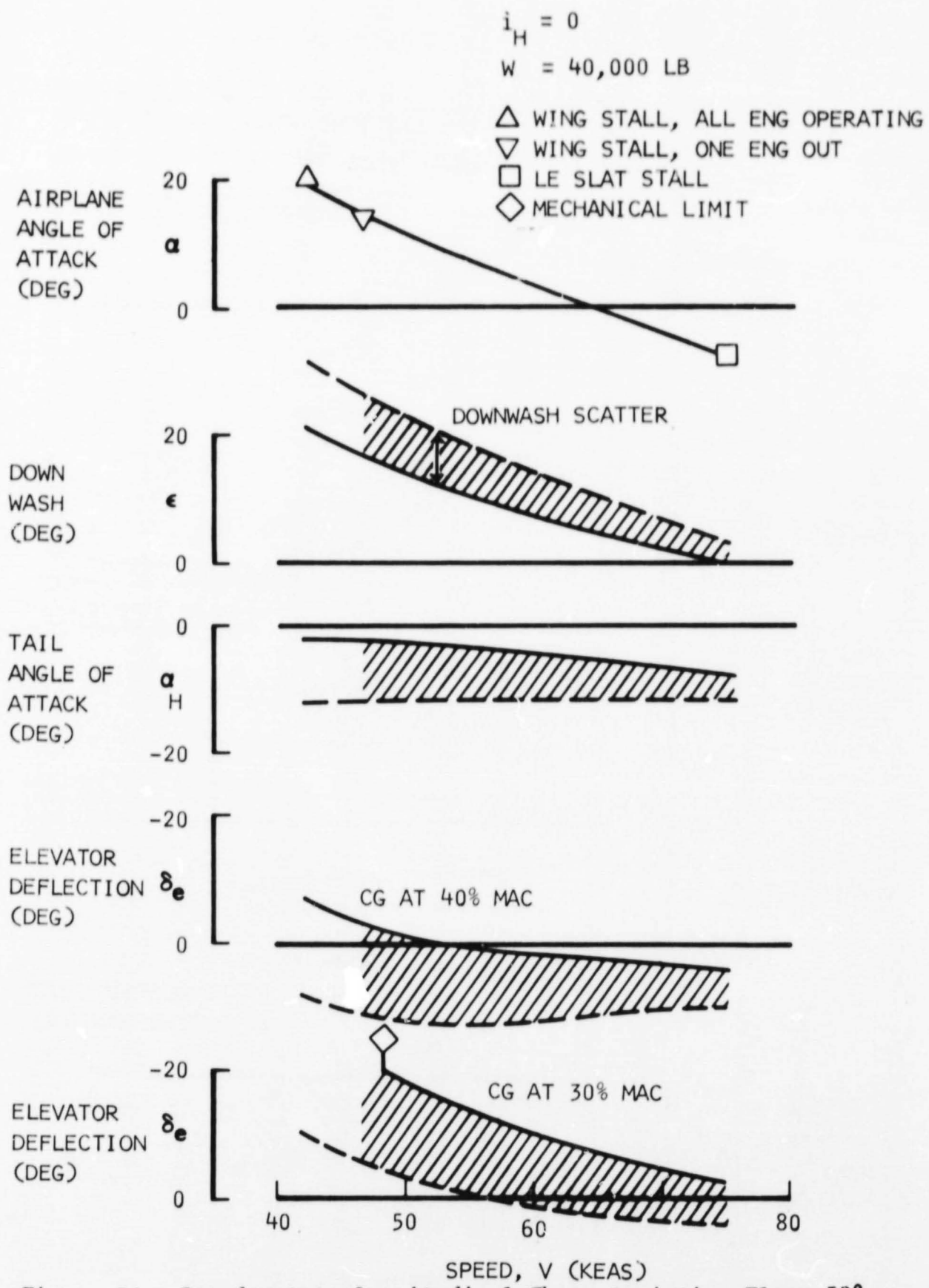


Figure 54. Steady-state Longitudinal Characteristics Flaps 50°, Max Augmentation, Idle Cruise Thrust

The previously mentioned values are based on the data presented in figures 55 through 58. In these, tail-off lift,  $L$ , is presented in the nondimensional form of  $L/T_0$  and plotted versus the speed parameter  $q/(T_0/S)$ . Herein,  $q$  is the freestream dynamic pressure,  $T_0$  is the static force vector existing when the wing flaps are being blown, and  $S$  is the wing reference area. The first two of these figures show data for 50 degrees flaps and for 80 degrees flaps with the associated downwash angles. In the other two figures, the lift data are identical, and the only difference lies in the different downwash.

The lift data are all taken from the NASA/Ames test 294 and presented in this form for easy use. For a given  $T_0$ , the stall speed for a required wing lift  $L$  can easily be obtained, and the variation of the maneuver margin with speed can easily be visualized. Effects of changing  $T_0$ , for example, due to RPM change or engine failure, can rapidly be identified. Also, for a given airplane weight, the angle of attack and downwash is obtained from these curves once  $T_0$  and the difference between the wing lift and the airplane weight (or trim lift) is known.

The lift from the wind tunnel data is converted to the present form using

$$\frac{L}{T_0} = \frac{C_L q S}{T_0} = \frac{C_L}{\left(\frac{T_0}{qS}\right)} = \frac{C_L}{C_J} \quad (99)$$

The speed parameter is obtained from the tunnel data using:

$$\frac{q}{\left(\frac{T_0}{qS}\right)} = \frac{1}{C_J} \quad (100)$$

The value of  $T_0$  is related to the thrust output  $T_C$  at the wing nozzle. Figure 59 shows a sketch with the definition of  $T_0$  and  $T_C$ . A higher ejector efficiency of the flap system results in a higher value of  $T_0$  for a given value of  $T_C$ . Values of  $T_0/T_C$  for various tests and various flap angles are presented in this figure, and later tests show improved values.

A high efficiency results not only in a high lift at zero forward velocity, but also throughout the entire STOL speed range which is obtained here by multiplication of  $T_0/T_C$  with  $L/T_0$ :

$$L = \left(\frac{L}{T_0}\right) \left(\frac{T_0}{T_C}\right) T_C \quad (101)$$

FLAPS 50°

DOWNWASH FROM TEST 294

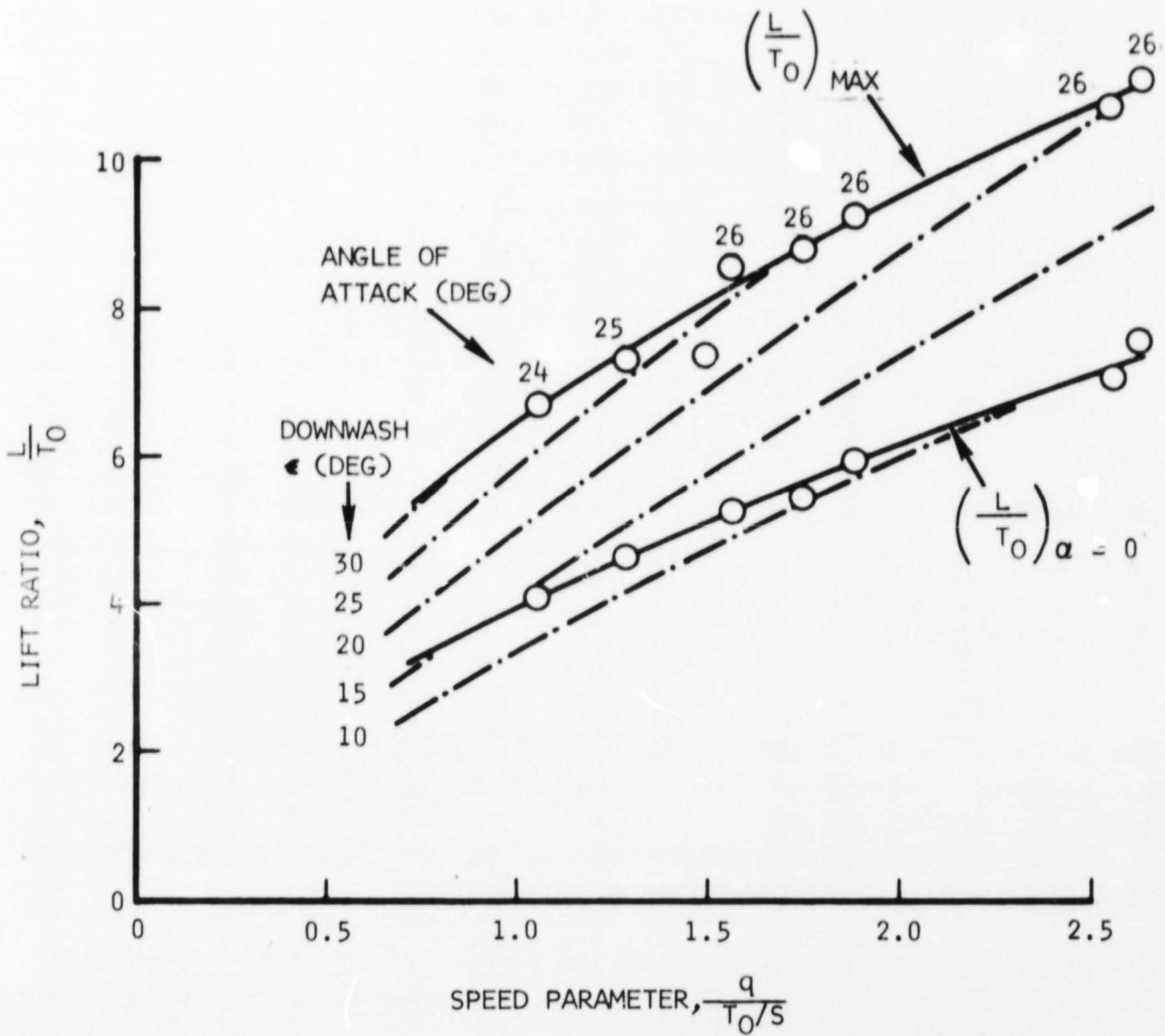


Figure 55. Lift, Angle of Attack, and Downwash Relation Vs Speed Parameter

FLAPS 80°

DOWNWASH FROM TEST 294

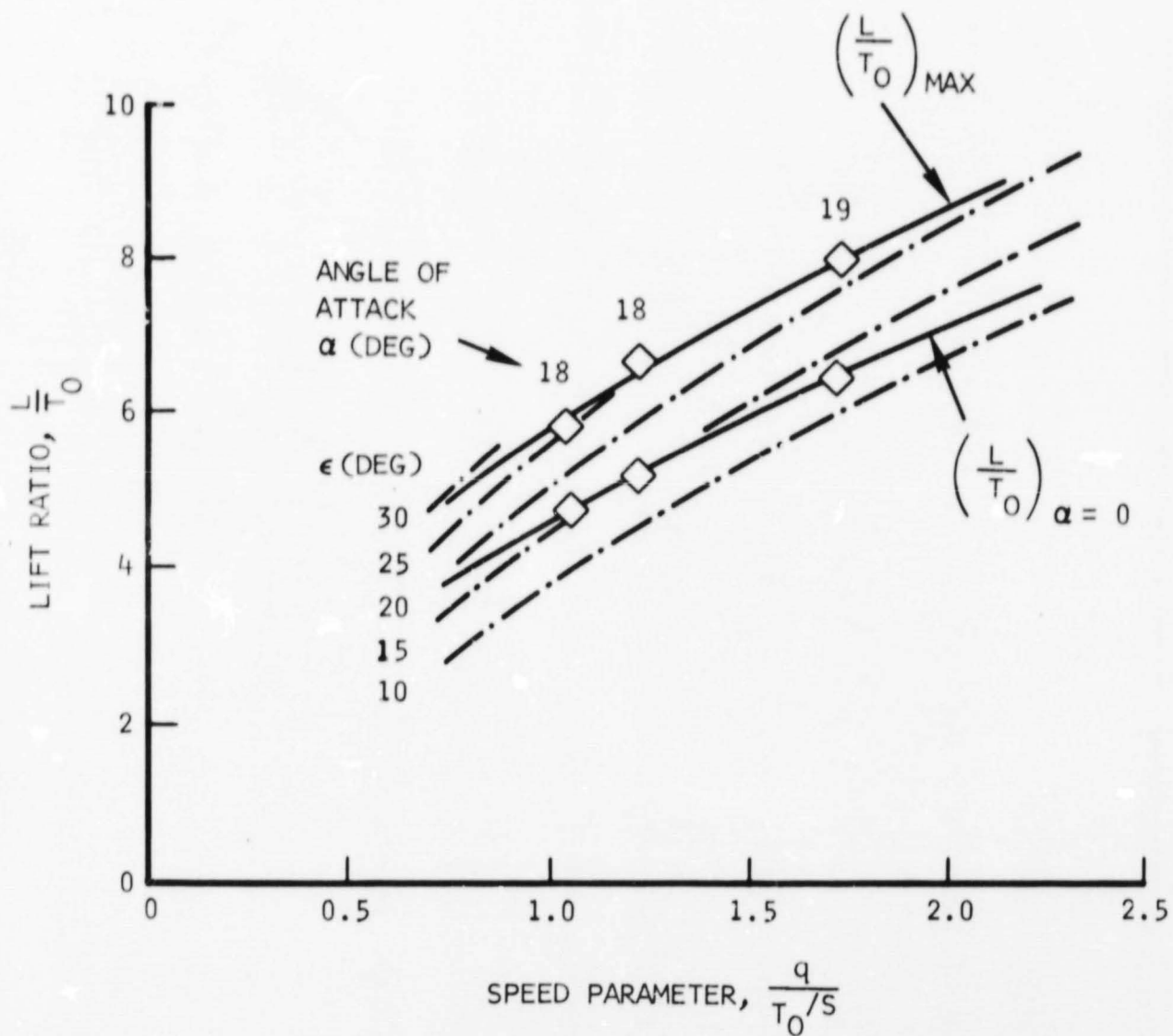


Figure 56. Lift, Angle of Attack, and Downwash Relation Vs Speed Parameter



FLAPS 50°

DOWNWASH FROM T.N. D-4610

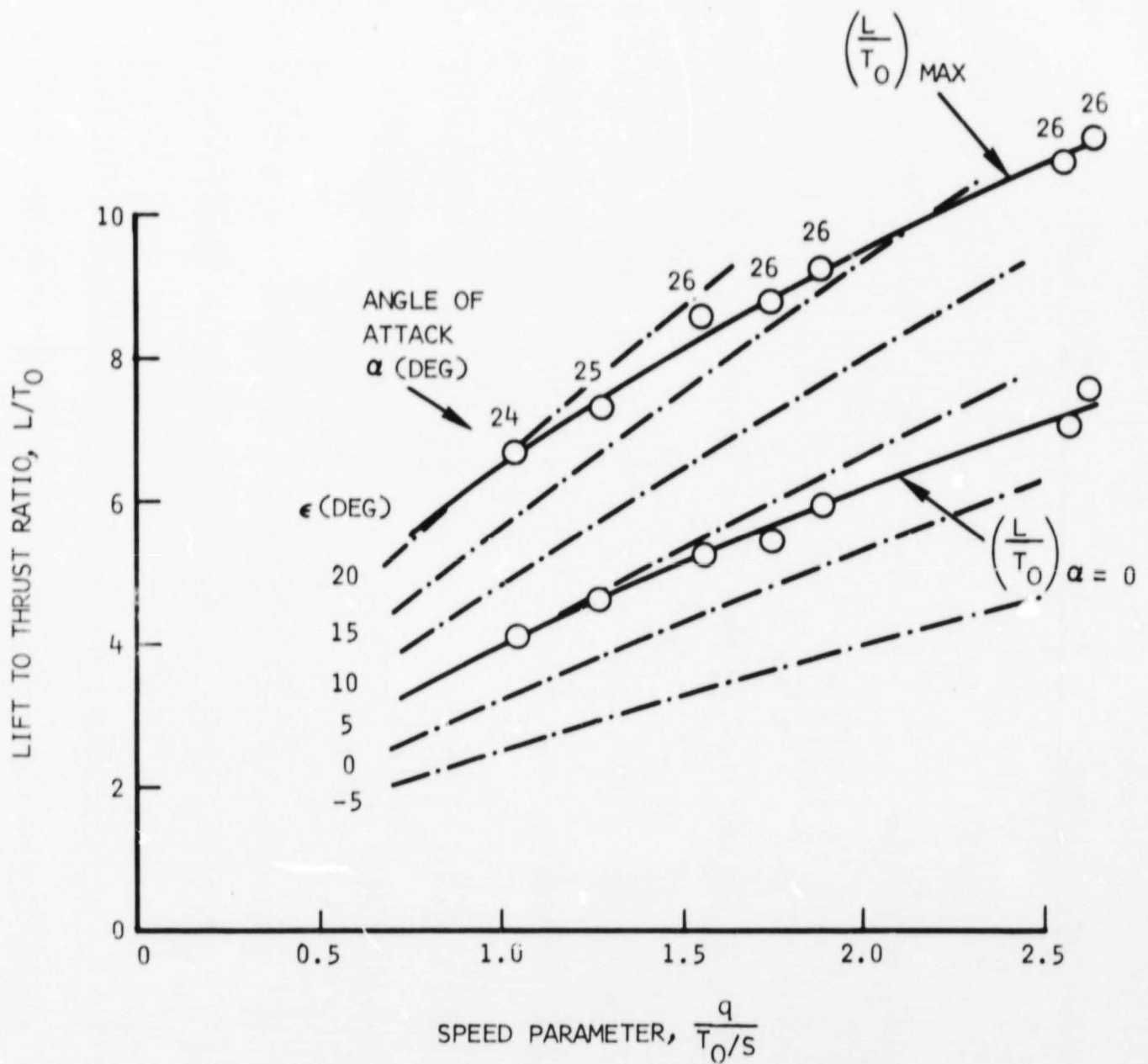


Figure 57. Lift, Angle of Attack, and Downwash Relation Vs Speed Parameter

FLAPS 80°

DOWNWASH FROM TN D-4610

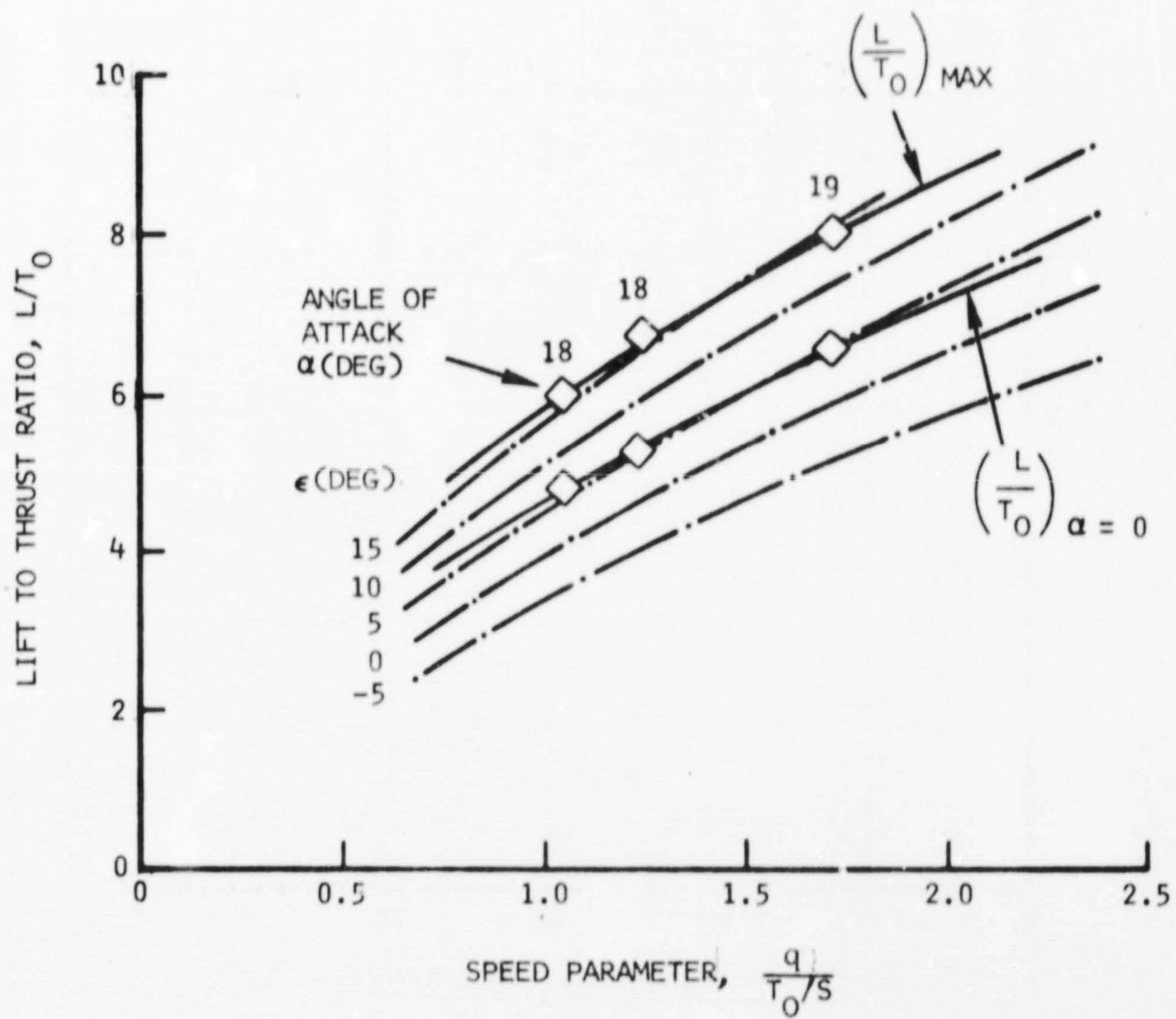


Figure 58. Lift, Angle of Attack, and Downwash Relation Vs Speed Parameter

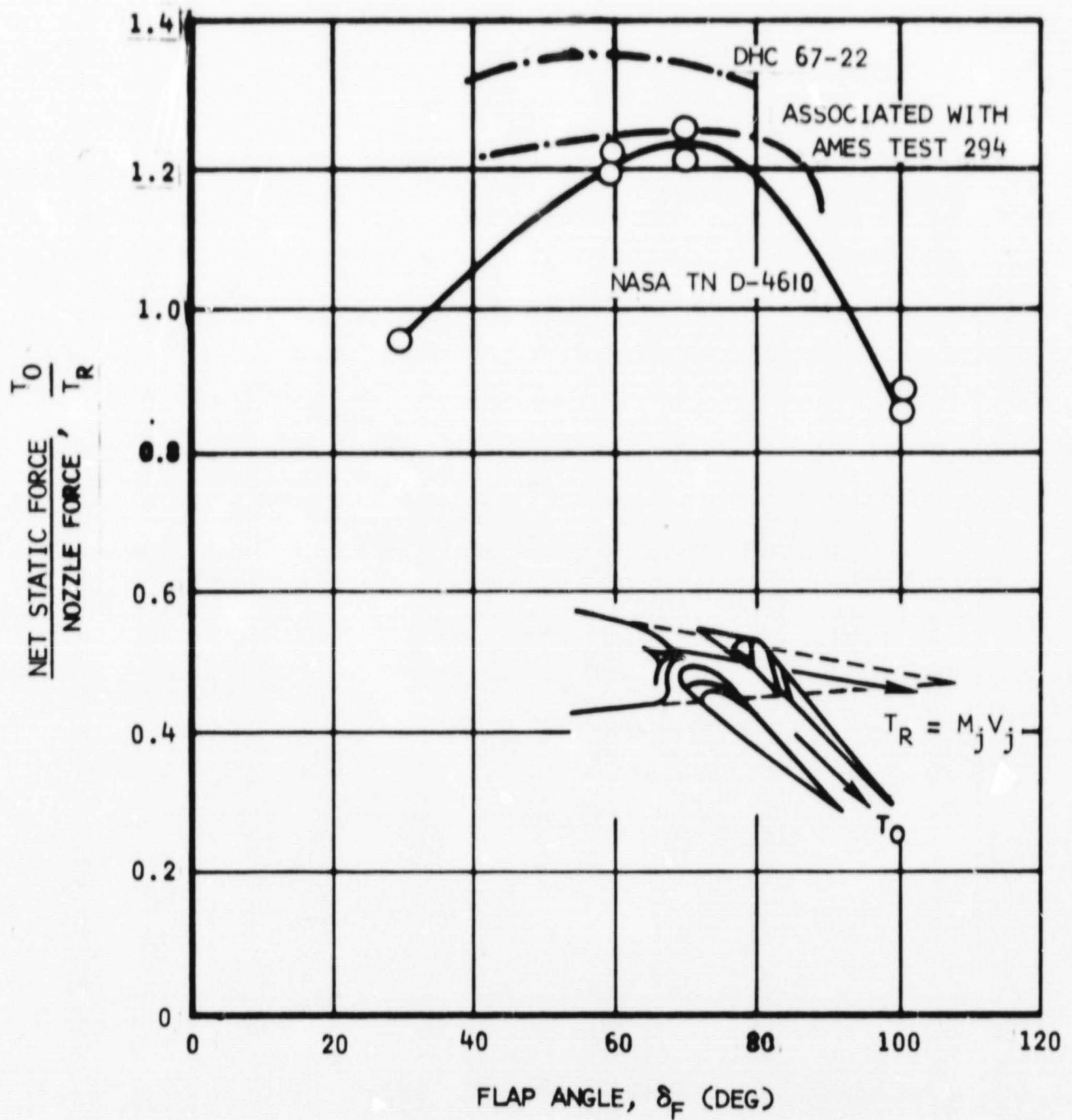


Figure 59. Static Force Augmentation

Some improvements in lift at forward speed have been obtained by improving the geometry of the wing-body intersection. Since these improvements are not incorporated in the present Buffalo modification, a relatively low value of  $T_O/T_C$  is used here to account for this when multiplied with the  $L/T_O$  data from the Ames 294 test. Also, the location of the fuselage side-mounted T64 engines are expected to represent an obstruction in the flap downwash, probably lowering the lift somewhat. Furthermore, a somewhat lower lift value is obtained by using only 20 degrees aileron droop instead of the 45 degrees used in the NASA tests. The following values are chosen for direct application to the  $L/T_O$  data of test 294:

$$\frac{T_O}{T_C} = 1.15 \text{ for } \delta_F = 50^\circ \quad (102)$$

$$\frac{T_O}{T_C} = 1.24 \text{ for } \delta_F = 65^\circ \quad (103)$$

$$\frac{T_O}{T_C} = 1.21 \text{ for } \delta_F = 80^\circ \quad (104)$$

The nozzle thrust used for normal T64 engine operation is  $T_C = 8,600$  pounds which is the static engine thrust for four engines minus duct losses. Seventy five percent of this value is taken for the one-engine-out operation; i.e., no emergency overrating is used.

The aforementioned values of  $T_C$  and  $T_O$  were also used in the tail-off pitching moment characteristics  $M/(T_O c)$  versus the speed parameter. Test 294 data were used to obtain

$$\frac{M}{T_O c} = \frac{C_m q S c}{T_O c} = \frac{C_m}{C_J} \quad (105)$$

The tail-off pitching moments of this test are considered directly applicable because the length and width in relation to the wing chord and span is almost identical between the wind tunnel model and the Buffalo airplane.

Large differences in the downwash angles at constant angles of attack have been found for two different tests (NASA/Ames test 294 and tests reported in TN D-4610). These differences are believed to stem also from the different geometry of the wing-body intersection. Because the wing-lift coefficient  $C_L$  is high, relatively minor changes in the shape of the wingload distribution near the fuselage results in relatively significant local changes in the strength of the trailing vortices; and, this may strongly affect the downwash

at the tail. Because the wing-body intersection of the modified Buffalo is relatively unsophisticated, it is believed that the downwash level will be closer to that of TN D-4610 than of the test 294.

It is suggested that close attention be given to the fairings of the wing-body intersections during the up-coming wind tunnel tests so that a better downwash prediction can be made and that the confidence in the flying qualities prediction can be improved. Also, if during the lifetime of the airplane, the fairings are improved, serious considerations must be given to the change of the downwash level.

In view of the difference in downwash level, a difference in the downwash distribution over the span of the horizontal tail was expected. This could lead to different tail angles of attack at which the tail stalls. Tail stall is one of the considerations that could limit the speed ranges previously shown. However, a comparison of the tail characteristics at practically constant tail angle of attack and varying elevator angle shows no significant differences. (See figure 60.) Thus, the tail characteristics are presently assumed to be independent of downwash distortions.

The tail characteristics used are presented in figure 61. They are derived from DHC 67-20 and are the tail characteristics of the unmodified Buffalo. A check of the tail lift curve slope shows agreement with the Weisinger lifting surface theory.

Another speed limitation is the flow separation of the leading edge slat lower surfaces (L.E. slat stall). The lift coefficients at which this occurs is plotted versus  $C_L$  at  $\alpha = 0$  in figure 62, and obtained from test 294 for various levels of  $C_J$ . The ordinate  $C_L$  at  $\alpha = 0$  is a measure of the flap effect on lift and its value is increasing with flap deflection as well as blowing.

At lower lift coefficients than those for stall onset, the wind tunnel data have shown an increase in longitudinal stability for all flaps-down cases. A decrease in stability was noticed in the flaps-up case. While it is not expected that this is critical, a closer analysis of the modified aircraft should be made during the design phase. Airplane buffeting is expected in the stalled region.

The elevator versus speed characteristics shown in the beginning of this section were given only for idle cruise engine thrust ( $T_{CR} = 0$ ). Some aft center-of-gravity cases from those data are now repeated in figure 63, and compared with characteristics with maximum cruise engine thrust at  $T_{CR} = 10,000$  pounds. It is seen that the elevator angle versus speed relation (flaps down) is significantly less stable with the thrust than without. Also, it is seen that conditions with thrust require a much larger elevator-down deflection.

$i_H$	$C_J$	REF.
○ 3.5	.80	TEST 294, DHC 67-42 FIG. 78
□ 1.0	1.15	NASA TN D-4610 FIG. 19/20
△ 3.5	.54	TEST 294, RUNS 26, 13
● -15	0	TEST 294, RUNS 34, 35

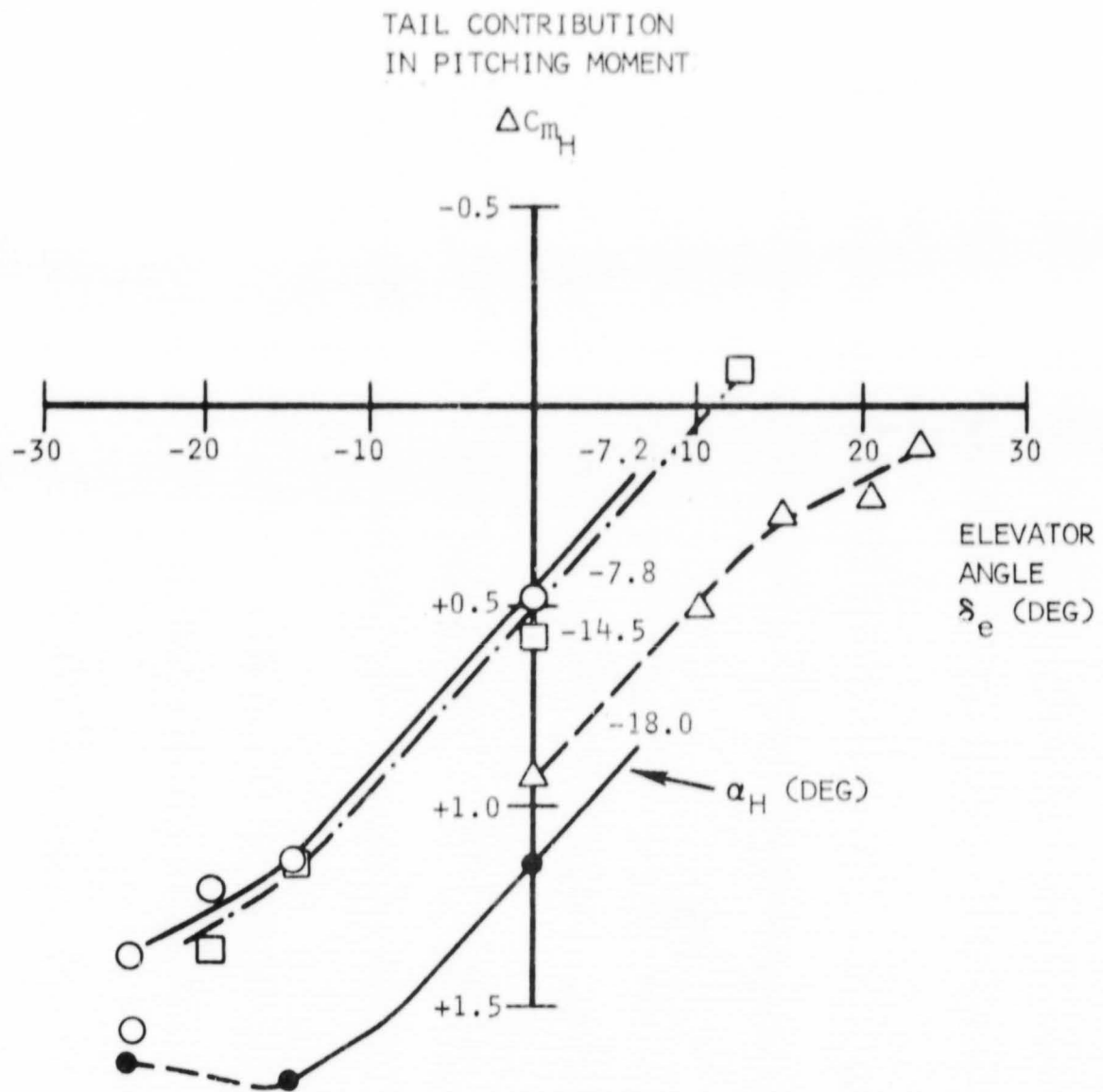


Figure 60. Ames Augmentor Wing Model Pitching Moment Due to Tail at  $\alpha = 0$

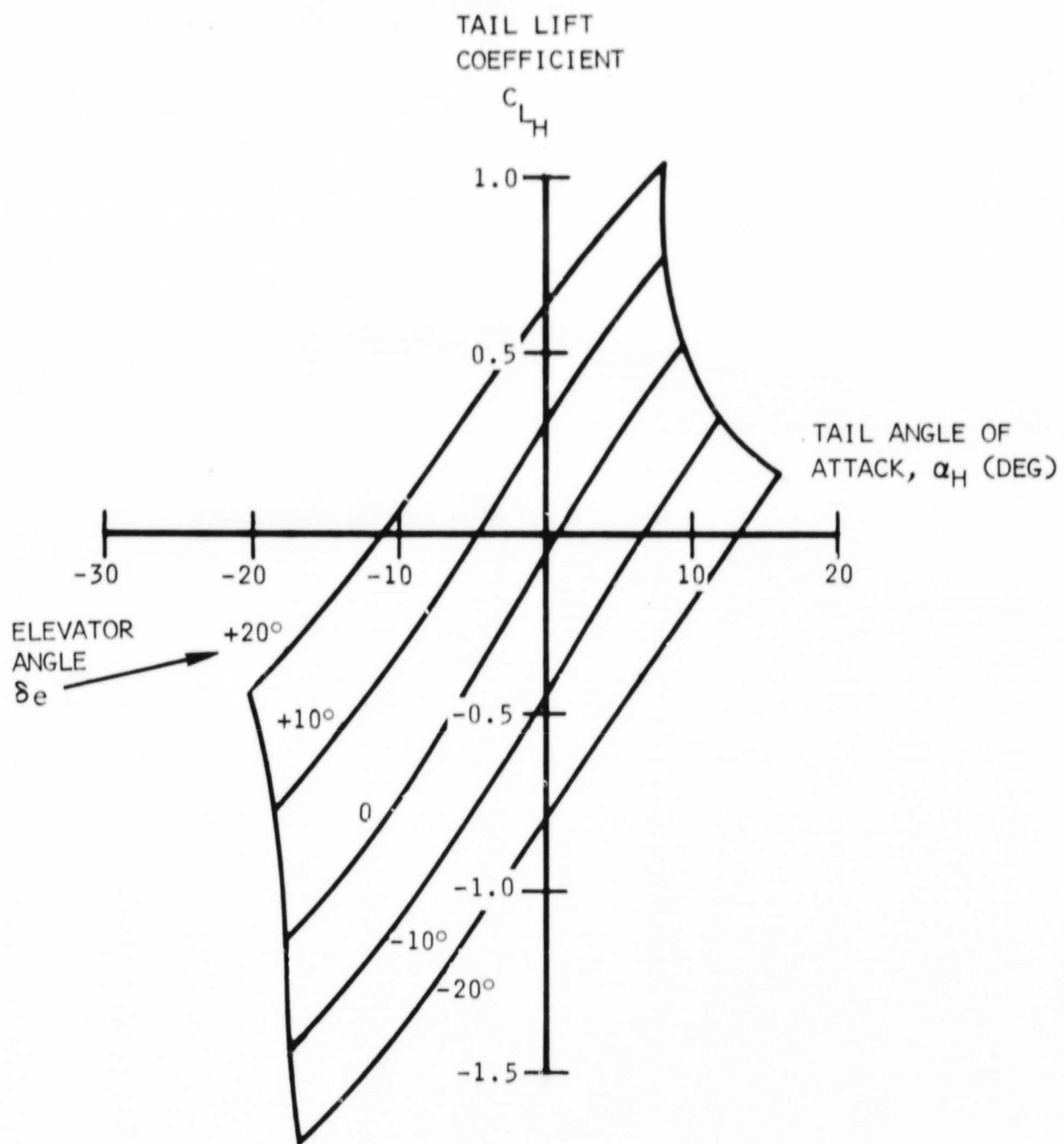


Figure 61. Horizontal Tail Characteristics

REF	RUN	FLAPS	SLATS
● TN D-4610		UP	ON
○ TEST 294	4	DOWN	60,60,40
△ TEST 294	9	DOWN	60,60,60
□ TEST 294	13	DOWN	70,60,60
◇ TEST 294	19	DOWN	70,60,60

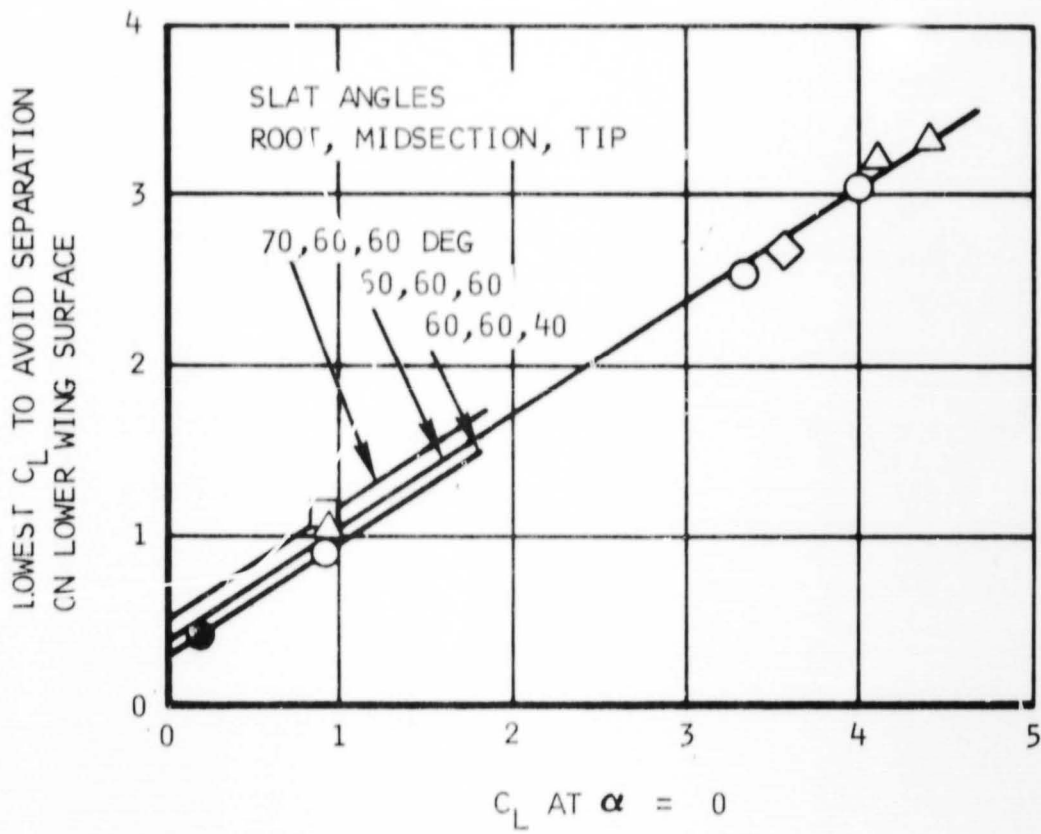


Figure 62. Slat Stall Correlation



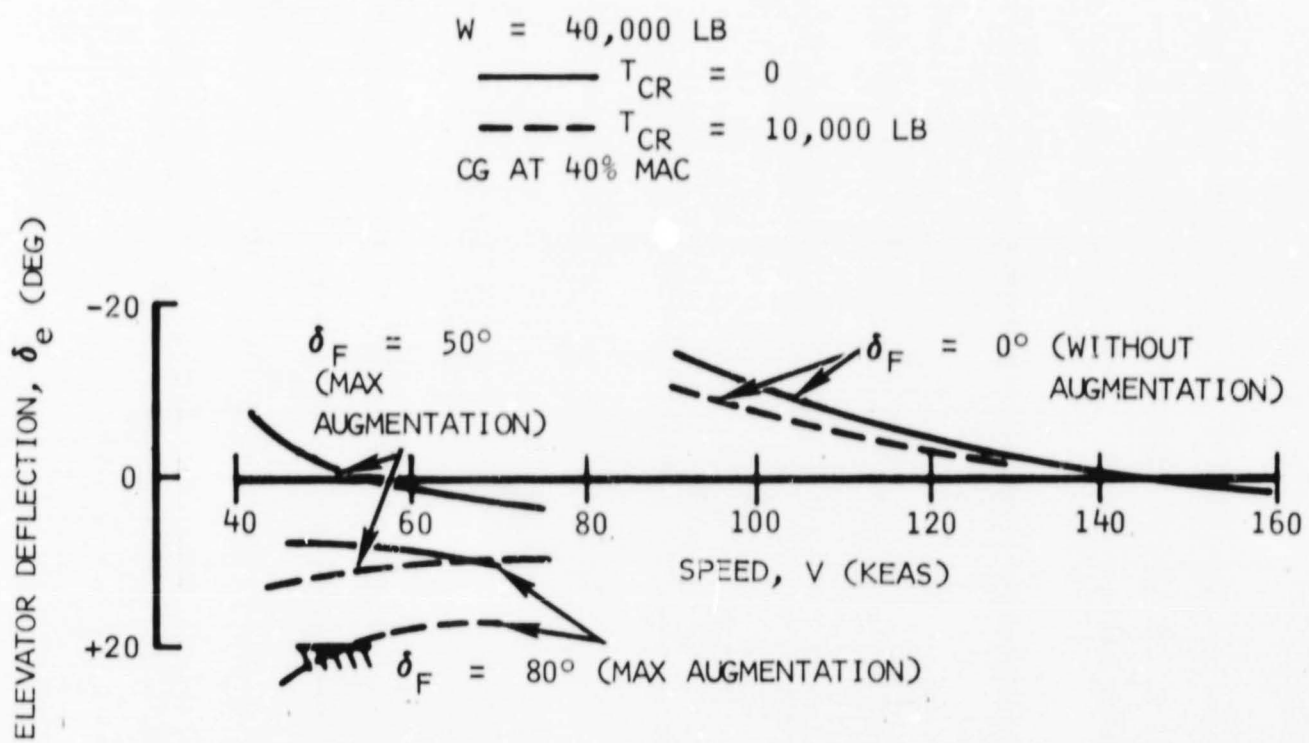


Figure 63. Steady-State Longitudinal Characteristics With and Without Cruise Engine Thrust

The effect of the cruise engine thrust is determined from

$$\Delta\delta_e = \frac{\Delta M}{\frac{\partial\left(\frac{M}{T_{OC}}\right)}{\partial\delta_e} (T_{OC})} \quad (106)$$

where  $\Delta M$  is the moment change due to the cruise engine thrust acting on a moment arm  $a$

$$M = a(T_{CR}) \quad (107)$$

The moment arm is approximately 3.7 feet, varying slightly with cruise thrust nozzle rotation. The magnitude of  $\Delta\delta_e$  is presented separately in figure 64.

It should be recalled that the data without cruise engine thrust at forward center-of-gravity locations and flaps 50 degrees show large upward elevator deflections, particularly at low speeds. Present data with the cruise engine thrust at aft center-of-gravity locations and flaps 80 degrees show large downward deflections, also at low speed. At some low speed, the full elevator travel is consumed. The stabilizer angle should be carefully adjusted so that the uplimit and downlimit is reached at the same speed. This speed is called here the longitudinal minimum control speed,  $V_{min}$ . The existing aircraft stabilizer installation provides some ground adjustment capability.

To obtain this speed, data have been plotted in figure 65, assuming that the spread between the fore and aft center-of-gravity limit is 10 percent MAC. A similar plot is made in figure 66, assuming that this spread is 5 percent MAC. Resultant values of  $V_{min}$  are presented in figure 67, showing 51 knots for the 10-percent case, and 39 knots for the 5-percent case. The 51 knots speed limit is compatible with the 50 knots stall speed with one T64 engine inoperative, shown before for  $\delta_F = 80$  degrees.

Stick-fixed longitudinal stability  $d(M/c)/dL$  versus speed is shown in figure 68 for flaps 50 degrees and maximum lift augmentation. The airplane shows a slight instability at very low speeds which is common to many V/STOL airplanes. At a higher flap angle, the airplane is slightly more stable. At less lift augmentation the airplane is significantly more stable.

The data is derived from  $dC_m/dC_L$  in figure 69, using

$$\frac{d\frac{M}{C}}{dL} = \frac{d\frac{M}{T_{OC}}}{d\frac{L}{T_O}} = \frac{d\frac{C_m q S c}{T_{OC}}}{d\frac{C_L q S}{T_O}} = \left(\frac{dC_m}{dC_L}\right)_A \quad (108)$$

CHANGE OF  
ELEVATOR ANGLE  
DUE TO CRUISE THRUST,  
 $\Delta\delta_e$  (DEG)

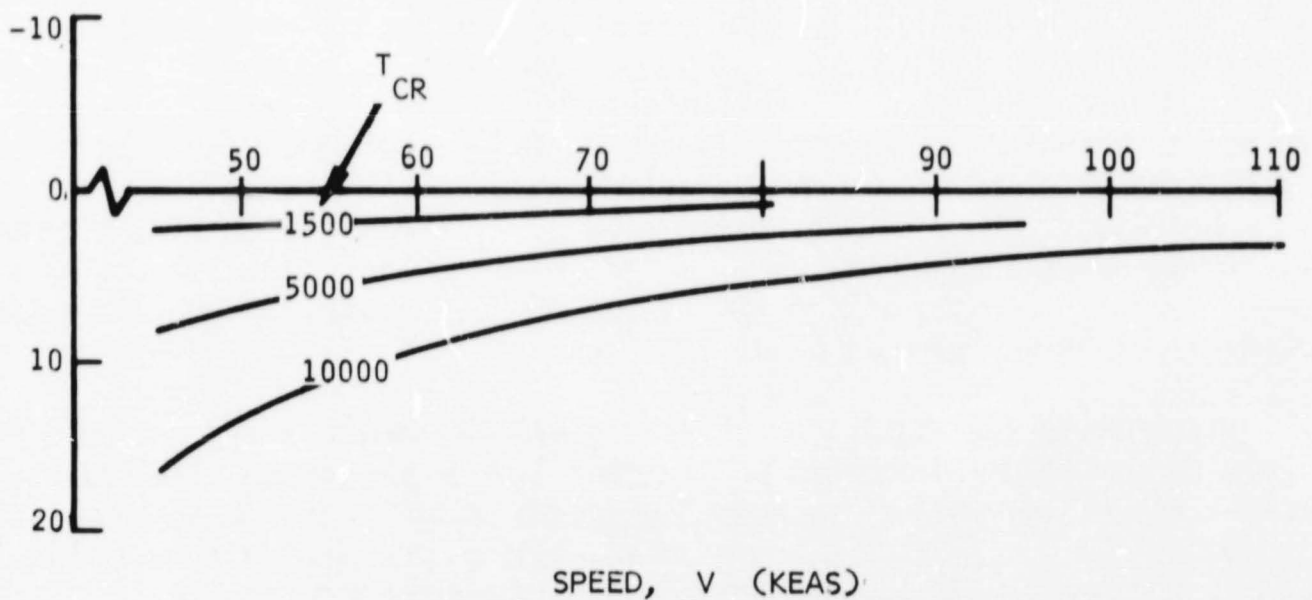
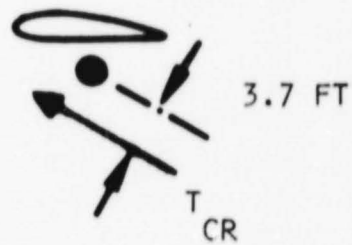
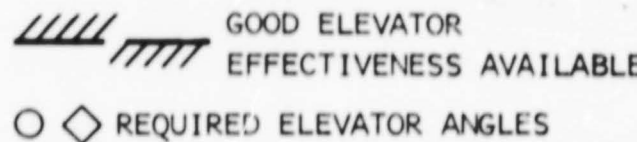
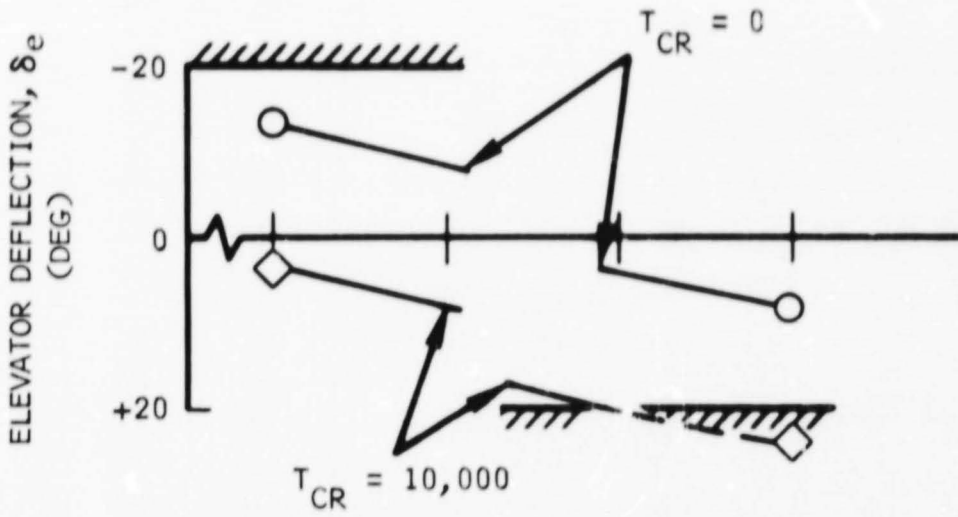


Figure 64. Effect of Maximum Cruise Thrust on Elevator Angle in Steady-state Flight



MAX. AUGMENTATION  
 WITH AND WITHOUT CRUISE THRUST  $T_{CR}$   
 $i_H = 0$   


$V = 45 \text{ KEAS}$



$V = 50 \text{ KEAS}$

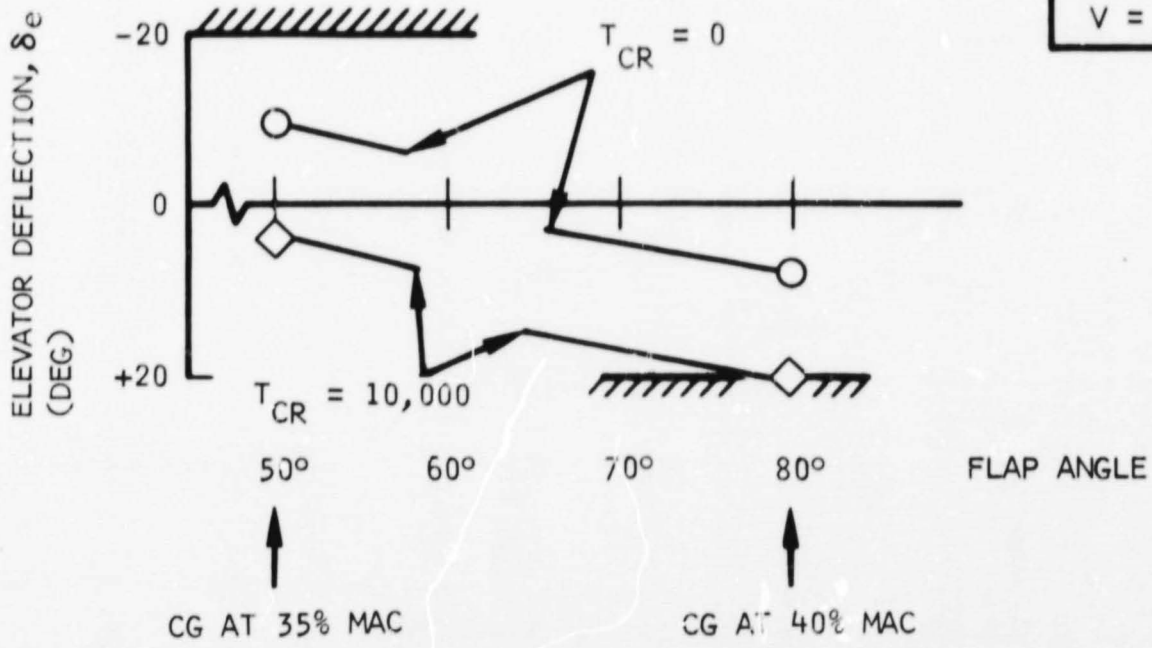


Figure 66. Available and Required Elevator Capability for a Center of Gravity Shift of 5-percent MAC

W = 40,000 LB

AFT CG LOCATION AT 40% MAC

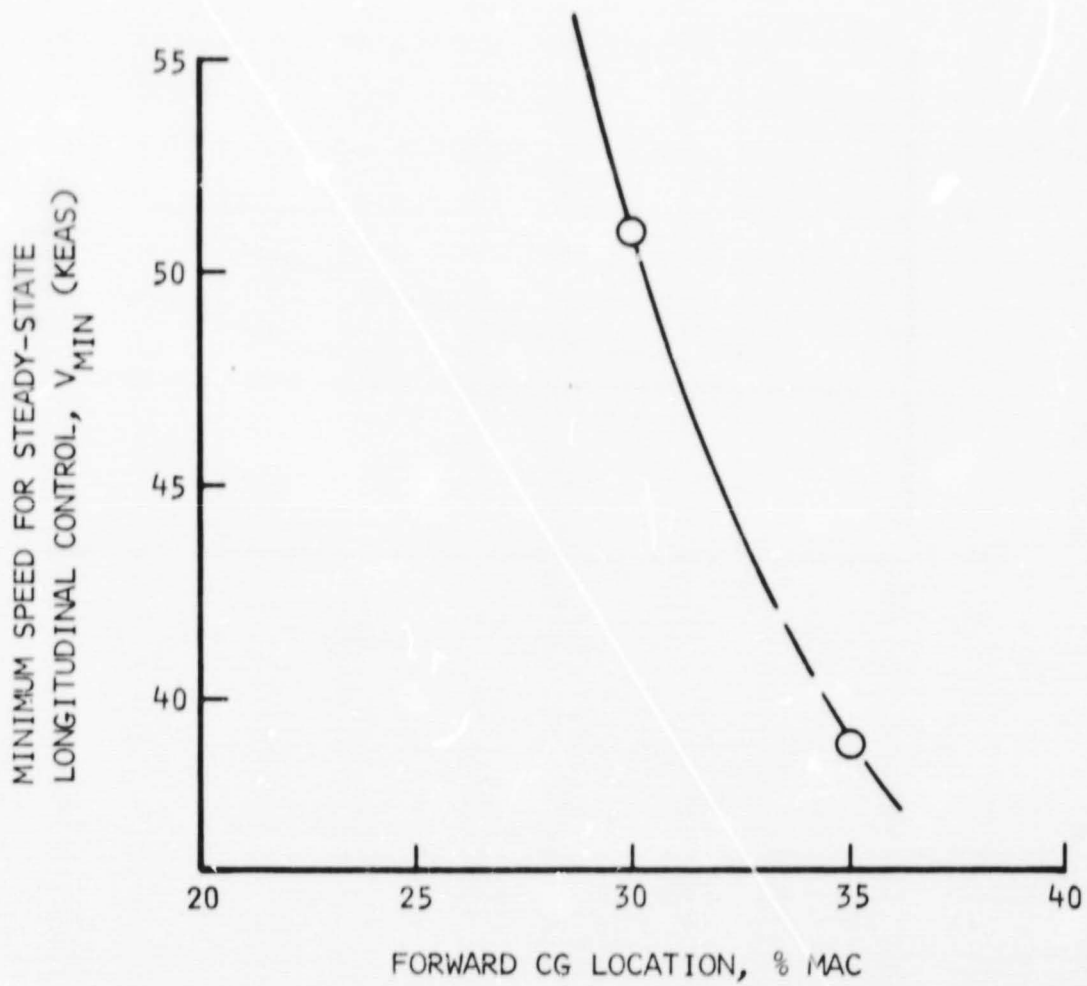


Figure 67. Minimum Speed for Steady-state Longitudinal Control

ELEVATOR FIXED  
FLAPS 50°  
MAX LIFT AUGMENTATION  
W = 40,000 LB

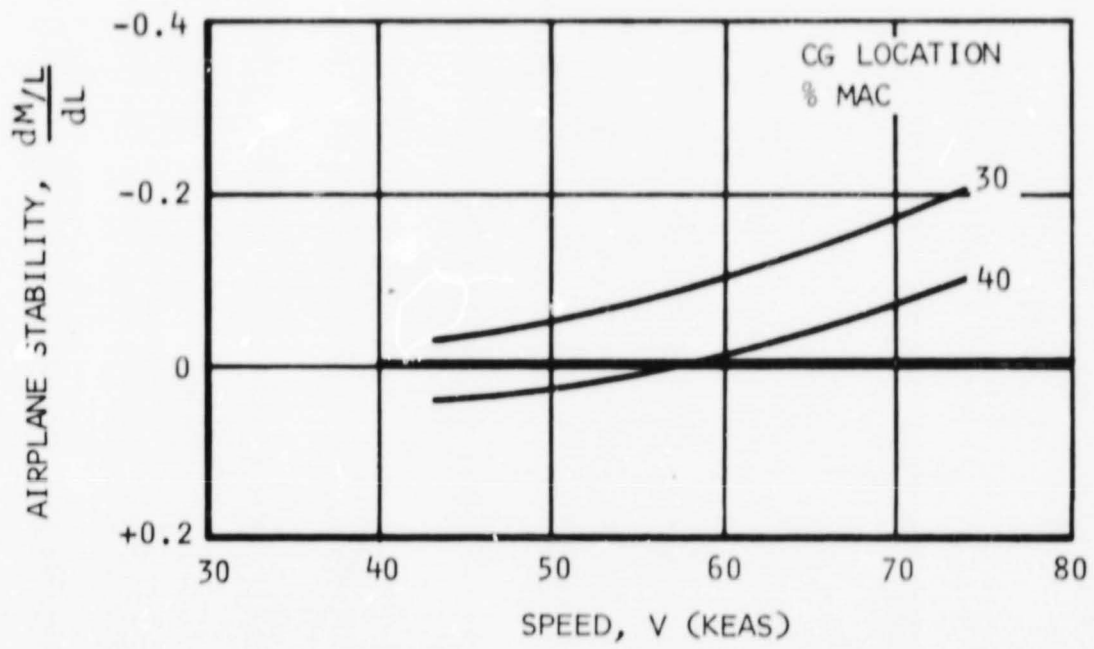


Figure 68. Airplane Longitudinal Stability Versus Speed

ELEVATOR FIXED

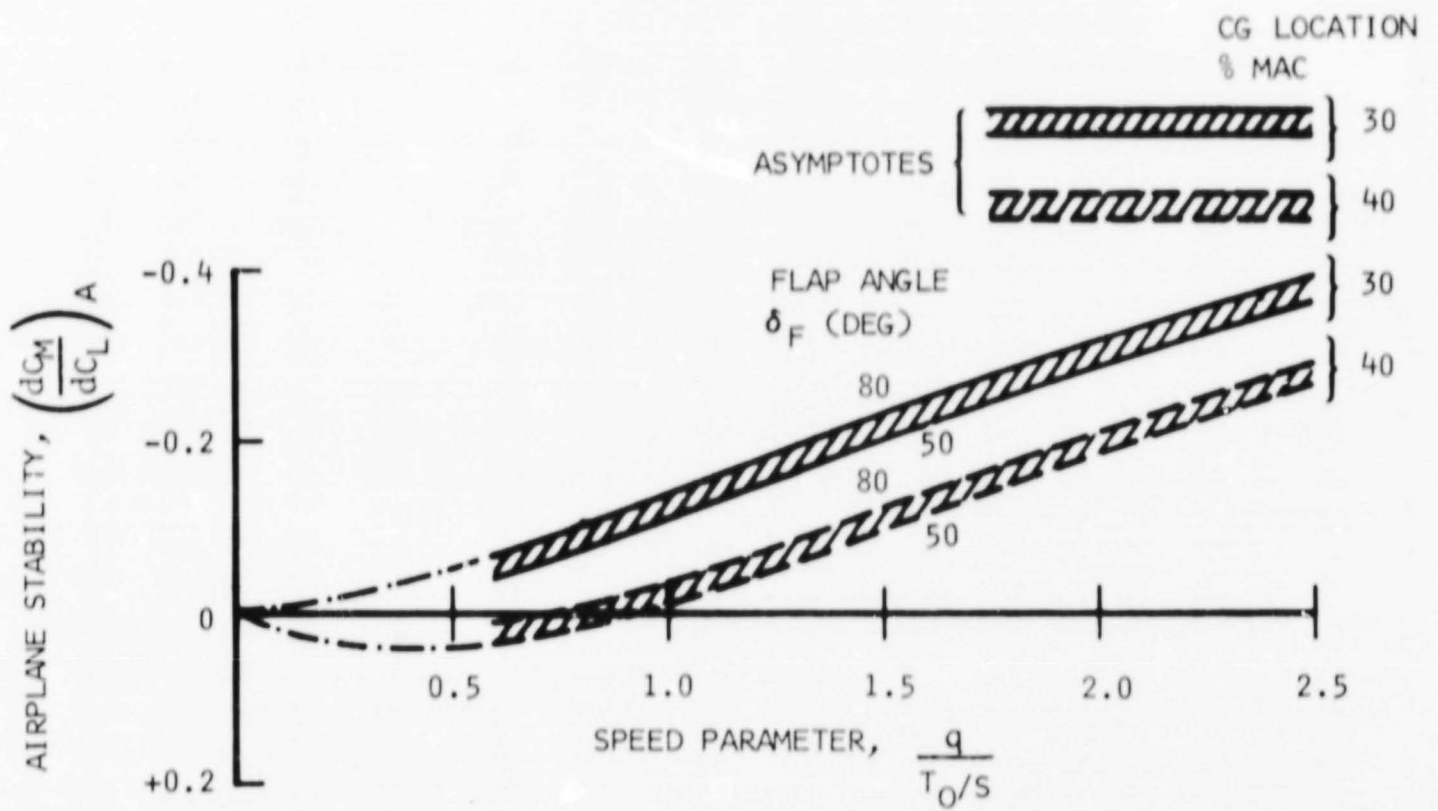


Figure 69. Airplane Longitudinal Stability Versus Speed Parameter



This stability level  $(dC_m/dC_L)_A$  is derived from a tail-off value and a tail contribution, both shown in figure 70. The tail contribution is derived from

$$\frac{dC_m}{d\alpha_H} = \left(1 - \frac{d\epsilon}{d\alpha}\right) C_{L_{\alpha_H}} \cdot \bar{V}_H \quad (109)$$

where  $d\epsilon/d\alpha$  is obtained from test 294 as a function of the speed parameter as shown in the Supporting Aerodynamic Data section. The tail-off values also are based on test 294 data and presented in figure 71.

The initial nose-up pitch acceleration capability,  $\ddot{\theta}$ , is shown in figure 72 with the stabilizer adjusted such that  $V_{min}$  can be reached. With the center of gravity located at 30-percent MAC (in conjunction with an aft limit of 40 percent), no pitch acceleration is available at  $V_{min}$  since all elevator capability is consumed for steady-state equilibrium. With an increase of speed, an increase in  $\ddot{\theta}$  capability is obtained, but the target value of 0.36 rad/sec<sup>2</sup> is reached only at speeds above 70 knots.

To obtain the target value at landing speeds of 60 to 65 knots, the center of gravity for STOL landings should not exceed the forward limit of 35- to 33-percent MAC. This forward limit is exceeded in the full-fuel condition because the fuselage side-mounted T64 engines force the fuel to be located forward in the fuselage.

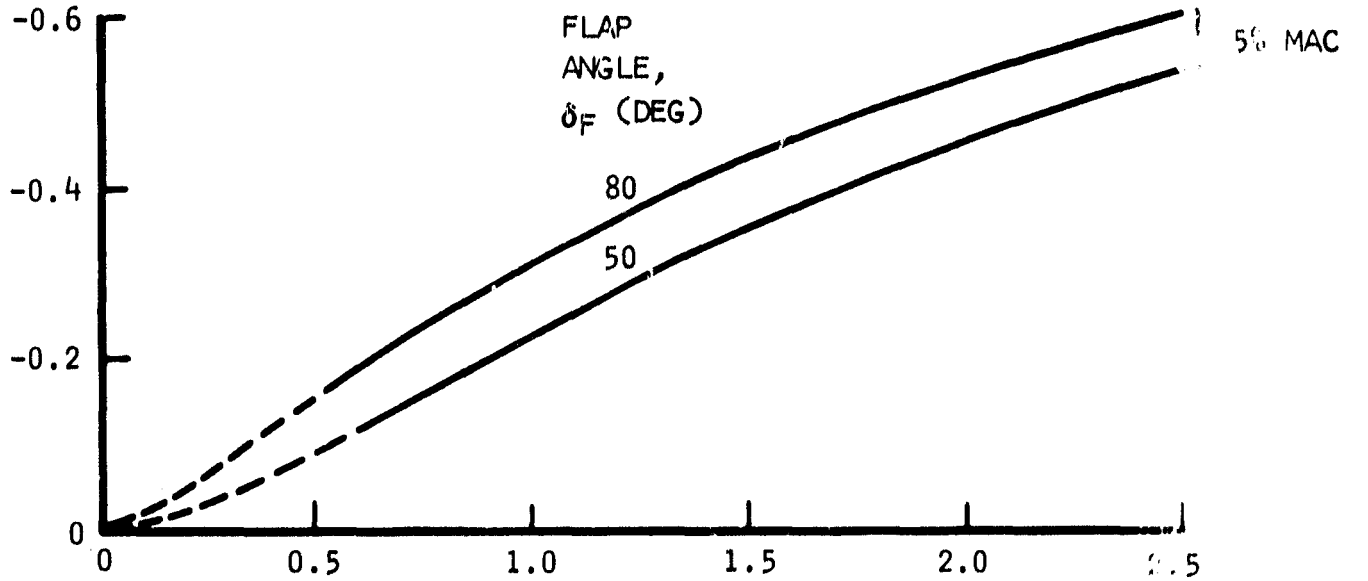
The sum of the pitch-down and pitch-up capability is presented in figure 73. The above pitch acceleration capability is presented for an airplane weight of 40,000 pounds. At a lower weight, fuel has been consumed from near the center of the airplane, and the moment of inertia is, therefore, not significantly reduced. Since the pitch acceleration is primarily a function of the ratio of the forward speed to the moment of inertia (for given center of gravity locations), the pitch acceleration is expected to be adequate for low airplane weights only when these landing speeds are not reduced.

Thrust vectoring with the rotatable cruise engine nozzles has been analyzed for the landing approach. Results for 40,000 and 30,000 pounds gross weight are presented in figure 74 and 75. The level of the cruise thrusts is assumed to be  $T_{CR} = 1,500$  pounds total. In this analysis, before entering the final approach, the flaps are first deflected in such a way that thrust and drag equilibrium exists in level flight at  $\alpha = 0$ , using this cruise engine thrust of 1,500 pounds. Simultaneously, a lift and weight equilibrium is established at this flap angle and  $\alpha = 0$  by properly adjusting the T64 engines. Subsequently, the landing glide is commenced without readjusting the lift augmentation. This is done by rotating the flaps to 80 degrees and rotating the cruise nozzles a certain amount forward for flight path control commensurate with the sink rate of 13 ft/sec.

STABILITY INCREMENT  
DUE TO TAIL

$$\left( \Delta \frac{dc_M}{dc_L} \right)_H$$

ASYPMTOTE



TAILOFF STABILITY  $\left( \frac{dc_M}{dc_L} \right)_{H0}$

FLAP ANGLE  $\delta_F$  (DEG)

CG LOCATION

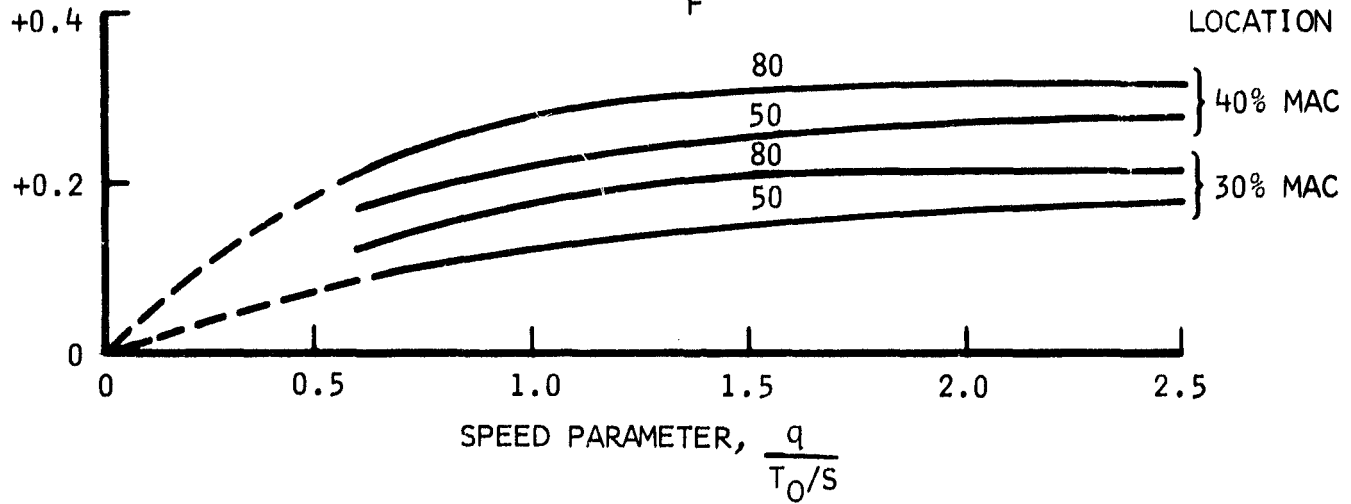


Figure 70. Longitudinal Stability Components Versus Speed Parameter

TEST 294

$\alpha = 0$

REF: 25% MAC

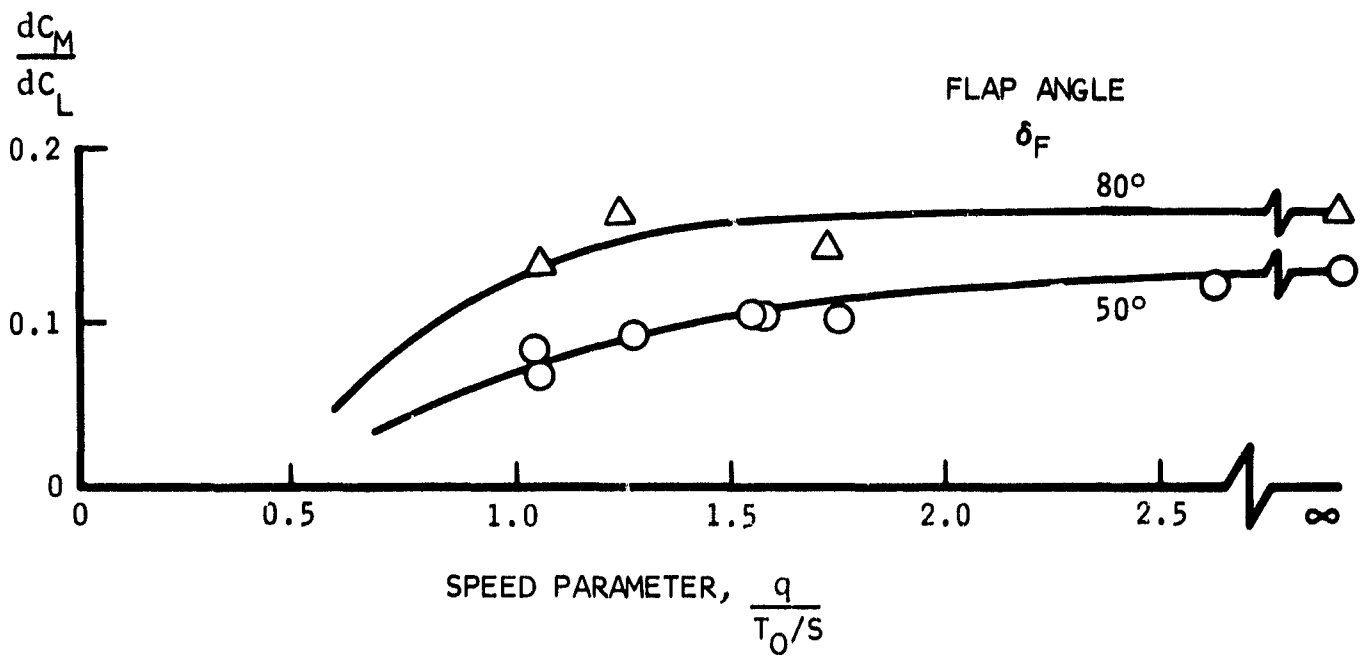


Figure 71. Ames Augmentor Wing Model  
Tailoff Longitudinal Stability Versus Speed Parameter

$W = 40,000 \text{ LB}$   
 $I = 212,000 \text{ SLUG-FT}^2$   
 AFT CG LOCATION = 40% MAC

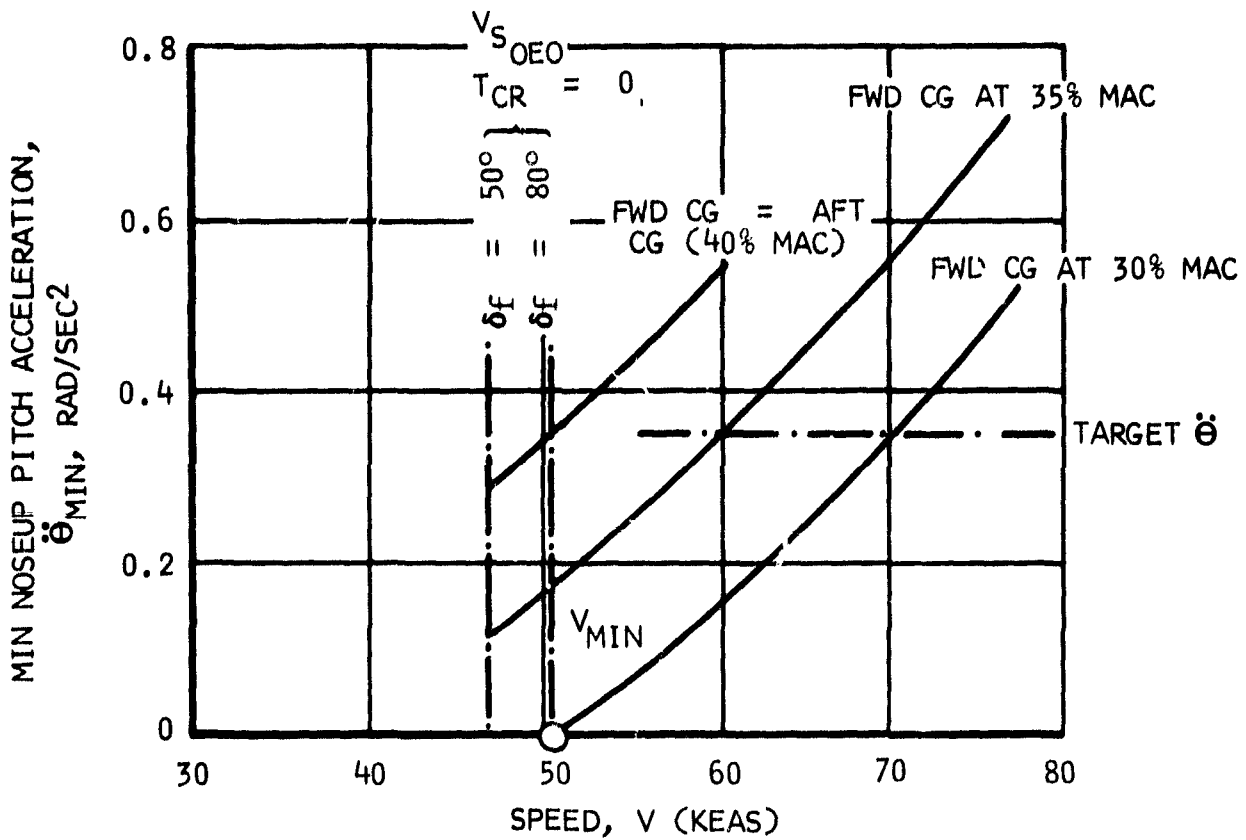


Figure 72. Minimum Noseup Pitch Acceleration Capability

I = 212,000 SLUG-FT<sup>2</sup>  
W = 40,000 LB

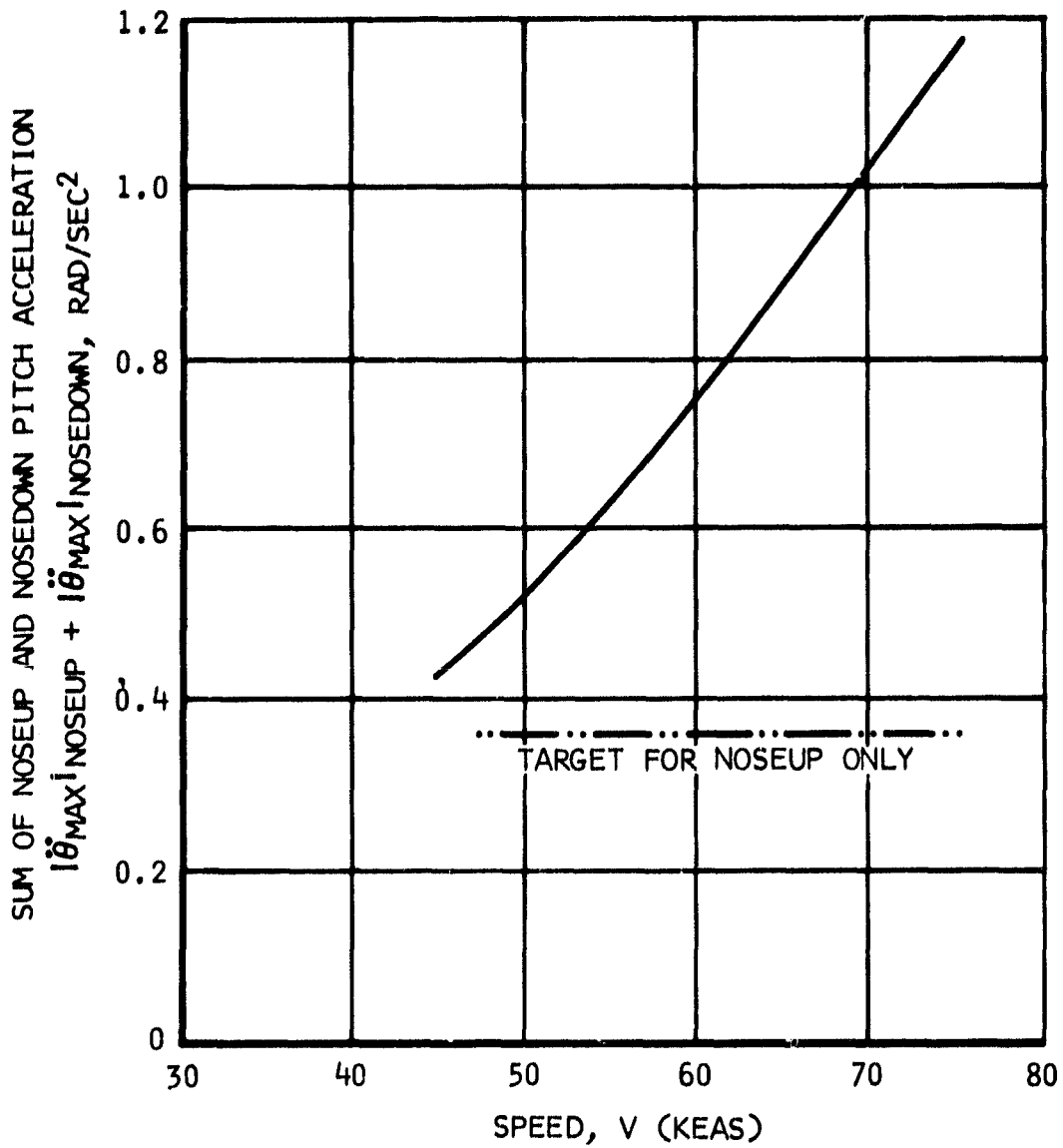


Figure 73. Maximum Noseup and Nosedown Pitch Acceleration

$$\alpha = 0^\circ$$

$$W = 40,000 \text{ LB}$$

◆ LEVEL FLIGHT WITH  $T_{CR} = 1,500 \text{ LB MAX AFT}$

● FINAL APPROACH WITH  $T_{CR} = 1,500 \text{ LB ROTATED FWD}$

→ VECTOR OF CRUISE NOZZLE FORCE

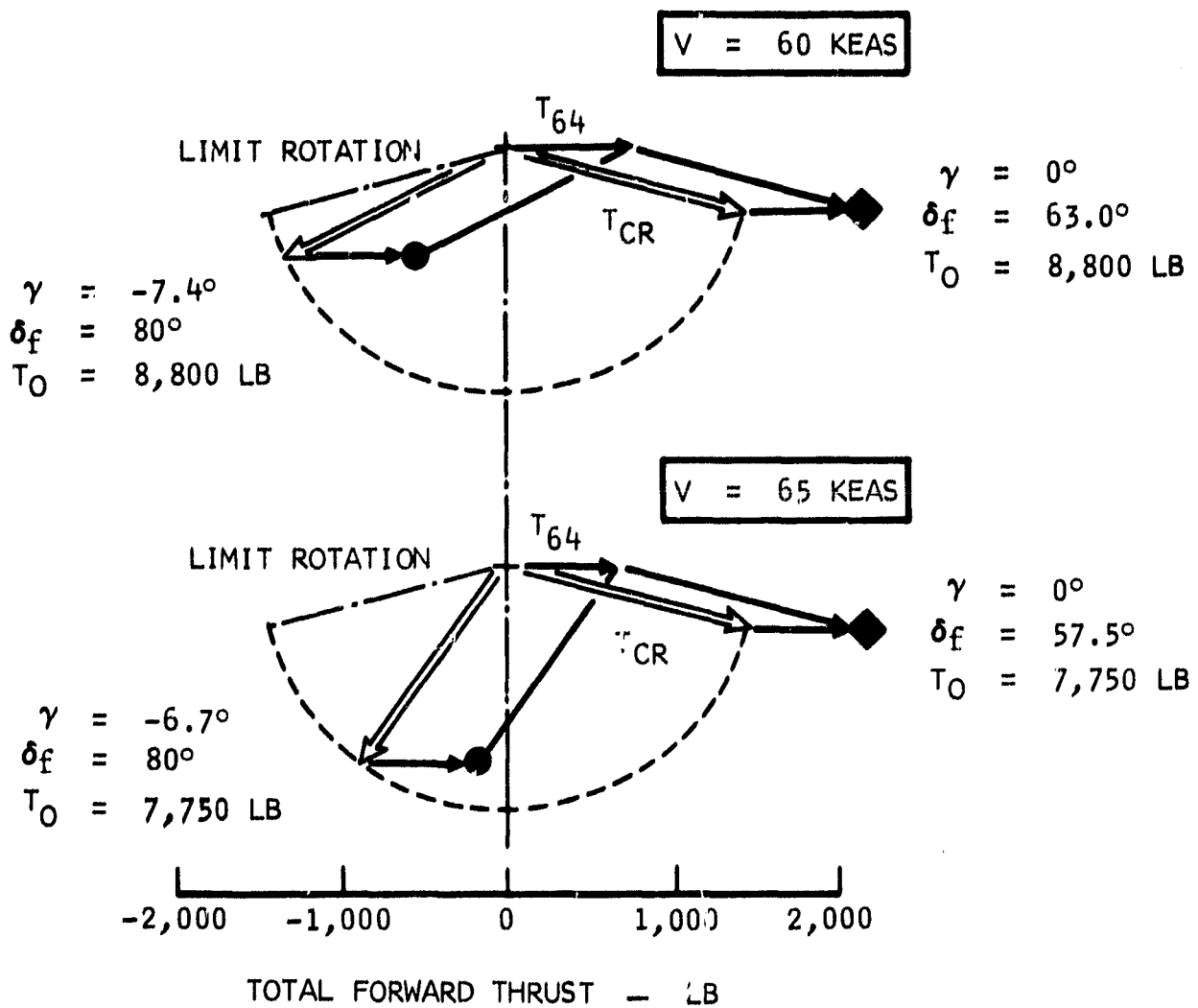


Figure 74. Thrust Vector Diagram for Landing

$$\alpha = 0^\circ$$

$$W = 30,000 \text{ LB}$$

◆ LEVEL FLIGHT WITH  $T_{CR} = 1,500 \text{ LB MAX AFT}$

● FINAL APPROACH WITH  $T_{CR} = 1,500 \text{ LB ROTATED FWD}$

→ VECTOR OF CRUISE NOZZLE FORCE

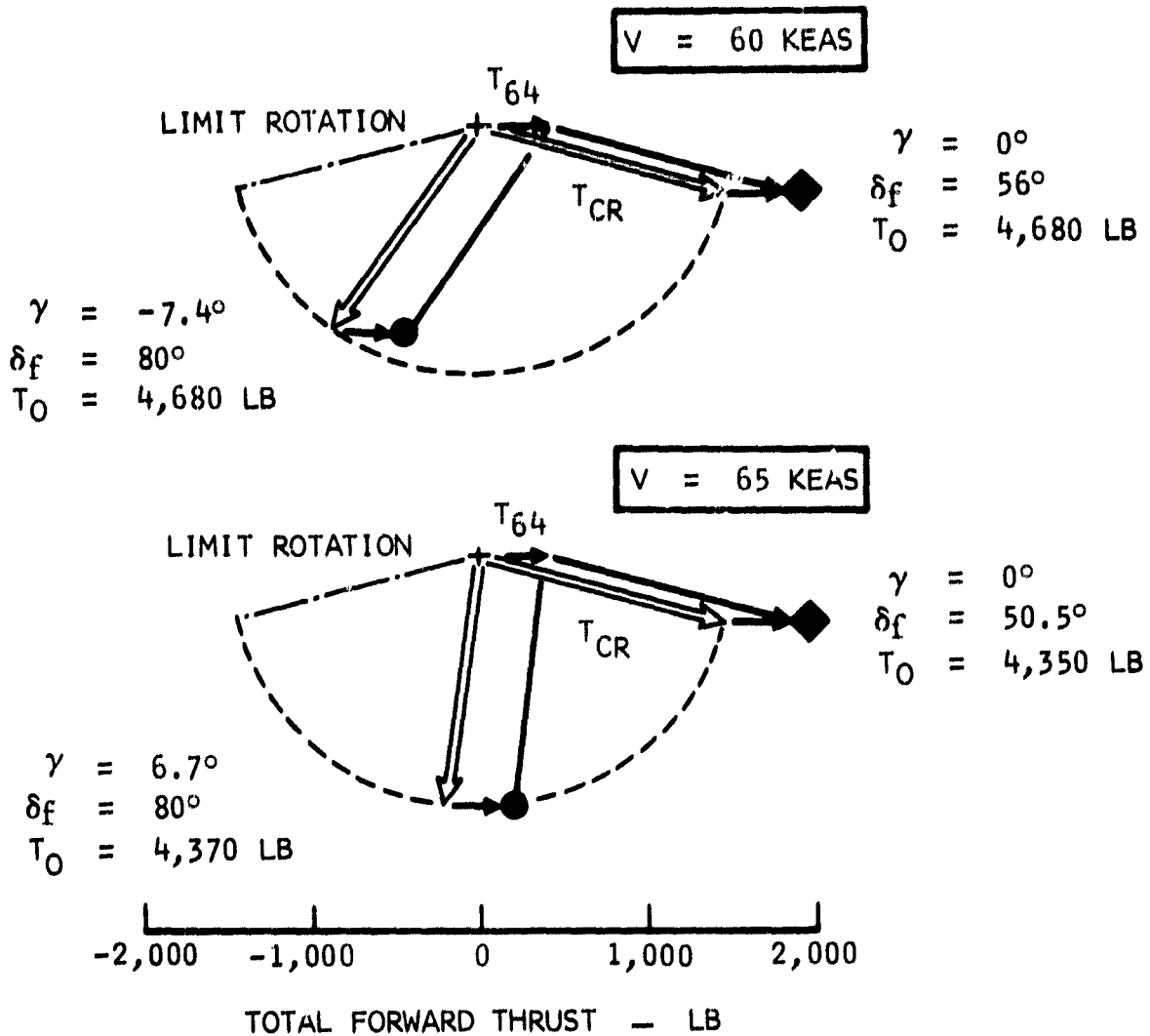


Figure 75. Thrust Vector Diagram for Landing

The figures show that  $T_{CR} = 1,500$  is about the minimum level for the flight path control. It is expected that normal STOL landings are carried out with minimum thrust levels of the cruise engines, in general, in order to conserve fuel, to reserve a good thrust margin for waveoff, to minimize hot gas ingestion, foreign object damage (FOD), and possibly ground erosion just prior to landing. It should be noted that the inlets of the fuselage side-mounted T64 engines may be prone to this hot gas ingestion and FOD, (if no screens are used) and relocation of these engines forward on the fuselage is recommended.

The landing analysis also shows that thrust levels of the T64 engines used in the lift equilibrium ( $T_0$ ) does not exceed the one-engine-out level of

$$T_0 = \left(\frac{T_0}{T_C}\right) T_{C_{max}} \cdot \frac{3}{4} = 1.24 (8600) \left(\frac{3}{4}\right) = 8,000 \text{ pounds} \quad (110)$$

in all cases except at high weight at 60 knots. An increase of  $T_{CR}$ ,  $\alpha$  or speed may alleviate this condition. No ground effects are considered in the aforementioned computations.

The above equilibrium conditions at level flight at  $\alpha = 0$  are obtained from figure 76, where the lift coefficient is presented as a function of the flap angle for various values of the speed parameter. Also, the coefficient  $C_D$  of the net drag (which includes the thrust from the augmentation but no thrust from the cruise engines) is indicated.

It is seen that a change of flap angle does not significantly change the lift so that merely a decrease in flap angle is not adequate to accommodate lightweight conditions at speeds of 60 to 65 knots. However, the effect of a variation in augmentation is strong. Also, a change in angle of attack does not vary the lift adequately to accommodate the light weights. This indicates, that lift control is most efficiently accomplished by augmentation control. Flight path control is accomplished by cruise engine thrust and nozzle angle control. Figure 76 is based directly on the NASA/Ames wind tunnel test 294.

The nose wheel lift-off speed is presented in figure 77 as a function of airplane weight. It is shown that the airplane can be rotated at speeds much lower than needed for takeoff.

The speed is computed by using moment equilibrium equations about the reference point indicated in figure 78.

$$\frac{M_H}{T_{OC}} + \frac{M_W}{T_{OC}} + \frac{M_{CP}}{T_{OC}} + \frac{M_T}{T_{OC}} = 0 \quad (111)$$



$\delta_F$	SYM	$\frac{T_0/S}{q}$			
		50°	○	0	0.38
60°	□	0	0.60	0.83	0.98
70°	△	0	0.57	0.80	1.0

FROM AMES TEST 294

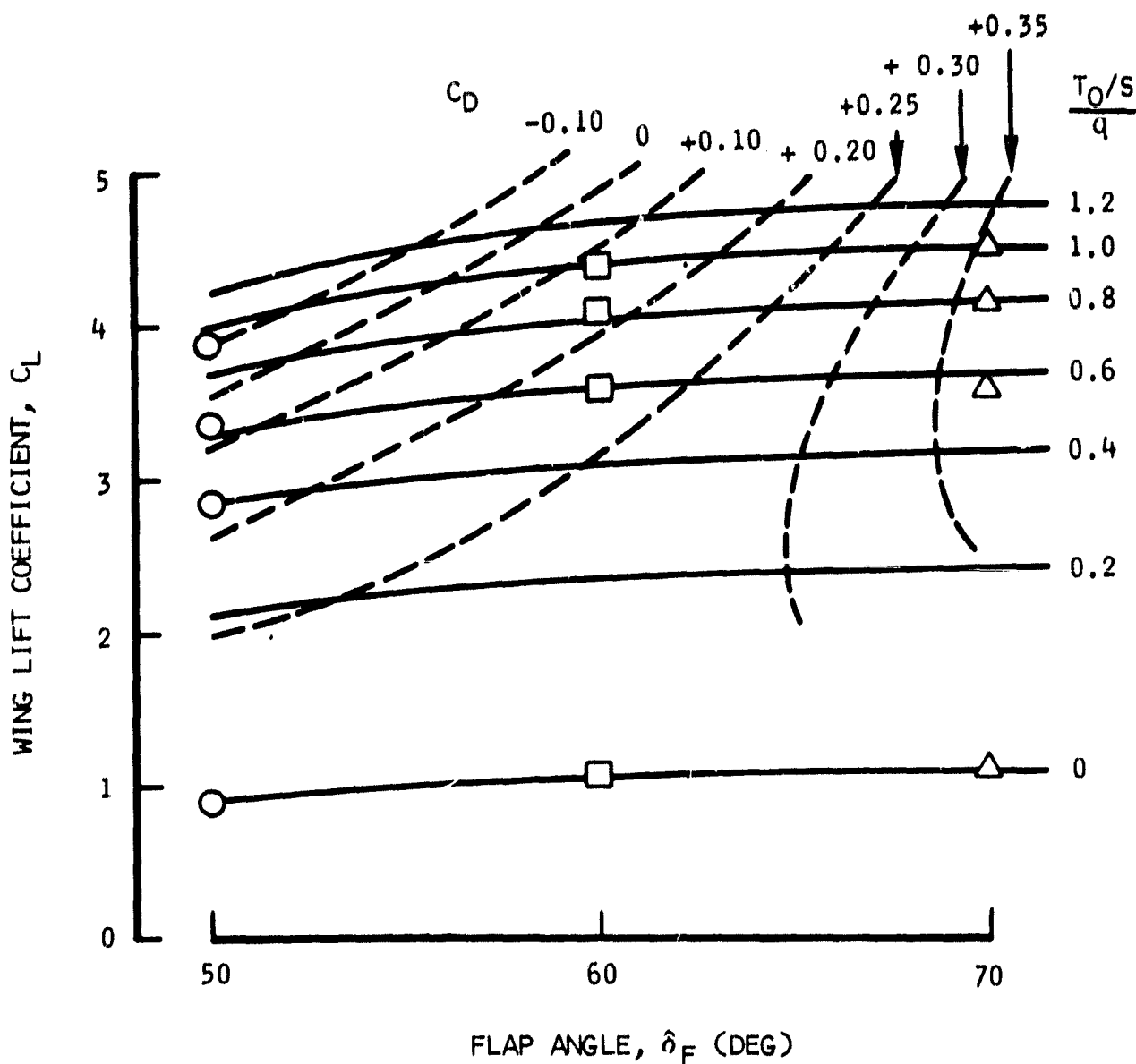


Figure 76. Lift and Drag Coefficient at Zero Angle of Attack

$\delta_F = 50^\circ$   
 $\alpha = 0^\circ$   
 $\mu = 0.05$

CG AT 35% MAC

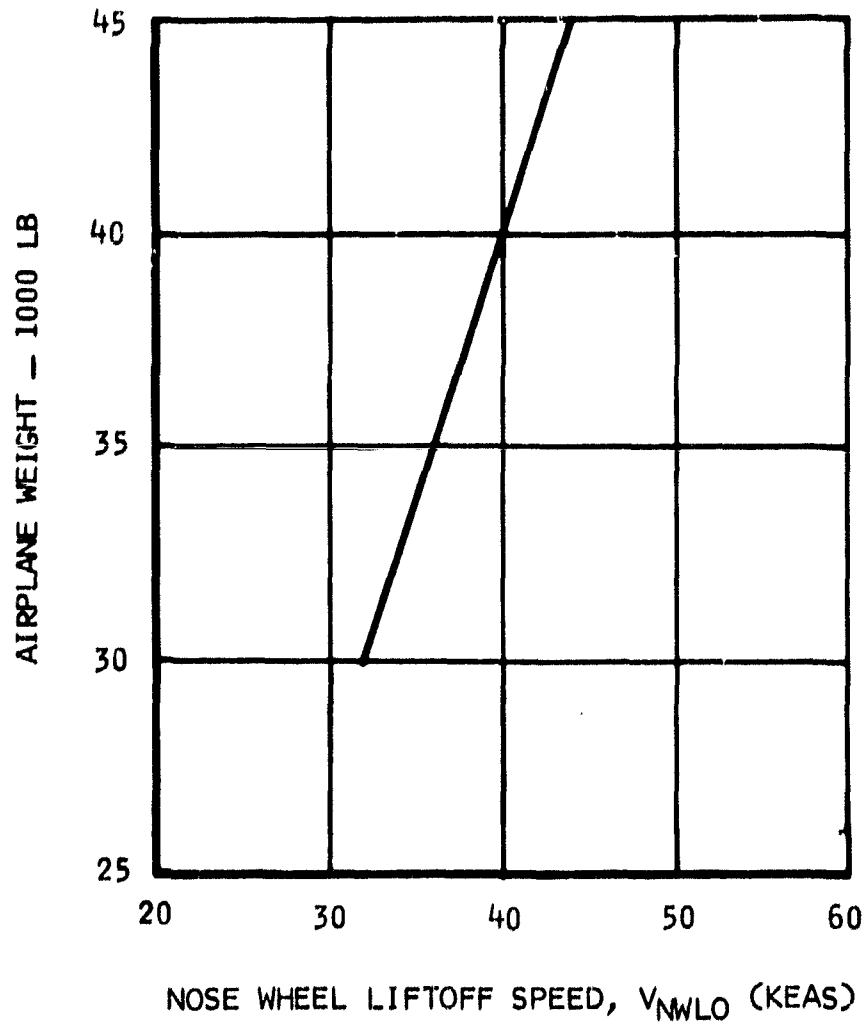


Figure 77. Nose Wheel Liftoff Speed With Maximum Augmentation

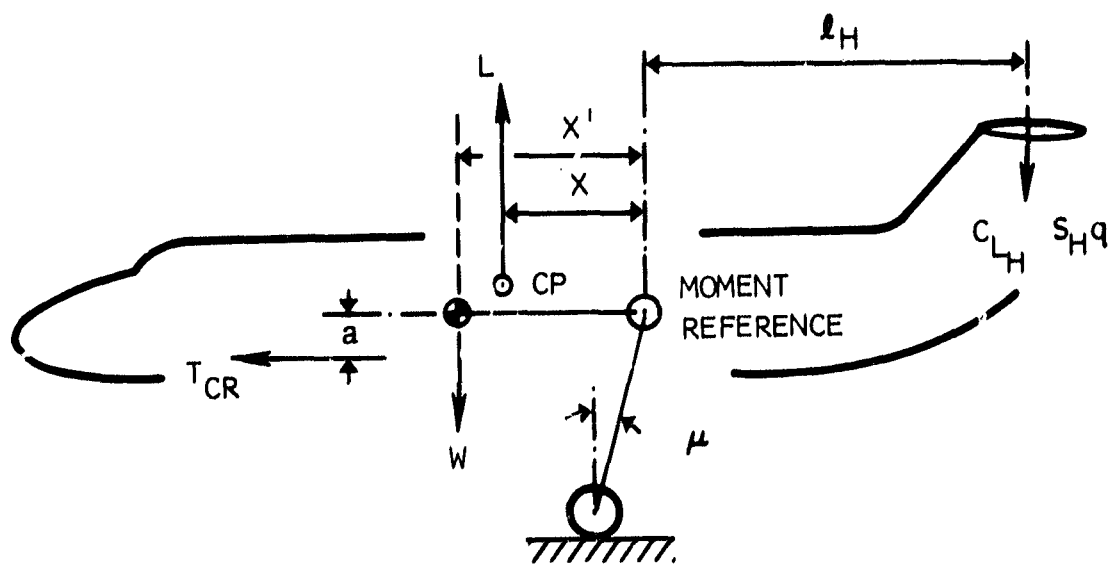


Figure 78. Definition for Nose Wheel Liftoff Computations

where

$$\frac{M_H}{T_{OC}} = C_{LH} \left( \frac{S_H}{S} \right) \left( \frac{L_H}{c} \right) \left( \frac{q}{T_0} \right) \left( \frac{q}{S} \right) \quad (112)$$

$$\frac{M_W}{T_{OC}} = \frac{W \cdot x'}{T_{OC}} \quad (113)$$

$$\frac{M_{cp}}{T_{OC}} = \frac{L}{T_0} \left( \frac{X}{c} \right) \quad (114)$$

$$\frac{M_T}{T_{OC}} = \left( \frac{a}{c} \right) \left( \frac{T_{CR}}{T_0} \right) \quad (115)$$

The value of  $x/c$  as a function of  $L/T_0$  is obtained using figure 79, where the location of the center of gravity can be found from the ratio of  $M/(T_{OC})$  to  $L/T$ . The figure is based on test 294 data.

Main gear lift-off speeds at the ground roll attitude ( $\alpha = 0$ ) and maximum augmentation are presented in figure 80. The figure shows that the main gear tends to lift off before the desired lift-off speed of 60 knots is reached. It is recommended to use less than maximum lift augmentation during the takeoff ground roll until the desired speed is obtained. Lift-off will then occur when maximum augmentation is applied.

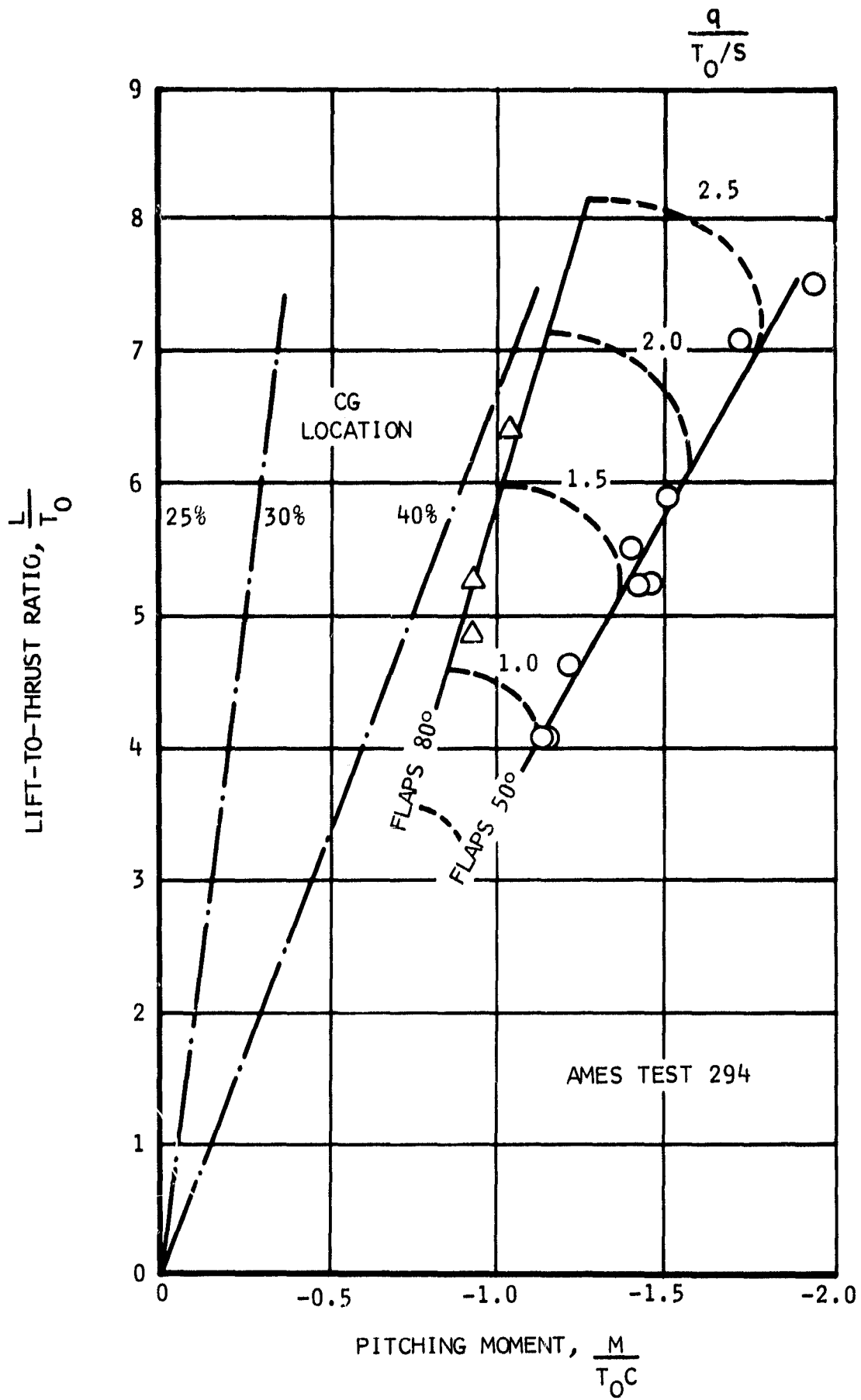


Figure 79. Pitching Moment Versus Lift at  $\alpha = 0$

$$\delta_f = 50^\circ$$
$$\alpha = 0^\circ$$

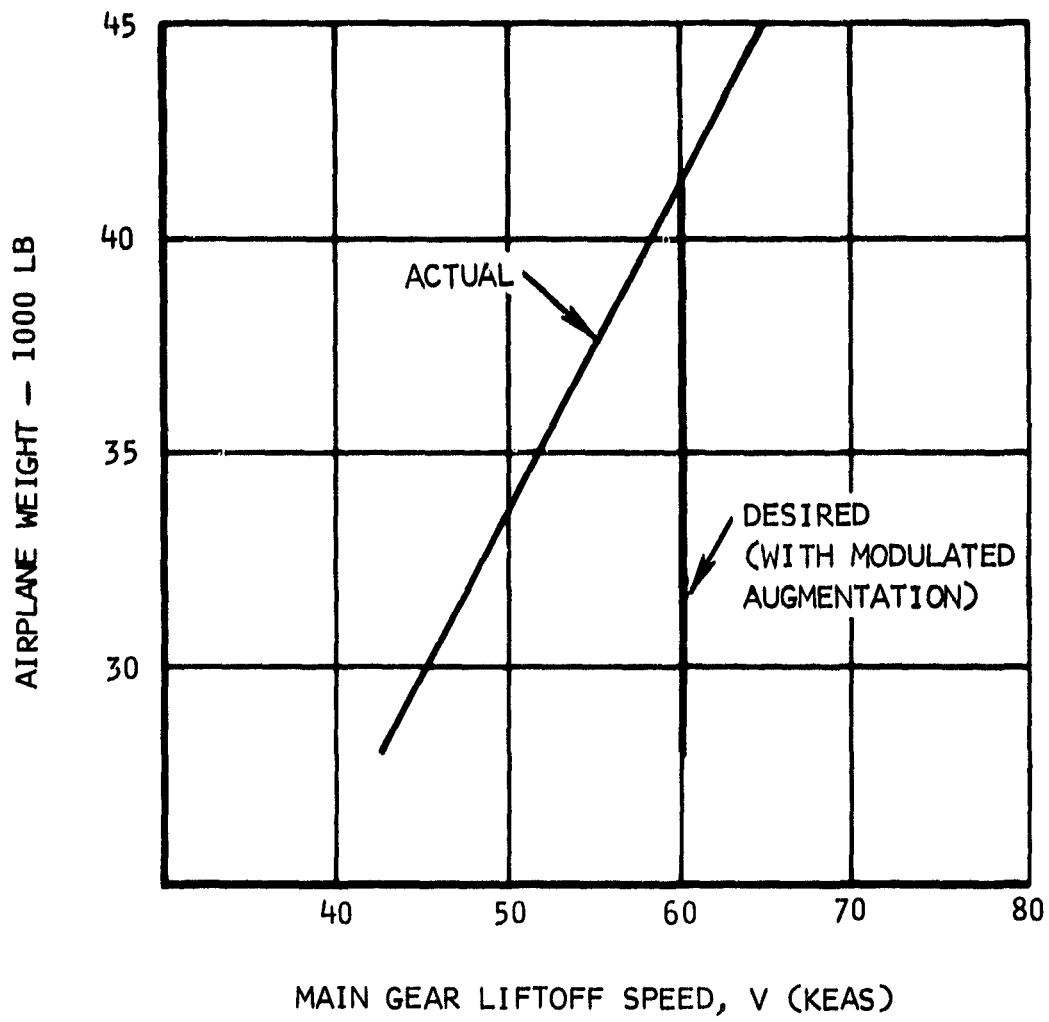


Figure 80. Main Gear Liftoff Speed With Maximum Augmentation

Lateral and directional stability and control. - The aileron deflections used in the present analysis are shown in figure 81 as a function of speed. At speeds below 65 knots, the deflections are mechanically limited to 16 degrees up, and 75 degrees down with a droop neutral position of 20 degrees. At higher speeds, the downward deflections are hinge moment limited. At speeds above approximately 100 knots, the droop is reduced to zero.

The deflections shown are the minimum deflections obtainable within 0.5 second for speeds below 100 knots, and 1.0 second for higher speeds. Larger deflections are possible at a lower deflection rate, except where mechanically limited. The large deflections at low speed are aerodynamically effective because of the use of boundary layer control (BLC) on the aileron upper surface. Because of this, no aerodynamic nose balance is used, and the hinge moments are relatively high.

In case of a hydraulic system failure, at least half of the deflections from neutral are available at a decreased deflection rate. In case of a failure in one of the BLC systems, at least half of the aileron surface is aerodynamically effective to the deflection angles shown because half of the surfaces are still fully blown due to the dual BLC system. In case of a cruise engine failure, the hydraulic flow supply from the pumps of the remaining engines with full rpm is adequate to obtain full deflections with a reduced rate without accumulator. With accumulator, a normal rate is obtained.

Spoiler deflections are used in conjunction with the ailerons and are also shown in figure 81.

The rudder is identical to the unmodified airplane. The deflection capability (not graphically shown here) is 25 degrees. A large geared tab deflects to a total of 50 degrees in the same direction when the rudder deflects to 25 degrees. This produces a high effectiveness, but introduces a large hinge moment.

The reasons for the larger aileron deflection capability for that airplane than for the unmodified Bullalo at low speeds are twofold. First, the reduction in wing size reduced the portion of the wing area over which the aileron is effective so that a larger deflections is needed for the same roll control at the same speed. Secondly, the speed for landing and takeoff is reduced requiring an additional deflection capability to obtain compatible roll accelerations. Target value for roll acceleration capability was set originally by NR at  $40 \text{ rad/sec}^2$ , but accelerations as high as reasonably possible beyond that value are desired for testing purposes.

The maximum deflection of 75 degrees is chosen because higher deflections tend to show a diminishing return for the surface effectiveness with BLC,

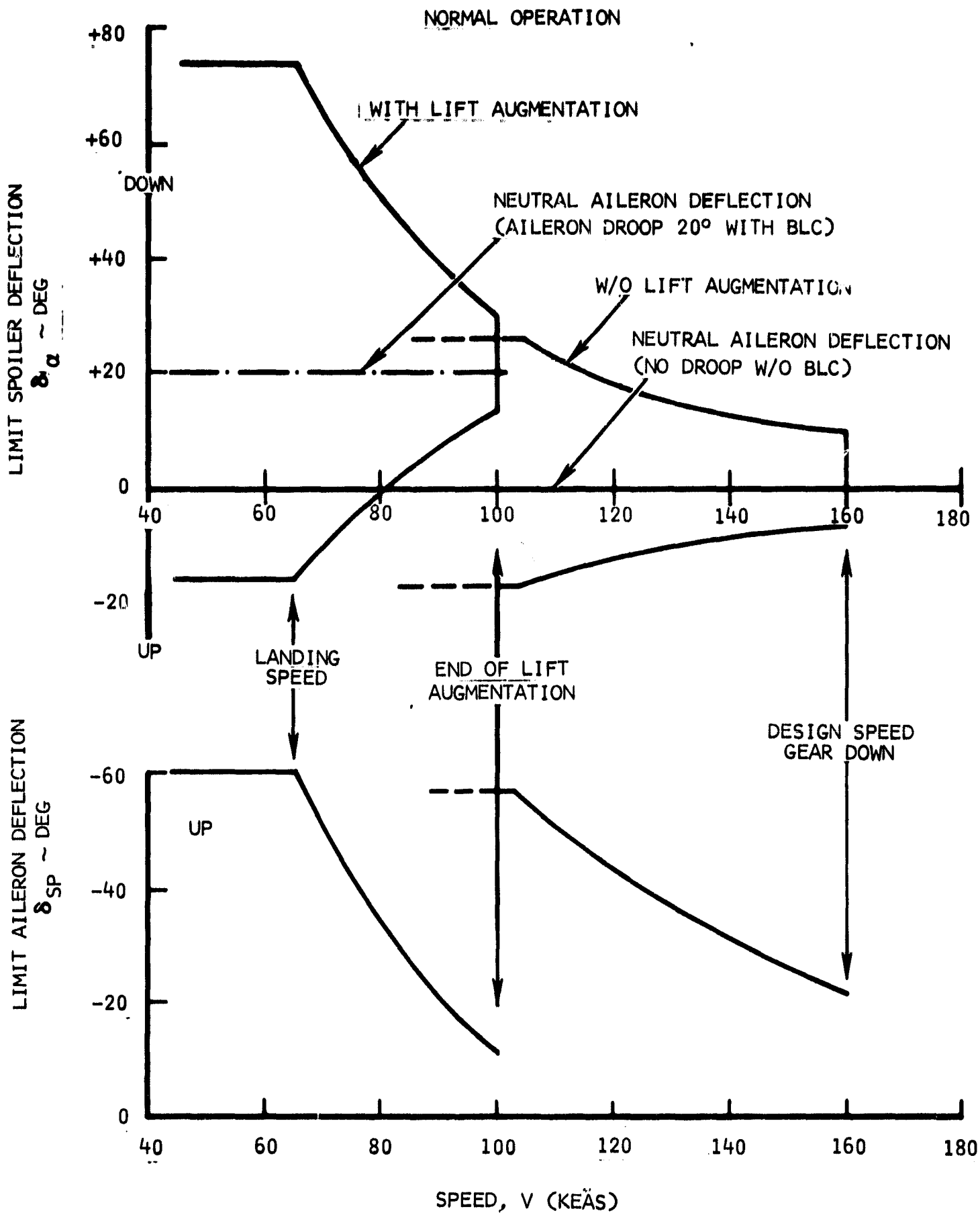


Figure 81. Aileron Deflection Limits Versus Speed



particularly at high angles of attack (See figure 82.) The blowing for the BLC is limited to the critical momentum coefficient (reference 9).

$$C_{\mu \text{ CRIT}} = 0.015 \frac{S_{\text{eff}}}{S_{\text{wing}}} \tan \alpha_a \quad (116)$$

At higher momentum coefficients, a diminishing return from the effectiveness of the BLC is encountered as evidenced by a series of experimental correlations, an example of which is shown in figure 83. At these higher momentum coefficients supercirculation is produced which is reserved more effectively to the augmentor flap blowing. The BLC nozzles are sized to meet this critical coefficient at half the thrust output of the T64 engines so that full BLC is available at the reduced lift augmentation associated with low-weight landings.

The maximum trailing edge up deflections of the aileron at low speeds is limited to approximately 15 degrees because higher deflections decrease the effectiveness of the spoiler. (See figure 84.) This based on experimental data found in NACA ACR 1D07. Figure 84 shows that application of a spoiler system is beneficial to obtain maximum roll control.

At low speed, the ailerons are drooped at neutral deflection. It was felt that the droop should be held to within 20 degrees because of (1) hinge moment considerations at the conversion speed of 100 knots, and (2) large adverse yawing moment due to aileron deflection when the droop is large (figure 85). The figure is valid for relatively small deflections starting from the drooped condition.

The favorable yaw from the spoiler deflection is not strong enough to overcome the adverse yaw characteristics of the ailerons, especially at high angles-of-attack. (See figure 86.) The figure is presented for maximum deflections, and includes nonlinear aerodynamic effects.

A number of airplane characteristics were analyzed based on the previously described control surface deflection capability.

The steady-state sideslip characteristics with full-rudder deflection in the positive direction are presented in figure 87 as a function of speed. The figure shows that the aileron change with sideslip is stable. The figure also shows that sideslip angles of 17 to 19 degrees can be maintained with full rudder at landing speeds of 60 to 65 knots. Ample aileron control is available at those speeds. However, with increase of speed the aileron deflection limit becomes lower and is marginally inadequate at the high-speed end attainable in conventional flight, as well as in the transition flight regime near 100 knots.

One reason for insufficient aileron control in conventional flight with full rudder is found in the fact that the aileron span has been reduced in

NACA TR 1369  
 NASA TN D-4610

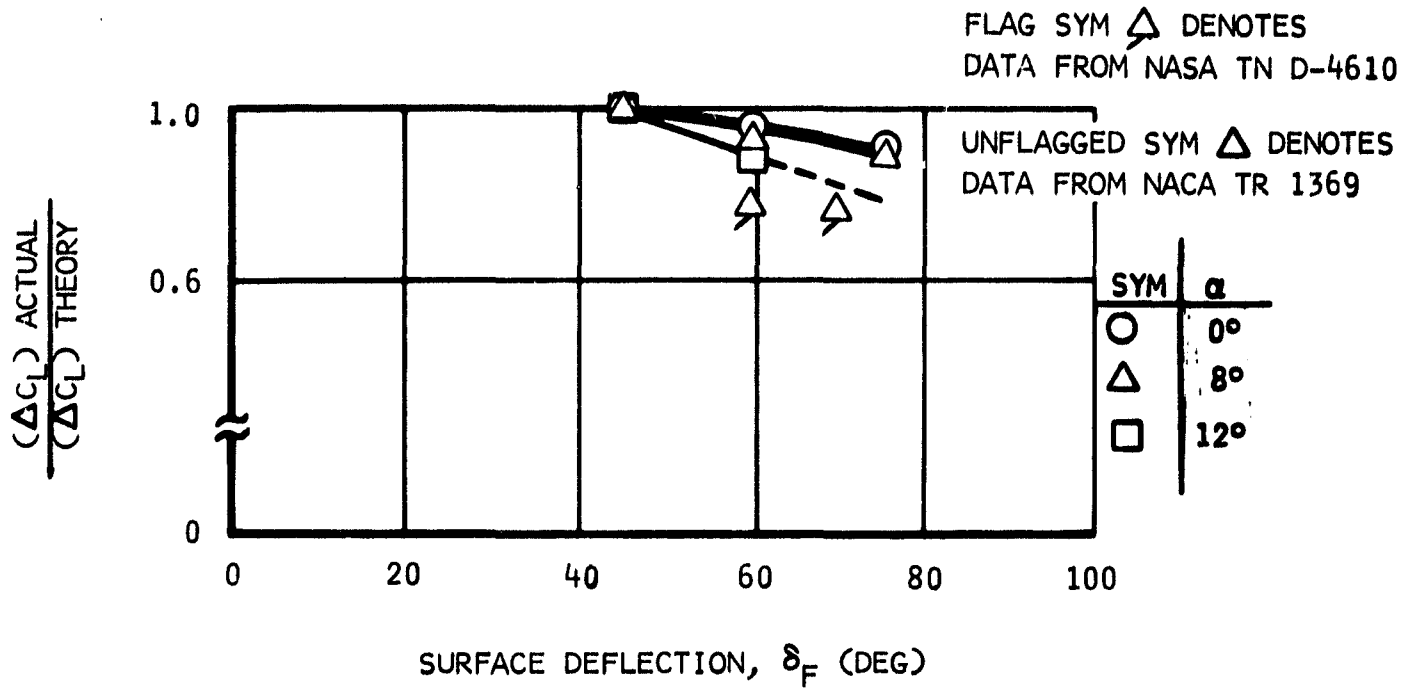
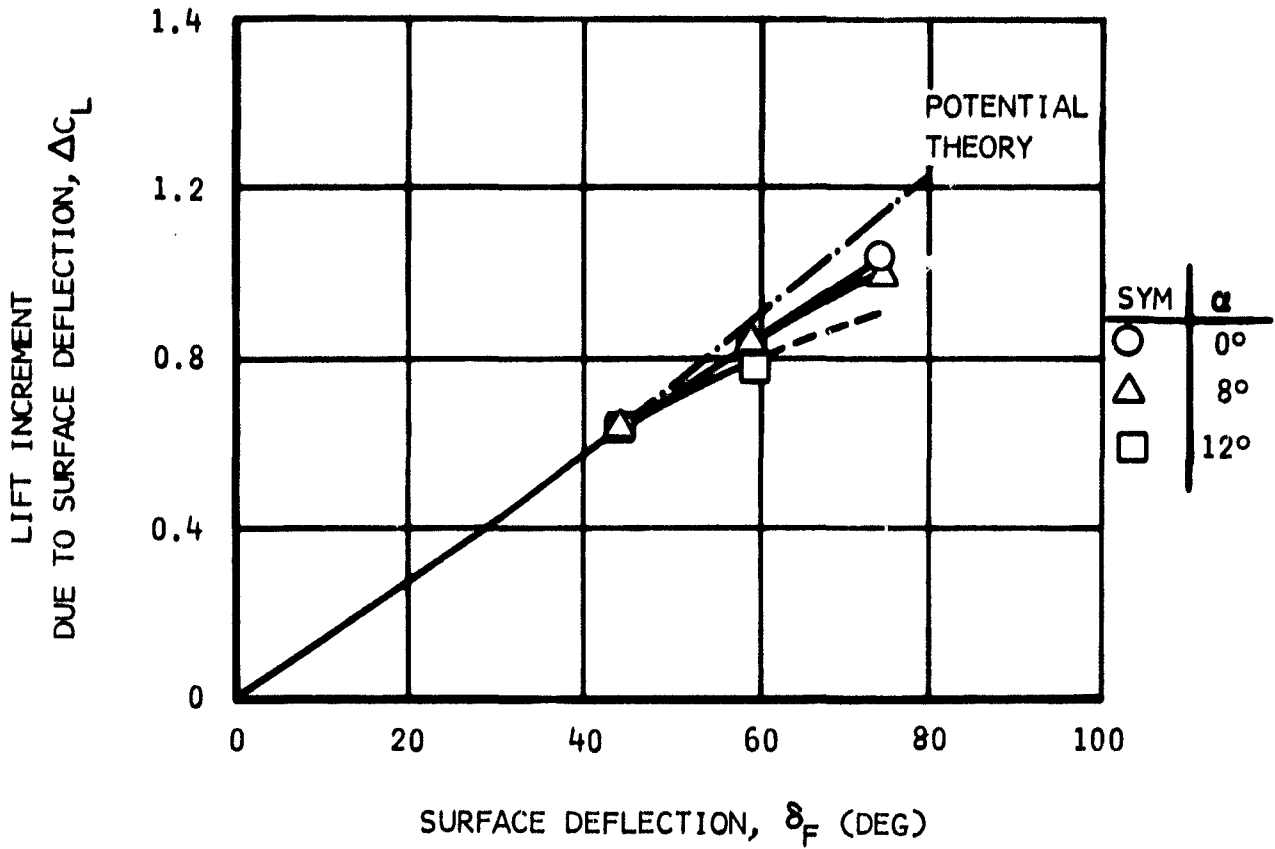


Figure 82. Effectiveness of a Surface With Boundary Layer Control at the Critical Momentum Coefficient for Blowing

$\delta_F = 60^\circ$

SYM  $\alpha$

○  $0^\circ$

△  $8^\circ$

□  $12^\circ$

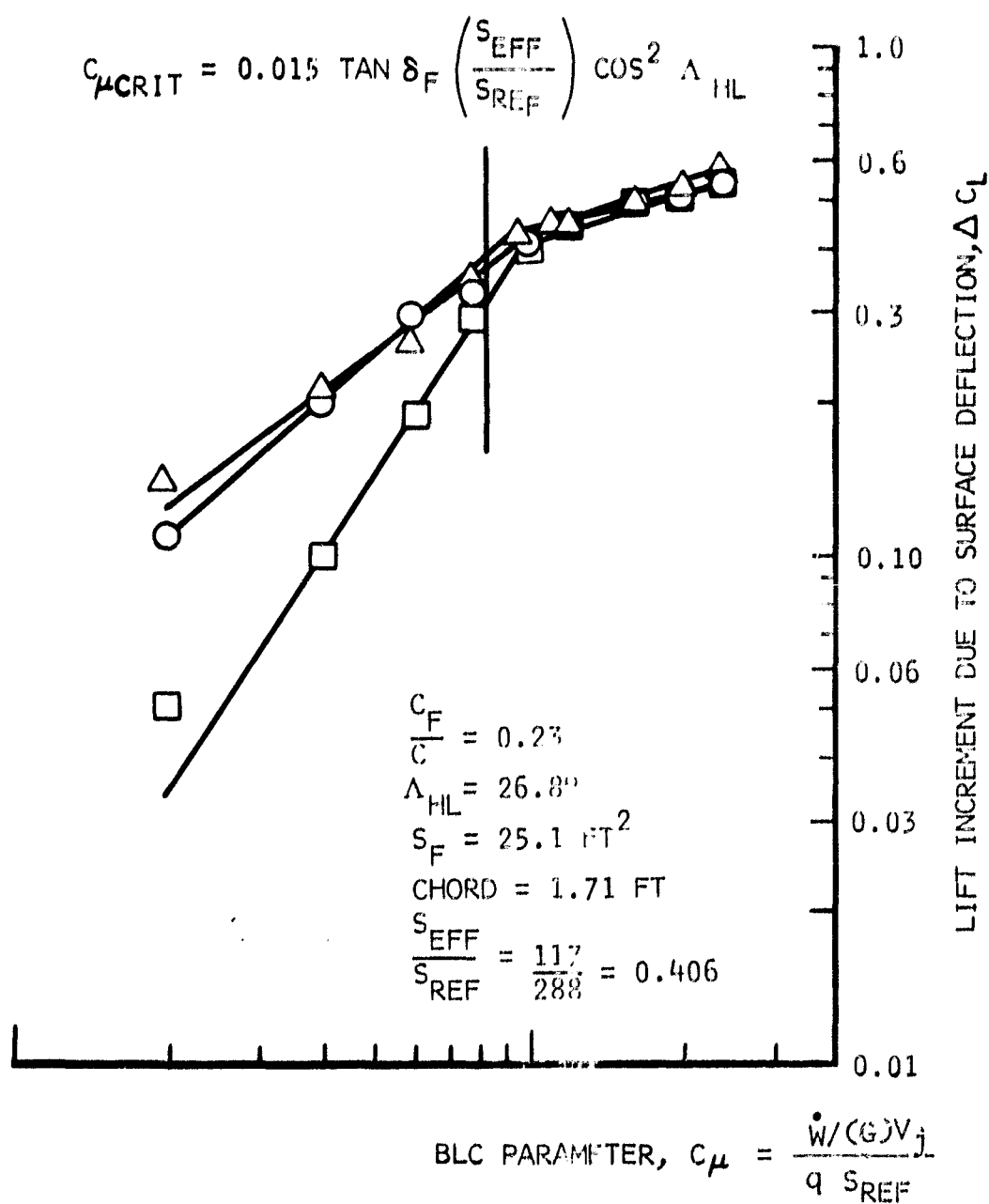


Figure 83. Effect of BLC On the Lifting Capability of a Deflected Surface

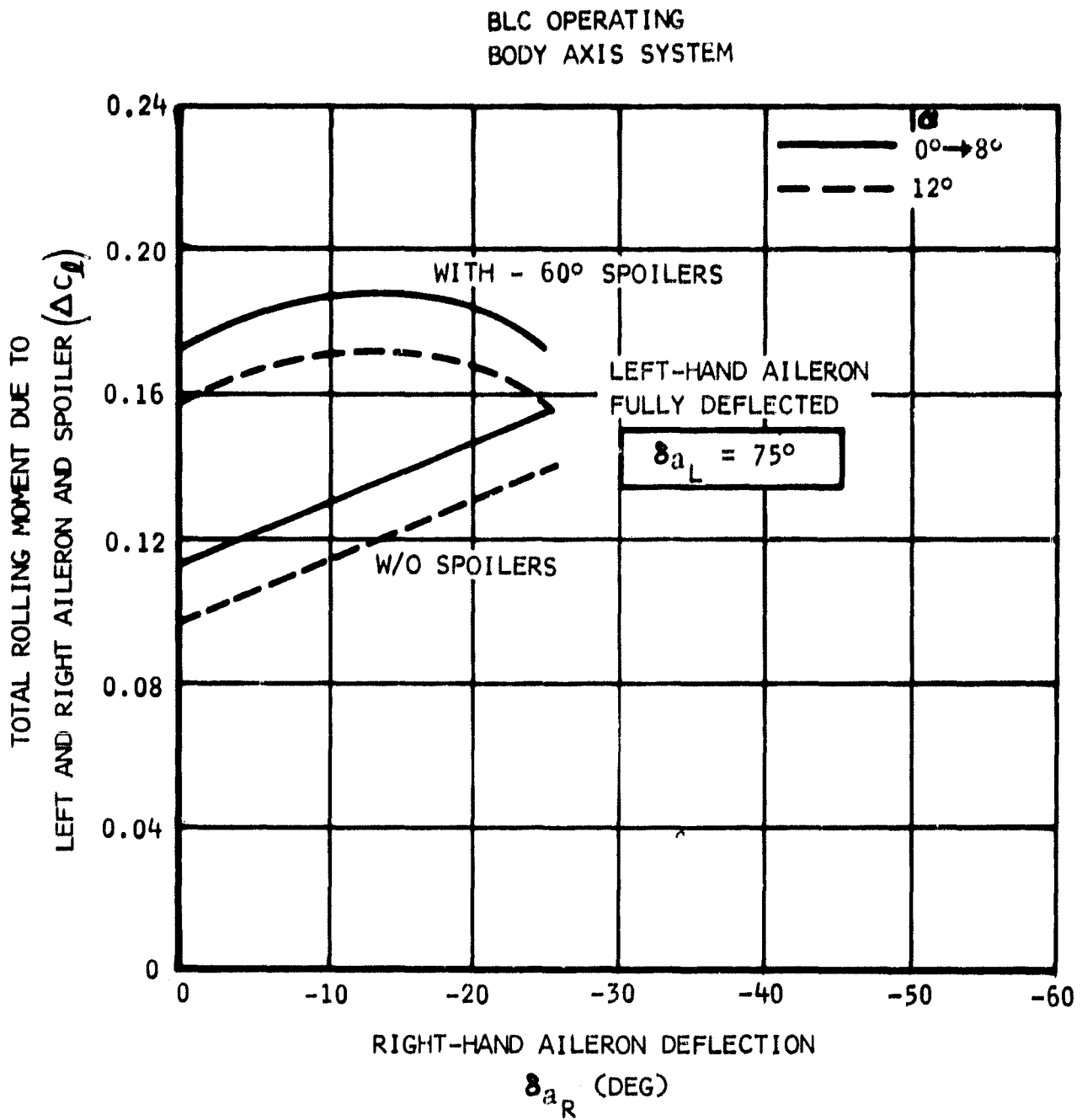


Figure 84. Rolling Moment Due to Aileron and Spoiler

AERO SPOILER DEFLECTION  
 3-D OPERATING  
 3-D AXIS SYSTEM

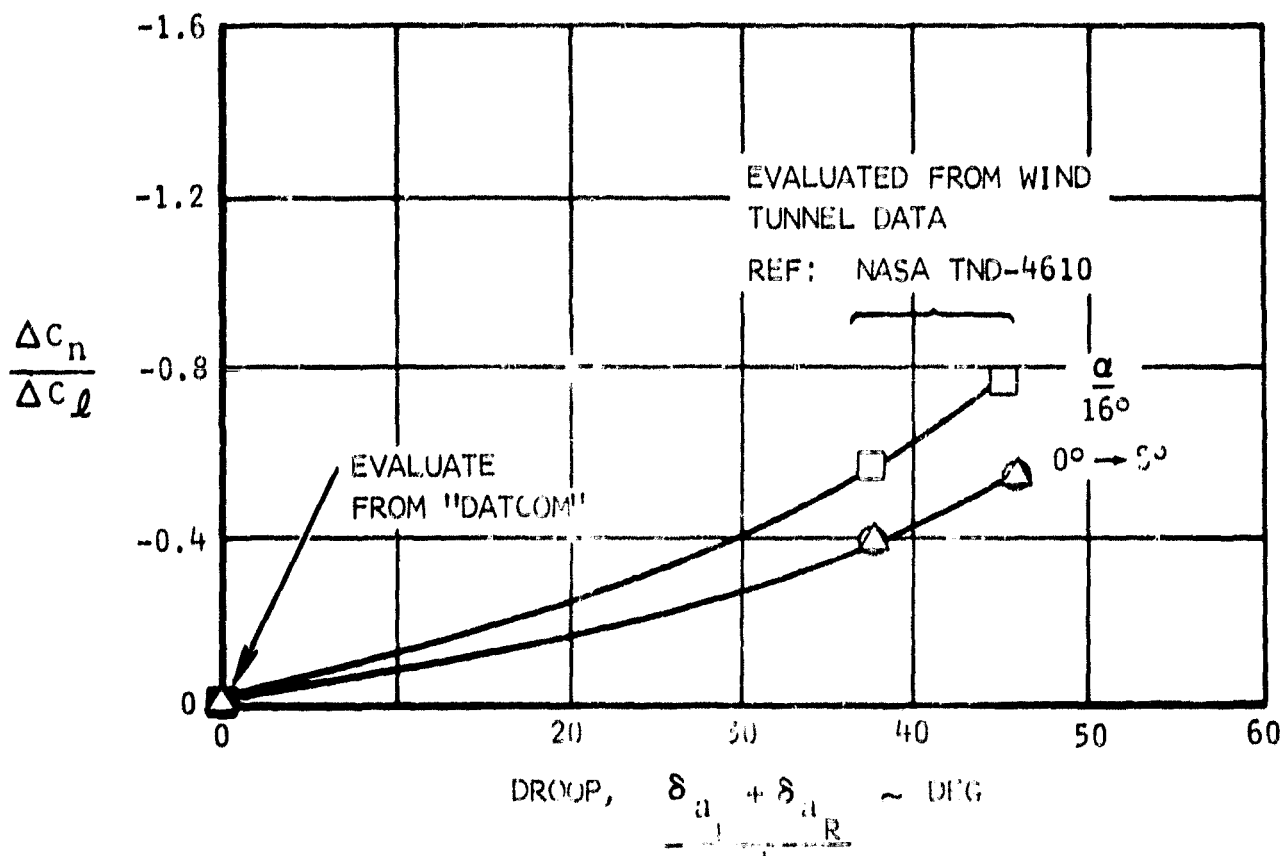


Figure 85. Yaw Due to Aileron Differentially Deflected About Various Values of Droop

BLC OPERATING  
BODY AXIS SYSTEM

MAX AILERON DEFLECTION  $\delta_{aL} = 75^\circ$  DOWN,  $\delta_{aR} = -15^\circ$  UP  
MAX SPOILER DEFLECTION  $\delta_{SPR} = -60^\circ$  UP

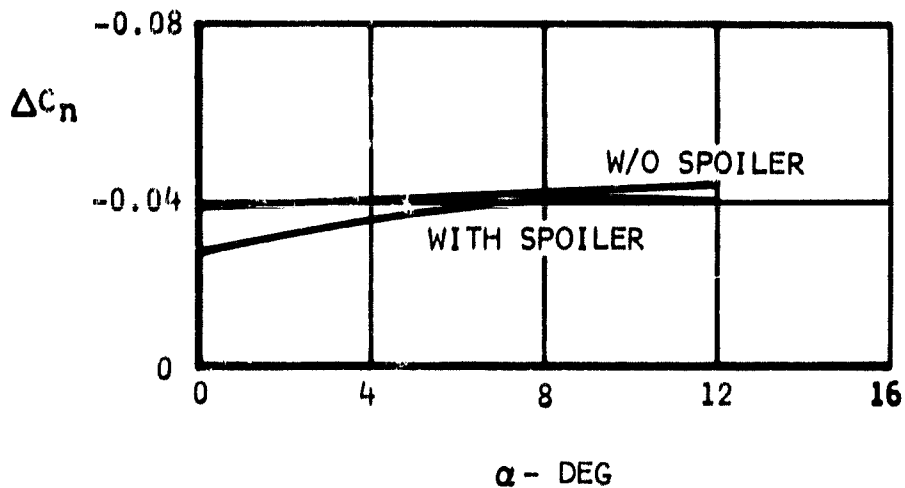


Figure 86. Yaw Due to Maximum Aileron and Spoiler Deflection

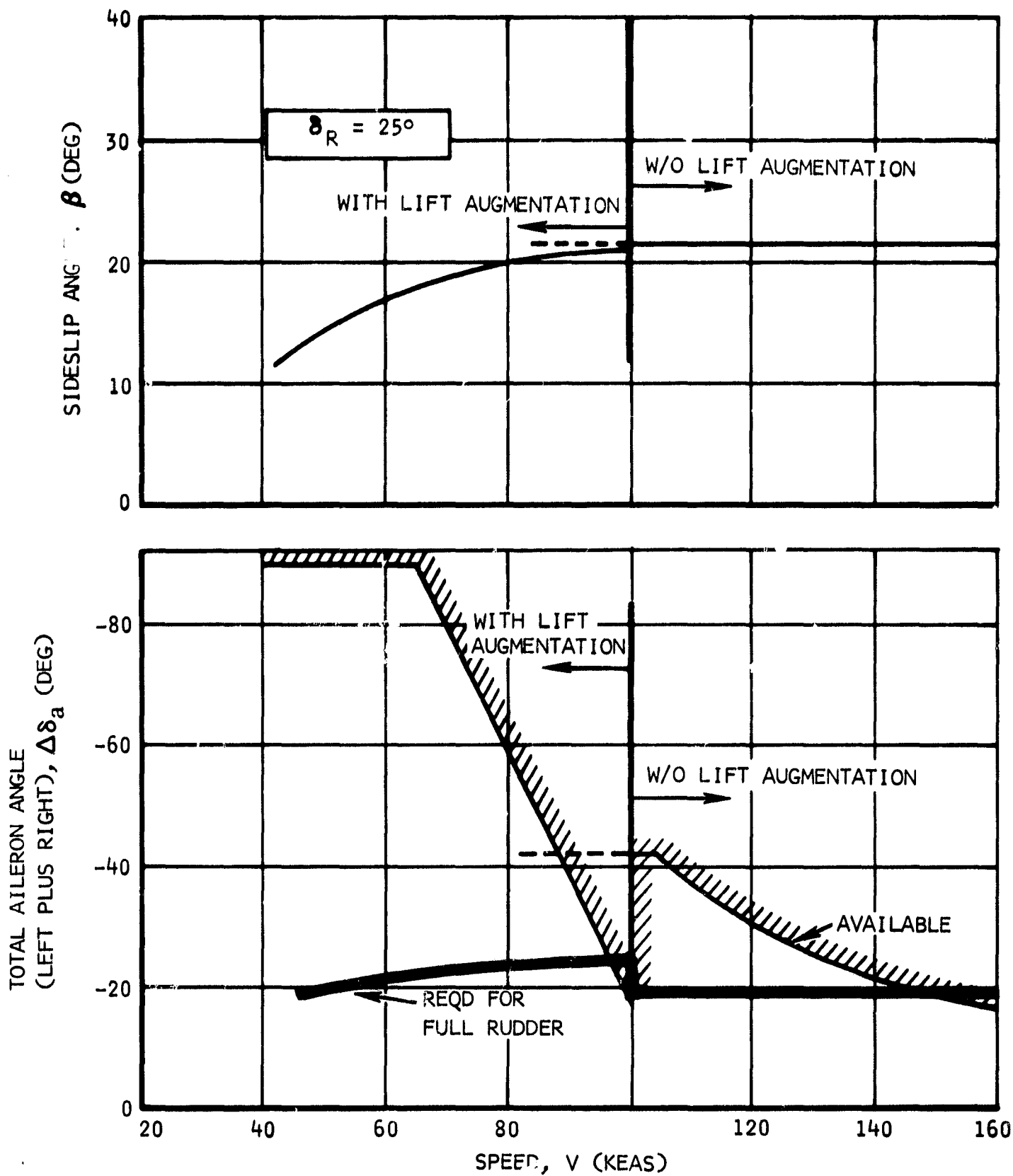


Figure 87. Steady-State Sideslip Characteristics With Full Rudder

comparison with the unmodified airplane. Since no BLC is used in this flight mode, a reduction in span results in less roll control capability.

To avoid control problems, a choice of the following limitations or changes may be made:

1. Restrict the rudder mechanically to about one-half of its maximum travel at speeds in excess of 90 knots.
2. Restrict sideslip angles to less than 10 degrees at speeds in excess of 90 knots.

The second item is recommended.

The sideslip angles and aileron deflections in figure 87 are computed from

$$\delta_a = \frac{\frac{\partial \mathcal{L}}{\partial \beta} \left( \frac{\Delta N}{T_{ob}} \right) \delta_{RMAX} - \frac{\partial N}{\partial \beta} \left( \frac{\Delta \mathcal{L}}{T_{ob}} \right) \delta_{RMAX}}{\Delta} \quad (117)$$

where

$$\beta = \frac{\left( \frac{\Delta \mathcal{L}}{T_{ob}} \right) \delta_{RMAX} \left( \frac{\partial N}{\partial \delta_a} \right) \left[ 1 + \frac{\frac{\partial N}{\partial \delta SP}}{\frac{\partial N}{\partial \delta_a}} \left( \frac{d \delta SP}{d \delta_a} \right) \right]}{\Delta} \quad (118)$$

$$\left( \frac{\Delta N}{T_{ob}} \right)_{RMAX} \left( \frac{\partial \mathcal{L}}{\partial \delta_a} \right) \frac{\left[ 1 + \frac{\frac{\partial \mathcal{L}}{\partial \delta SP}}{\frac{\partial \mathcal{L}}{\partial \delta_a}} \left( \frac{\partial \delta SP}{\partial \delta_a} \right) \right]}{\Delta}$$



and

$$\Delta = \frac{\partial \frac{\mathcal{L}}{T_{ob}}}{\partial \beta} \left( \frac{\partial \frac{N}{T_{ob}}}{\partial \delta_a} \right) \left[ 1 + \frac{\frac{\partial \frac{N}{T_{ob}}}{\partial \delta_{SP}} \left( \frac{d\delta_{SP}}{d\delta_a} \right)}{\frac{\partial \frac{N}{T_{ob}}}{\partial \delta_a}} \right] - \frac{\partial \frac{N}{T_{ob}}}{\partial \beta} \left( \frac{\partial \frac{\mathcal{L}}{T_{ob}}}{\partial \delta_a} \right) \left[ 1 + \frac{\frac{\partial \frac{\mathcal{L}}{T_{ob}}}{\partial \delta_{SP}} \left( \frac{d\delta_{SP}}{d\delta_a} \right)}{\frac{\partial \frac{\mathcal{L}}{T_{ob}}}{\partial \delta_a}} \right] \quad (119)$$

All terms in these equations are a function of the speed parameter  $q/(T_0/S)$ . Nonlinear effects are also included in figure 87.

Result in terms of this speed parameter are presented in figure 88. It is seen that the sideslip angle with full rudder decreases when the speed parameter decreases. This decrease stems from an increase of airplane directional stability due to power effect as discussed under Directional Data. Conversion for the speed parameter to the velocity  $V$  is carried out using  $T_0 = 9,900$  pounds.

A large sideslip capability is available for crosswind landings. The present capability depends on a large aileron deflection which, in turn, depends on a large aileron BLC. Thus, the lift augmentation which supplies the air for the BLC should not be reduced to less than half after landing touch-down until considerable weight is carried by the main landing gear.

Figure 89 shows the helix angle  $pb/(2V)$  as a function of speed as another important lateral control parameter. It is seen that the target value of 0.07 per radian is met at all speeds with ailerons fully deflected. This target value is taken from MIL-F-8785.

The values of the helix angle are determined from

$$\frac{pb}{2v} = \frac{\left( \frac{\Delta \mathcal{L}}{T_{ob}} \right)_{MAX}}{\left( \frac{\partial \frac{\mathcal{L}}{T_{ob}}}{\partial \frac{pb}{2v}} \right)} \quad (120)$$

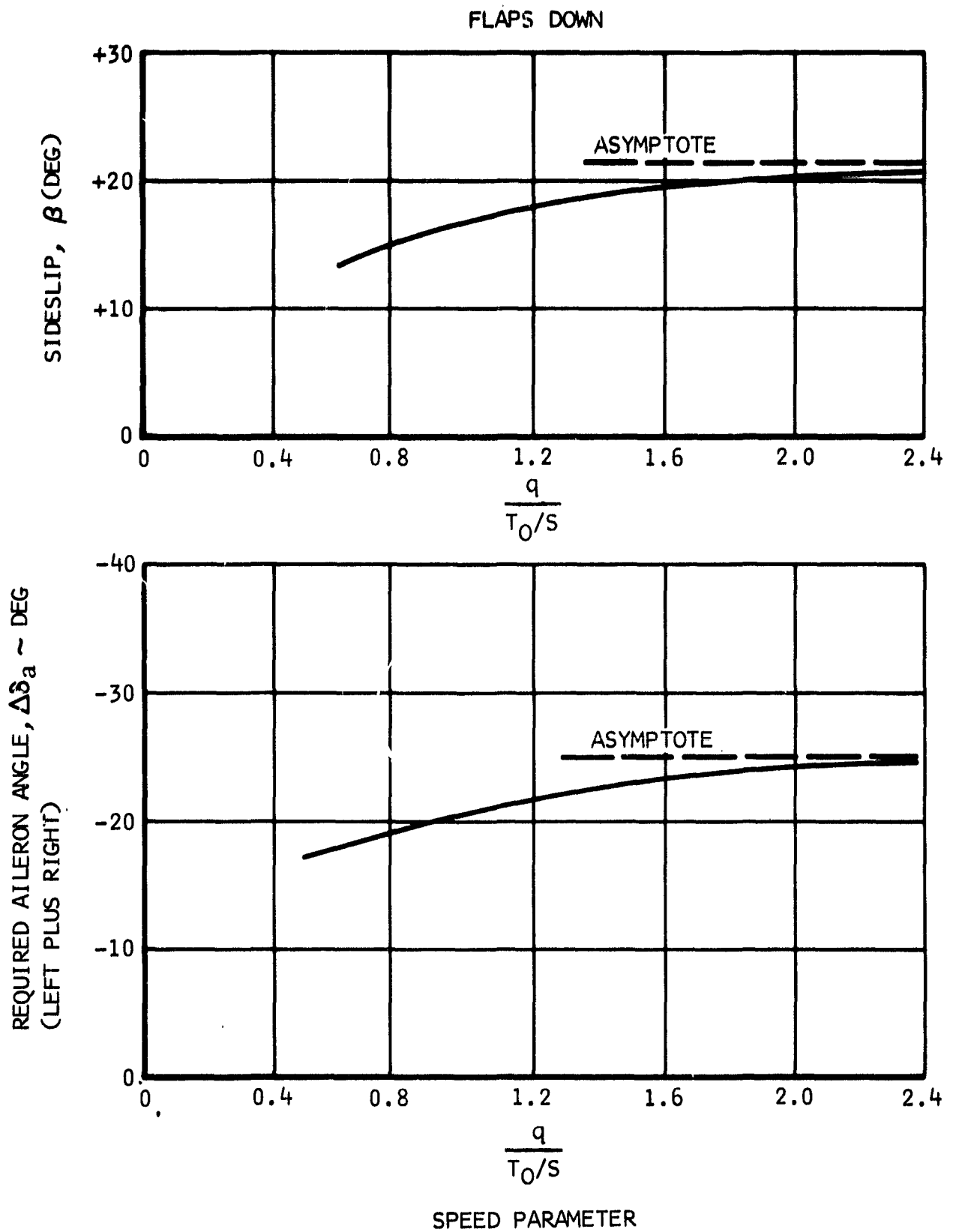


Figure 88. Effect of Full Rudder on Steady-State Sideslip and Aileron Deflection as a Function of Speed Parameter

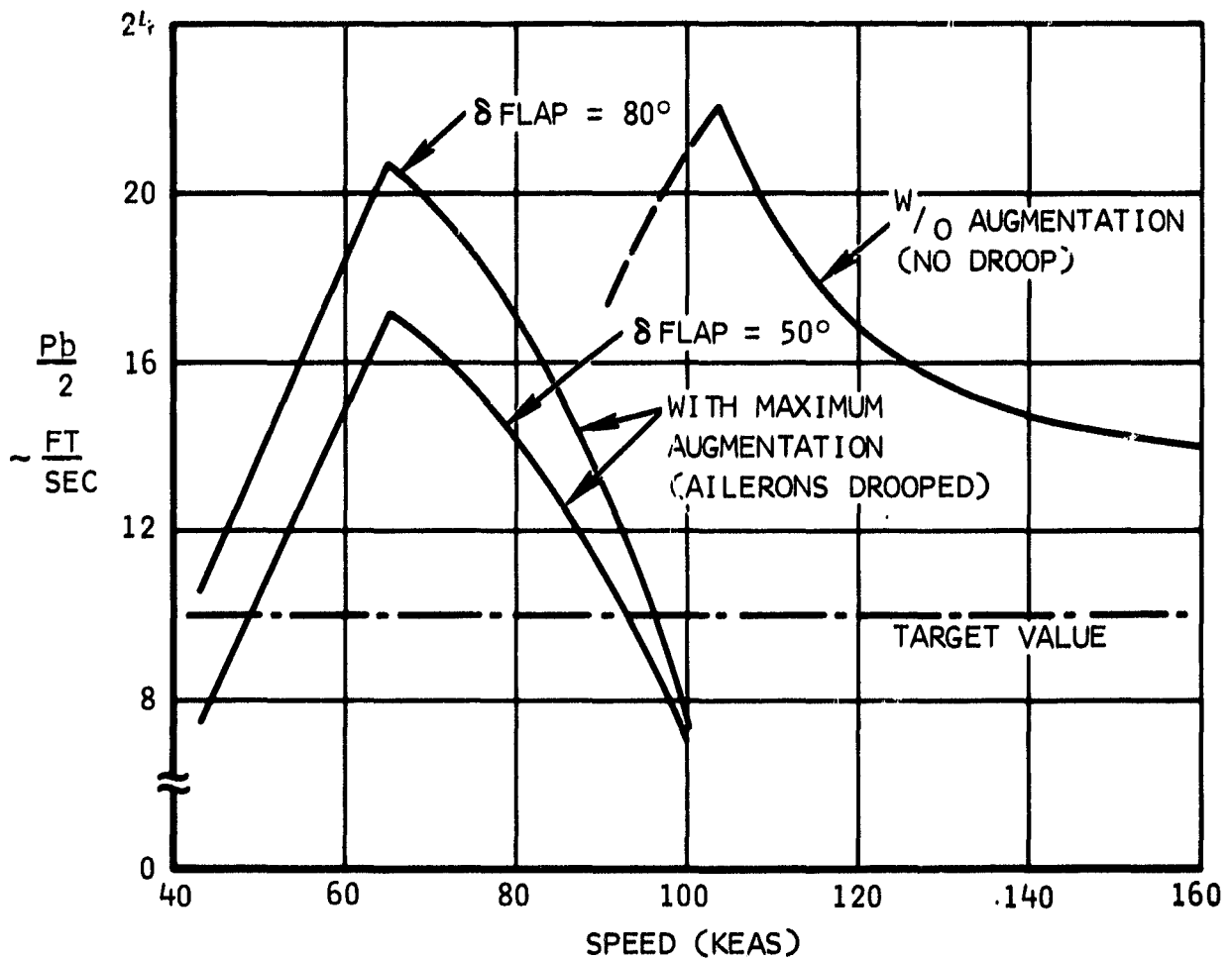
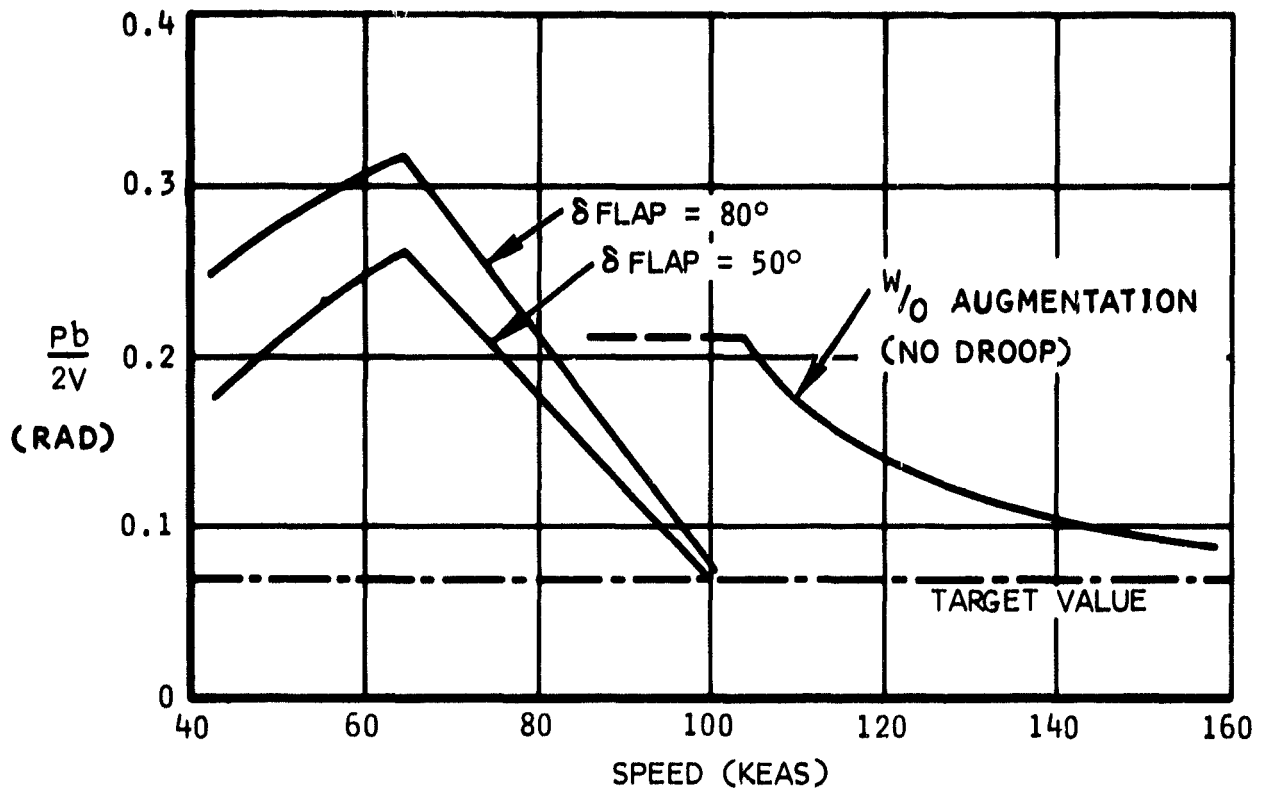


Figure 89.  $Pb/2V$  and  $Pb/2$  Versus Speed for Limit Aileron Deflection

where

$$\left(\frac{\Delta \mathcal{L}}{T_o b}\right)_{\max} = (\Delta C_l)_{\delta a_{\max}, \delta s_{\max}} \left(\frac{q}{T_o S}\right) \quad (121)$$

The vertical velocity of the wingtip,  $p(b/2)$ , is also shown in the figure. The target value of 10 ft/sec is met at speeds higher than 50 knots except near the transition speed with ailerons drooped. This target value is also taken from MIL-F-8783.

The initial roll acceleration capability is presented in figure 90 as a function of speed. At the minimum control speed of 51 knots (longitudinal characteristics), the roll acceleration is 0.60 rad/sec<sup>2</sup>; and, at a minimum landing speed of 60 knots, the acceleration is 0.85. This compares favorably to the target value of 0.40 set previously by NR. The acceleration is computed from the simplified form

$$\ddot{\phi} = \frac{\left(\frac{\Delta \mathcal{L}}{T_o b}\right)_{\max} (T_o b)}{I_{\text{roll}}} \quad (122)$$

The initial yaw acceleration capability is given versus speed in figure 91. The NR target value of 0.18 rad/sec<sup>2</sup> is met at speeds above 50 knots, and a value of 0.27 is reached at a minimum landing speed of 60 knots. The yaw acceleration capability is reduced by about one-third when the rudder has to overcome the adverse yaw from full aileron deflections.

The acceleration to obtain from the simplified form

$$\ddot{\psi} = \frac{\left(\frac{\Delta N}{T_o b}\right)_{\max} (T_o b)}{I_{\text{yaw}}} \quad (123)$$

where in case of zero roll inputs

$$\left(\frac{\Delta N}{T_o b}\right)_{\max} = (\Delta C_l)_{\text{vertical tail}_{\max}} \left(\frac{q}{T_o S}\right) \bar{V}_v \quad (124)$$

$$\begin{aligned} \Delta\delta_a &= -75^\circ + 15^\circ = 90^\circ \\ \Delta\delta_{SP} &= -60^\circ \\ I_{XX} &= 166,000 \text{ SLUG-FT}^2 \end{aligned}$$

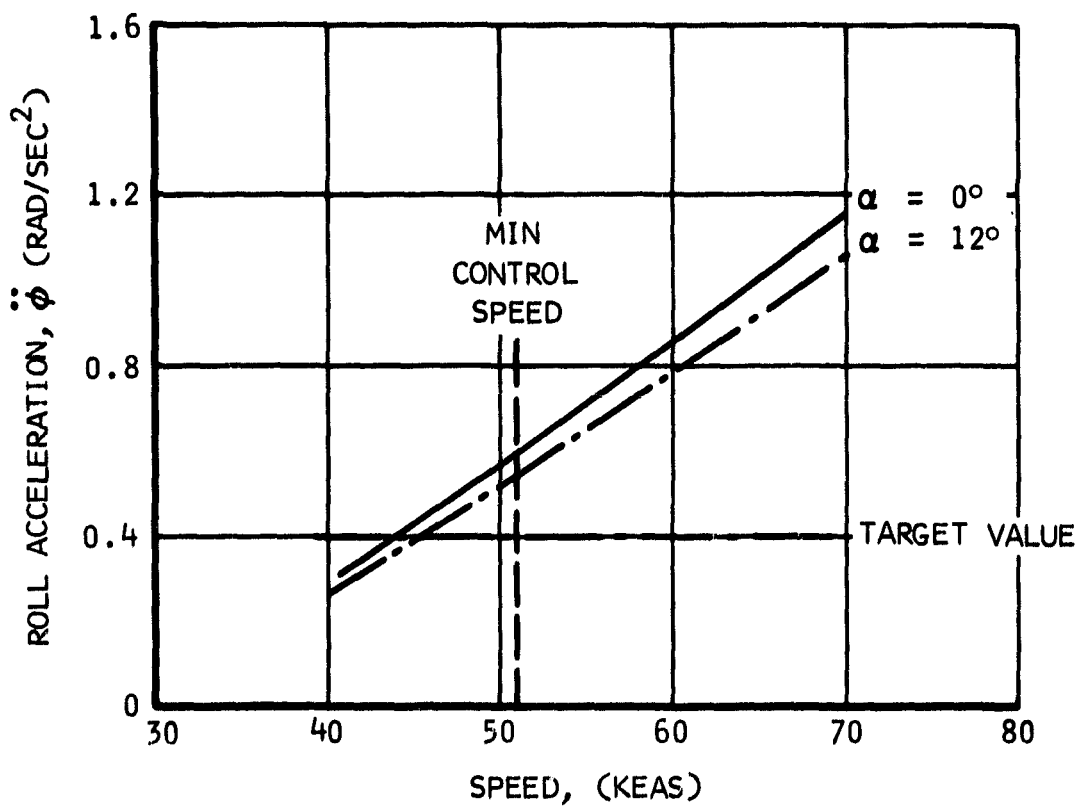


Figure 90. Roll Acceleration Capability

$$\delta_R = -25^\circ$$

$$I_{YY} = 331,000 \text{ SLUG-FT}^2$$

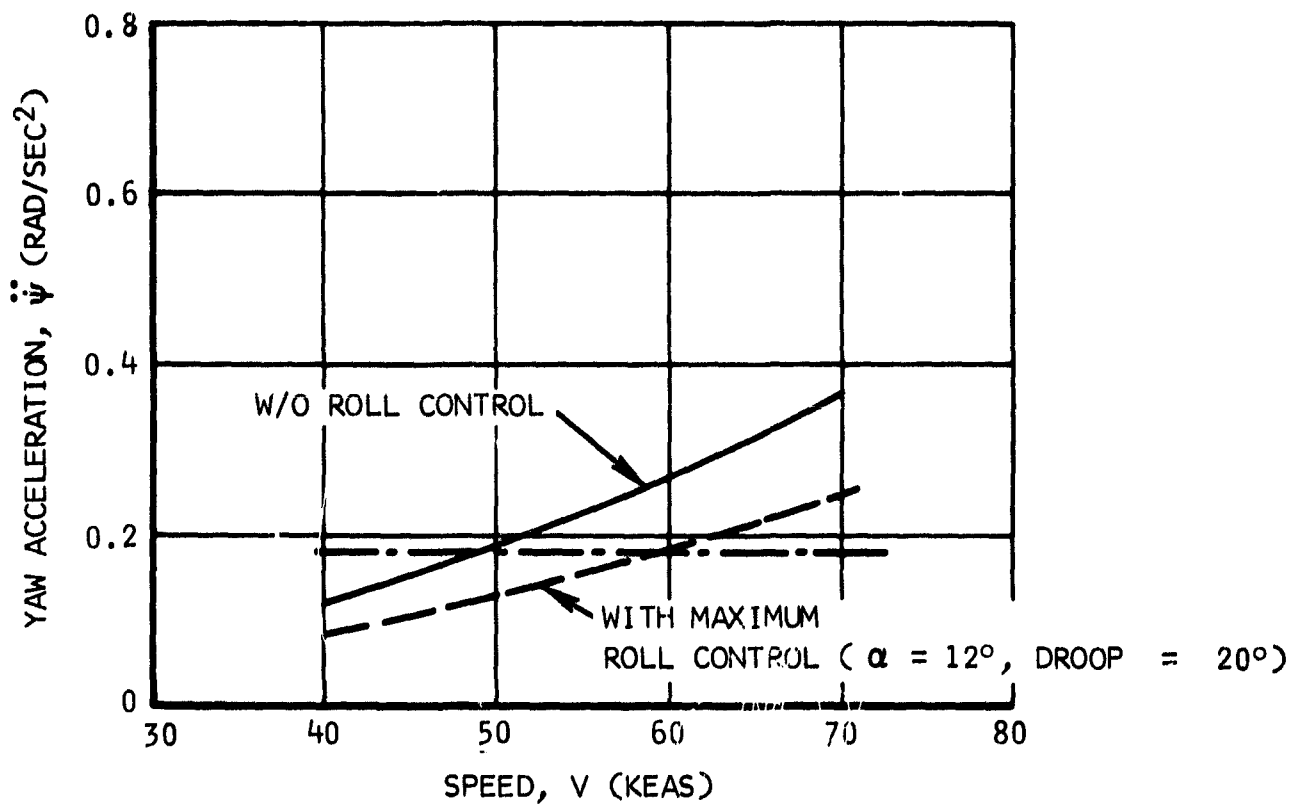


Figure 91. Yaw Acceleration Capability

The minimum speed for one-engine-out roll control is 44 knots (independent of weight) and is determined from figure 92. The available roll control shown in this figure is computed from

$$\phi = \left( \frac{\Delta Z}{T_o b} \right)_{\max} (T_o b) \quad (125)$$

Full-roll control is available even though one hydraulic pump is inoperative. The required roll control is computed from a 100-percent rpm Orpheus engine thrust with the exhaust nozzle rotated to the vertical position.

The available aerodynamic yawing moment for the critical one-engine-out condition in yaw is presented in figure 93 in parametric form. The maximum sideslip angle used is equal to the maximum level flight sideslip with full rudder and symmetric power. However, the use of a larger sideslip angle is possible with approximately 5 degrees bank.

The values in the figure are derived using the following equation for the given sideslip  $\beta$  and maximum rudder deflection  $\delta_{R_{\max}}$ :

$$\left( \frac{T_{cr}}{W} \right) \left( \frac{a}{b} \right) = \frac{\frac{\partial \frac{N}{T_o b}}{\partial \beta} \beta_{\max} + \frac{\partial \frac{N}{T_o b}}{\partial \delta_R} \delta_{R_{\max}} + \frac{\partial \frac{N}{T_o b}}{\partial \delta_a} \delta_a + \frac{\partial \frac{N}{T_o b}}{\partial \delta_{Sp}} \delta_{Sp}}{\left( \frac{q}{T_o S} \right)} \left( \frac{q^5}{W} \right) \quad (126)$$

The aileron and spoiler deflection for this equation is derived from the rolling moment equilibrium

$$\frac{\partial \frac{L}{T_o b}}{\partial \beta} \beta_{\max} + \frac{\partial \frac{L}{T_o b}}{\partial \delta_R} \delta_{R_{\max}} + \frac{\partial \frac{L}{T_o b}}{\partial \delta_a} \delta_a + \frac{\partial \frac{L}{T_o b}}{\partial \delta_{Sp}} \delta_{Sp} = 0 \quad (127)$$

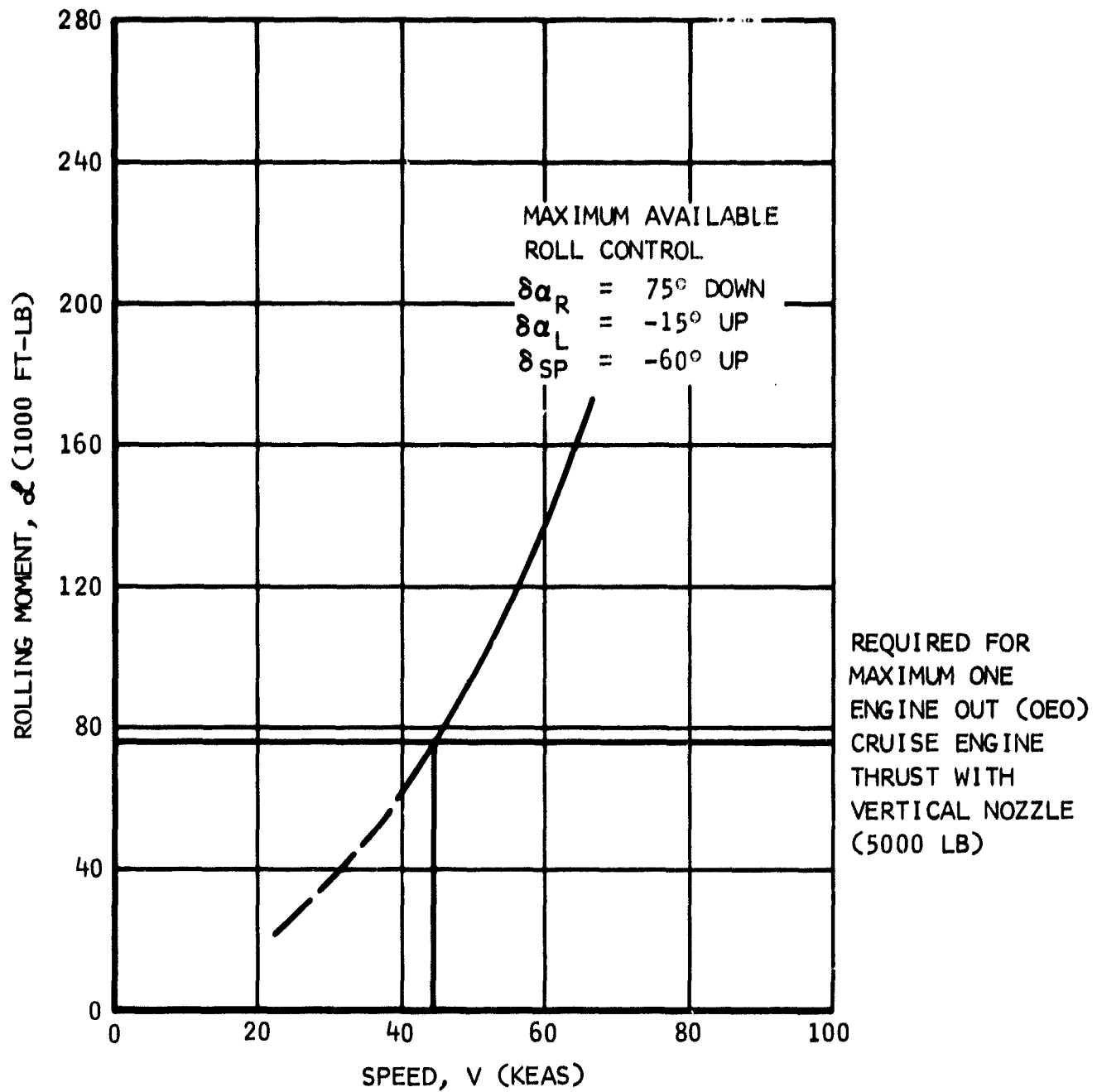


Figure 92. Minimum Speed for One Engine Out Roll Control



WITH LIFT AUGMENTATION  
 SPEED PARAMETER =  $\frac{q}{T_0/S} = 0.6$

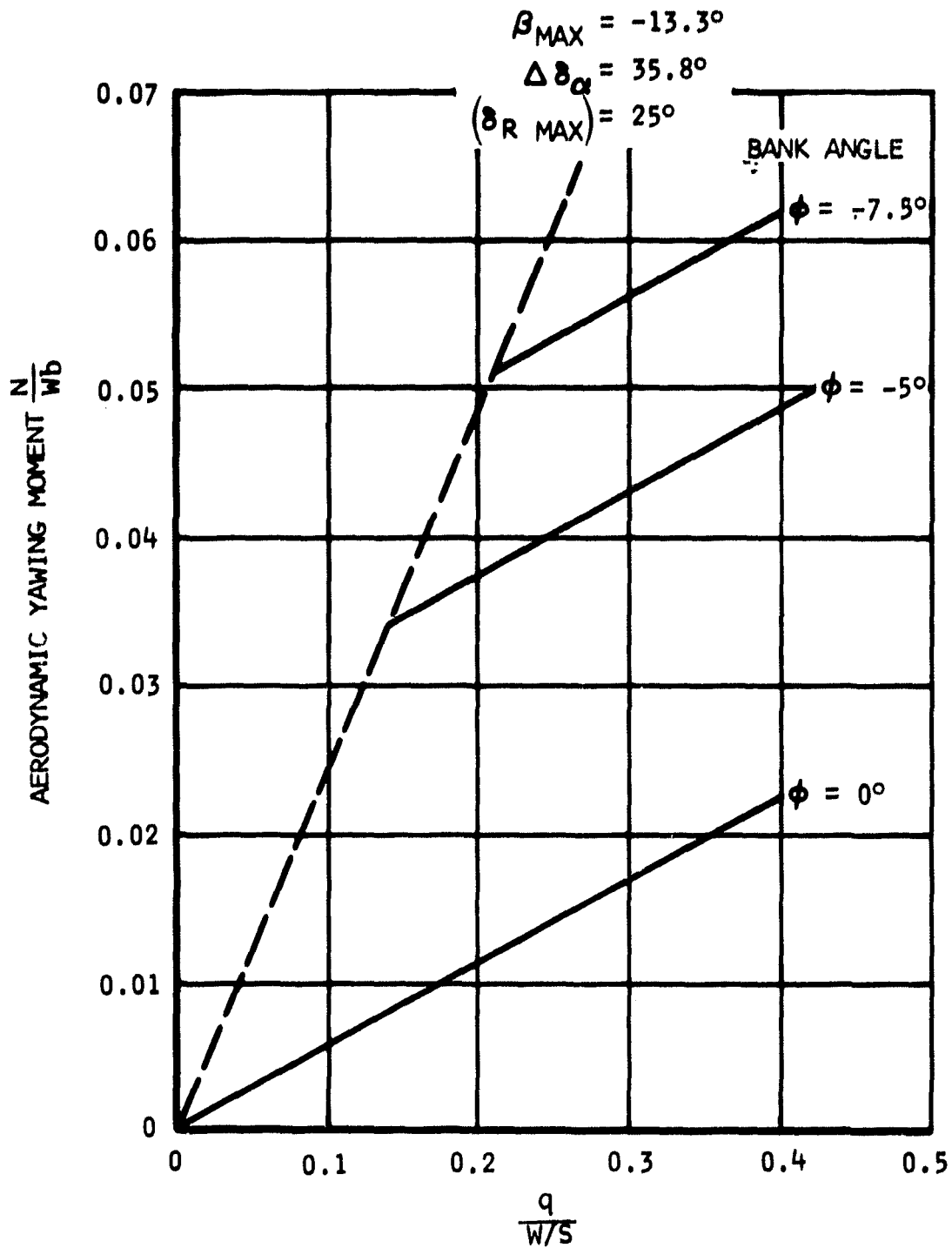


Figure 93. Available Aerodynamic Yawing Moment for One Engine Out Condition

Associated bank angles  $\phi$  are computed from

$$\left(\frac{T_{cr}}{W}\right)\left(\frac{a}{b}\right) = \frac{\frac{\partial \frac{N}{T_o b}}{\partial \beta}}{\frac{\partial \frac{Y}{T_o}}{\partial \beta}} \sin \phi + \frac{\frac{\partial \frac{N}{T_o b}}{\partial \delta_R} \delta_R + \frac{\partial \frac{N}{T_o b}}{\partial \delta_a} \delta_a + \frac{\partial \frac{N}{T_o b}}{\partial \delta_{sp}} \delta_{sp}}{\left(\frac{q}{T_o}\right) \left(\frac{S}{S}\right)}$$

$$\left[ \begin{array}{c} \frac{\partial \frac{Y}{T_o}}{\partial \delta_R} \delta_R \\ \frac{q}{T_o} \\ \frac{S}{S} \end{array} \right] \left( \frac{\partial \frac{N}{T_o b}}{\partial \beta} \right) \left( \frac{qS}{W} \right) \quad (128)$$

The equation is derived by eliminating the sideslip angle from the yawing moment equation with the help of sideforce relations.

The available aerodynamic yawing moment is converted in figure 94 to a function of speed for the maximum sideslip angle. The bank angle is found not to be limiting because its magnitude is approximately 5 degrees. Comparison in this figure with the yawing moment required to make equilibrium with an asymmetric yawing moment from an Orpheus engine at 100-percent rpm yields a minimum control speed of 40 knots.

Comparison with longitudinal characteristics shows that the minimum control speeds in yaw and roll from one-engine-out considerations are less than the longitudinal minimum control speed:

TABLE XXXVI

<u>Condition</u>	<u>V<sub>min</sub></u>
One-engine-out yaw	40 KEAS
One-engine-out roll	44 KEAS
Longitudinal control limit	51 KEAS

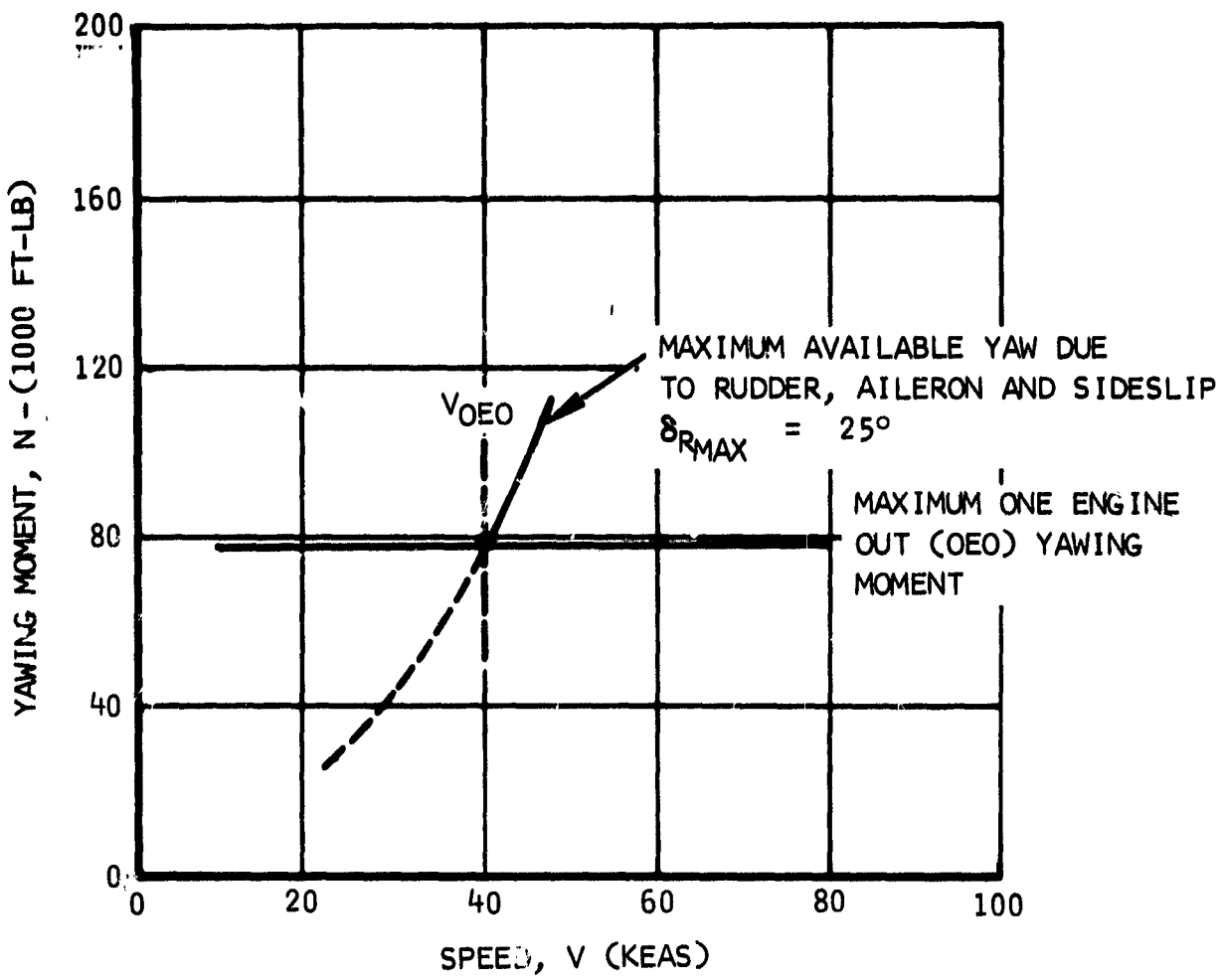


Figure 94. Minimum Speed for One Engine Out Yaw Control

Conclusions and recommendations. - The takeoff distance is 890 feet and the landing distance with 100 percent thrust reversal is 883 feet. These distances are computed for all engines operating, an obstacle height of 50 feet, a gross weight of 40,000 pounds, sea-level standard-day conditions, and a landing and takeoff speed of 60 knots. Adequate speed margins, maneuver margins, and rate of climb exists at this speed with one engine inoperative.

Ferry distance is 135 nautical miles and six STOL takeoffs and landings can be made with full fuel in a normal STOL takeoff and landing pattern.

The minimum permissible flying speed at 40,000 pounds gross weight is computed to be 51 knots. This speed is set by the one T64 engine out stall speed. At this speed, a higher weight may be carried with improved wing-body intersections.

STOL landings at speeds from 60 to 68 KEAS are expected to be safe. The lift augmentation for conversion between the conventional and STOL flight mode should be activated at 100 to 105 KEAS. In the conventional mode, flaps should be operated between 110 and 125 KEAS. The maximum aerodynamic flight limit is 160 KEAS for fixed wing leading edge slats. This coincides with the gear limit speed.

The target pitch acceleration of  $0.36 \text{ rad/sec}^2$  is obtained at 60 KEAS and center-of-gravity locations aft of 35-percent MAC. The roll and yaw accelerations at that speed are  $0.85$  and  $0.27 \text{ rad/sec}^2$ , respectively. Lightweight landings are not recommended, at lower speeds in order to preserve the pitch acceleration capability. Minimum control speeds in roll and yaw are not critical.

It is recommended that the fuselage side-mounted T64 engines be relocated to the front or top of the fuselage in order to avoid center-of-gravity locations that are too far forward for low speed STOL landings with nearly full fuel. Possible hot air reingestion and FOD near the ground prior to touchdown, and possible adverse aerodynamic interference on lift may also be alleviated by a relocation.

#### Aerodynamics Supporting Data

Axis system and sign convention. - The stability axis system is used for all longitudinal data. The body-axis system is used for all lateral-directional data.

The sign convention used is presented in figure 95.

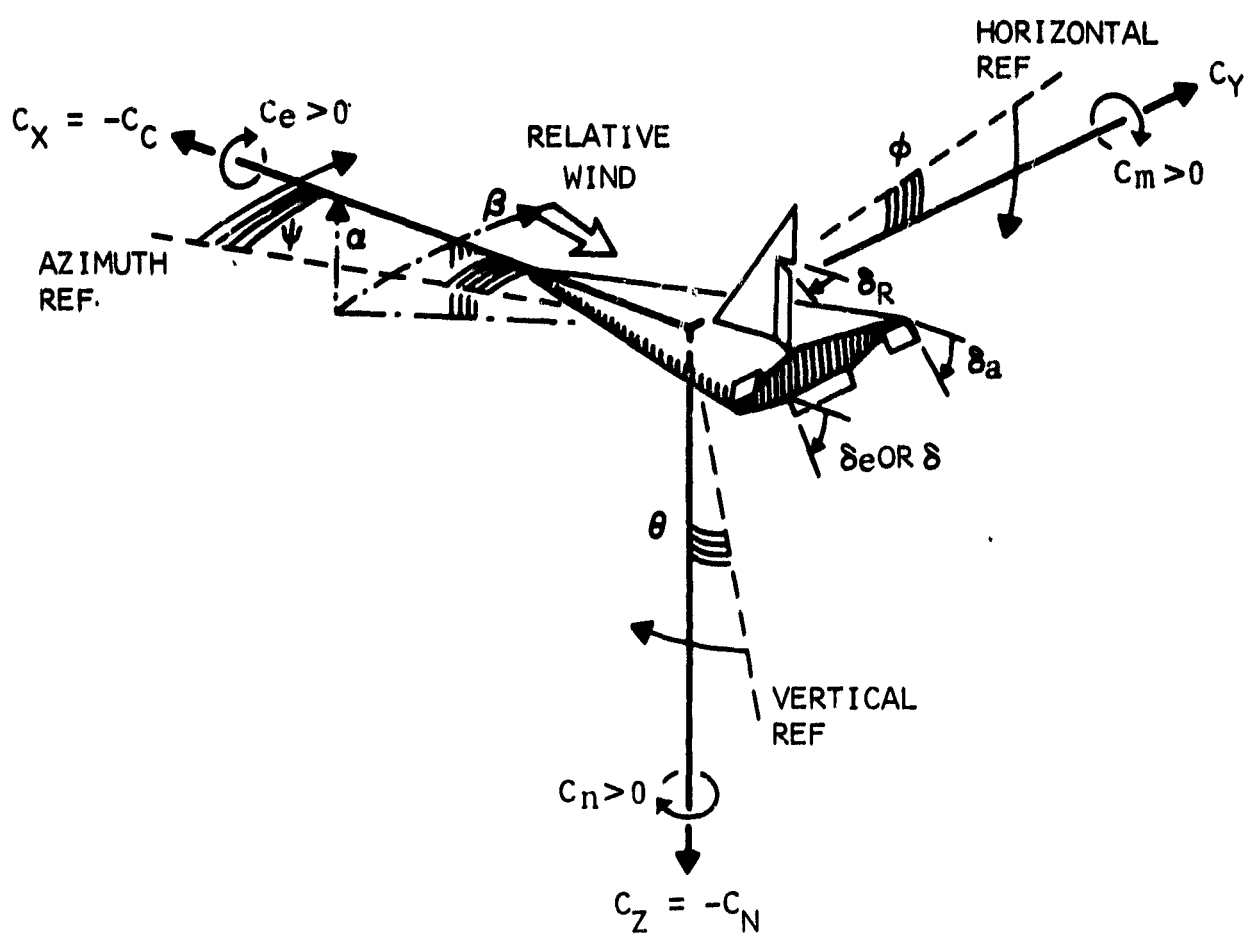


Figure 95. Body Axis System

Aircraft drag and longitudinal data. - Power-off drag data (fixed landing gear) are shown in figure 96 for the wing with and without leading edge slats. An equivalent  $C_F = 0.0070$  was used for defining the minimum drag coefficient. At the wetted area of 4,837 square feet transport aircraft vary from a  $C_F = 0.0045$  to 0.0080, and the 0.0070 is selected and accounts for all the interference effects of the various nacelles and engine pods and the T64 engines shut down during cruise. The minimum drag coefficient of 0.0424 is based on a wing area of 800 square feet for the air vehicle without gear. The landing gear drag is estimated and indicates a drag increment of 0.062 at the minimum drag  $C_L$ . To complete the drag polars shown, the drag due to lift and slat drag representative of the slats on and off is taken from the model data presented in figure 7 of NASA TN D-4160.

Power effects on drag are shown in figures 97 and 98 for 50-degree and 80-degree flap angle at zero angle of attack. The data are obtained from the NASA/Ames test 294. They include the effect of the lift augmentation without intake momentum drag, and do not include the thrust effects of the Orpheus cruise engines.

The asymptotes in the figures are obtained from

$$\frac{D}{T_0} = \frac{C_{D_{\text{power off}}} qS}{T_0} = C_{D_{\text{power off}}} \left( \frac{q}{\frac{T_0}{S}} \right) \quad (129)$$

Lift cruise slopes are presented in figure 99 for the tail-off case, and in figure 100 for the tail-on case. The data points of figure 100 are obtained from the Ames test 294 using

$$\frac{\frac{dL}{T_0}}{d\alpha} = \frac{dC_L}{d\alpha} \left( \frac{qS}{T_0} \right) = \frac{C_{L\alpha}}{C_J} \quad (130)$$

The asymptote represents the power-off case and is determined from

$$\frac{\frac{dL}{T_0}}{d\alpha} = (C_{L\alpha})_{\text{power off}} \left( \frac{q}{\frac{T_0}{S}} \right) \quad (131)$$

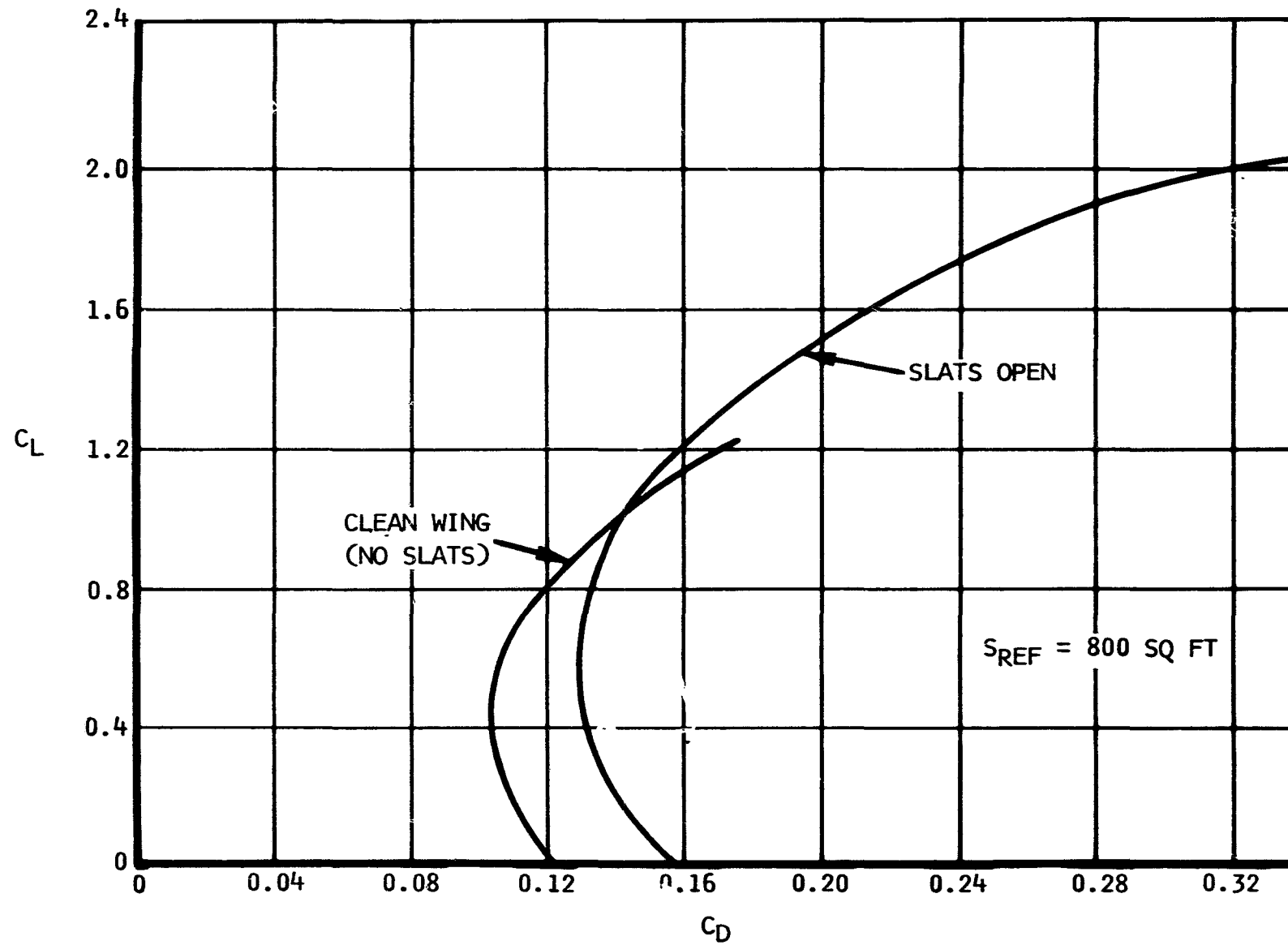


Figure 96. Modified Buffalo Drag Data  
Gear Down, Flaps Up  
Augmentor Wing

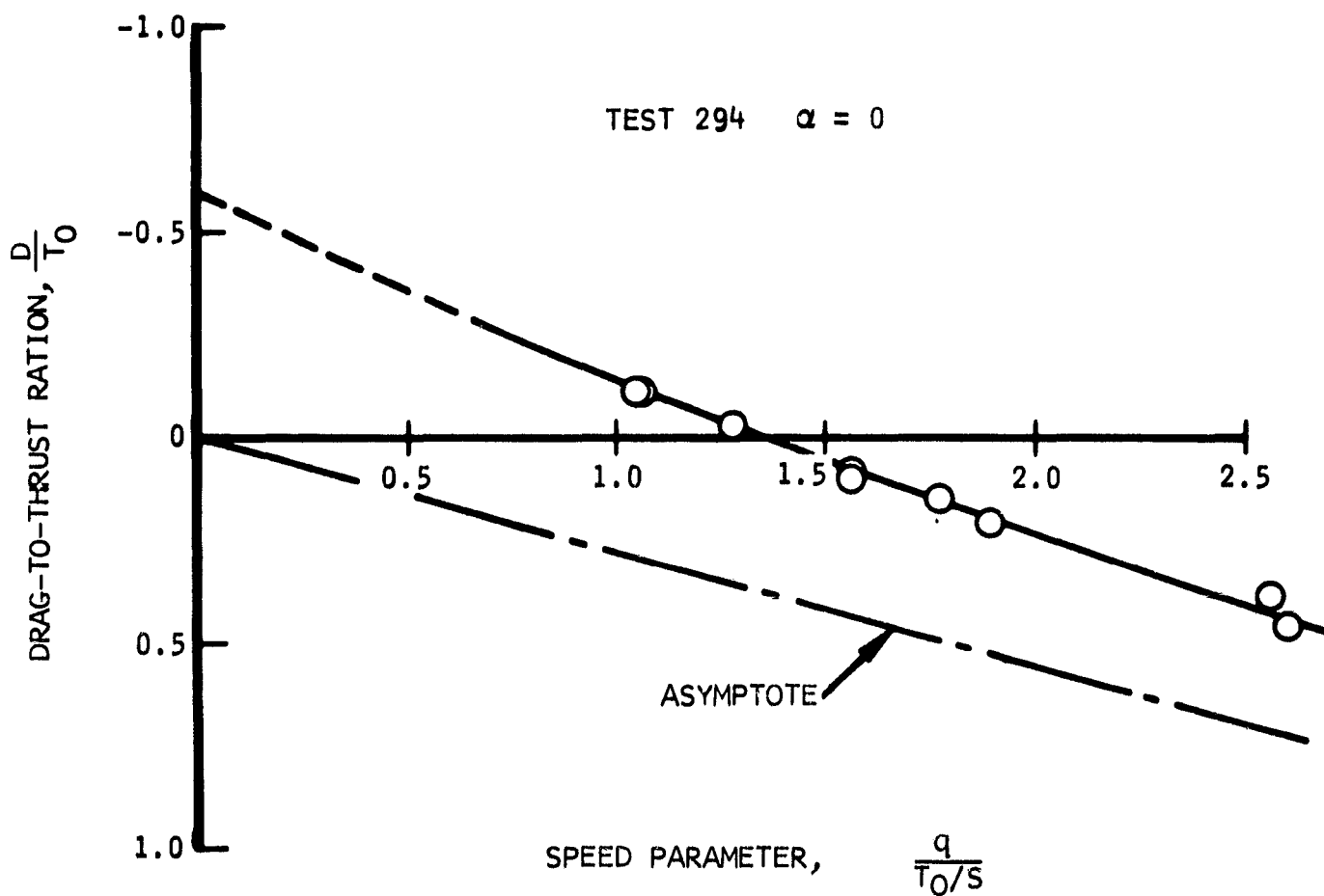


Figure 97. Net Drag Versus Speed Parameter at Flaps 50 Degrees



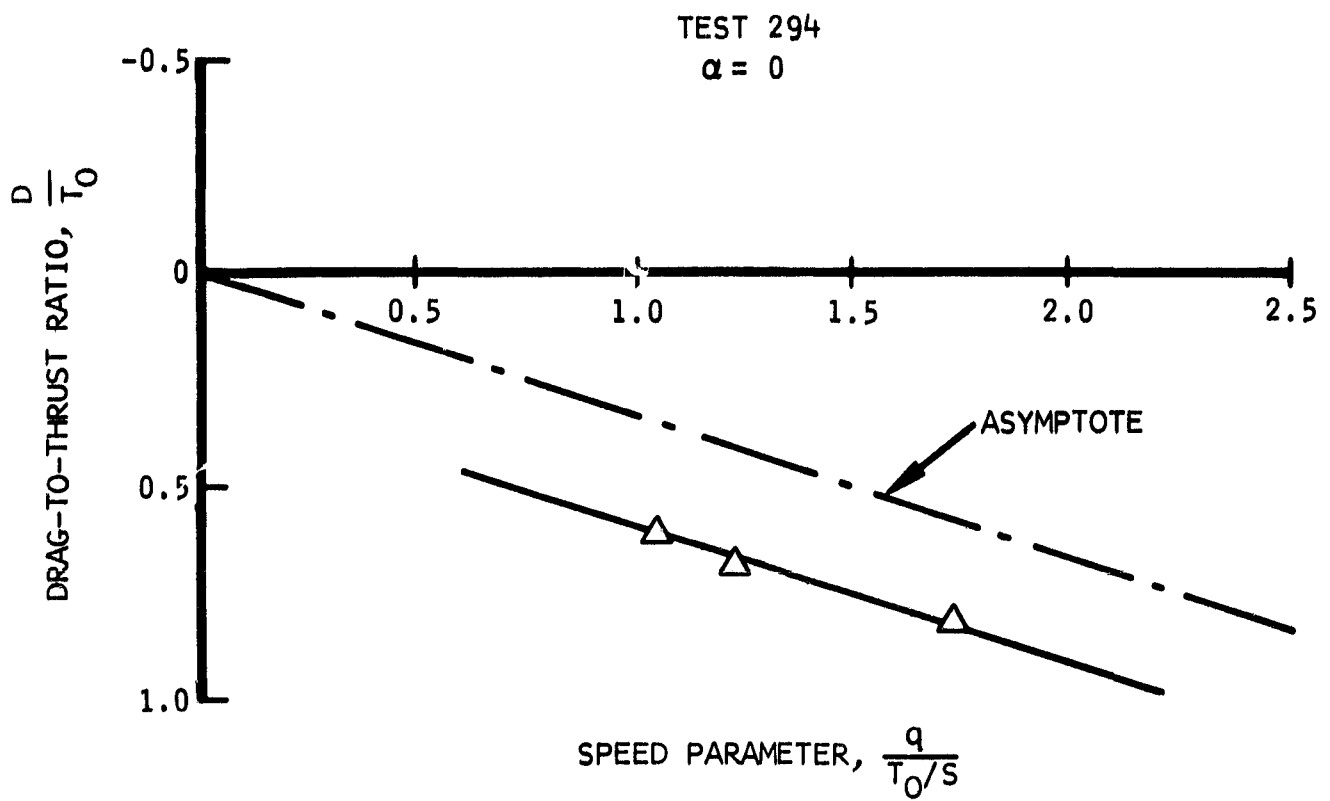


Figure 98. Net Drag Versus Speed Parameter at Flaps 80 Degrees

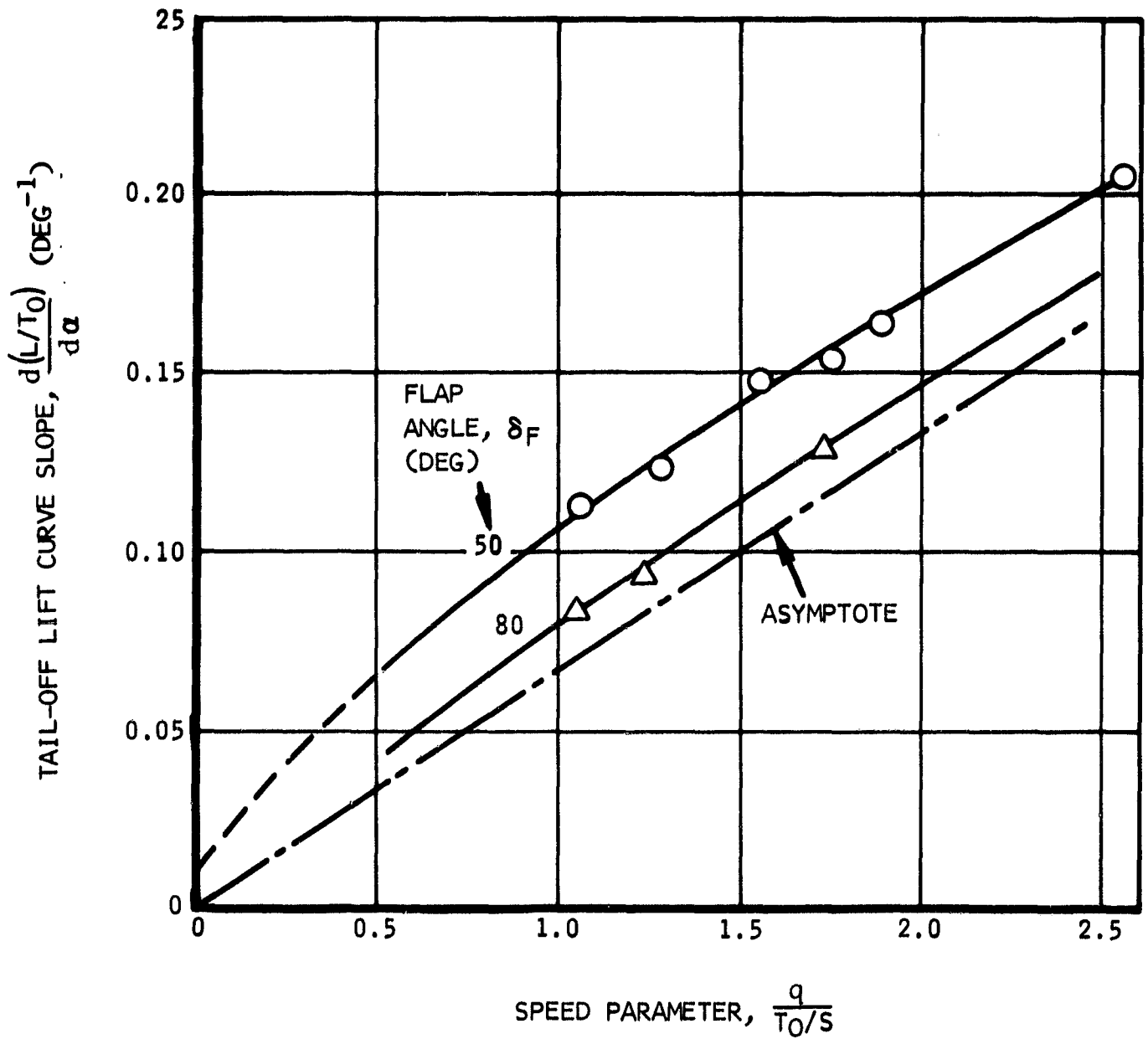


Figure 99. Tail-off Lift Curve Slopes Versus Speed Parameter

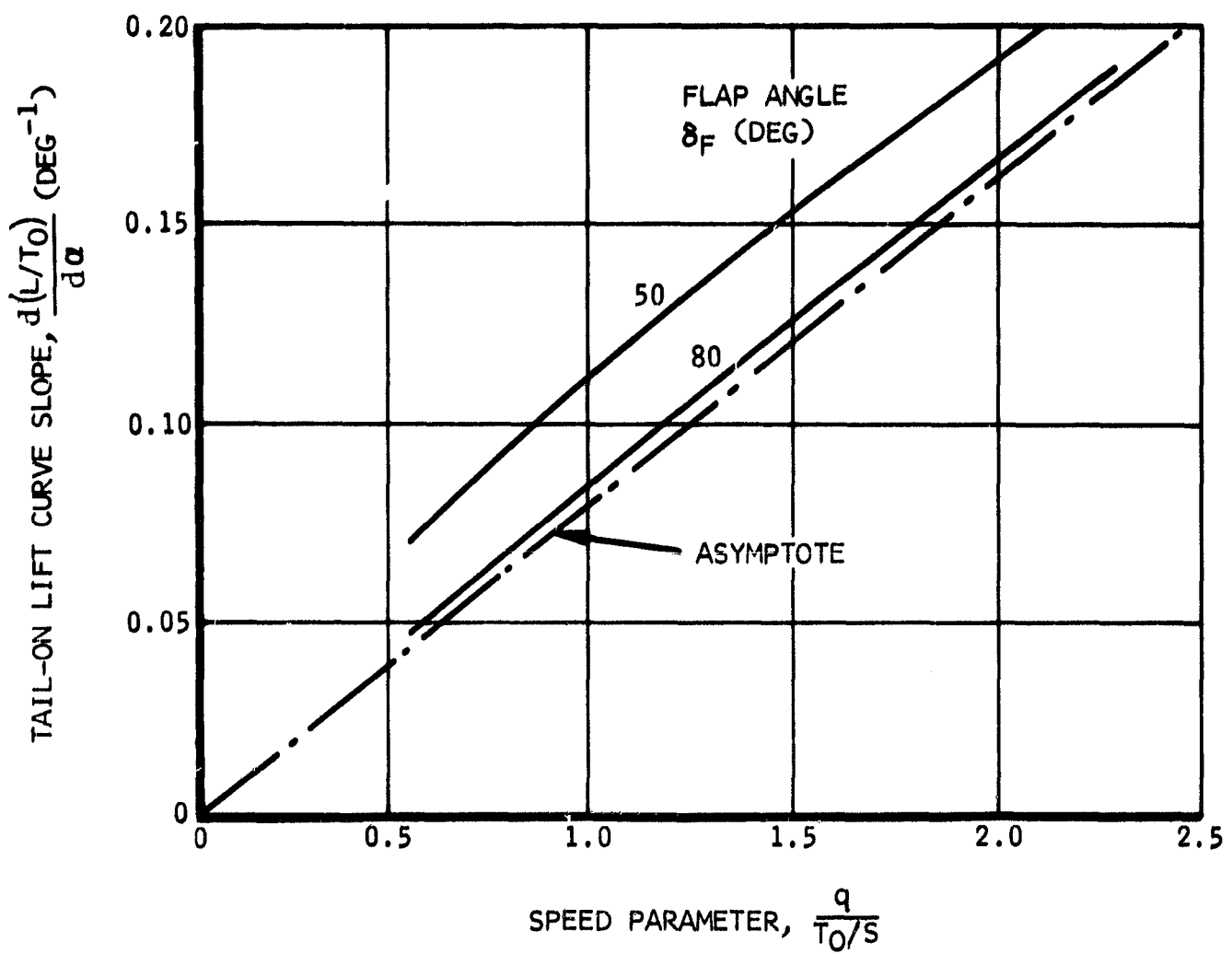


Figure 100. Tail-on Lift Curve Slopes Versus Speed Parameter

At zero forward speed, a point is computed for guidance in the extrapolation of the data, and is obtained from

$$\frac{d \frac{L}{T_0}}{d \alpha} = - \frac{D}{T_0} \left( \frac{d \sin \alpha}{d \alpha} \right) = \left( - \frac{D}{T_0} \right) \left( \frac{1}{57.3} \right) \quad (132)$$

where  $D/T_0$  is taken from above drag curves at zero speed.

The downwash at zero angle of attack is given in figure 101 as obtained from NASA/Ames test 294, and in figure 102 as obtained from TN D-4610. Large differences in downwash levels are found between these tests. However, the rate of downwash as a function of the speed parameter is almost identical between these two sources. (See figures 103 and 104.)

The downwash data are assumed directly applicable to the modified Buffalo, because of the very similar wing aspect ratio and because the tail surface is sufficiently far aft so that the effect of the bound vortices (i.e., the tail length difference) is minor in comparison to the effect of the trailing vortices.

Elevator effectiveness is presented in figure 105. It is obtained from

$$\frac{\partial \frac{M}{T_0 c}}{\partial \delta_e} = \frac{(-C_{L\delta_e})_H S_H l_H q}{T_0 c} = - (C_{L\delta_e}) \left( \bar{v}_H \right) \left( \frac{q}{S} \right) \quad (133)$$

Airplane damping in pitch is given in figure 106 and obtained using

$$\frac{\partial \frac{M}{T_0 c}}{\partial \frac{\dot{\theta} c}{V}} = \frac{(C_{L\alpha})_H S_H l_H q \left( \frac{\dot{\theta} l_H}{V} \right)}{T_0 c \left( \frac{\dot{\theta} c}{V} \right)} = C_{L\alpha} H \left( \frac{l_H}{c} \right) \left( \frac{q}{T_0} \right) \bar{v}_H \quad (134)$$

NASA AMES TEST 294  
DHC-DIR 67-42

$C_U$   
 ○ 0.56  
 ◇ 0.78 (APPROXIMATE)  
 △ 0.92 (APPROXIMATE)  
 □ 0.92 (APPROXIMATE)

DOWNWASH  
FROM TEST 294

FLAGGED SYMBOLS:  $\delta_F = 50^\circ$   
 PLAIN SYMBOLS:  $\delta_F = 70^\circ$

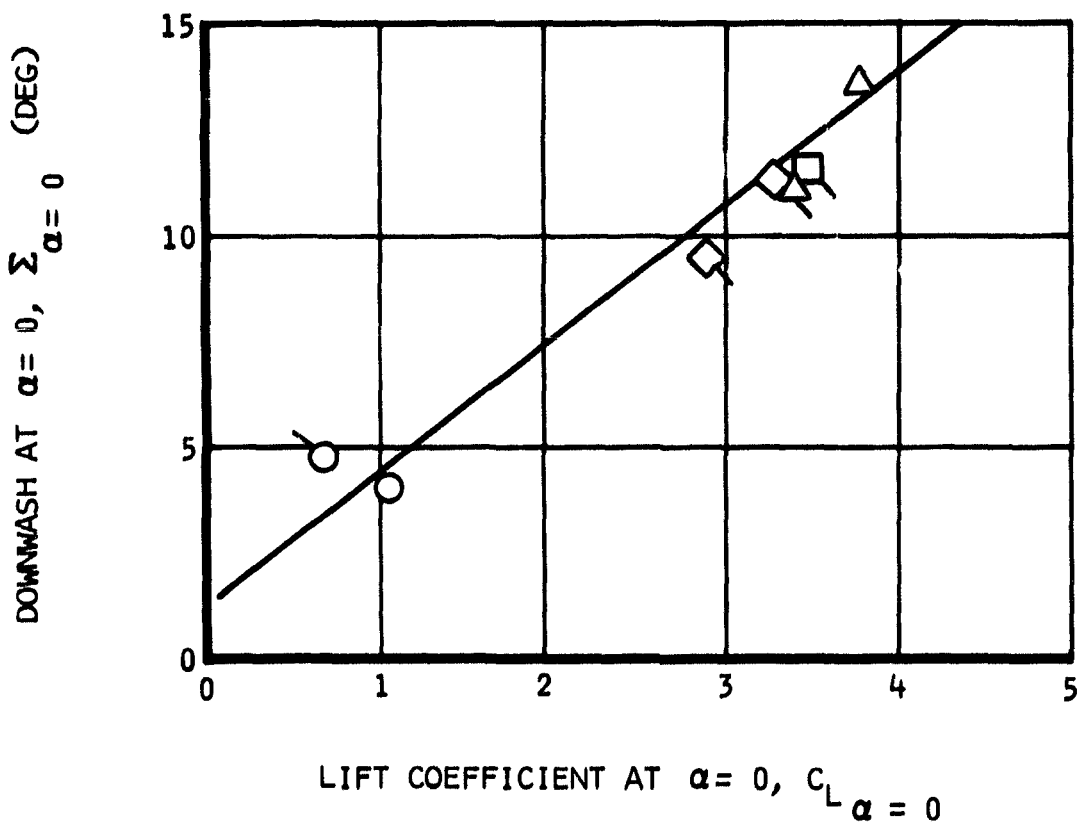


Figure 101. Downwash at Zero Angle of Attack as Affected by Power

DOWNWASH  
FROM TN D-4610

$\delta_F = C_J$
$\square 30^\circ = 0.75$
$\triangle 60^\circ = 1.21$
$\nabla 70^\circ = 1.22$
$\triangleleft 100^\circ = 0.74$

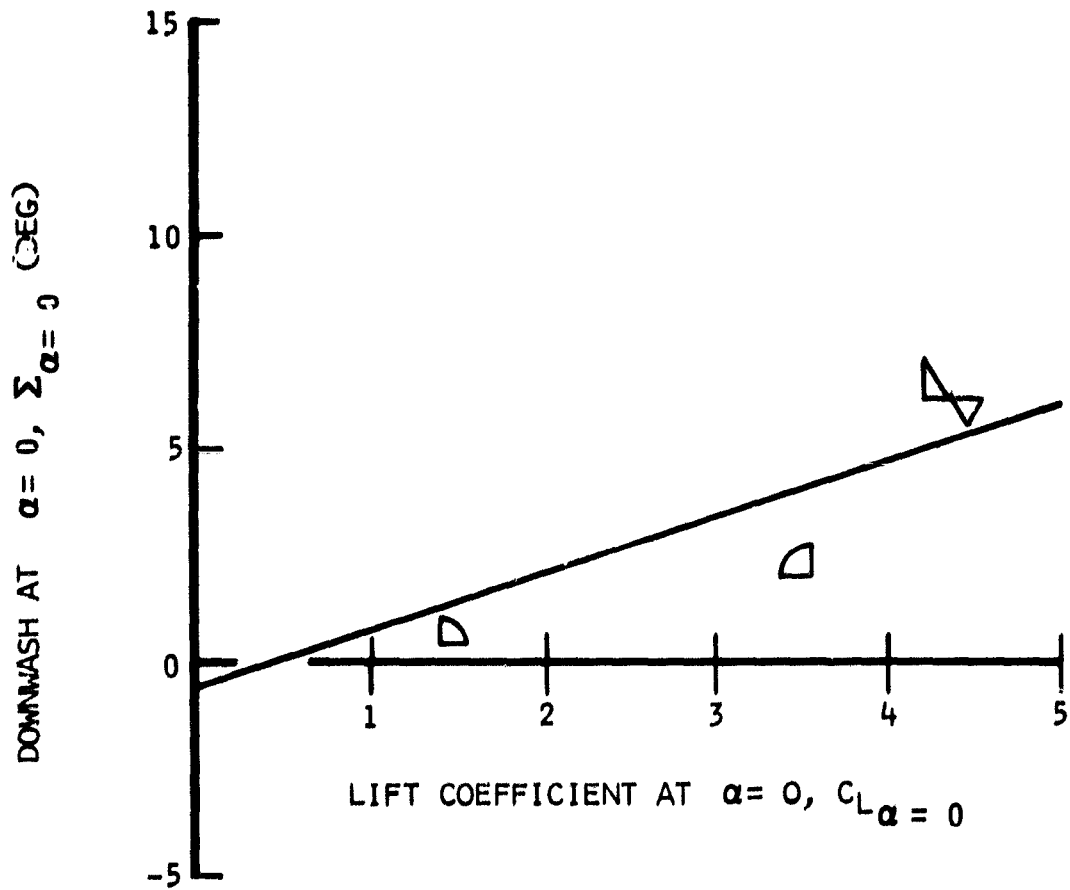


Figure 102. Ames Augmentor Wing Model.  
Effect of Power on Downwash Slope

DHC-DIR 67-42  
 NASA AMES TEST 294

- $C_J$
- 0
  - ◇ 0.56
  - △ APPROXIMATELY 0.78
  - APPROXIMATELY 0.92

DOWNWASH  
 FROM TEST 294

FLAGGED SYMBOLS:  $\delta_F = 50^\circ$   
 PLAIN SYMBOLS:  $\delta_F = 70^\circ$

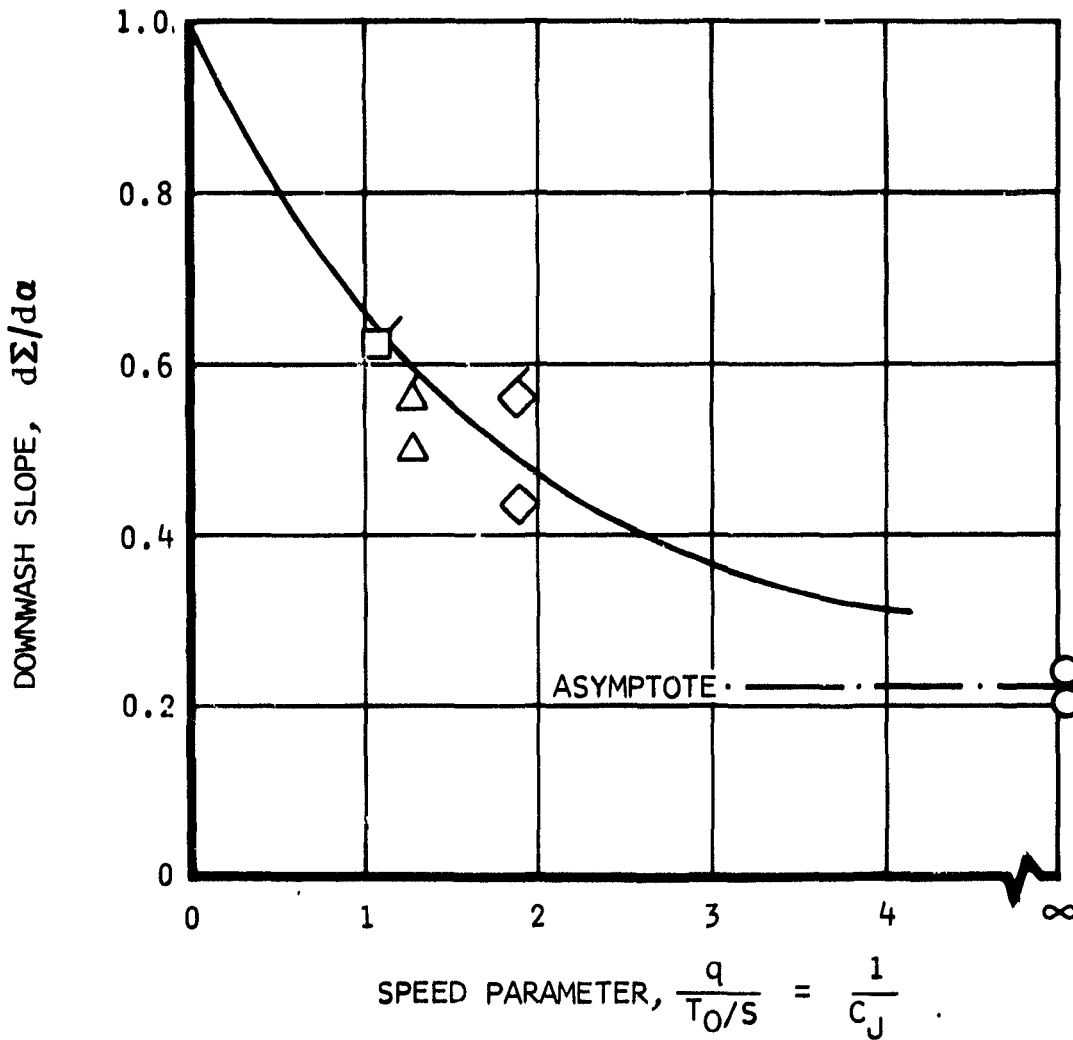


Figure 103. Ames Augmentor Wing Model  
 Effect of Power on Downwash Slope

	$\delta_F$	$C_J$
D	30°	0.75
▷	60°	1.21
▽	70°	1.22
◁	100°	0.74

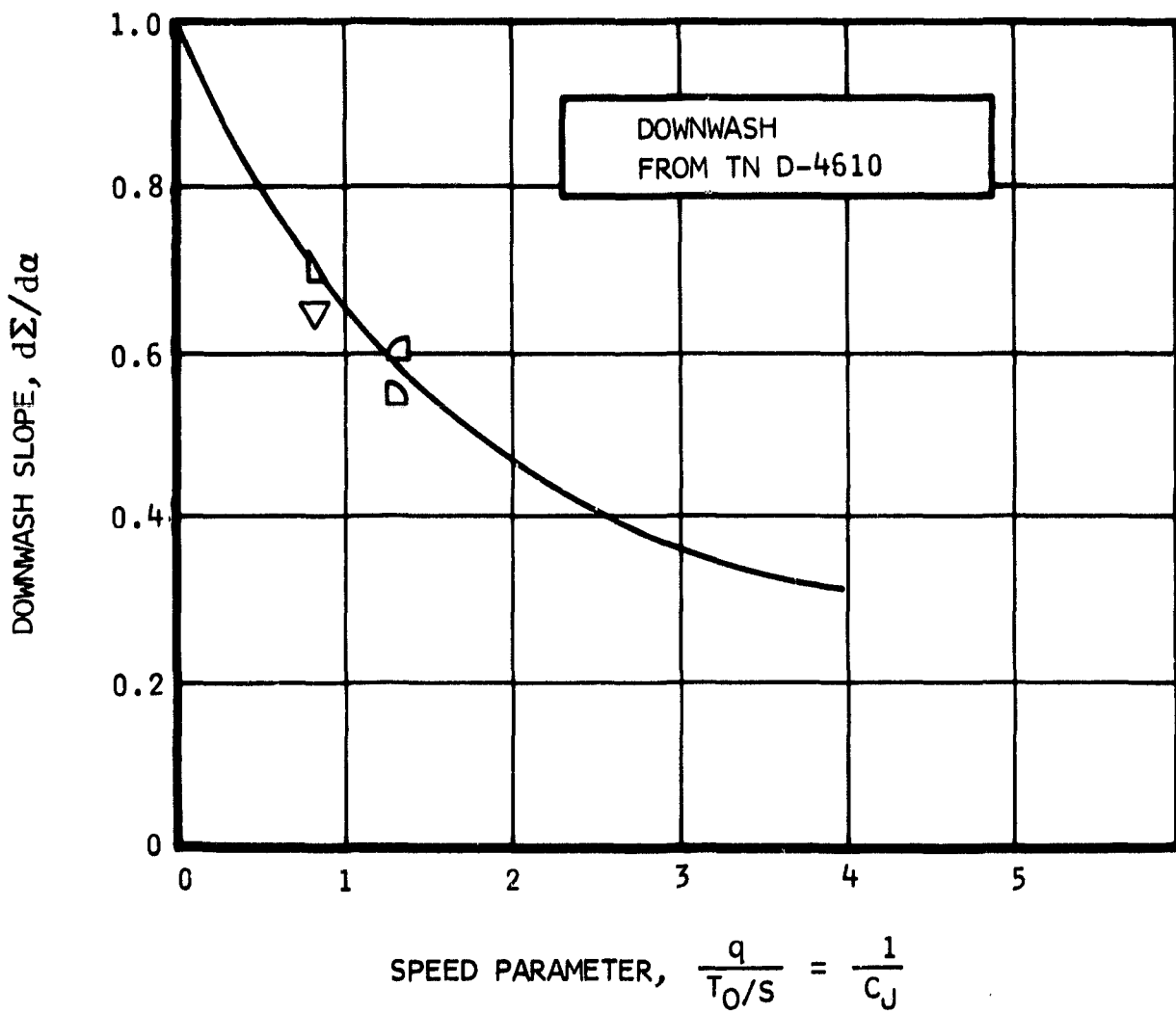


Figure 104. Ames Augmentor Wing Model-Effect of Power on Downwash Slope



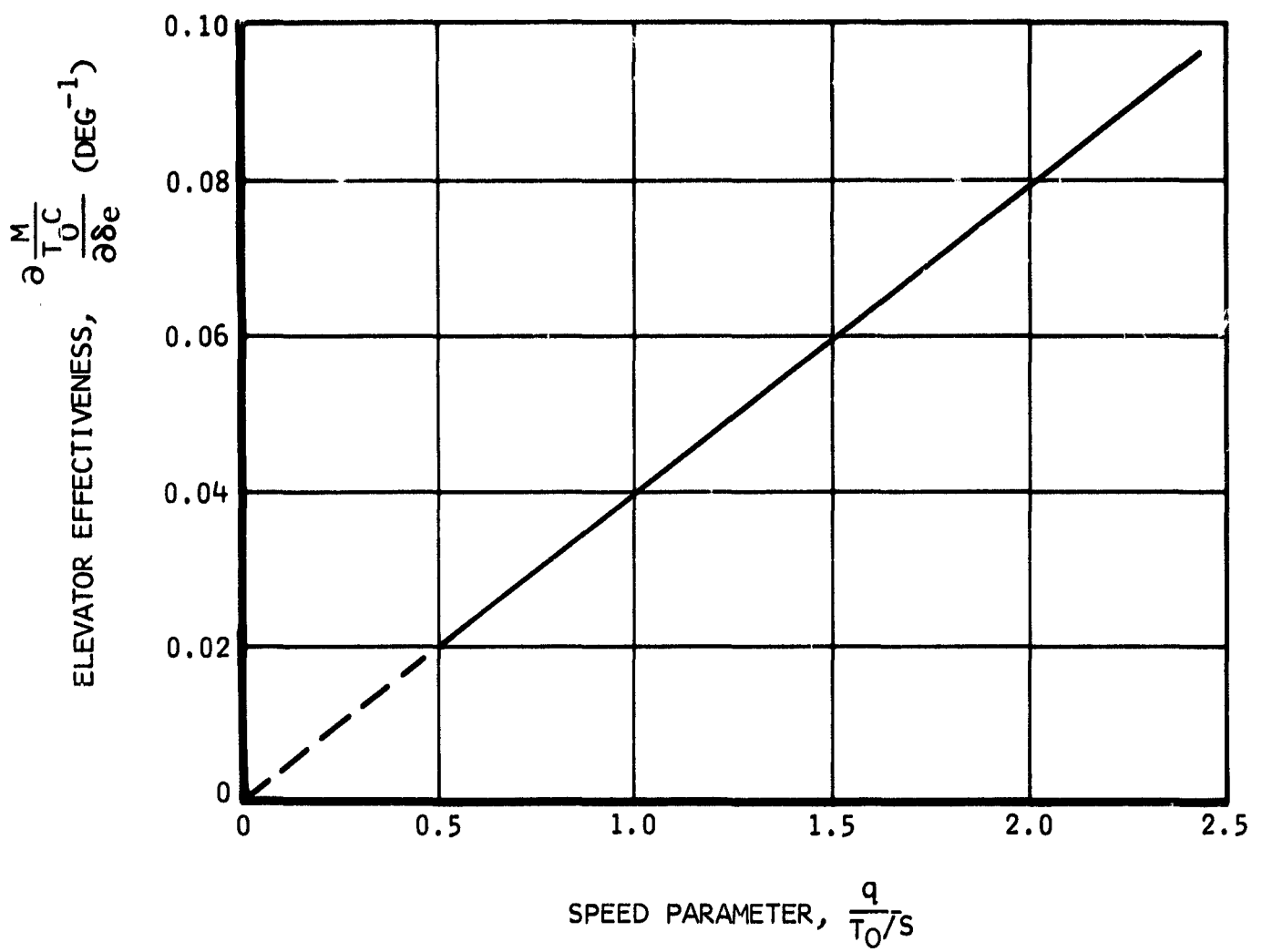


Figure 105. Elevator Effectiveness

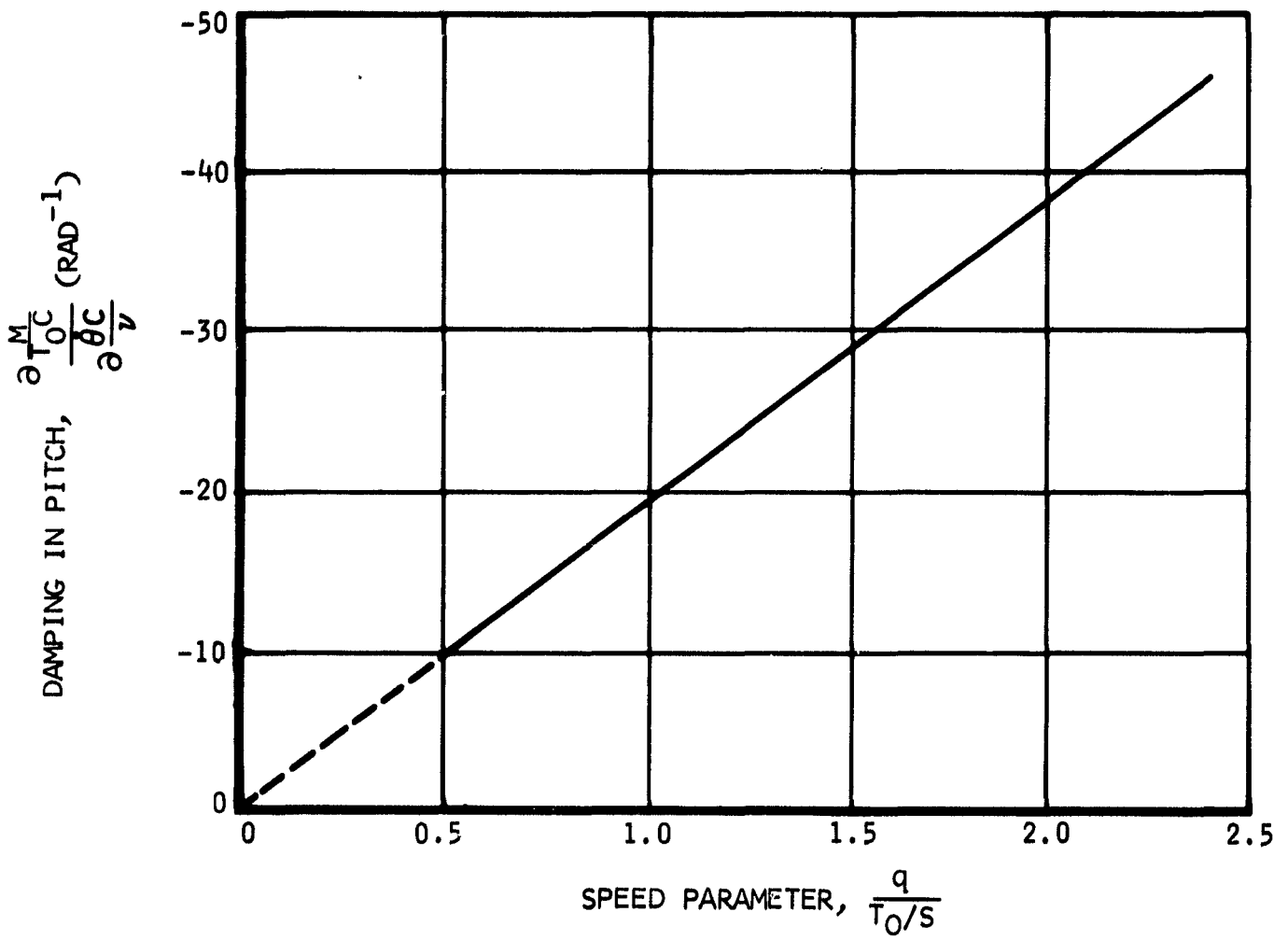


Figure 106. Airplane Damping in Pitch

The airplane damping in angle of attack in figure 107 is derived from

$$\frac{\partial \frac{M}{T_o c}}{\partial \frac{\dot{\alpha} c}{V}} = \frac{\partial \frac{M}{T_o c}}{\partial \frac{\dot{\theta} c}{V}} \left( \frac{d\epsilon}{d\alpha} \right) \quad (135)$$

Lateral and directional data.

Aileron characteristics: The rolling moment due to aileron deflection in the conventional coefficient form  $\Delta C_l$  is presented in figure 108. It is estimated using Weissinger lifting surface theory, to which an experimental factor is applied to account for the aileron-to-wing chord ratio with BLC as shown in the section of aerodynamics control system considerations.

Figure 109 shows the aileron effectiveness in a form more suitable for the STOL investigation, using

$$\frac{\partial \frac{L}{T_o b}}{\partial \delta_a} = \frac{C_{l \delta_a} q S b}{T_o b} = C_{l \delta_a} \frac{q}{\frac{T_o}{S}} \quad (136)$$

Similarly, the yawing moment due to aileron deflection in figure 110 is obtained from

$$\frac{\partial \frac{N}{T_o b}}{\partial \delta_a} = C_{n \delta_a} \left( \frac{q}{\frac{T_o}{S}} \right) \quad (137)$$

Herein  $C_{n \delta_a}$  is a function of aileron droop as shown in the section describing aerodynamics characteristics of the control system.

With spoilers deflected, the aileron trailing edge up deflection (from horizontal) is taken as only 55 percent effective. This is based on NACA ACR 1D07. A reduction is expected because of the spoiler wake.

The aileron hinge moments are shown in figure 111 and are based on DATCOM.

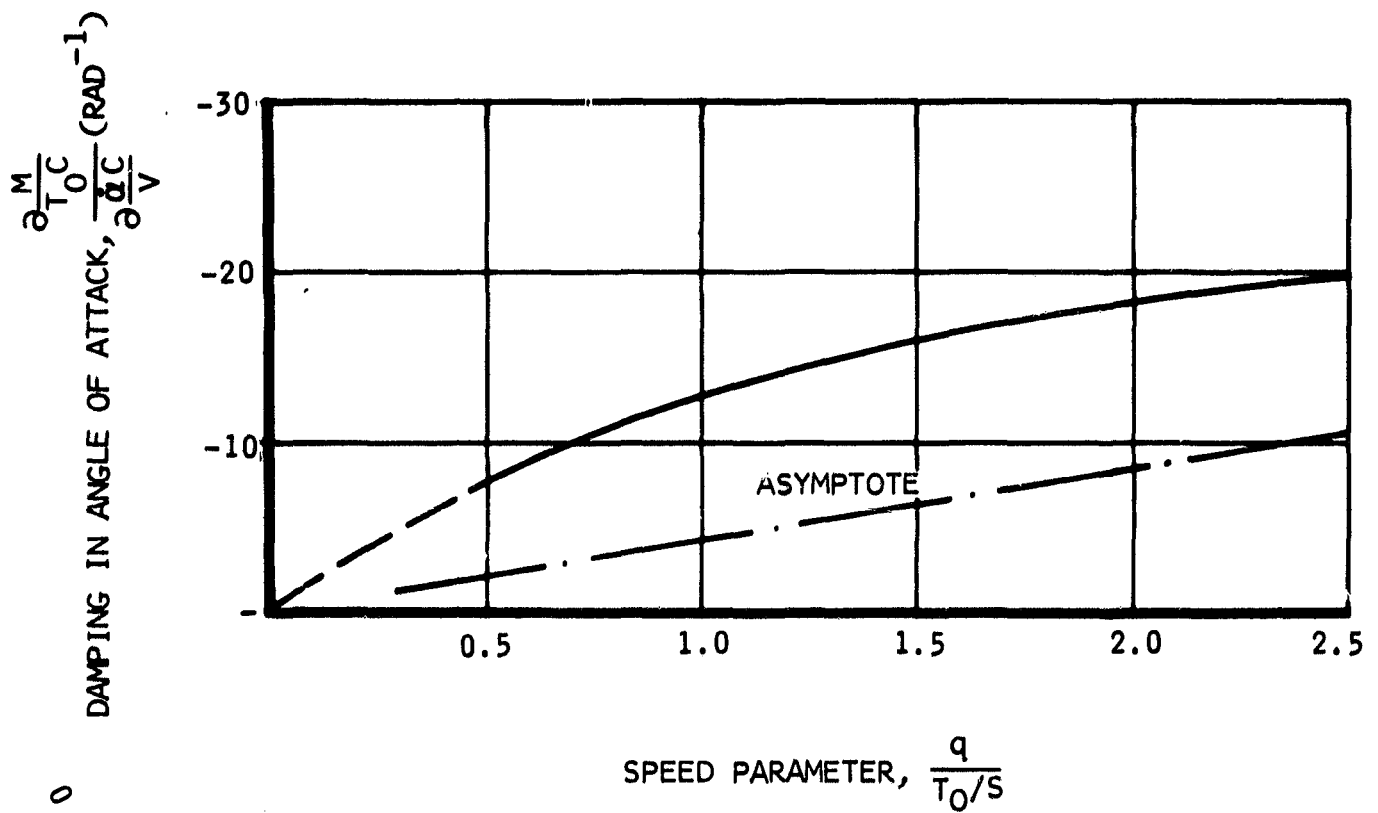


Figure 107. Airplane Damping in Angle of Attack

WITHOUT SPOILER DEFLECTION

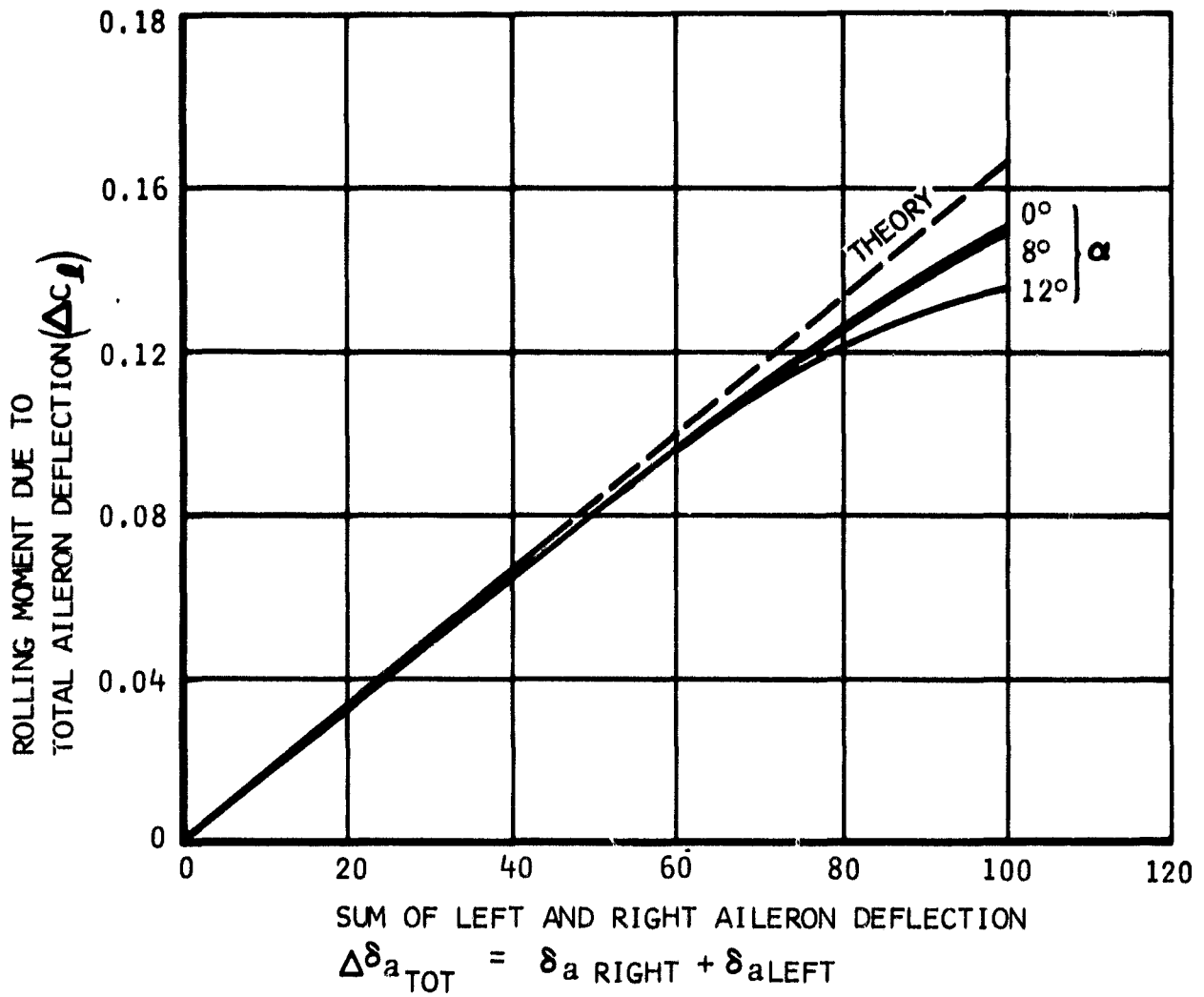


Figure 108. Aileron Effectiveness at the Critical Momentum Coefficient for Blowing

ZERO SPOILER DEFLECTION  
 BODY AXIS SYSTEM  
 SMALL AILERON DEFLECTIONS

$\alpha = 0^\circ \rightarrow 12^\circ$

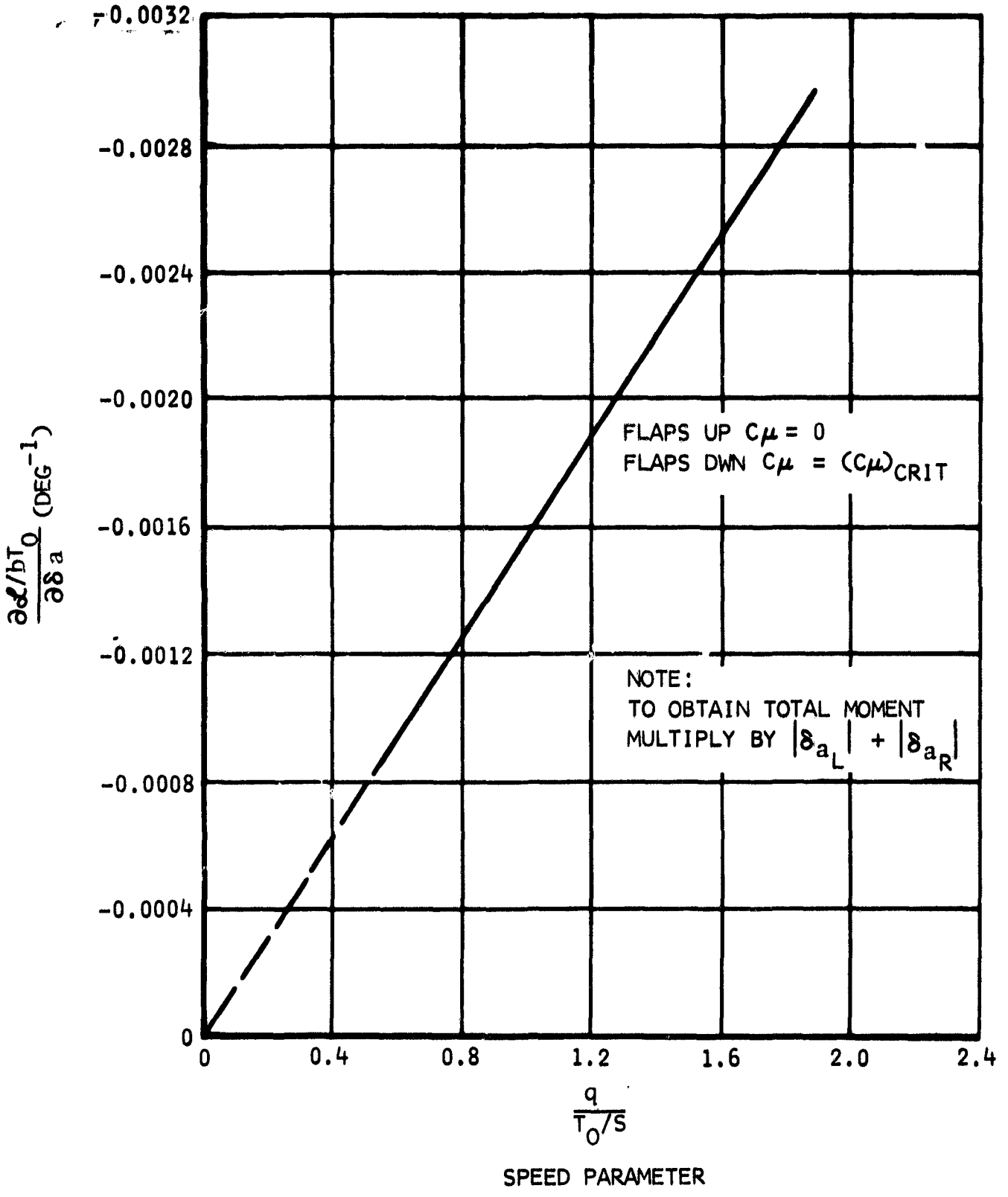
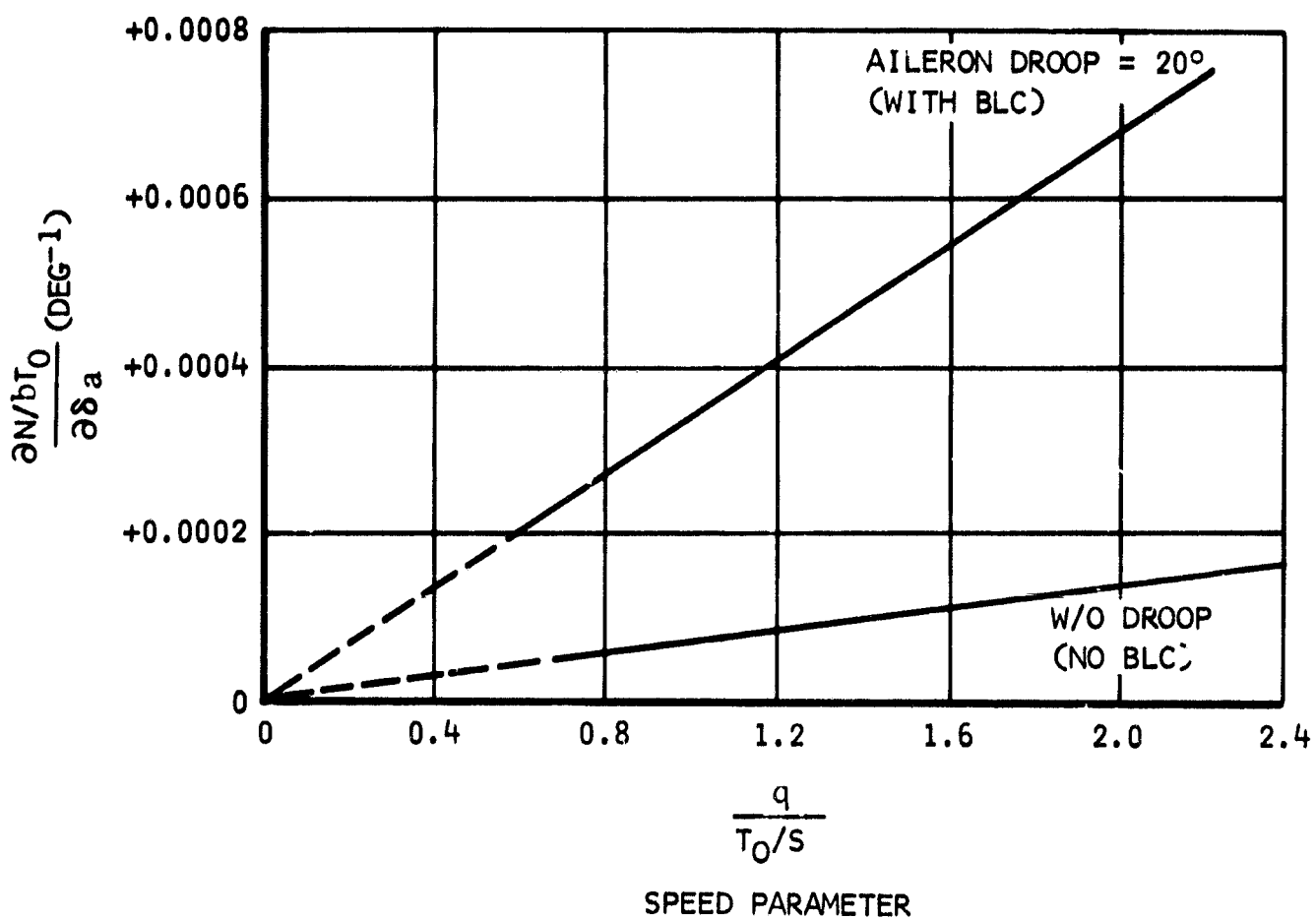


Figure 109. Aileron Effectiveness Versus Speed Parameter

ZERO SPOILER DEFLECTION  
 SMALL AILERON DEFLECTIONS  
 BODY AXIS SYSTEM

$\alpha = 0^\circ \rightarrow 8^\circ$



NOTE: TO OBTAIN TOTAL MOMENT  
 MULTIPLY BY  $|\delta_{a_L}| + |\delta_{a_R}|$

Figure 110. Yaw Due to Aileron Deflection Versus Speed Parameter

$\alpha$   
 ————— 0°  
 - - - - - 8°  
 - · - - - 12°  
 BASED ON AILERON  
 $S_a = 30.0$  SQ FT  
 $\bar{C}_a = 2.77$  FT

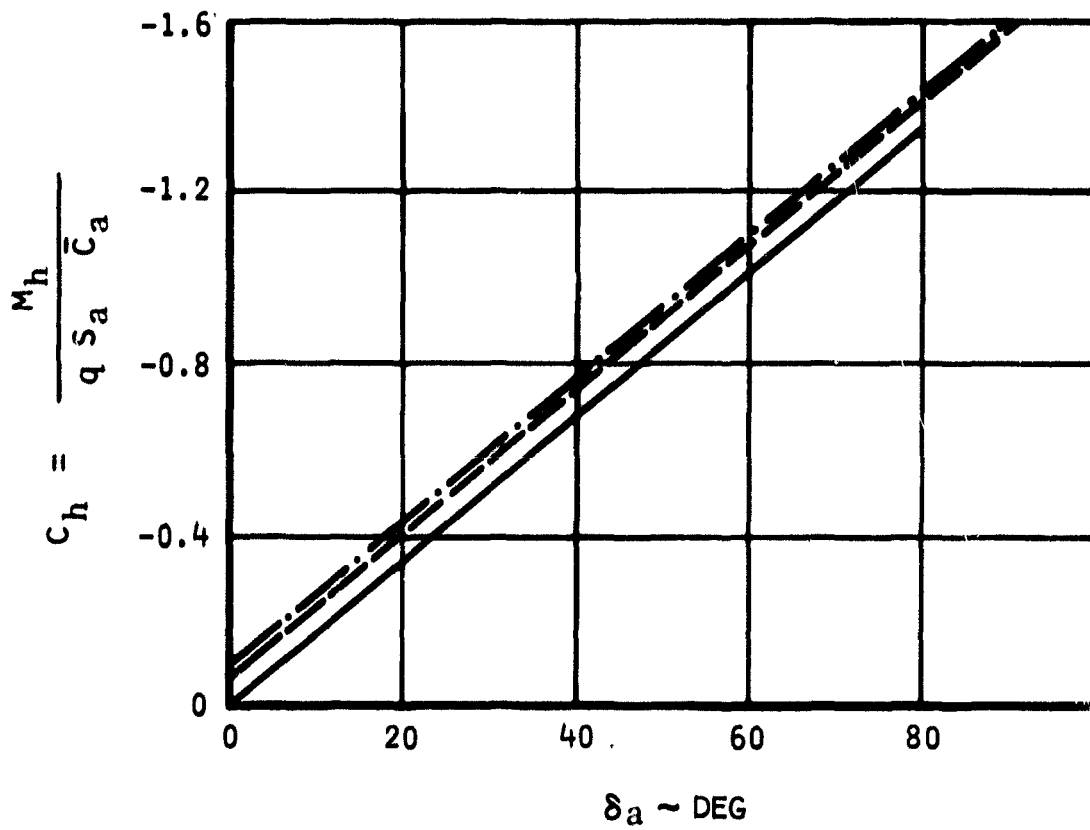


Figure 111. Aileron Hinge Moment



**Spoiler characteristics:** The rolling moment and yawing moment coefficients in their conventional form are presented in figure 112 and are based on DATCOM. They can be used in conjunction with aileron deflections, provided the ailerons are deflected downward. Conversion to STOL parameters is carried out in figures 113 and 114 using

$$\frac{\partial \frac{L}{T_o b}}{\partial \delta_{sp}} = C_{l_{\delta_{sp}}} \left( \frac{q}{\frac{T_o}{S}} \right) \quad (138)$$

$$\frac{\partial \frac{N}{T_o b}}{\partial \delta_{sp}} = C_{n_{\delta_{sp}}} \left( \frac{q}{\frac{T_o}{S}} \right) \quad (139)$$

Spoiler hinge moment characteristics are based on the correlations presented in figure 115.

**Rudder characteristics:** The lift coefficient of the vertical tail as a function of rudder deflection is given in figure 116. It is estimated on the basis of Weissinger lifting surface theory and experimental values of  $\partial \alpha / \partial \delta$ . Note that the rear portion of the rudder rotates to a total of 50 degrees when  $\delta_R = 25$  degrees.

STOL sideforce derivatives, yawing moment derivatives, and rolling moment derivatives are presented in figure 117, 118, and 119, and obtained from

$$\frac{\partial \frac{Y}{T_o}}{\partial \delta_R} = \left[ \left( \frac{\partial C_L}{\partial \delta_R} \right)_v \frac{S_v}{S} \right] \frac{q}{\frac{T_o}{S}} \quad (140)$$

$$\frac{\partial \frac{N}{T_o b}}{\partial \delta_R} = \left[ \left( \frac{\partial C_L}{\partial \delta_R} \right)_v \frac{S_v}{S} \right] \left( \frac{l_v}{b} \right) \left( \frac{q}{\frac{T_o}{S}} \right) = \left( \frac{\partial C_L}{\partial \delta_R} \right)_v \left( \frac{q}{\frac{T_o}{S}} \right) \bar{V}_v \quad (141)$$

RIGHT-HAND WING  
 ZERO AILERON DEFLECTION  
 BODY AXIS SYSTEM

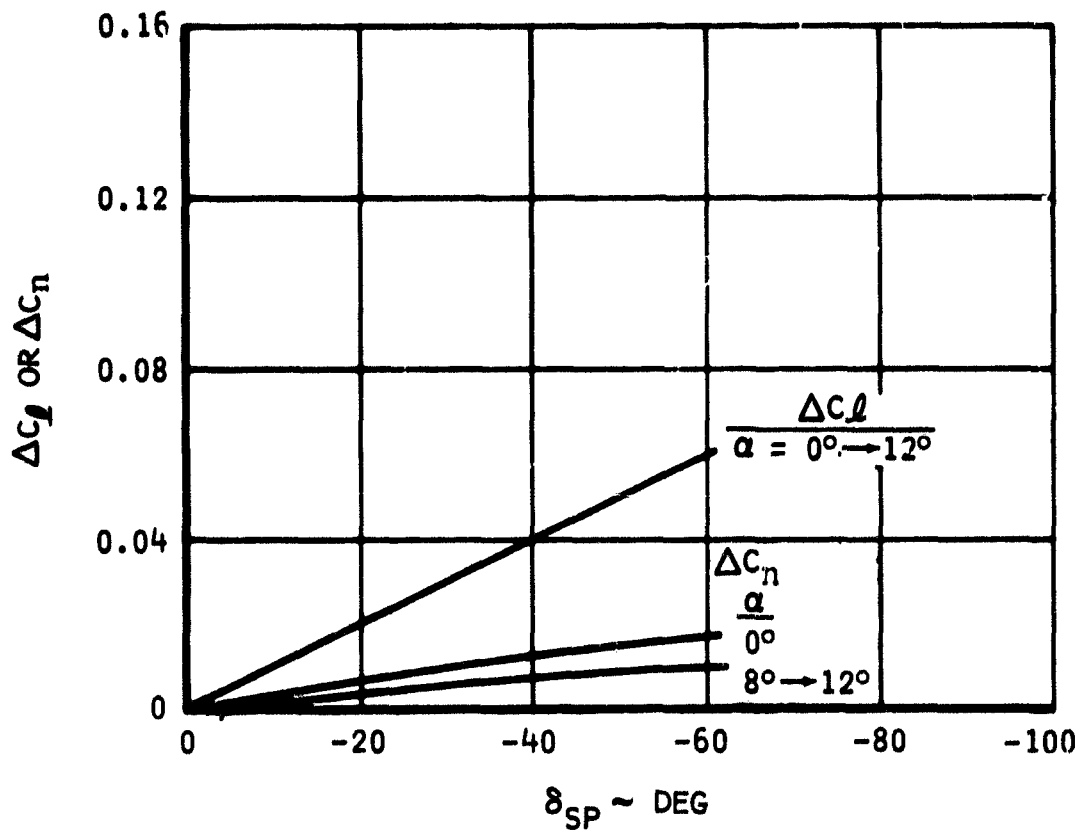


Figure 112. Spoiler Effectiveness and Yawing Moment Due to Spoiler

ZERO AILERON DEFLECTION  
BODY AIXS SYSTEM  
 $\alpha = 0^\circ \rightarrow 12^\circ$

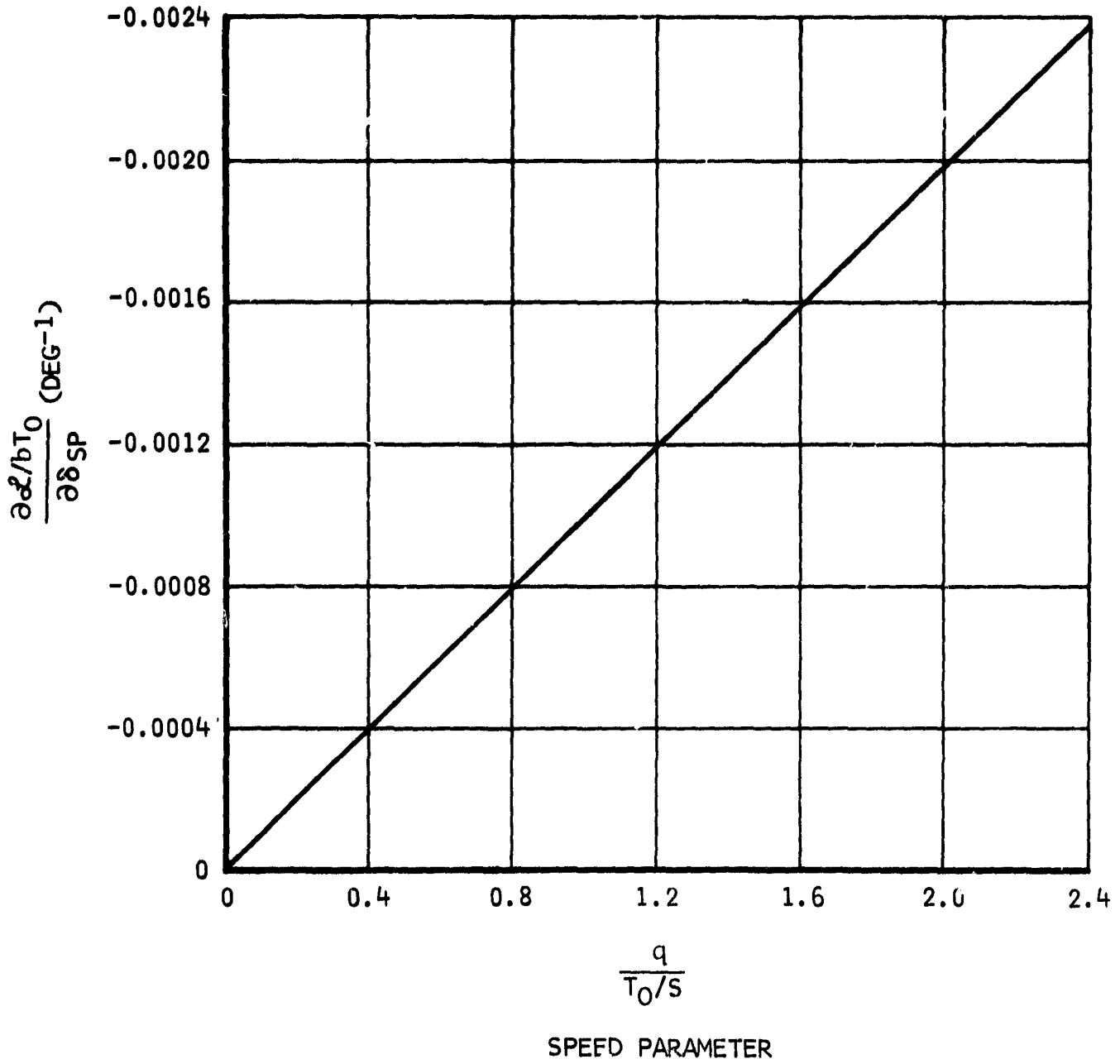


Figure 113. Spoiler Effectiveness Versus Speed Parameter

ZERO AILERON DEFLECTIONS  
 FOR SMALL SPOILER DEFLECTIONS  
 $\alpha = 0^\circ$

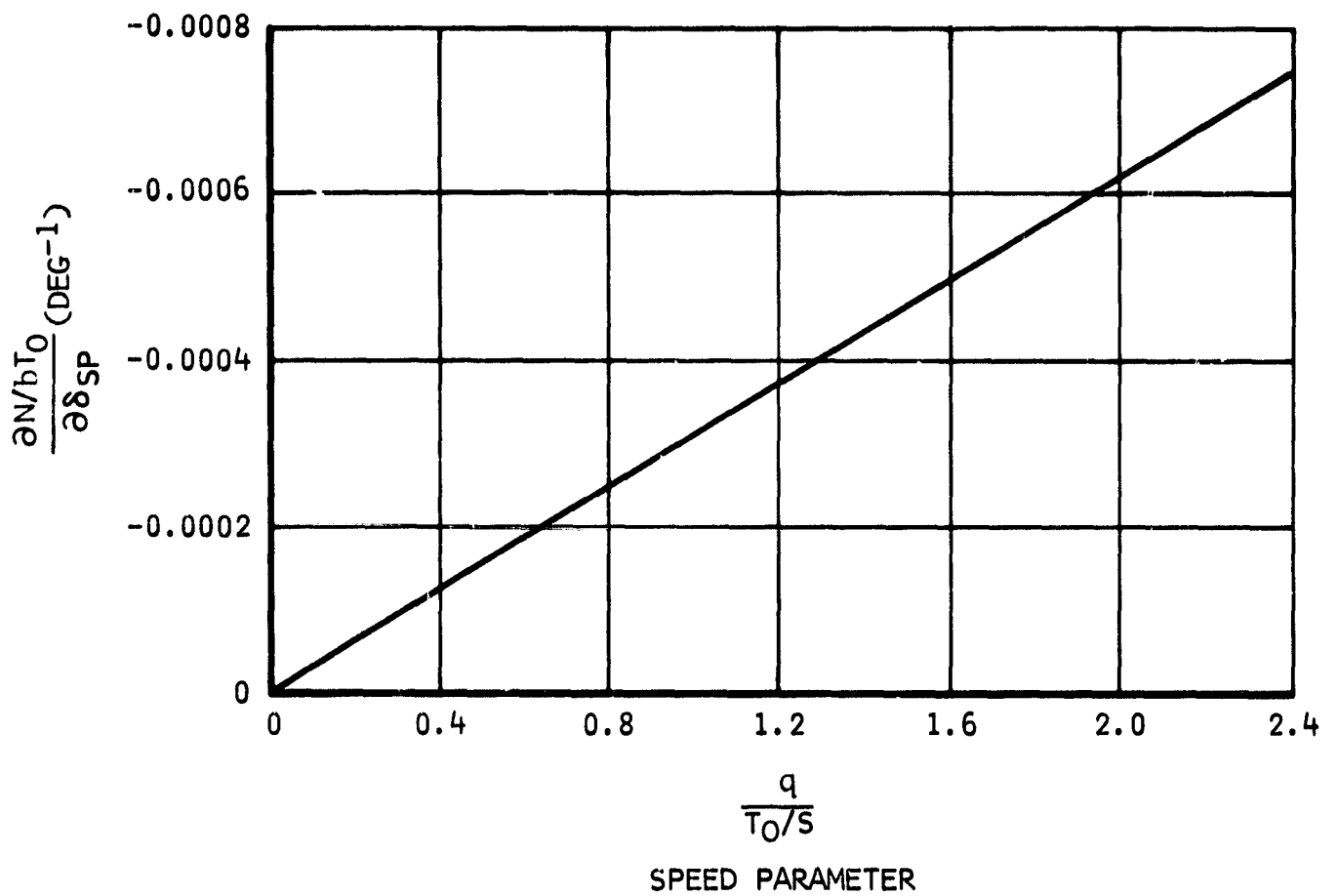


Figure 114. Yawing Moment Due to Spoiler Deflection Versus Speed Parameter

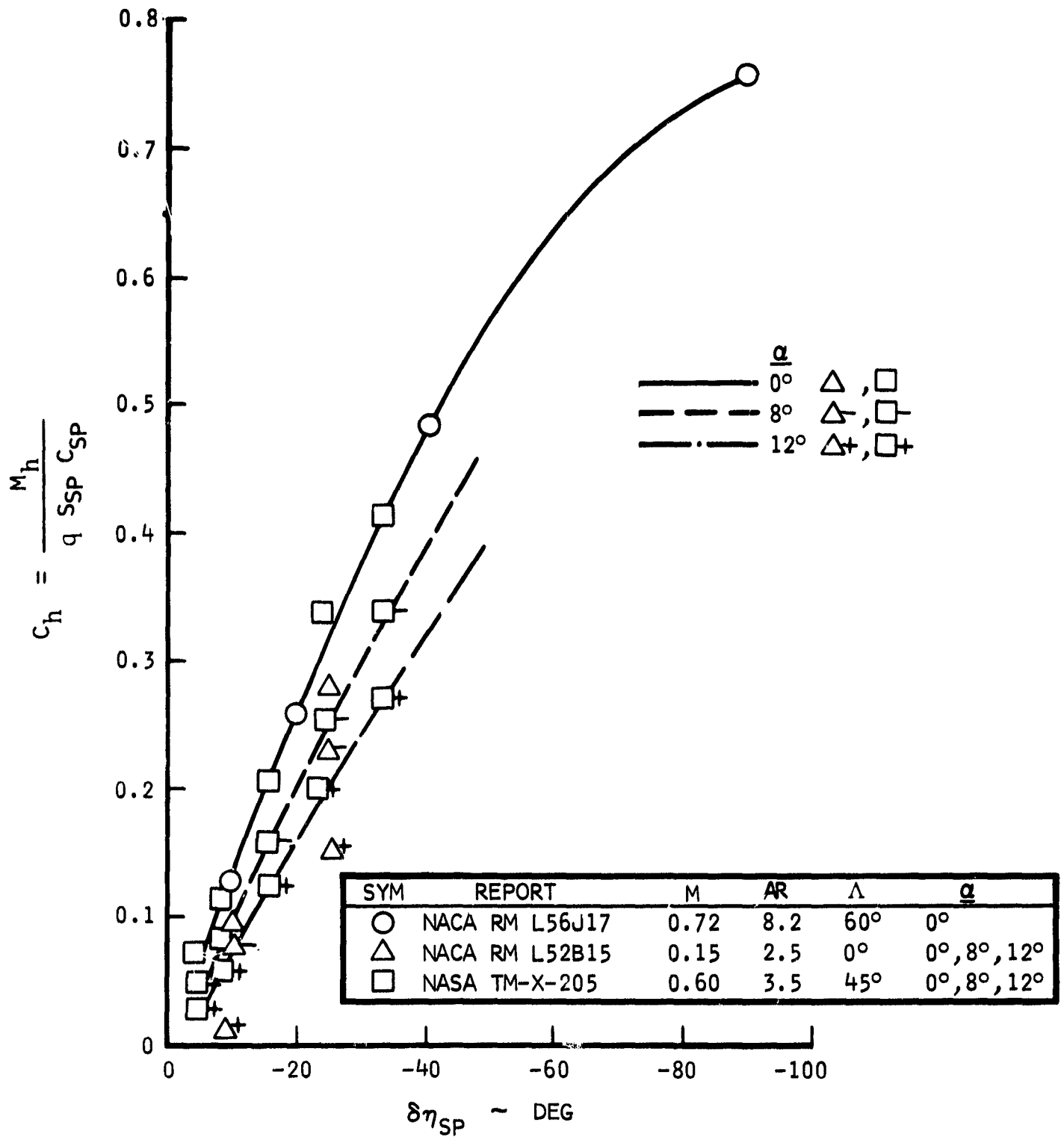
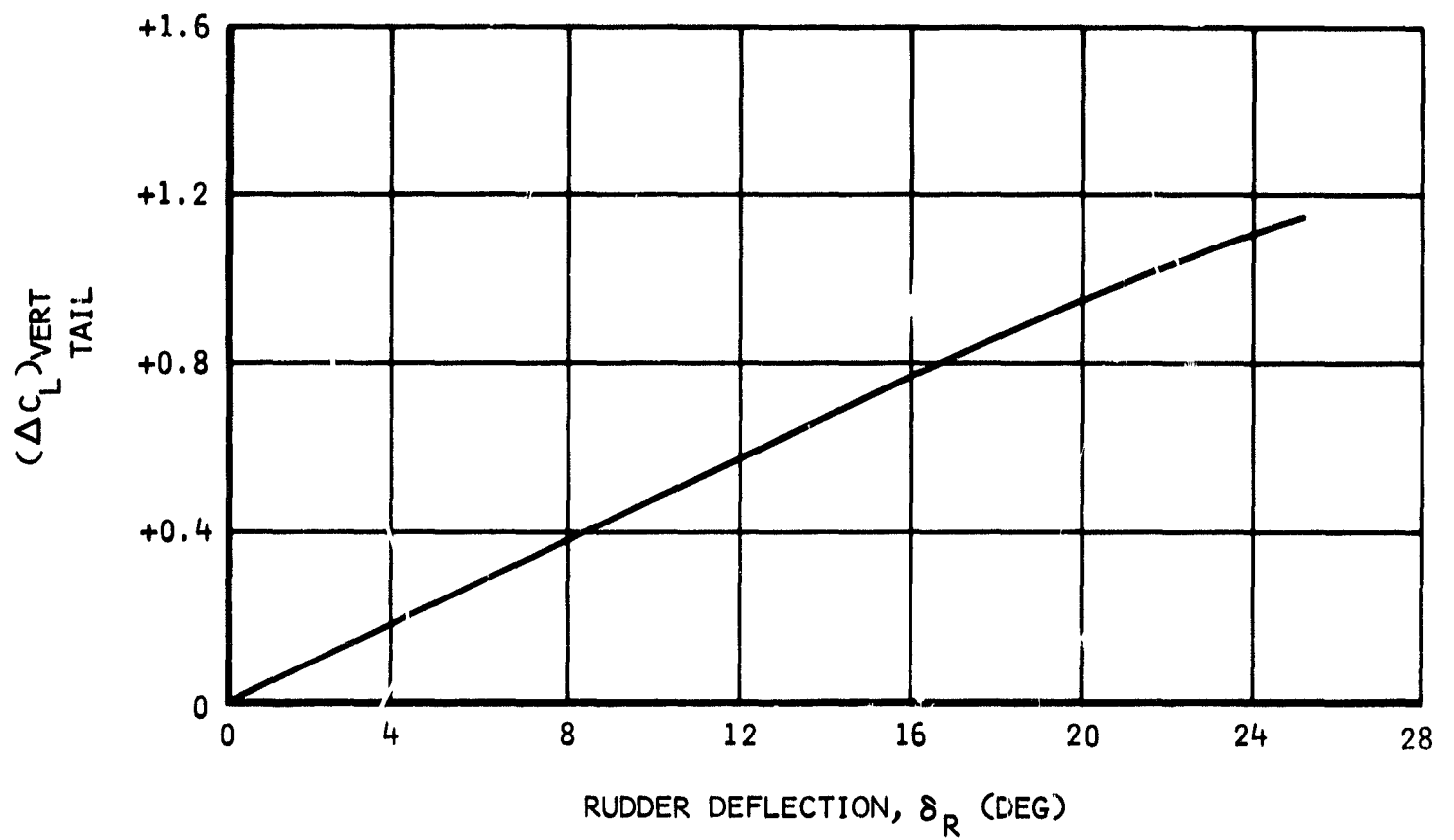


Figure 115. Spoiler Hinge Moment



NOTE: VERTICAL REFERENCE AREA = 151 FT<sup>2</sup>

Figure 116. Side Force Due to Rudder

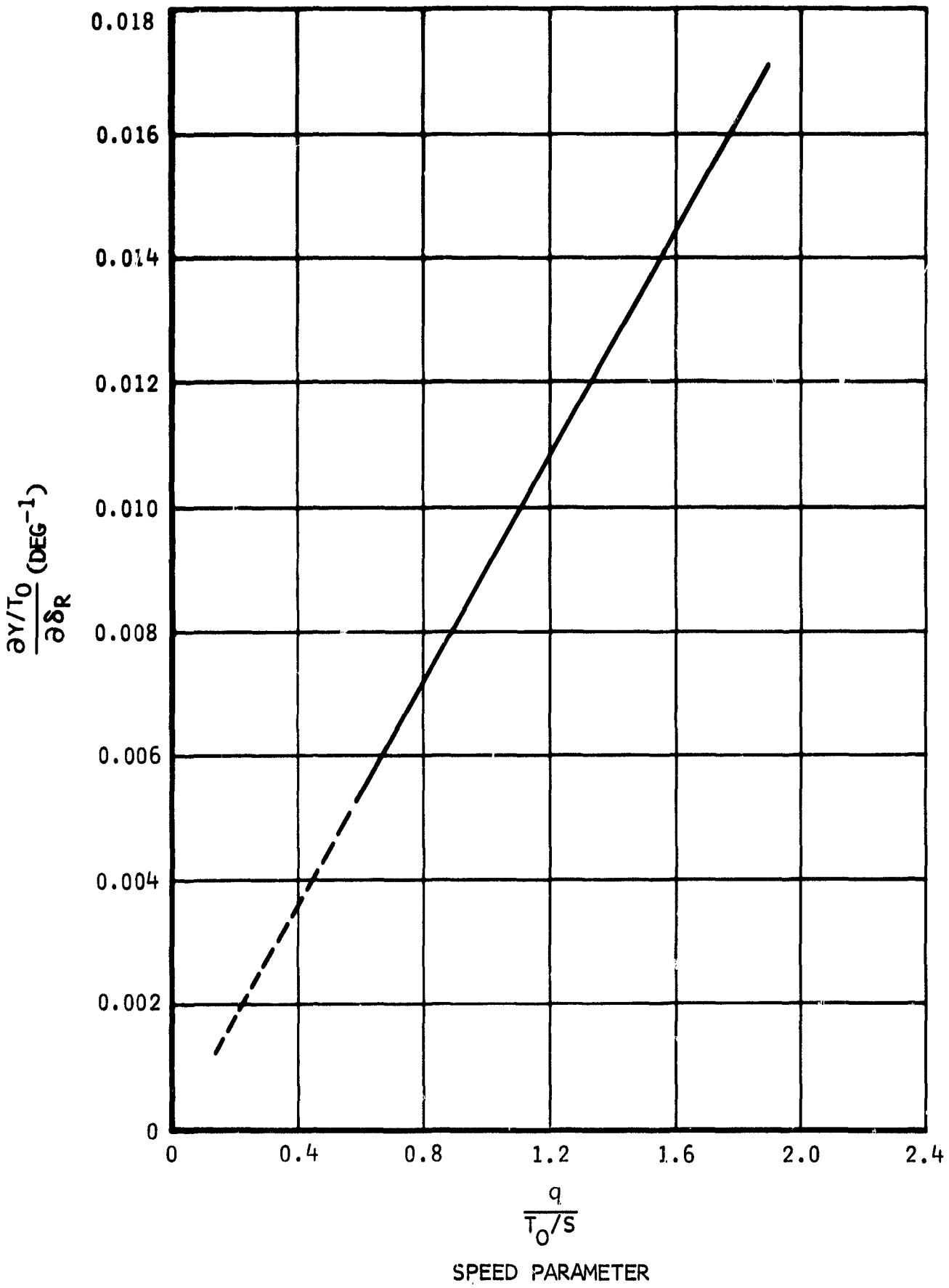


Figure 117. Rudder Side Force Derivative Versus Speed Parameter

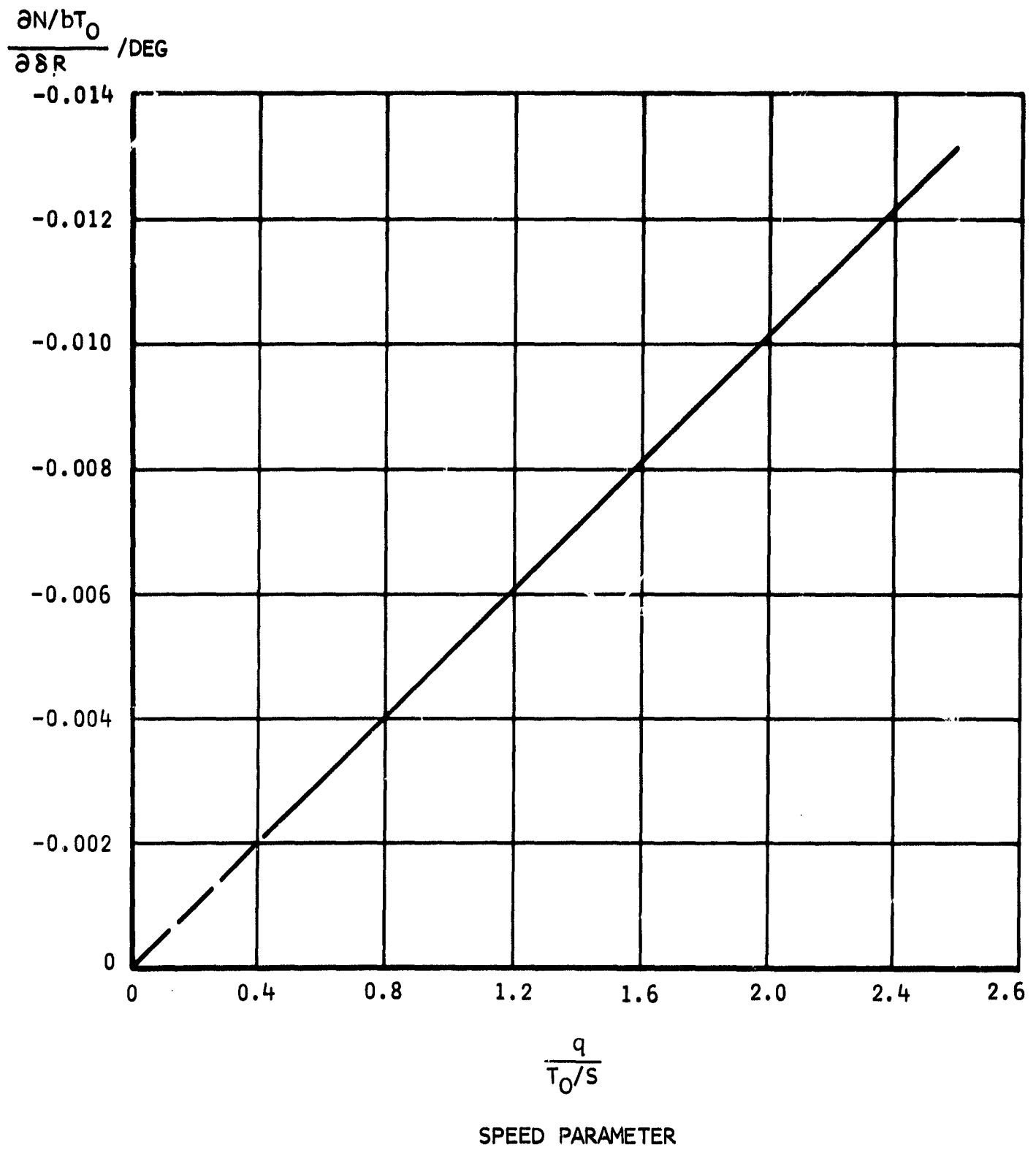


Figure 118. Rudder Effectiveness Versus Speed Parameter



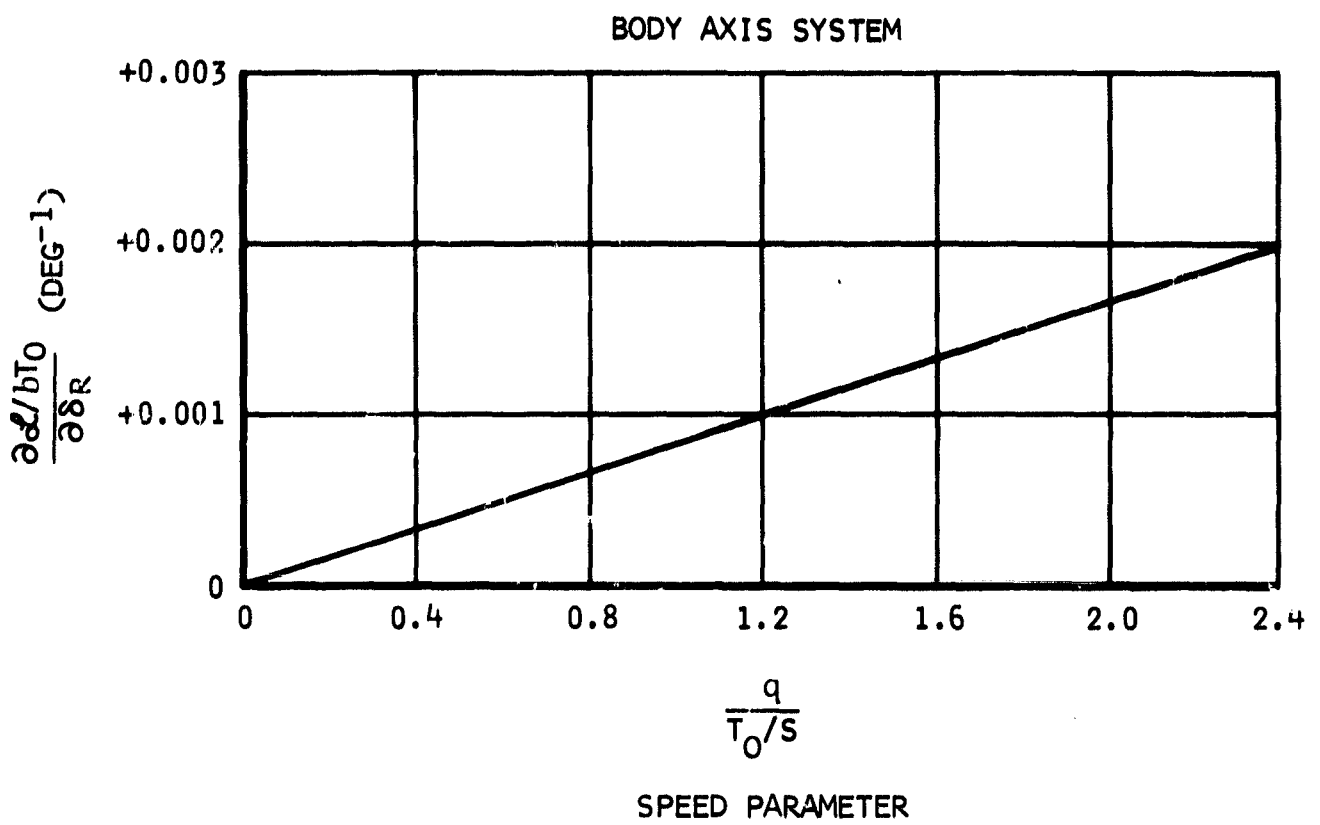


Figure 119. Rolling Moment Due to Rudder Deflection Versus Speed Parameter

$$\frac{\partial \frac{L}{T_o b}}{\partial \delta_R} = \left[ \left( \frac{\partial C_L}{\partial \delta_R} \right)_v \frac{S_v}{S} \right] \left( \frac{z}{b} \right) \left( \frac{q}{T_o S} \right) \quad (142)$$

Sideslip derivatives: The rolling moment due to sideslip is given in figure 120. The asymptote shown represents the condition at zero thrust from the lift augmentation engines. The asymptote is derived from

$$\left( \frac{\partial \frac{L}{T_o b}}{\partial \beta} \right) = (C_{l\beta})_{\text{power off}} \left( \frac{q}{T_o S} \right) \quad (143)$$

where  $(C_{l\beta})_{\text{power off}}$  is taken equal to the unmodified Buffalo characteristics based on DHC information. (The effect of wing aspect ratio difference is negligible.)

The power-on values are obtained by applying increments to the power-off value. These increments are taken from NASA/Ames wind tunnel test 294.

Similarly, the yawing moment and sideforce derivatives are obtained (also considering the change in the wing reference area), and are presented in figures 121 and 122.

Roll derivatives: The asymptote for the damping in roll in figure 123 is obtained from the Weissinger lifting surface theory. It represents the power-off portion according to

$$\frac{\partial \frac{L}{T_o b}}{\partial \left( \frac{pb}{2V} \right)} = \frac{(C_{lp})_{\text{power off}} q S b}{T_o b} = (C_{lp})_{\text{power off}} \left( \frac{q}{T_o S} \right) \quad (144)$$

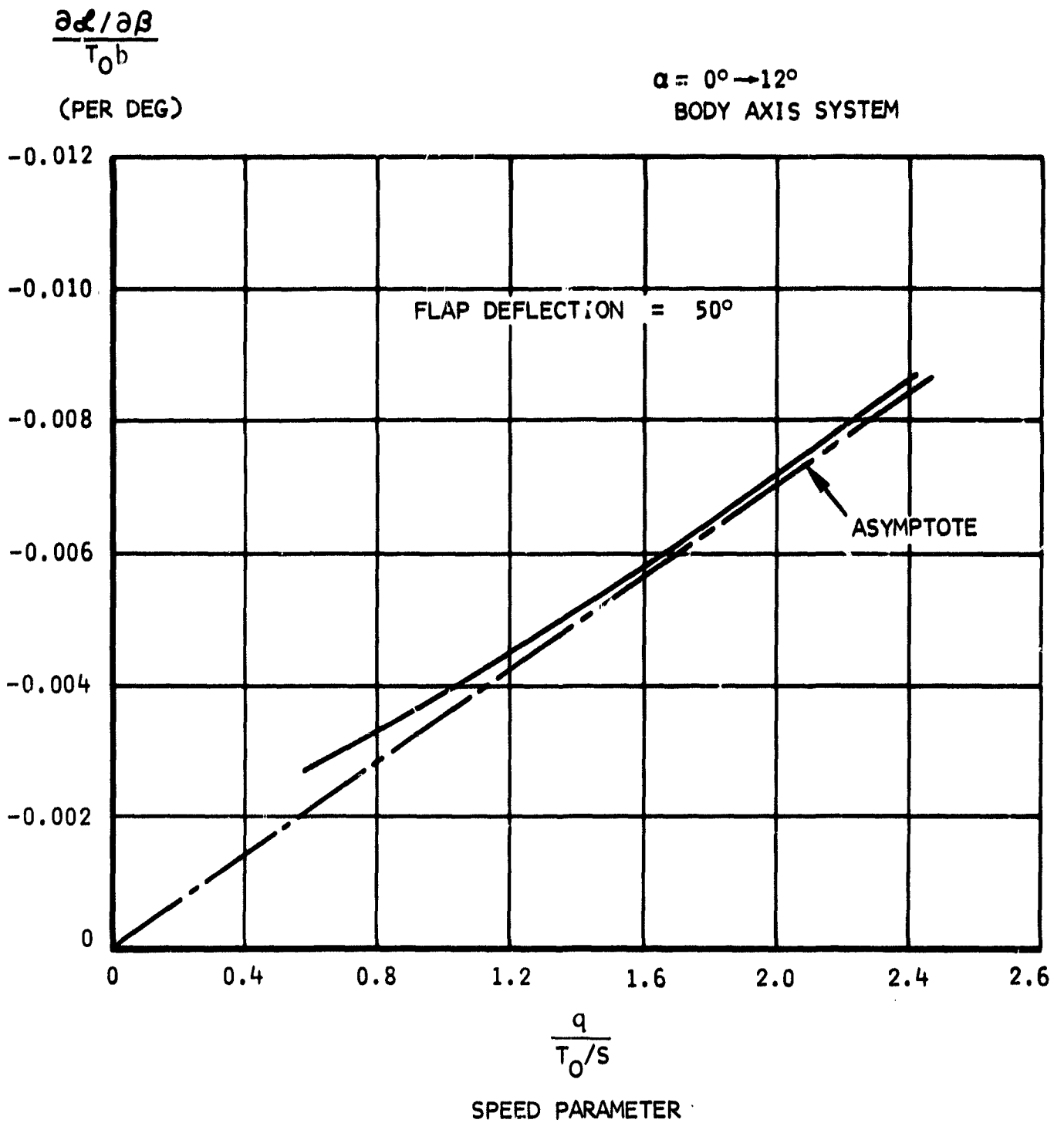


Figure 120. Rolling Moment Due to Side-Slip Versus Speed Parameter

$\frac{\partial N/\partial \beta}{T_{0b}}$   
(PER DEG)

$\alpha = 0^\circ \rightarrow 12^\circ$   
BODY AXIS SYSTEM

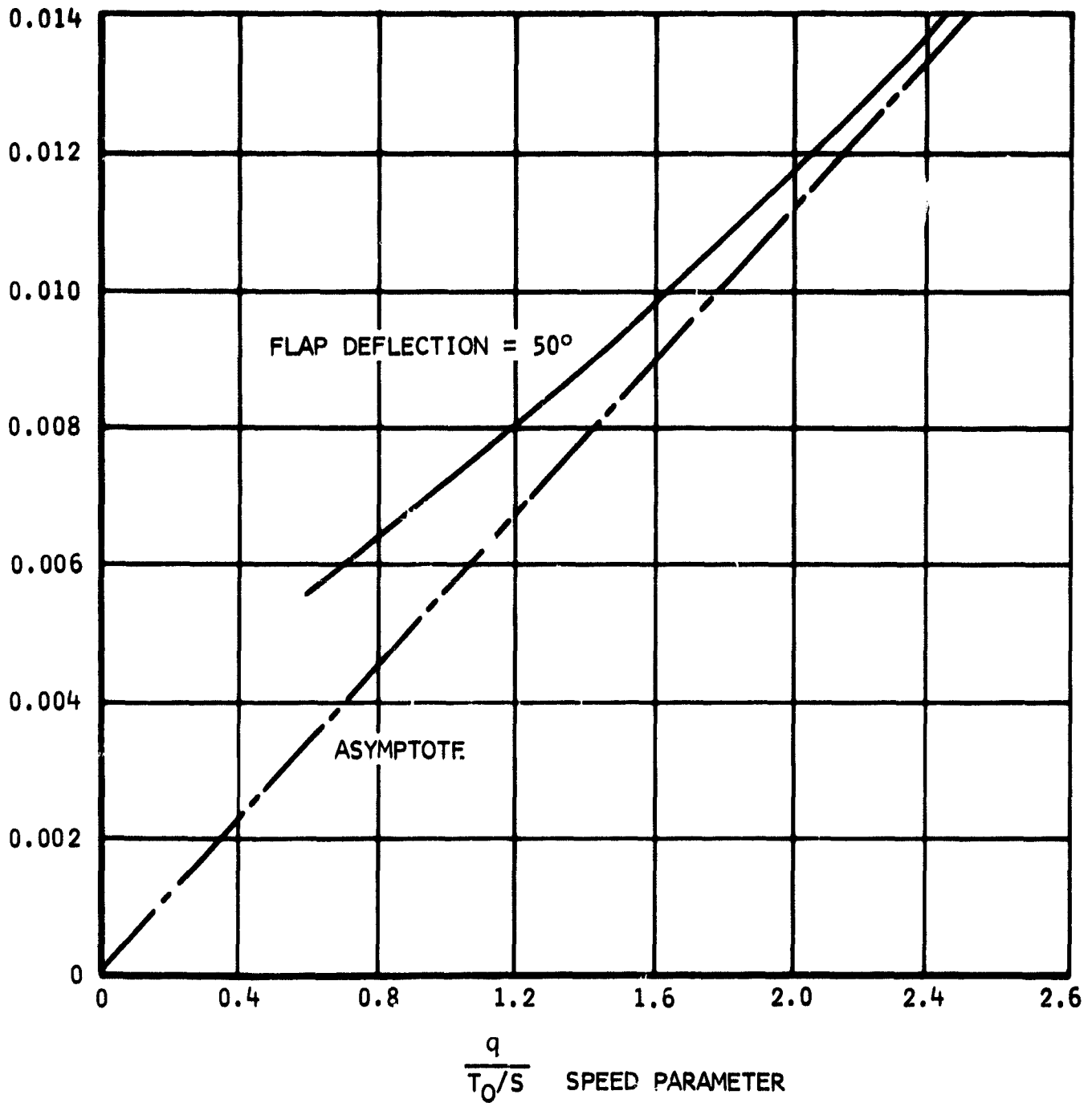


Figure 121. Yawing Moment Due to Side-Slip Versus Speed Parameter

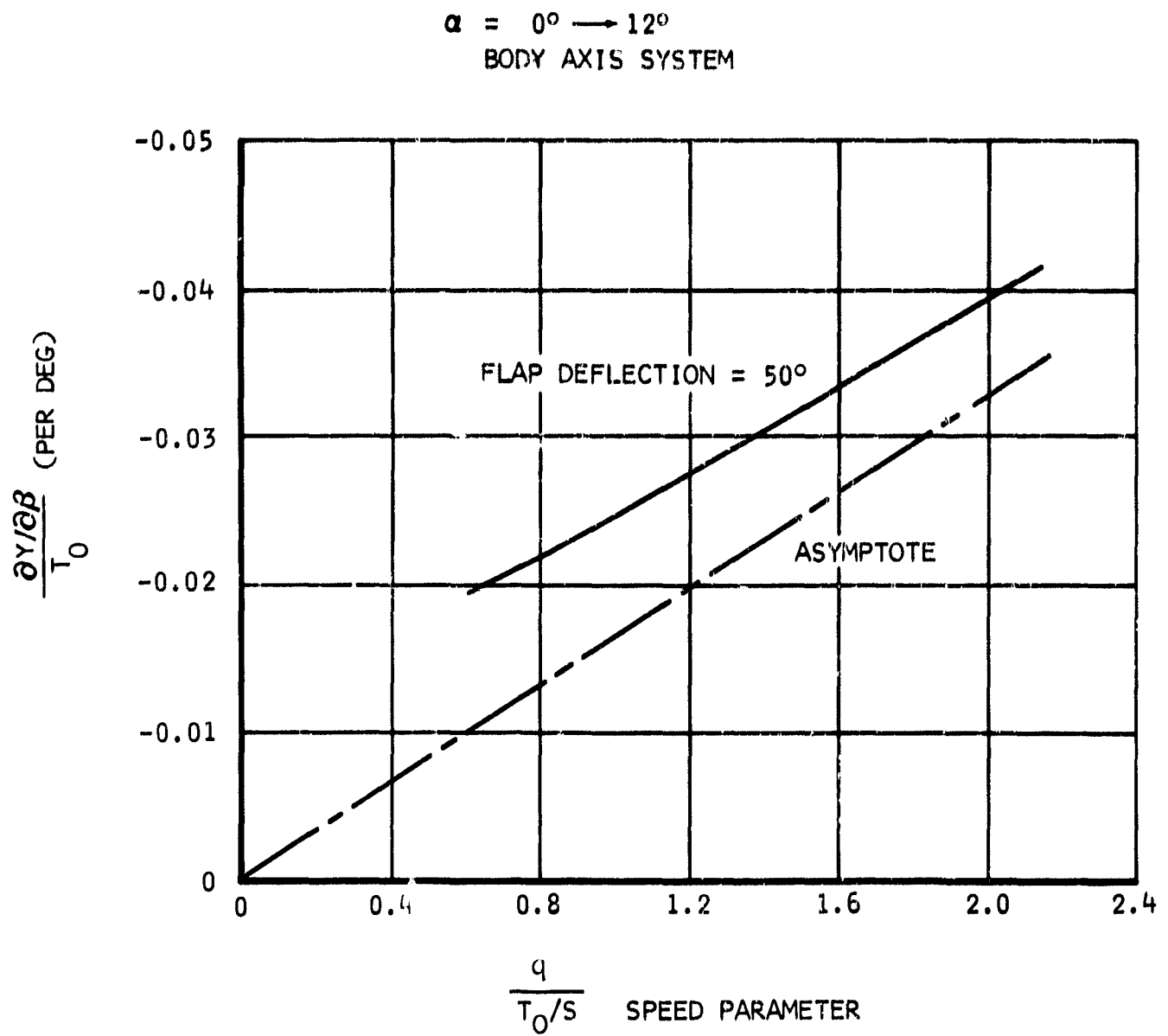


Figure 122. Side-Force Derivative Versus Speed Parameter

$\frac{\partial \mathcal{L}/T_0}{\partial \left(\frac{Pb}{2V}\right)}$   
 (PER RAD)

$\alpha = 0$

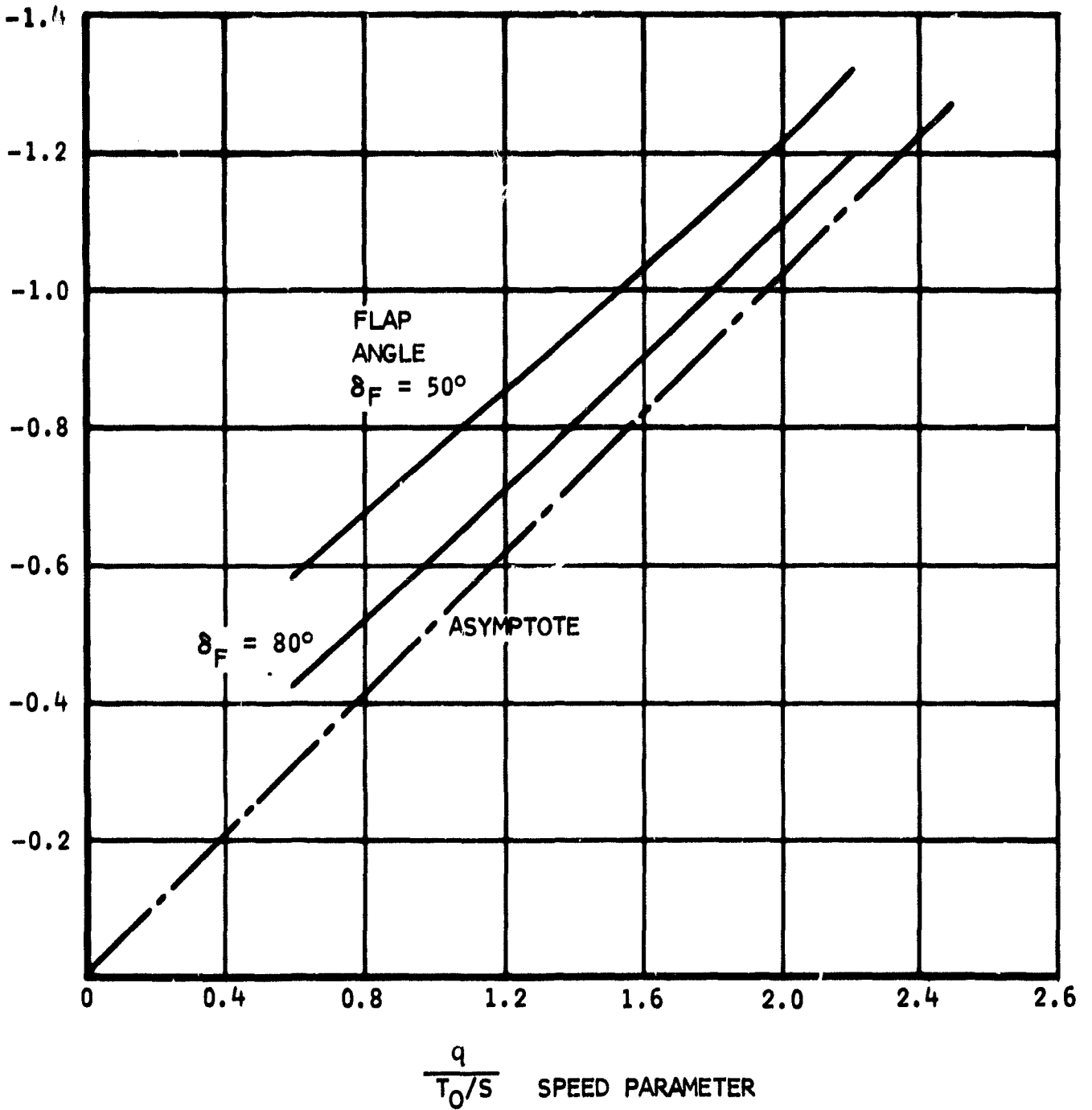


Figure 123. Damping Derivative in Roll as a Function of Speed Parameter

The power effects are obtained by applying to it the ratio of the power-on to power-off lift curve slopes from the longitudinal section of the report

$$\frac{\left[ \frac{\partial \frac{L}{T_0 b}}{\partial \left( \frac{pb}{2V} \right)} \right]_{\text{power on}}}{\left[ \frac{\partial \frac{L}{T_0 b}}{\partial \left( \frac{pb}{2V} \right)} \right]_{\text{power off}}} = \frac{\left( \frac{\partial \frac{L}{T_0}}{\partial \alpha} \right)_{\text{power on}}}{\left( \frac{\partial \frac{L}{T_0}}{\partial \alpha} \right)_{\text{power off}}} = \frac{(C_{L\alpha})_{\text{power on}}}{(C_{L\alpha})_{\text{power off}}} \quad (145)$$

The derivative of yaw due to rolling is presented in figure 124. The asymptote is determined from

$$\frac{\partial \frac{N}{T_0 b}}{\partial \left( \frac{pb}{2V} \right)} = (C_{np})_{\text{power on}} \left( \frac{q}{S} \right) \quad (146)$$

The yawing moment due to roll with power effect is computed from an equation which is derived as follows: The yawing moment depends on local drag changes  $(\partial D/T_0)/\partial \alpha$  and a rotation of the local lift vector  $L/T_0$  through an angle  $\Delta \alpha$ , where  $\tan \Delta \alpha = (\partial Y)/V$ . Calling  $y^*$  the lateral distance where the local drag and lift vector changes can be presented as one force change and calling  $f^*$  a factor representing the reduction of the forces due to three dimensional effects in the roll mode (rather than in the pitch mode), the yawing moment can be expressed as

$$N = f^* \left( \frac{1}{2} \frac{\partial \frac{D}{T_0}}{\partial \alpha} \right) \left( \frac{\partial y^*}{V} \right) (57.3) (2y^*) T_0 -$$

$$f^* \frac{L}{T_0} (\sin \Delta \alpha) (2y^*) T_0 \quad (147)$$

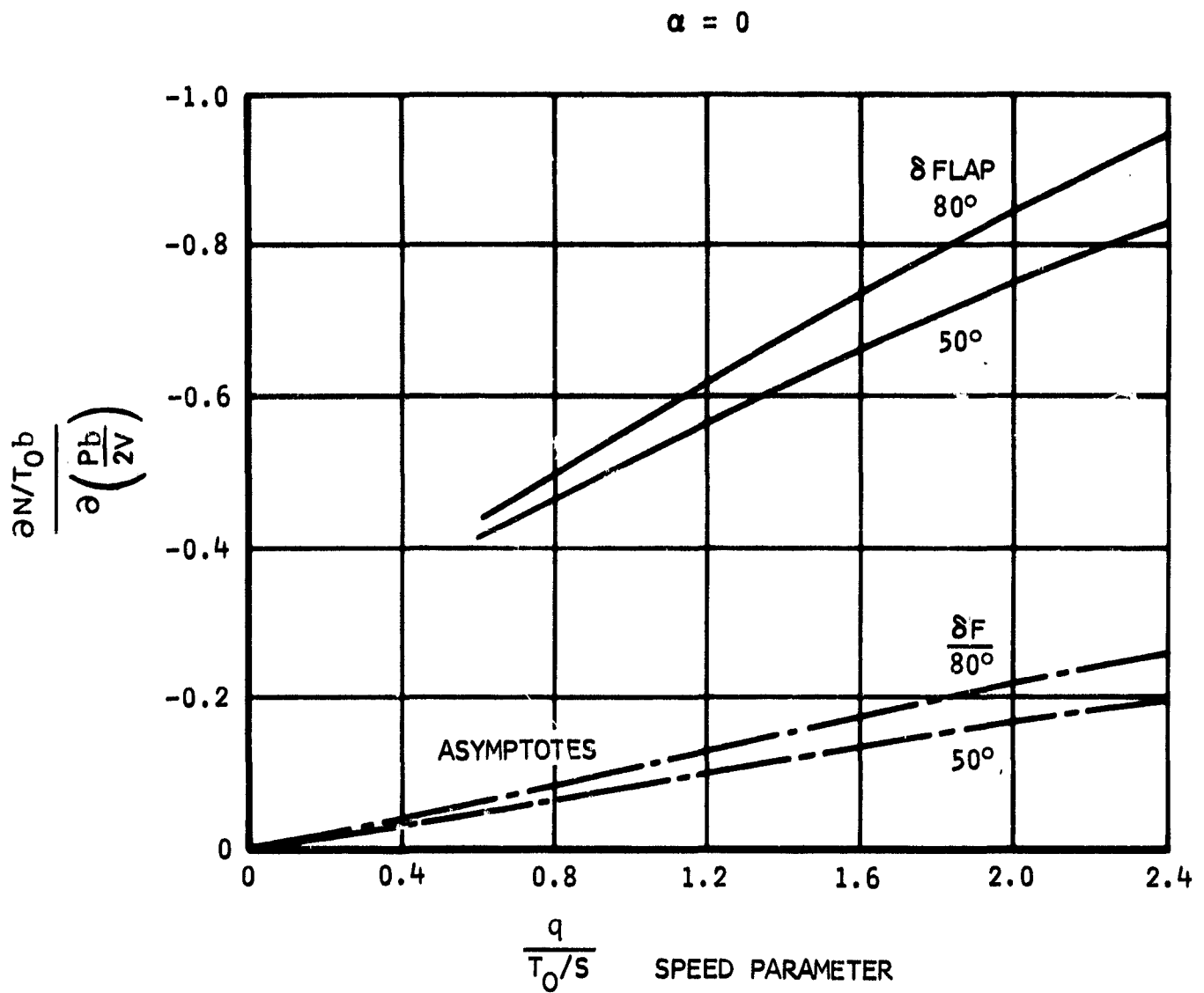


Figure 124. Yawing Moment Due to Roll as a Function of Speed Parameter



Assuming that  $\Delta\alpha$  is small, i.e., that  $V$  is not relatively small, yields

$$\frac{N}{T_0 b} = f^* \left( \frac{y^*}{\frac{b}{2}} \right) \left[ \left( \frac{1}{2} \frac{\partial \frac{D}{T_0}}{\partial \alpha} \right) \left( \frac{\dot{y} y^*}{V} \right) 57.3 - \frac{L}{T_0} \left( \frac{\dot{y} y^*}{V} \right) \right] \quad (148)$$

or

$$\frac{\partial \frac{N}{T_0 b}}{\partial \frac{pb}{2V}} = f^* \left( \frac{y^*}{\frac{b}{2}} \right)^2 \left[ \left( \frac{1}{2} \frac{\partial \frac{D}{T_0}}{\partial \alpha} \right) 57.3 - \frac{L}{T_0} \right] \quad (149)$$

This equation is used for figure 124 assuming that  $f^* = 1/2$ , and  $y^* = 0.58 b/2$ .

Yaw derivatives: The rolling moment due to yaw is presented in figure 125. The asymptote representing power-off values is determined using the DATCOM methods. The power-on values are obtained from an equation derived as follows. The forward velocity at the local wing station is

$$V_{LOC} = V + ry \quad (150)$$

so that

$$d V_{LOC} = d (ry) \quad (151)$$

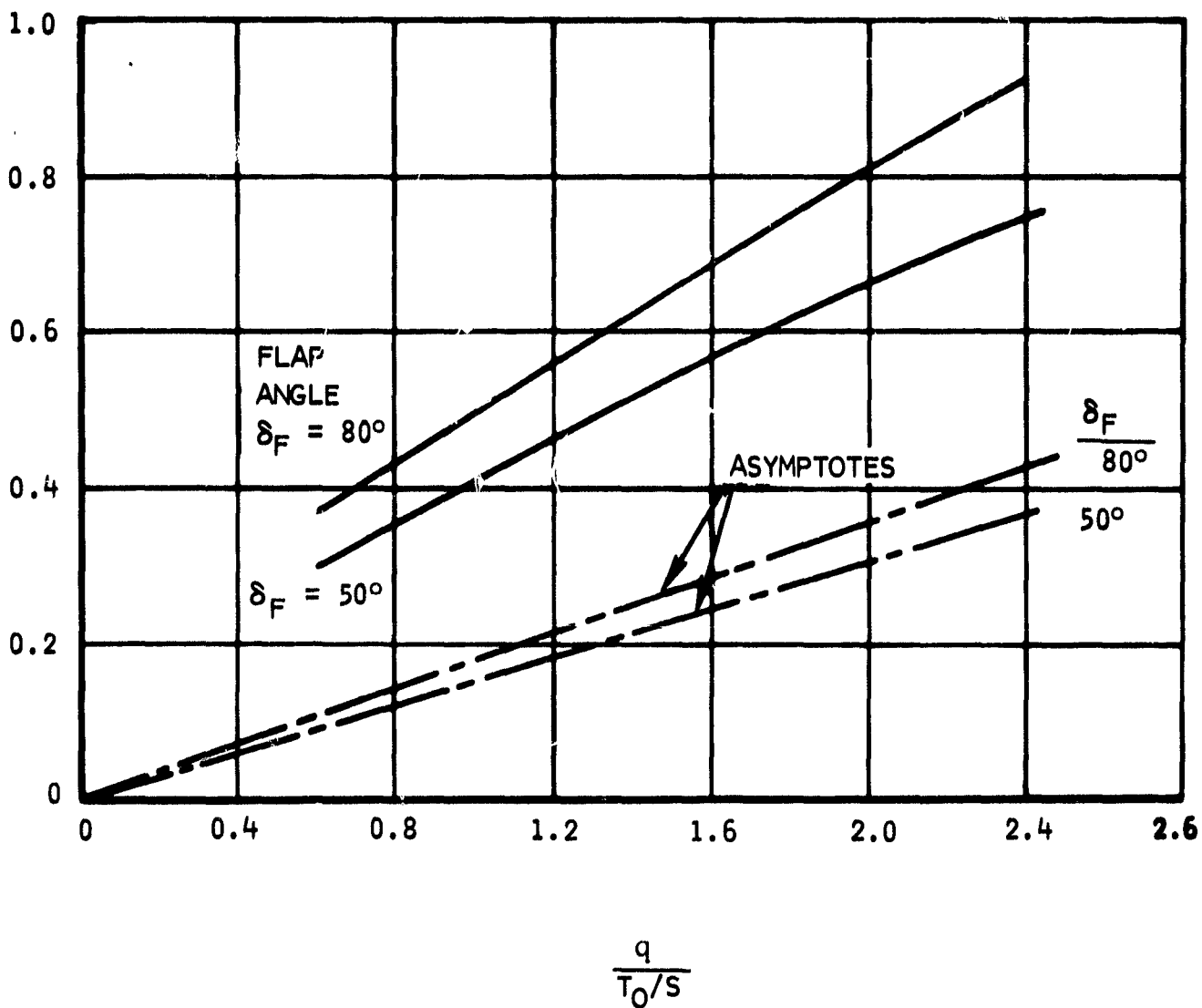
$$dq = d \left( \frac{1}{2} \rho V_{LOC}^2 \right) = \rho V_{LOC} dV_{LOC} = \rho V_{LOC} \cdot d(ry) \quad (152)$$

At a lateral station  $y^*$  the local lift forces from the  $q$ -changes can, per definition, be considered concentrated into one force at each wing panel. This force amounts to (using  $f^*$  to account for three dimensional effects in the rolling mode).

$$\frac{\partial \alpha / T_0 b}{\partial \left( \frac{rb}{2V} \right)}$$

$\alpha = 0$

(PER RAD)



SPEED PARAMETER

Figure 125. Rolling Moment Due to Yaw as a Function of Speed Parameter

$$d \frac{L}{T_o} = f'' \left( \frac{1}{2} \frac{\partial \frac{L}{T_o}}{\partial q} \right) \rho (V + ry^*) d (ry^*) \quad (153)$$

so that

$$d \frac{\mathcal{L}}{T_{ob}} = d \frac{\mathcal{L}}{T_o} \frac{y^*}{b} \cdot 2 = f^* \left( \frac{1}{2} \frac{\partial \frac{L}{T_o}}{\partial q} \right) \rho \left( V + rb \frac{y^*}{b} \right) \frac{y^*}{b} \cdot 2 d \frac{rb \left( \frac{y^*}{b} \right)}{b} \quad (154)$$

$$d \frac{\mathcal{L}}{T_{ob}} = f^* \left( \frac{1}{2} \frac{\alpha \frac{L}{T_o}}{\alpha \frac{q}{T_o}} \right) \frac{\rho}{S} \left( V + \frac{rb}{2V} \frac{y^*}{b} V \right) \frac{y^*}{b} d \left( \frac{rb}{2V} \frac{y^*}{b} V \right) \quad (155)$$

$$\frac{\partial \frac{\mathcal{L}}{T_{ob}}}{\partial \frac{rb}{2V}} = f^* \left( \frac{\alpha \frac{L}{T_o}}{\alpha \frac{q}{T_o}} \right) \frac{q}{S} \left( 1 + \frac{rb}{2V} \frac{y^*}{b} \right) \left( \frac{y^*}{b} \right)^2 \quad (156)$$

Numerical data presented here are based on  $f^* = 1/2$ ,  $y^* = 0.58 b/2$ , and  $r = 0$ .

The damping in yaw is presented in figure 126. The damping is determined mainly from the vertical tail using

$$\frac{\partial \frac{N}{T_{ob}}}{\partial \frac{rb}{2V}} = \left[ \left( \frac{\partial C_L}{\partial \alpha} \right)_v \frac{S_v}{S} \right] \frac{l_v}{b} \cdot \frac{q}{T_o} \cdot \frac{l_v}{b} = \left( \frac{\partial C_L}{\partial \alpha} \right)_v \cdot \bar{V}_v \cdot \frac{q}{S} \cdot \frac{l_v}{b} \quad (157)$$

An additional contribution is taken into account for the wing, based on DATCOM. Power effects on the wing contribution are negligible.

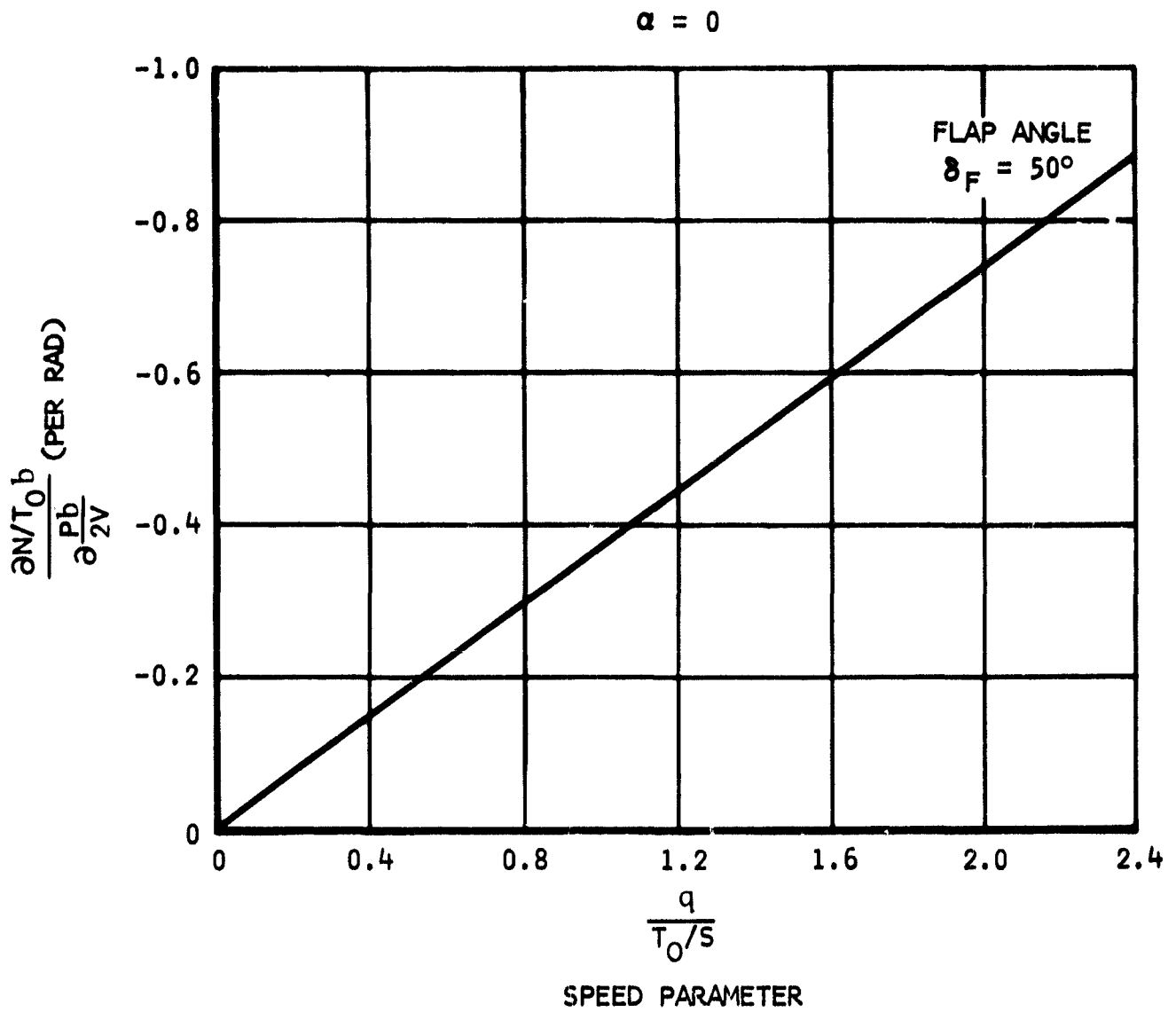


Figure 126. Damping Derivative in Yaw as a Function of Speed Parameter

## REFERENCES

1. DHC 67-20, "Augmentor Wing Flight Test Vehicle Program - Volume I - Technical Plan," de Havilland Aircraft of Canada LTD, no date.
2. Ames Research Center Working Paper No. 236, "Aerodynamic Characteristics of a Large-Scale Unswept Augmented - Jet Flap Model," by D. Koenig, V. Corsiglia, J. Morelli, no date.
3. Ames Research Center Unpublished Data (follow on test to reference 2 above.)
4. NA68-995, "Configuration Evaluations of a CV-7A Buffalo Modification to a Jet-Powered, Augmentor Wing STOL Aircraft," E. H. Kemper, Los Angeles Division of North American Rockwell Corporation, December 1968.
5. E.O. 05-2004-2B, Description and Maintenance Instructions, Hydraulics and Pneumatic System-Buffalo.
6. Military Specification Flying Qualities of Piloted Airplanes MIL-F-008785A, 31 October 1968.
7. V/STOL Flying Qualities Criteria Development Volume 1, A Proposed Military Specification for V/STOL Flying Qualities, AFFDL, October 1968.
8. V/STOL Flying Qualities Criteria Development Volume II, Background Information and User Guide for the Proposed Military Specification for V/STOL Flying Qualities, AFFDL, October 1968.
9. G. V. Lachmann, Pergamon Press 1961, "Boundary Layer and Flow Control."